

ON-LINE ANALYSIS OF THE
STABILITY AND OTHER FEATURES
OF FROTHS AND FOAMS BY USE OF
DIGITAL IMAGE PROCESSING

René Ellis



Thesis submitted in partial fulfilment of the
requirements for the degree of
Master of Science (Chemical Engineering)
at the University of Stellenbosch

Supervisor: Prof. C. Aldrich

STELLENBOSCH
MARCH 2002

DECLARATION

I, the under-signed, hereby declare that the work contained in this thesis is my own original work, except where specifically acknowledged in the text. The present thesis has not previously in its entirety or in part been submitted at any university for a degree.

October 2001

SYNOPSIS

The objective of this study is the assessment of the usefulness of an industrial machine vision system for laboratory studies of especially flotation froths and other foams. With this in mind it was attempted to meet three objectives. The first objective is the adjudication of the machine vision system's ability through image analysis to differentiate between characteristics of two-phase and three-phase systems. Secondly, through the use of image analysis the effect of varying surfactant concentration, as well as the addition of quartz particles on the foam/froth stability was quantified and thirdly it was attempted to define the nature of foam decay as stochastic or deterministic. While not as important in the industrial setting, the last objective is quite important when a laboratory system is concerned, even more so owing to the difficulty of quantifying the collapse or decay of foams and froths.

Two experimental set-ups were used to attain above-mentioned objectives. A Leeds flotation cell was used for the flotation of the quartz with cetyltrimethylammonium bromide (CTAB) and octadecylamine (ODA) and as well as for the characterisation of the CTAB and ODA foam. A glass column was used to investigate the CTAB foam column decay. In both set-ups the foam/froth structures were monitored with an ELMO charged coupled device (CCD). The CCD was connected to a personal computer equipped with frame grabber, which captured and digitised the images.

The following conclusions can be drawn from the experimental results:

- i The machine vision system can differentiate accurately between surfactant groups of different concentration and thus groups with unique characteristics.
- ii The stability of foam is highly correlated with all other foam variables extracted from the image analysis system. In particular, the movement of the foam/froth in the flotation cell has a substantial influence on the stability values obtained for the foam/froth.

- iii As far as the experimental system was concerned, small quartz particles (-75 μm) stabilised the froth, while coarser particles (75-106 μm , 106-150 μm and 150+ μm) destabilised the froth.
- iv Likewise, the decay of CTAB foam in a column was non-linear and deterministic. When observed manually, the decay of long life foams follow the same trend as short-life foams and short-life emulsions in that a specific decay constant can be calculated for a specific surfactant system.
- v The machine vision system is a viable alternative for current stability measurements. Firstly, no data processing need to be done to calculate a indirect stability parameter as it computes a direct stability parameter and secondly it also computes the bubble size distribution of the sample.

The following recommendations are made:

- i The experimental design of the system needs to be altered to minimise the effect the experimental environment has on results. The possibility of a different camera set-up must be investigated. The focus of the camera on the foam surface needs to be accurate as the computation of the stability value depends on the quality of the image obtained.
- ii The four factors that affect the stability of a flotation froth, namely solid concentration, particle size, particle type and particle hydrophobicity should be investigated in the same study. There exists many conflicting studies on this subject as many studies for different particles with a variety of sizes, hydrophobicity and concentration are performed. One study should be conducted where all four these factors are investigated under the same experimental conditions.
- iii The method with which the image analysis system deal with fine froth need to be addressed. In laboratory systems a typical system investigated will show a dense foam with small bubble distributions as in the case of CTAB. The extent to which the grouping of fine froth as one bubble influence the instability values obtained needs to be investigated.

OPSOMMING

Die doelwit van hierdie studie is die evaluering van die toepassing van 'n industriële masjienvisiesistiem in 'n laboratorium studie van hoofsaaklik flottasie skuim. Die doel van hierdie toepassing is drie-ledig. Die eerste doelwit is om die onderskeidingsvermoë van die masjienvisiesistiem tussen groepe met verskillende eienskappe te evalueer deur intydse beeld verwerking. Tweedens is die invloed van oppervlakmiddelkonsentrasie veranderinge asook die byvoeging van kwarts partikels op die stabiliteit van die skuim ondersoek. Derdens is die aard van die skuim verval ondersoek om vas te stel of die proses deterministies of stochasties is. Alhoewel laasgenoemde doelwit nie so belangrik is in die industriële toepassing nie, is dit van uiterse belang in die laboratorium studies, veral as gevolg van die probleme wat ondervind word in die kwantifisering van skuimverval.

Twee eksperimentele opstellings is gebruik om bogenoemde doelwitte te bereik. 'n Leeds flottasiesel is gebruik vir die flottasie van kwarts met CTAB en ODA asook vir die karakterisering van CTAB en ODA skuimeienskappe. 'n Glaskolom is gebruik vir die ondersoek van die aard van skuimverval. In beide opstellings is die beelde gemonitor deur 'n ELMO CCD. Die CCD is verbind met 'n rekenaar wat toegerus is met 'n raam-vanger wat die beelde vang en digitiseer.

Die volgende gevolgtrekkings kan uit die eksperimentele resultate gemaak word:

- i Die masjienvisiesistiem differensieer akkuraat tussen oppervlakmiddel groepe van verskillende konsentrasies en dus ook tussen groepe met unieke eienskappe.
- ii Die skuim stabiliteit korreleer met die ander skuim eienskappe naamlik gemiddelde area, gemiddelde omtrek, aantal borrels, fynheid van die beeld (SNE), beweging van die skuim en kleur van die skuim. Veral die beweging van die skuim in die flottasiesel het 'n beduidende invloed op die skuimstabiliteit.

- iii In die genoemde eksperimentele sisteem is gevind dat klein kwartspartikels ($-75\ \mu\text{m}$) skuim stabiliseer terwyl groter partikels ($75\text{-}106\ \mu\text{m}$, $106\text{-}150\ \mu\text{m}$ en $150+\ \mu\text{m}$) skuim destabiliseer.
- iv Die verval van CTAB skuim in 'n kolom is nie-lineêr en deterministies. In die geval waar die verval van die CTAB met die hand gemeet is, is gevind dat die verval van 'n lang-lewe skuim dieselfde tendens as kort-lewe skuim en kort-lewe emulsies volg. 'n Spesifieke verval konstante kan bereken word vir 'n spesifieke oppervlakmiddel sisteem.
- v Die masjienvisiesisteem is 'n werkbare alternatief in die meting van skuimstabiliteit. Anders as in bestaande stabiliteitsmetings waar 'n indirekte stabiliteitsparameter bereken moet word, bereken die sisteem 'n direkte stabiliteitsparameter asook die borrelverspreiding van die skuim monster.

Die volgende aanbevelings kan gemaak word:

- i Die eksperimentele ontwerp van die sisteem moet aangepas word om sodoende die invloed van eksperimentele kondisies op die resultate te verminder. Die moontlikheid van 'n alternatiewe kamera opstelling moet ook ondersoek word, aangesien die verkrygte stabiliteitswaardes afhanklik is van die kwaliteit van die skuimbeelde.
- ii Daar is talle teenstrydige studies ten opsigte van die vier faktore wat die stabiliteit van flotasie skuim beïnvloed naamlik erts tipe, partikel grootte, partikel hidrofobisiteit en vastestof konsentrasie. Hierdie faktore moet gelyktydig in 'n studie ondersoek word onder dieselfde eksperimentele kondisies.
- iii Die masjienvisiesisteem groepeer fyn skuim gedeeltes saam as een borrel. Hierdie wyse van fyn skuim hantering moet aangespreek word aangesien 'n tipiese oppervlakmiddel sisteem in die laboratorium, soos in die geval

van CTAB, digte skuim met 'n fyn borrelverspreiding toon. Die mate waarin die onvermoë van die sisteem om fyn borrels te herken die stabiliteitswaardes beïnvloed, moet ondersoek word.

ACKNOWLEDGEMENTS

my supervisor, Chris Aldrich, for teaching me about patience and future vision and for inspiring me

Juliana Steyl for the endless organisation she did effortlessly; for always being prepared to help and for walking the extra mile

the workshop staff, in particular Anton and Howard for the many urgent orders that they delivered every time, on time

the library staff, Corinna Truter, Lizette Baard and Maryna Horn for their willingness to help and for the endless library requests that had no destination

my mother in who's footsteps I have always wished to follow to understand that I have fallen short of that is a relief as I surely now can say that I know, love and respect a truly great mind and a wonderful person

my father for being brilliant in taking the pressure off; for caring and for being proud

my fiancé and husband to be, Richard, for being the most positive person I have ever met; for never lacking encouragement and understanding

my friends for bearing each day with me and for making it so much more than worth it

the use of Crusader Systems' Fluxar[®] software for the digital analysis of the froth images is gratefully acknowledged

To my Creator;
without His grace this work would not be possible

TABLE OF CONTENTS

SYNOPSIS	I
OPSOMMING	III
ACKNOWLEDGEMENTS	VI
TABLE OF CONTENTS	VIII
LIST OF FIGURES	XVI
LIST OF TABLES	XX
CHAPTER 1 - INTRODUCTION	1
1.1 MOTIVATION FOR STUDY	1
1.1.1 FOAM AND FROTH STABILITY	1
1.1.2 IMAGE ANALYSIS	3
1.2 SPECIFIC OBJECTIVES OF THIS STUDY	4
CHAPTER 2 - FOAM PHENOMENA	6
2.1 OBJECTIVES	6
2.2 STRUCTURE AND CLASSIFICATION OF FOAM	7
2.2.1 DEFINITION	7
2.2.2 CLASSIFICATION OF FOAM	7
2.2.3 STRUCTURE	8

2.2.3.1 Liquid Films	9
2.2.3.2 Plateau Borders	9
2.3 FOAM STABILITY	10
2.4 SURFACE ACTIVITY	11
2.4.1 SURFACE TENSION	12
2.4.2 SURFACE-ACTIVE AGENTS	12
2.4.2.1 Surfactant Characteristics	13
2.4.2.2 Foam stabilisation mechanisms	15
2.5 FOAM FORMATION	17
2.5.1 FACTORS INFLUENCING FOAM FORMATION	17
2.5.1.1 Elasticity	17
2.5.1.2 The Gibbs adsorption isotherm	18
2.5.1.3 Gibbs effect	19
2.5.1.4 Marangoni effect	19
2.5.2 FOAM FORMATION METHODS	20
2.5.2.1 Pneumatic methods	21
2.5.2.2 Shaking tests	21
2.5.2.3 Pour test	22
2.5.2.4 Other methods	22
2.6 FOAM LIFETIME (STABILITY)	23
2.6.1 DRAINAGE OF FILMS AND PLATEAU BORDERS	24
2.6.1.1 Films	24
2.6.1.2 Capillary Pressure	24
2.6.1.3 Mechanisms of drainage through gravity	25
2.6.1.4 Viscous flow to Plateau borders	26
2.6.1.5 Prevention of drainage	27
2.6.1.6 Marginal regeneration	27
2.6.1.7 Plateau borders	29
2.6.2 DIFFUSION OF GAS THROUGH LAMELLAE (DISPROPORTIONATION)	29
2.6.2.1 Definition	29
2.6.2.2 Effect of solubility of gas on disproportionation	31
2.6.2.3 Retardation of disproportionation	31
2.6.3 FACTORS DETERMINING FILM PERSISTENCE	32
2.6.3.1 Repulsion Force	32
2.6.3.2 Dilational viscosity	33
2.6.4 SPECIAL APPLICATION: FOAM COLUMN COLLAPSE	34
2.7 CONCLUDING REMARKS	35

2.8 SYMBOLS USED IN CHAPTER 2	37
2.8.1 SYMBOLS	37
2.8.2 GREEK SYMBOLS	38
2.8.3 SUBSCRIPTS	38
CHAPTER 3 - LITERATURE SURVEY	39
<hr/>	
3.1 OBJECTIVES	39
3.2 STABILITY OF FOAM	39
3.2.1 FOAMABILITY	40
3.2.2 FOAM STABILITY	41
3.3 MEASUREMENT TECHNIQUES OF FOAM STABILITY	41
3.4 STABILITY MEASUREMENTS OF DYNAMIC FOAM	42
3.4.1 BIKERMAN'S DYNAMIC METHOD	42
3.4.1.1 Theory	42
3.4.1.2 Variations on Bikerman's method	45
3.4.1.3 Comments on Bikerman's dynamic method and variations	46
3.4.2 OTHER APPLICATIONS	48
3.4.2.1 Application of a two-phase foam	49
3.4.2.2 Application of a three-phase foam: Foamed emulsion	51
3.4.2.3 Comments on the stability parameter calculation followed by Iglesias et al. (1995) and Turner et al. (1999)	53
3.4.3 OTHER METHODS	54
3.5 STABILITY MEASUREMENTS OF STATIC FOAMS	55
3.5.1 EXCESS PRESSURE	55
3.5.1.1 Theory	56
3.5.1.2 Further analysis of data	58
3.5.1.3 Comments on the Excess Pressure method	58
3.5.2 LIGHT TRANSMISSION METHODS AND REFLECTOMETRY	61
3.5.2.1 Theory on light transmission	61
3.5.2.2 Comments on the Light Transmission Method	62
3.5.2.3 Theory on reflectometry	62
3.5.2.4 Comments on Reflectometry Method	63
3.5.3 OTHER METHODS	64
3.6 IMAGE ANALYSIS	64
3.6.1 OVERVIEW OF DEVELOPMENT	65

3.6.2 IMAGE PROCESSING	67
3.6.2.1 Static Analysis	67
Bubble segmentation	67
Other textural properties	69
Fine froth segmentation	71
3.6.2.2 Dynamic Analysis	71
3.6.2 PARAMETER EXTRACTION	71
3.6.2.1 Extractable parameters	71
Area	72
Bubble count	72
Bubble base motion	72
Colour information	73
Perimeter	73
3.6.3.2 Statistics	73
3.6.3.3 Histogramming	73
3.6.4 CHARACTERISATION OF FROTH/FOAM STABILITY	74
3.6 CONCLUDING REMARKS	75
3.7 SYMBOLS USED IN CHAPTER 3	77
3.7.1 SYMBOLS	77
3.7.2 GREEK SYMBOLS	78
3.7.3 SUBSCRIPTS	78
CHAPTER 4 - FLOTATION FROTH FEATURES	79
4.1 OBJECTIVES	79
4.2 THE FLOTATION PROCESS	80
4.2.1 DEFINITION	80
4.2.2 PROCESS DESCRIPTION	81
4.2.2.1 Bubble generation	81
4.2.2.2 Bubble/Suspended matter contact	82
4.2.2.3 Bubble/Suspended matter attachment	84
4.2.3 TYPES	86
4.2.4 FACTORS INFLUENCING FLOTATION RATE	87
4.2.4.1 Bubble size	87
4.2.4.2 Agitation	87
4.2.4.3 Particle density	88

4.2.5 EFFECT OF PARTICLES ON FROTH STABILITY	88
4.2.5.1 Particles hydrophobicity	89
4.2.5.2 Particle Size	91
4.3 CASE STUDY: THE FLOTATION OF QUARTZ	92
4.3.1 EXPERIMENTAL SET-UP	92
4.3.2 QUARTZ AND REAGENTS	93
4.3.3 TEST PROCEDURE	94
4.3.4 IMAGE ANALYSIS	95
4.4 RESULTS AND DISCUSSION	96
4.4.1 FOAM AND FROTH STRUCTURES	96
4.4.1.1 System without solids	96
Principal component analysis	96
Correlations between variables	101
4.4.1.2 System with solids	103
Principal component analysis	103
Classification of groups	108
4.4.2 COMPARISON OF THE STABILITY OF FOAM AND FROTH	112
4.4.2.1 Influence of surfactant concentration on stability	113
Stability of foam	113
Stability of froth	119
4.4.2.2 Influence of particles on stability	121
4.4.3 RECOVERY	126
4.4.3.1 Influence of surfactant concentration on recovery	126
4.4.3.2 Influence of particles size on recovery	127
4.5 CONCLUDING REMARKS	128
CHAPTER 5 - DYNAMIC MODELLING OF FROTH STABILITY	130
5.1 OBJECTIVES OF THIS CHAPTER	131
5.2 OUTLINE OF THIS CHAPTER	131
5.3 CASE STUDY: CETYLTRIMETHYLAMMONIUM BROMIDE	133
5.3.1 EXPERIMENTAL SET-UP	133
5.3.2 REAGENTS	134
5.3.3 TEST PROCEDURE	134
5.4 EXPERIMENTAL DATA	135
5.4.1 INSTABILITY CURVES	135

5.4.2 TRANSFORMATION OF DATA	144
5.4.2.1 Series A: Instability differences	144
5.4.2.2 Series B: Residual value from linear regression	148
5.5 SAMPLING DISTRIBUTIONS	151
5.6 EMBEDDING USING SINGULAR SPECTRUM ANALYSIS	155
5.6.1 SERIES A	156
5.6.2 SERIES B	159
5.7 SURROGATE DATA	161
5.7.1 SERIES A	162
5.7.2 SERIES B	163
5.8 MODELLING	166
5.8.1 SERIES A	166
5.8.2 SERIES B	167
5.8.3 MODELS	168
5.9 CONCLUDING REMARKS FOR TIME SERIES ANALYSIS	171
5.10 CALCULATION OF STABILITY PARAMETER THROUGH MANUAL METHOD	171
5.11 SYMBOLS USED IN CHAPTER 5	177
CHAPTER 6 - CONCLUSIONS AND RECOMMENDATIONS	178
<hr/>	
6.1 CONCLUSIONS	178
6.1.1 CASE STUDY: FLOTATION OF QUARTZ	178
6.1.1.1 System differentiating	178
6.1.1.2 Correlation between extracted variables	179
6.1.1.3 Identification of groups	179
6.1.1.4 Stability of foam and froth	180
6.1.1.5 Recovery	181
6.1.2 CASE STUDY: DECAY OF CETYLTRIMETHYLAMMONIUM BROMIDE	182
6.1.2.1 Instability curves	182
6.1.2.2 Time series analysis	182
6.1.2.3 Stability as measured by manual method	184
6.2 RECOMMENDATIONS FOR FURTHER RESEARCH	185
6.3 FLOW DIAGRAM OF FOAM STABILITY EVALUATION PROCEDURE	188
REFERENCES	189
<hr/>	

APPENDIX A - ADDITIONAL TABLES AND FIGURES FOR CHAPTER 4	204
A.1 FACTOR LOADINGS	204
A.1.1 PARTICLE SIZE –75 MICRON	206
A.1.2 PARTICLE SIZE 75-106 MICRON	207
A.1.3 PARTICLE SIZE 150+ MICRON	209
A.2 FACTOR ANALYSIS GRAPHS	210
A.2.1 PARTICLE SIZE –75 MICRON	210
A.2.2 PARTICLE SIZE 75-106 MICRON	212
A.2.3 PARTICLE SIZE 150+ MICRON	214
A.3 CLASSIFICATION OF DATA	215
A.3.1 CLASSIFICATION BETWEEN GROUP WITH SOLIDS AND GROUP WITHOUT SOLIDS	216
A 3.1.1 Particle size –75 micron	216
A 3.1.2 Particle size 75-106 micron	216
A 3.1.3 Particle size 150+ micron	217
A 4.2 CLASSIFICATION BETWEEN ALL GROUPS	218
A 4.2.1 Particle size –75 micron	218
A 4.2.2 Particle size 75-106 micron	219
A 4.2.3 Particle size 150+ micron	220
APPENDIX B - ADDITIONAL THEORY FOR CHAPTER 5	221
B.1 EMBEDDING OF TIME SERIES	221
B.2 SINGULAR SPECTRUM ANALYSIS	222
B.3 TESTING FOR NONLINEARITIES	224
B.3.1 SURROGATE DATA	224
B.3.2 CORRELATION DIMENSION	225
B.4 MODELLING	227
B.4.1 MODEL CLASS	227
B.4.2 MODEL VALIDATION	228
B.5 SYMBOLS USED IN APPENDIX B	229
B.5.1 SYMBOLS	229
B.5.2 GREEK SYMBOLS	229
B.5.3 SUBSCRIPTS	229

APPENDIX C - ADDITIONAL TABLES AND FIGURES FOR CHAPTER 5	230
C.1 FOAM IMAGES	231
C.2 SAMPLING DISTRIBUTION	235

LIST OF FIGURES

FIGURE 2.1 SCHEMATIC ILLUSTRATION OF EVENTS DURING FOAM FORMATION (WALSTRA, 1989).	9
FIGURE 2.2 SECTION THROUGH A PLATEAU BORDER (AVEYARD ET AL., 1999).	10
FIGURE 2.3 SCHEMATIC REPRESENTATION OF A SURFACTANT	13
FIGURE 2.4 SCHEMATIC REPRESENTATION OF THE FORMATION OF MICELLES	14
FIGURE 2.5 VELOCITIES OF FLOW ACROSS LIQUID FILMS OF (A) PURE LIQUID AND (B) LIQUID BOUNDED BY MONOLAYERS OF ADSORBED SURFACTANTS (AVEYARD ET AL., 1999).	16
FIGURE 2.6 ILLUSTRATION OF ELASTICITY MECHANISM (ROSEN, 1978).	18
FIGURE 2.7 SCHEMATIC REPRESENTATION OF THE PROCESS OF MARGINAL REGENERATION (PRINS, 1988).	28
FIGURE 3.1 SCHEMATIC DIAGRAM OF APPARATUS FOR MEASUREMENT OF DYNAMIC FOAM STABILITY (BENEVENTI ET AL., 2001).	43
FIGURE 3.2 CONICAL FOAM METER (NISHIOKA ET AL., 1996).	55
FIGURE 3.3 DICKINSON'S PRESSURE CHAMBER (WILSON, 1996).	60
FIGURE 3.4 WATERSHED SEGMENTATION OF FROTH	69
FIGURE 4.1 MECHANISMS OF BUBBLE/SOLID CONTACT (BENNETT, 1988).	83
FIGURE 4.2 SCHEMATIC DIAGRAM OF GAS PHASE (BUBBLE) ADHERING TO SOLID PHASE (PRUD' HOMME & WARR, 1996).	85
FIGURE 4.3 FILM BREAKING BY HYDROPHOBIC PARTICLES (WALSTRA, 1989).	90
FIGURE 4.4 EXPERIMENTAL SET-UP FOR FLOTATION CELL STUDY	93
FIGURE 4.5 CHEMICAL STRUCTURE OF CETYLTRIMETHYLAMMONIUM BROMIDE	94
FIGURE 4.6 CHEMICAL STRUCTURE OF OCTADECYLAMINE	94
FIGURE 4.7 PRINCIPAL COMPONENT ANALYSIS FOR THE TWO-PHASE SYSTEM (RUN A)	100
FIGURE 4.8 PRINCIPAL COMPONENT ANALYSIS FOR THE TWO-PHASE SYSTEM (RUN B)	100
FIGURE 4.9 PRINCIPAL COMPONENT ANALYSIS FOR TWO-PHASE AND THREE-PHASE SYSTEM CONTAINING -75 μM PARTICLES	107
FIGURE 4.10 PRINCIPAL COMPONENT ANALYSIS FOR TWO-PHASE AND THREE-PHASE SYSTEM CONTAINING 75-106 μM PARTICLES	107
FIGURE 4.11 PRINCIPAL COMPONENT ANALYSIS FOR TWO-PHASE AND THREE-PHASE SYSTEM CONTAINING 106-150 μM PARTICLES	108
FIGURE 4.12 PRINCIPAL COMPONENT ANALYSIS FOR TWO-PHASE AND THREE-PHASE SYSTEM CONTAINING 150+ μM PARTICLES	113
FIGURE 4.13 FOAM IMAGES SHOWING 100% CTAB, 90% CTAB AND 80% CTAB	114
FIGURE 4.14 INFLUENCE OF SURFACTANT CONCENTRATION ON FOAM STABILITY	115
FIGURE 4.15 STABILITY TEST	115
FIGURE 4.16 FROTH IMAGES AT DIFFERENT TIME STEPS IN STABILITY TEST	116
FIGURE 4.17 COMPARISON OF STABILITY OF FOAM IN FLOTATION CELL AND STABILITY TEST CURVE	117
FIGURE 4.18 AVERAGE SPEED AND STABILITY OF FOAM FOR 100% CTAB	118

FIGURE 4.19 AVERAGE SPEED AND STABILITY OF FOAM FOR 90% CTAB	118
FIGURE 4.20 AVERAGE SPEED AND STABILITY OF FOAM FOR 80% CTAB	119
FIGURE 4.21 INFLUENCE OF SURFACTANT CONCENTRATION ON FROTH STABILITY CONTAINING –75 μM QUARTZ PARTICLES	120
FIGURE 4.22 INFLUENCE OF SURFACTANT CONCENTRATION ON FROTH STABILITY CONTAINING 75-106 μM QUARTZ PARTICLES	120
FIGURE 4.23 INFLUENCE OF SURFACTANT CONCENTRATION ON FROTH STABILITY CONTAINING 106-150 μM QUARTZ PARTICLES	121
FIGURE 4.24 INFLUENCE OF SURFACTANT CONCENTRATION ON FROTH STABILITY CONTAINING 150+ μM QUARTZ PARTICLES	122
FIGURE 4.25 INFLUENCE OF PARTICLE SIZE ON FROTH STABILITY FOR 100% CTAB	123
FIGURE 4.26 INFLUENCE OF PARTICLE SIZE ON FROTH STABILITY FOR 90% CTAB	123
FIGURE 4.27 INFLUENCE OF PARTICLE SIZE ON FROTH STABILITY FOR 80% CTAB	125
FIGURE 4.28 AVERAGE SPEED OF FOAM FOR 100% CTAB CONTAINING 106-150 μM QUARTZ PARTICLES	125
FIGURE 4.29 AVERAGE SPEED OF FOAM FOR 90% CTAB CONTAINING 106-150 μM QUARTZ PARTICLES	126
FIGURE 4.30 AVERAGE SPEED OF FOAM FOR 80% CTAB CONTAINING 106-150 μM QUARTZ PARTICLES	127
FIGURE 4.31 INFLUENCE OF SURFACTANT CONCENTRATION ON SOLID RECOVERY	128
FIGURE 5.1 EXPERIMENTAL SET-UP FOR FLOTATION COLUMN STUDY	134
FIGURE 5.2 INSTABILITY CURVE FOR RUN A	137
FIGURE 5.3 FOAM IMAGES FOR RUN A	137
FIGURE 5.4 INSTABILITY CURVE FOR RUN B	138
FIGURE 5.5 FOAM IMAGES FOR RUN B	138
FIGURE 5.6 INSTABILITY CURVE COMPARISON FOR RUN A AND RUN B	139
FIGURE 5.7 INSTABILITY CURVE FOR RUN C	140
FIGURE 5.8 FOAM IMAGES FOR RUN C	140
FIGURE 5.9 INSTABILITY CURVE FOR RUN D	141
FIGURE 5.10 FOAM IMAGES FOR RUN D	141
FIGURE 5.11 INSTABILITY CURVE COMPARISON FOR RUN C AND RUN D	142
FIGURE 5.12 INSTABILITY CURVE COMPARISON FOR RUN B AND RUN C	143
FIGURE 5.13 INSTABILITY CURVE FOR SERIES A, RUN A	145
FIGURE 5.14 INSTABILITY CURVE FOR SERIES A, RUN B	146
FIGURE 5.15 INSTABILITY CURVE FOR SERIES A, RUN C	147
FIGURE 5.16 INSTABILITY CURVE FOR SERIES A, RUN D	148
FIGURE 5.17 INSTABILITY CURVE FOR SERIES B, RUN A	149
FIGURE 5.18 INSTABILITY CURVE FOR SERIES B, RUN B	149
FIGURE 5.19 INSTABILITY CURVE FOR SERIES B, RUN C	150
FIGURE 5.20 INSTABILITY CURVE FOR SERIES B, RUN D	150

FIGURE 5.21 HISTOGRAM ILLUSTRATING NORMAL DISTRIBUTION	151
FIGURE 5.22 HISTOGRAM SHOWING DISTRIBUTION OF ORIGINAL TIME SERIES, RUN B	152
FIGURE 5.23 HISTOGRAM SHOWING DISTRIBUTION OF SERIES A, RUN B	153
FIGURE 5.24 HISTOGRAM SHOWING DISTRIBUTION OF SERIES B, RUN B	154
FIGURE 5.25 ATTRACTOR DESCRIBING STOCHASTIC PROCESS	156
FIGURE 5.26 ATTRACTOR FOR SERIES A, RUN A	156
FIGURE 5.27 ATTRACTOR FOR SERIES A, RUN B	157
FIGURE 5.28 ATTRACTOR FOR SERIES A, RUN C	157
FIGURE 5.29 ATTRACTOR FOR SERIES A, RUN D	158
FIGURE 5.30 ATTRACTOR FOR SERIES B, RUN A	159
FIGURE 5.31 ATTRACTOR FOR SERIES B, RUN B	159
FIGURE 5.32 ATTRACTOR FOR SERIES B, RUN C	160
FIGURE 5.33 ATTRACTOR FOR SERIES B, RUN D	161
FIGURE 5.34 SURROGATE DATA CURVES FOR SERIES A, RUN A	162
FIGURE 5.35 SURROGATE DATA CURVES FOR SERIES A, RUN B	162
FIGURE 5.36 SURROGATE DATA CURVES FOR SERIES A, RUN C	163
FIGURE 5.37 SURROGATE DATA CURVES FOR SERIES A, RUN D	163
FIGURE 5.38 SURROGATE DATA CURVES FOR SERIES B, RUN A	164
FIGURE 5.39 SURROGATE DATA CURVES FOR SERIES B, RUN B	164
FIGURE 5.40 SURROGATE DATA CURVES FOR SERIES B, RUN C	165
FIGURE 5.41 SURROGATE DATA CURVES FOR SERIES B, RUN D	165
FIGURE 5.42 MULTI-LAYER PERCEPTRON MODEL FOR SERIES B, RUN B	169
FIGURE 5.43 PREDICTED DATA VS OBSERVED DATA FOR SERIES B, RUN B	169
FIGURE 5.44 MULTI-LAYER PERCEPTRON MODEL FOR SERIES B, RUN D	170
FIGURE 5.45 PREDICTED DATA VS OBSERVED DATA FOR SERIES B, RUN D	170
FIGURE 5.46 FOAM HEIGHT VERSUS TIME FOR RUN A, RUN B AND RUN C	173
FIGURE 5.47 DIMENSIONLESS FOAM DECAY CURVES OVER 20 PERCENT TO 80 PERCENT OF DECAY TIME	174
FIGURE 5.48 NON-UNIFORM FOAM COLLAPSE OF CTAB CONTAINING 1 PERCENT (%) NaCl	176
FIGURE 6.1 FLOW DIAGRAM OF FOAM STABILITY EVALUATION PROCESS	188
FIGURE A.1 PRINCIPAL COMPONENT ANALYSIS FOR TWO-PHASE AND THREE-PHASE SYSTEM CONTAINING –75 μm PARTICLES AT 100% CTAB	210
FIGURE A.2 PRINCIPAL COMPONENT ANALYSIS FOR TWO-PHASE AND THREE-PHASE SYSTEM CONTAINING –75 μm PARTICLES AT 90% CTAB	211
FIGURE A.3 PRINCIPAL COMPONENT ANALYSIS FOR TWO-PHASE AND THREE-PHASE SYSTEM CONTAINING –75 μm PARTICLES AT 80% CTAB	211
FIGURE A.4 PRINCIPAL COMPONENT ANALYSIS FOR TWO-PHASE AND THREE-PHASE SYSTEM CONTAINING 75-106 μm PARTICLES AT 100% CTAB	212
FIGURE A.5 PRINCIPAL COMPONENT ANALYSIS FOR TWO-PHASE AND THREE-PHASE SYSTEM CONTAINING 75-106 μm PARTICLES AT 90% CTAB	212

FIGURE A.6 PRINCIPAL COMPONENT ANALYSIS FOR TWO-PHASE AND THREE-PHASE SYSTEM CONTAINING 75-106 μM PARTICLES AT 80 % CTAB	213
FIGURE A.7 PRINCIPAL COMPONENT ANALYSIS FOR TWO-PHASE AND THREE-PHASE SYSTEM CONTAINING 150+ μM PARTICLES AT 100% CTAB	214
FIGURE A.8 PRINCIPAL COMPONENT ANALYSIS FOR TWO-PHASE AND THREE-PHASE SYSTEM CONTAINING 150+ μM PARTICLES AT 90% CTAB	214
FIGURE A.9 PRINCIPAL COMPONENT ANALYSIS FOR TWO-PHASE AND THREE-PHASE SYSTEM CONTAINING 150+ μM PARTICLES AT 80% CTAB	215
FIGURE B.1 SCHEMATIC REPRESENTATION OF A TYPICAL MULTI-LAYER PERCEPTRON NETWORK TOPOLOGY	228
FIGURE C.1 FOAM IMAGES FOR RUN A	231
FIGURE C.2 FOAM IMAGES FOR RUN B	232
FIGURE C.3 FOAM IMAGES FOR RUN C	233
FIGURE C.4 FOAM IMAGES FOR RUN D	234
FIGURE C.5 HISTOGRAM SHOWING DISTRIBUTION OF ORIGINAL TIME SERIES, RUN A	235
FIGURE C.6 HISTOGRAM SHOWING DISTRIBUTION OF SERIES A, RUN A	236
FIGURE C.7 HISTOGRAM SHOWING DISTRIBUTION OF SERIES B, RUN A	237
FIGURE C.8 HISTOGRAM SHOWING DISTRIBUTION OF ORIGINAL TIME SERIES, RUN C	238
FIGURE C.9 HISTOGRAM SHOWING DISTRIBUTION OF SERIES A, RUN C	239
FIGURE C.10 HISTOGRAM SHOWING DISTRIBUTION OF SERIES B, RUN C	240
FIGURE C.11 HISTOGRAM SHOWING DISTRIBUTION OF ORIGINAL TIME SERIES, RUN D	241
FIGURE C.12 HISTOGRAM SHOWING DISTRIBUTION OF SERIES A, RUN D	242
FIGURE C.13 HISTOGRAM SHOWING DISTRIBUTION OF SERIES B, RUN D	243

LIST OF TABLES

TABLE 2.1 SURFACE TENSION DATA FOR TYPICAL INTERFACES	12
TABLE 4.1 VARIANCE EXPLAINED BY PRINCIPAL COMPONENTS IN TWO-PHASE SYSTEM	97
TABLE 4.2 FACTOR LOADINGS FOR THREE SURFACTANT RATIOS FOR RUN A	98
TABLE 4.3 FACTOR LOADINGS FOR THREE SURFACTANT RATIOS FOR RUN B	98
TABLE 4.4 CORRELATIONS BETWEEN SEVEN IMAGE VARIABLES DESCRIBING RUN A	101
TABLE 4.5 CORRELATIONS BETWEEN SEVEN IMAGE VARIABLES DESCRIBING RUN B	102
TABLE 4.6 VARIANCE EXPLAINED BY PRINCIPAL COMPONENTS IN TWO-PHASE AND THREE-PHASE SYSTEMS	104
TABLE 4.7 FACTOR LOADINGS FOR THREE-PHASE SYSTEM WITH 100% CTAB AND SOLID PARTICLE SIZE 106-150 μm	104
TABLE 4.8 FACTOR LOADINGS FOR THREE-PHASE SYSTEM WITH 90% CTAB AND SOLID PARTICLE SIZE 106-150 μm	105
TABLE 4.9 FACTOR LOADINGS FOR THREE-PHASE SYSTEM WITH 80% CTAB AND SOLID PARTICLE SIZE 106-150 μm	105
TABLE 4.10. CLASSIFICATION RESULTS BETWEEN TWO MAIN GROUPS FOR THE SOLID PARTICLE SIZE 106-150 μm	109
TABLE 4.11 CLASSIFICATION RESULTS FOR SIX GROUPS FOR THE SOLID PARTICLE SIZE 106-150 μm	110
TABLE 4.12 CLASSIFICATION RESULTS BETWEEN TWO MAIN GROUPS FOR ALL SOLID PARTICLE SIZES	112
TABLE 4.13. CLASSIFICATION RESULTS FOR SIX GROUPS FOR THE ALL SOLID PARTICLE SIZES	112
TABLE 5.1 DESCRIPTIVE STATISTICS OF NORMAL DISTRIBUTION	152
TABLE 5.2 DESCRIPTIVE STATISTICS OF ORIGINAL TIME SERIES, RUN B	153
TABLE 5.3 DESCRIPTIVE STATISTICS OF SERIES A, RUN B	154
TABLE 5.4 DESCRIPTIVE STATISTICS OF SERIES B, RUN B	156
TABLE 5.5 TABLE OF R^2 VALUES FOR TRAINING AND CROSS VALIDATION FOR SERIES A	167
TABLE 5.6 TABLE OF R^2 VALUES FOR TRAINING AND CROSS VALIDATION FOR SERIES B	168
TABLE 5.7 CHARACTERISTICS OF LINEAR REGRESSION CURVES DESCRIBING RUN A, RUN B AND RUN C	172
TABLE 5.8 CHARACTERISTICS OF LINEAR REGRESSION CURVES DESCRIBING RUN A, RUN B AND RUN C IN DIMENSIONLESS PLOT	175
TABLE A.1 FACTOR LOADINGS FOR TWO-PHASE SYSTEM (RUN C)	204
TABLE A.2 FACTOR LOADINGS FOR TWO-PHASE SYSTEM (RUN D)	205
TABLE A.3 FACTOR LOADINGS FOR TWO-PHASE SYSTEM (RUN E)	205
TABLE A.4 FACTOR LOADINGS FOR THREE-PHASE SYSTEM WITH 100% CTAB AND SOLID PARTICLE SIZE -75 μm	206
TABLE A.5 FACTOR LOADINGS FOR THREE-PHASE SYSTEM WITH 90% CTAB AND SOLID PARTICLE SIZE -75 μm	206

TABLE A.6 FACTOR LOADINGS FOR THREE-PHASE SYSTEM WITH 80% CTAB AND SOLID PARTICLE SIZE - 75 μM	207
TABLE A.7 FACTOR LOADINGS FOR THREE-PHASE SYSTEM WITH 100% CTAB AND SOLID PARTICLE SIZE 75-106 μM	207
TABLE A.8 FACTOR LOADINGS FOR THREE-PHASE SYSTEM WITH 90% CTAB AND SOLID PARTICLE SIZE 75-106 μM	208
TABLE A.9 FACTOR LOADINGS FOR THREE-PHASE SYSTEM WITH 80% CTAB AND SOLID PARTICLE SIZE 75-106 μM	208
TABLE A.10 FACTOR LOADINGS FOR THREE-PHASE SYSTEM WITH 100% CTAB AND SOLID PARTICLE SIZE +150 μM	209
TABLE A.11 FACTOR LOADINGS FOR THREE-PHASE SYSTEM WITH 90% CTAB AND SOLID PARTICLE SIZE +150 μM	209
TABLE A.12 FACTOR LOADINGS FOR THREE-PHASE SYSTEM WITH 80% CTAB AND SOLID PARTICLE SIZE +150 μM	210
TABLE A.13 CLASSIFICATION RESULTS BETWEEN TWO MAIN GROUPS FOR THE SOLID PARTICLE SIZE -75 μM	216
TABLE A.14 CLASSIFICATION RESULTS BETWEEN TWO MAIN GROUPS FOR THE SOLID PARTICLE SIZE 75- 106 μM	216
TABLE A.15 CLASSIFICATION RESULTS BETWEEN TWO MAIN GROUPS FOR THE SOLID PARTICLE SIZE +150 μM	217
TABLE A.16 CLASSIFICATION RESULTS BETWEEN SIX GROUPS FOR THE SOLID PARTICLE SIZE -75 μM	218
TABLE A.17 CLASSIFICATION RESULTS BETWEEN SIX GROUPS FOR THE SOLID PARTICLE SIZE 75-106 μM	219
TABLE A.18 CLASSIFICATION RESULTS BETWEEN SIX GROUPS FOR THE SOLID PARTICLE SIZE +150 μM	220
TABLE C.1 DESCRIPTION OF NUMBERING OF FOAM IMAGES	230
TABLE C.2 DESCRIPTIVE STATISTICS OF ORIGINAL TIME SERIES, RUN A	235
TABLE C.3 DESCRIPTIVE STATISTICS OF SERIES A, RUN A	236
TABLE C.4 DESCRIPTIVE STATISTICS OF SERIES B, RUN A	237
TABLE C.5 DESCRIPTIVE STATISTICS OF ORIGINAL TIME SERIES, RUN C	238
TABLE C.6 DESCRIPTIVE STATISTICS OF SERIES A, RUN C	239
TABLE C.7 DESCRIPTIVE STATISTICS OF SERIES B, RUN C	240
TABLE C.8 DESCRIPTIVE STATISTICS OF ORIGINAL TIME SERIES, RUN D	241
TABLE C.9 DESCRIPTIVE STATISTICS OF SERIES A, RUN D	242
TABLE C.10 DESCRIPTIVE STATISTICS OF SERIES B, RUN D	243

CHAPTER 1

INTRODUCTION

1.1 MOTIVATION FOR STUDY

Foams have extensive industrial applications in froth flotation, waste treatment, fire-fighting, enhanced oil recovery (Nutt & Burley, 1989; Rossen, 1996) the brewing industry and sewage disposal (Fruhner et al., 1999). There are two main types of foam, namely foamed liquids and more persistent foams in which the continuous phase is solid. Solid foams include expanded polystyrene cups, packaging and insulation (Askeland, 1996) as well as thermoset foams used in construction (Blaga, 1974). Liquid foams are thermodynamically unstable and will deteriorate back to two separate phases within a relatively short time, while most solid foams are rigid and thus totally stable (Wilson, 1996). The applications of liquid foams are endless. In everyday life, foams are used in toiletries such as shaving cream and hair mousse. Foams are present in the food industry in applications such as beer and aerated food such as chocolate mousse and whipped cream. All these applications have one thing in common: the product quality or production performance is dependent on the stability of the foam.

1.1.1 FOAM AND FROTH STABILITY

Foams are complicated physicochemical systems and therefore a satisfactory comprehensive theory of foam stability is still lacking (Malysa, 1992). The stability of a foam or its lifetime is dependent on film thinning mechanisms such as drainage and disproportionation, while liquid properties such as elasticity and viscosity oppose these mechanisms. The stability of liquid foams are of great practical importance, for example to extinguish liquid fuel fires, fire-fighting foams have to float on the surface of the liquid as to create a barrier between the vapour and the air. The most important feature of fire-fighting foams is their foam blanket stability (Croda fire fighting

chemicals, 2000). Likewise, the stability of aerated food such as whipped cream, ice-cream, chocolate, nougat and marshmallow are important in the competitive market as the user expects products of high quality. Foam can however also be unwanted, for instance in absorption or distillation columns. In these cases foam formation can affect the product quality as well as the separation efficiency negatively (Breward et al., 1997). It is thus equally important to investigate foam stability to enhance or suppress it.

In the mineral industry the state of the foam used in froth flotation, an extensively used method for the extraction of valuable minerals from their mineral ore, is vital. In froth flotation it is undesirable if the froth is not sufficiently stable, as the mineralised bubbles will rupture before being scraped over the weir (Feng & Aldrich, 2000). This will result in the mineral particles detaching and falling back into the pulp. If froth is too stable the froth could entrain gangue and this will lead to the recovery of a lower grade product (Dippenaar, 1982a). It is therefore desirable to have a froth that is stable enough to support the load prior to skimming. A froth of correct stability provides additional selectivity during flotation (Moolman et al., 1996). Although the stability is thus of importance in the industry, it is not explicitly measured for industrial processes. In the industry the focus falls mainly on the viscosity (mobility) of the froth (Moolman et al., 1996).

Foam and froth stability is thus important in a variety of applications, but is poorly understood due to the difficulty associated with the measurement of the variable. Existing foam stability measurements are of such a nature that a comparison between different studies is extremely difficult (Bikerman, 1973). The results are vulnerable to experimental conditions as the lifetime of foam relies on parameters such as the mode of generation, the vessel shape used and the foam type generated (Fruhner et al., 1999). The methods are case specific as not all foam can be analysed by the same method. In some methods the foam has to be transparent, as in the case of light transmission methods (Turner et al., 1999) while in others, such as the excess pressure method, the foam may not contain spherical cells (Nishioka, 1986). The existing methods have other drawback in common in that rigorous further processing of the data is required to finally obtain a comparable stability parameter. With the advent of

sophisticated image analysis algorithms, it is now possible to successfully study the stability of foam and froth systems on-line.

1.1.2 IMAGE ANALYSIS

Image analysis as a visual interpretation tool is widely used in plants where froth flotation is utilised to extract minerals from mineral ore (Botha et al., 1999b). As flotation extracts various minerals from their ores effectively, the process is easy to implement in the industry. As in all industrial processes, the aim is to operate the process as profitable as possible. To ensure this, the process has to deliver the best grade of mineral at the best recovery. This is achieved through effective control of the parameters that affects both grade and recovery namely stability, mobility, entrainment and drainage of particles (Mathe et al., 1998). Through application of an image analysis system, the flotation process can be optimised. The analysis of the froth structures in a flotation cell reflects on the performance of the cell (Moolman et al., 1994). The effective control of the process is directly linked to the appearance of the froth and the operators' interpretation of the froth. In the case of copper flotation foam with polyhedral bubbles indicate a well drained froth with a high grade, while froth with small spherical bubbles represents a non-drained froth with low mineral content (Moolman et al., 1995d). The industrial applications therefore focus on so-called key performance indicators such as the metallurgical properties of the froth namely bubble type, bubble size and the colour of the froth. The focus is thus on the classification of the froth rather than a quantitative description of the froth (Moolman et al., 1994) as the driving force behind decision making is optimal control.

There is however a vast difference in emphasis when comparing laboratory and industrial flotation systems. Although features from image analysis are extracted from industrial flotation processes, the froth features do not need to be physically interpretable. The grade and recovery of the mineral being floated is the main concern as this is the basis for productivity and delivery. In laboratory systems, the focus falls more on the physical structures of the froth itself. The objectives for a laboratory system include the understanding of the mechanisms and physical phenomena in the

froth structure to better surfactant development and classification of
froth character

This is not as falls on the development of certain flotation
characteristics for higher productivity. As energy in industrial systems increase,
The development of surfactants, the optimisation of surfactant mixtures and a
better understanding of froth phenomena are the three important factors that play
an important role in the performance of flotation process. These factors
can be successfully addressed by the application of machine vision systems in the
laboratory.

Thus, although machine vision has found widespread application as a powerful
technique for the detection of froth appearance in the mining industry, the
focus in this study is limited. The need exists to apply the same system in
fundamental research to determine the possible parameters that can be extracted from
such a system.

1.2 SPECIFIC OBJECTIVES OF THIS STUDY

The objectives of this study are to describe foam and froth behaviour with the use of an
on-line image analysis system. The first objective is to adjudicate the image analysis
system's ability to distinguish between foams of different characteristics to assess its
application in the mining industry and the second to quantify the effect of solids on foam
stability and rate of foam decay.

The specific objectives of this study are as follows:

- i. To investigate the complex phenomenon of foam formation and a large number of factors
affecting its formation, stability and decay. For the reader to understand the
difficulty associated with the measurements of foam stability, a background
explanation of the subject has to be understood. The first objective is to
establish a thorough background on foam phenomena,

accomplished in *Chapter 2*. The stability of foam is defined and the mechanisms responsible for the lifetime of the foam are identified.

- ii The existing methods of foam stability measurement are discussed in *Chapter 3* with specific focus on the drawbacks and shortcomings of these methods. An overview is given of the development of image analysis as a method to extract foam characteristics from images. The on-line machine vision platform used in this study, Fluxar[®]-SP is briefly discussed and the algorithms used to extract the foam characteristics are described.
- iii The on-line image analysis system's ability to differentiate between systems that have different characteristics is adjudicated by the application of quartz flotation. This is done by statistically analysing the image variables extracted for a specific group by principal component analysis and linear discriminant analysis. This case study is presented in *Chapter 4*. The correlations between the foam and froth characteristics, such as size, movement and colour are investigated to gain a better understanding of the underlying variables that affect foam stability.
- iv There are many contradictory studies concerning the effect of particle size on froth stability. The on-line image analysis system is used to investigate the effect of particle size as well as surfactant concentration on flotation foam stability. The effect of froth movement in a flotation cell on stability is investigated.
- v The use of the image analysis system as foam stability measurement is explored to determine whether such a system is a viable alternative to current stability measurements. The image analysis system is also applied to the process of foam decay in an effort to investigate the nature of foam decay. Time series analysis is used to characterise the dynamics of foam stability in *Chapter 5*.

CHAPTER 2

FOAM PHENOMENA

2.1 OBJECTIVES

This chapter gives a brief overview of the most important foam phenomena. The main objective is to establish a thorough background on this subject and to inform the uninitiated reader. The following specific areas will be discussed:

- i The definition of foam is given and the structure it attains as well as the characteristics associated with the structure is illustrated.
- ii Surface-active agents are chemical compounds necessary for the formation of stable foam. The structures of these chemical compounds are described and the mechanism by which they stabilise foam and the effect they have on the lifetime of foam are discussed.
- iii For the formation of a stable foam from a liquid, the liquid must have certain characteristics. These necessary characteristics are identified.
- iv There are two main methods used to generate foam, namely condensation methods and dispersion methods. The main dispersion methods are discussed.
- v The stability or lifetime of foam is discussed in the light of the three main mechanisms that play a role in foam decay. The factors that affect these mechanisms, as well as the opposing forces are described. Special attention is given to the decay of a foam column.

2.2 STRUCTURE AND CLASSIFICATION OF FOAM

2.2.1 DEFINITION

Foam is an agglomeration of gas bubbles separated from each other by a thin liquid film and belong to the first class of eight colloidal systems, namely *gas dispersed in liquid* (Bikerman, 1973). A distinction must be made between *foam* and *froth*. A foam is a gas-water macrocluster system which, when the structure is destroyed, leaves a homogeneous aqueous solution. A froth contains dispersed solid particles and when its structure is destroyed, a two-phase system remains: an aqueous solution of surfactant and solid particles (Sebba, 1987).

2.2.2 CLASSIFICATION OF FOAM

A *solid foam* is a dispersion of gas in liquid, which has changed into a gel or a solid after the dispersion process (Walstra, 1989). Solid foams are made up from gas bubbles surrounded by a framework of solid material. A liquid foam can be described as either transient (wet or unstable) foams or metastable (dry) foams. These two terms are often used to describe systems being near two opposite limits of the foam stability spectrum. A *wet* foam is an assembly of spherical bubbles separated by thick lamellae (Malysa, 1992). In a wet foam the quantity of liquid contained in the foam is significant. In the ideal 3D foam model, the liquid is incorporated in the cell edges, which becomes a network of Plateau borders (discussed in more detail in Section 2.4.2). As the liquid fraction increases, the Plateau borders swell and the cell faces shrink and disappear (Weaire et al., 1999). These foams can only exist in the presence of a foam formation agent and collapse very rapidly when foam formation is terminated. In *dry* or *metastable* foam the cells are entirely surrounded by thin films. The bubbles take on a polyhedral shape and are separated by very thin, slightly curved liquid films. In dry foams the liquid fraction is negligible, and most of the liquid drains away due to gravity so that the equilibrium state is reached fairly quickly. The

lifetime of a dry foam can be hours or days. All metastable foams pass through a stage where they consist of spherical bubbles separated by thick lamellae (Malysa, 1992).

2.2.3 STRUCTURE

Foam as a dispersed system is composed of air bubbles, liquid lamellae and Plateau borders. The properties of foam are determined by various factors of which solution composition, type, number and concentration of surface-active agent used, contaminations present and the conditions under which the foam was formed are the most important. The properties of a foam are mainly determined by three processes, namely (Fruhner et al., 1999):

- i The physicochemical properties of the solution, especially surface viscosity and surface tension.
- ii The interaction of the foam with its surroundings.
- iii The method of foam generation.

The structure of a foam does not depend on the chemical composition of the substance it is generated from or the average bubble size of the gas used as dispersion medium. The only parameter that drastically affects the bubble shape is the liquid contents (The diffusing light web site, 2000). The liquid between the bubbles drains rapidly from the top to the bottom so that the bubbles in the upper part of the foam become polyhedral. In this polyhedral structure the liquid lamellae are thin films, and the films are planar and are joined at Plateau borders. The bubbles in the lower part of the foam are spherical (Aveyard et al., 1999) and are separated by thick lamellae. The configuration where the gas cavities are spherical is called a gas emulsion (Callaghan, 1989). The change in structure, from spherical to polyhedral gas cavities is illustrated in Figure 2.1.

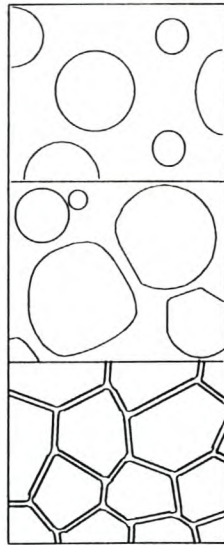


Figure 2.1 Schematic illustration of events during foam formation (Walstra, 1989).

In essence, the stability and lifetime of a foam are governed by two main structural units, namely thin liquid films and Plateau borders (Angarska et al., 1998).

2.2.3.1 Liquid Films

When a gaseous phase is introduced beneath the surface of a liquid, the liquid encloses the gas with a film of liquid. The gas cavities enclosed by thin liquid films give the foam a honeycomb structure. The thin liquid films that form the walls enclosing the gas cells, have approximately plane parallel sides, and are called the lamellae of the foam (Rosen, 1978).

2.2.3.2 Plateau Borders

The thin lamella of liquid between bubbles in a foam is not isolated. Plateau borders connect all lamellae enclosing gas cells to one another. When three or more gas bubbles meet, the lamellae are curved, concave to the gas cells, forming what is called a Plateau border. At the Plateau border, three plane films meet at 120° along a line as illustrated in Figure 2.2. The border has one radius of curvature r and the other radius is infinite so that the pressure in the border (p_B) is less than the pressure in the plane (p_A) (Aveyard et al., 1999).

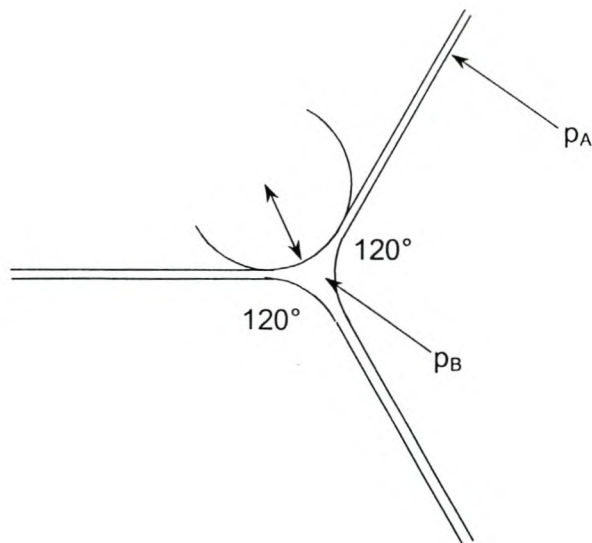


Figure 2.2 Section through a Plateau border (Aveyard et al., 1999).

2.3 FOAM STABILITY

There is no foam that is thermodynamically stable. Persistent foams (or *metastable* foams) are produced only when some mechanism exists to prevent rupture of the lamellae when most of the liquid has drained. These foams have a measurable lifetime for the following reasons (Bikerman, 1973):

- i The high viscosity (η) of the liquid retards rupture of bubble walls.
- ii The high surface viscosity (η_s) retards drainage and surface deformations prior to rupture.
- iii The Marangoni effect resists deformation.
- iv Electric double layer repulsion maintains lamellae.

The lifetime of persistent foams are measured in hours or days while unstable foams' (or *transient* foams') lifetimes are in the order of a few seconds or less (Rosen, 1978).

Specific forces of interaction (disjoining pressure), elasticity and viscosity are commonly referred to in the discussion about foam stability. However, care has to be

taken when ascribing forces to a foam's stability. Not all the forces are present in all types of foams. Disjoining pressure is only meaningful when the thickness of the lamellae reaches approximately 1000 Å. The stability of wet foams can thus not be explained in terms of disjoining pressure as the film ruptures at a much higher thickness. Surface elasticity forces are induced and operate only under dynamic conditions, thus the elasticity is a very important factor when the foam is formed. Surface elasticity forces are the main factor in the stability of wet foams, while the elasticity forces become less influential in well-drained dry foam (Malysa, 1992).

2.4 SURFACE ACTIVITY

When a surface property, such as surface tension is substantially changed by the addition of a small amount of some compound the phenomenon is called surface activity. A surface-active agent (surfactant) is a substance that lowers the surface tension of a solvent (Tsuji, 1998).

The amount of surfactant adsorbed per unit area of interface can be calculated by the Gibbs adsorption isotherm, which can be defined as follows (Walstra, 1989):

$$\Gamma = -\frac{1}{RT} \frac{d\gamma}{d \ln a} \quad 2.1$$

where a = activity of solute in bulk liquid [-]

R = gas constant [J/mol.K]

T = temperature [K]

γ = surface tension of the solution [N/m]

Γ = surface excess of solute per unit area of surface [mol/m²]

For a dilute solution, where no micelles are present, Equation 2.1 can be expressed as (Sebba, 1987):

$$\Gamma = -\frac{1}{RT} \frac{d\gamma}{d \ln C_L} \quad 2.2$$

where C_L = concentration of solute in the bulk liquid [mol/m^3]

2.4.1 SURFACE TENSION

The reduction of surface or interfacial tension is the most commonly measured property of surfactants in solution. It depends directly on the replacement of molecules of solvent at the interface by molecules of surfactant. The molecules at the surface of a liquid have potential energy that is higher than the molecules in the interior of the liquid. Since the potential energies of the molecules at the surface are greater than the energy of those in the interior of the phase, an amount of work equal to the difference in potential energy must be expended to bring a molecule from the interior to the surface. The *surface free energy per unit area* or *surface tension* is a measure of this work (Rosen, 1978).

Surface tension is dependent on the temperature of the interface. Some experimental surface tension data for various interfaces are summarised in Table 2.1 (Taylor, 2000).

Table 2.1 Surface tension data for typical interfaces

<i>Interface</i> [-]	<i>Temperature</i> [°C]	<i>Surface Tension</i> [mN/m]
<i>Water/Air</i>	20	72.75
<i>Hg/Air</i>	20	472.0
<i>Benzene/Air</i>	20	28.88
<i>Water/Air</i>	100	58.00

2.4.2 SURFACE-ACTIVE AGENTS

Surface-active agents (surfactants) consist of two parts, namely a hydrophilic head and a hydrophobic tail, as illustrated in Figure 2.3.

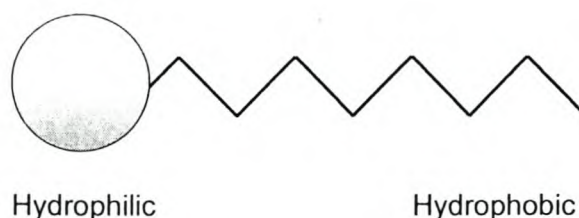


Figure 2.3 Schematic representation of a surfactant

The polar heads are hydrophilic and are attracted to the water. It is also by the hydrophilic group that surfactants can be classified into four categories. The anionic or negative charged groups contain one of four polar groups namely carboxylate, sulfonate, sulphate or phosphate. Anionic surfactants are the most widely used surfactant. Cationic surfactants are used in acidic (aqueous and non-aqueous) systems and adsorb more strongly than non-ionic surfactants. The cationic head group carries a positive charge on an amino or quaternary nitrogen group. Non-ionic groups include ethoxylates, carboxylic acid esters and carboxylic amides, and can be prepared to attain almost any hydrophilic-lipophilic balance (HLB). Amphoteric compounds may contain anionic or cationic groups. Ether or hydroxyl groups may also be present to enhance the hydrophilicity of the molecule. Amphoterics are compatible with both anionic and cationic surfactants and are used in personal care products (Siegel, 1996).

The non-polar tails are hydrophobic and tend to be as far from the water as possible. The hydrophobic group is usually a hydrocarbon chain, although it can also consist of fluorocarbon or silica chains and is often called a lipophilic group (Tsujii, 1998).

2.4.2.1 Surfactant Characteristics

All characteristic properties of surfactants originate from the behaviour of its hydrophobic group that avoids the water and the hydrophilic group that is drawn to the water. The hydrophobic group shows a strong tendency to escape from the water and thus likes to adsorb on the surface of the solution and/or the interfaces between

the aqueous solution and any hydrophobic solid or liquid particles present in the solution (Tsuji, 1998). When the surfactant adsorbs, it creates a new non-polar surface on the water. Since there are only dispersion forces between the hydrophobic non-polar tails, this surface has a lower surface energy than the previous water surface and thus the surface energy of the water is lowered (Nelson Chemistry, 2000). In general, good surface or interfacial tension reduction is shown only by those surfactants that have an appreciable, but limited solubility in the system (Rosen, 1978).

When more surfactant is added after all possible adsorption sites are already occupied, the surfactant molecules group together to avoid contact with the water molecules. The aggregates that form are called micelles and every surfactant has a critical micelle concentration (CMC) at which these aggregates form. The formation of these aggregates is illustrated in Figure 2.4.

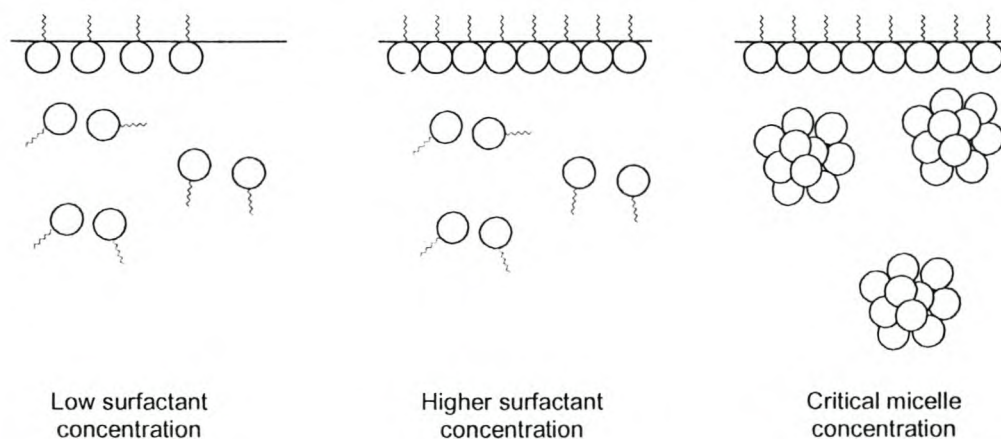


Figure 2.4 Schematic representation of the formation of micelles

Micelles consist of tens of surfactant molecules or more. The number of molecules in one micelle is called the *aggregation number* (Tsuji, 1998). The aggregation number depends on the concentration of the surfactant, as well as the concentration of any electrolytes present in the solution. The aggregation number of non-ionic surfactants will increase with temperature until the cloud point is reached, where the micelles will separate out as a separate liquid phase. The shapes of micelles are governed by the

packing of the hydrophobic chains of surfactant molecules. The solution properties of the surfactant depend strongly on the shape of the micelles, which can either be rod-like or plate-like. Above the CMC the formation of micelles bring variations in the relation between the concentration and the physico-chemical properties of the solution. The concentration of singly dispersed surfactant molecules is virtually constant and little variation can be seen in the value of the interfacial tension at concentrations higher than CMC (The Surfactants Virtual Library, 1996).

In comparing the performance of surface-active materials in interfacial phenomena, a distinction should be made between the amount of surfactant required to reduce the interfacial tension and the maximum reduction in tension that can be obtained regardless of concentration. These two parameters are *efficiency* and *effectiveness* (Rosen, 1978).

The efficiency of a surfactant is the bulk phase concentration of surfactant required to reduce the surface tension by some significant amount. The negative log of the bulk concentration necessary to reduce the interfacial tension by 20 mN/m is a good measure of this. The effectiveness is the maximum reduction in tension that can be obtained, regardless of the bulk concentration of surfactant, and is measured by the amount of reduction attained at the CMC (Rosen, 1978).

2.4.2.2 Foam stabilisation mechanisms

When considering a column of pure liquid, it can be stated that the drainage of a vertical film follows a plug-flow configuration, as there is no velocity gradient normal to the film. The films thin very rapidly as there is no force to stabilise it (Aveyard et al., 1999). To render the lamellae stable, it is necessary to have an adsorbed layer of surface-active material at the lamellae surfaces, as illustrated in Figure 2.5.

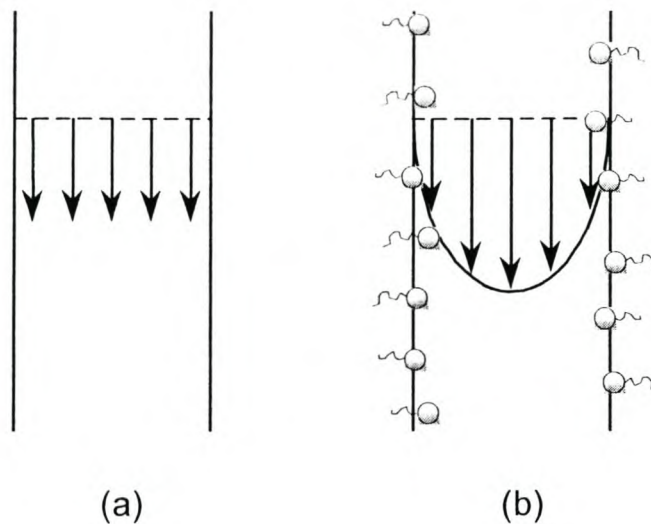


Figure 2.5 Velocities of flow across liquid films of (a) pure liquid and (b) liquid bounded by monolayers of adsorbed surfactants (Aveyard et al., 1999).

A surfactant adsorbs onto the air-liquid interface, thereby lowering the surface tension. However, the lowering of the surface tension is not the cause of foam stability. Rather, it is the variation of the surface tension with time or location that cause the stability (Walstra, 1989). The mass per unit of the surface-active agent is the surface excess concentration or the amount adsorbed. If the system is not in equilibrium, concentration gradients exist in the interface, which results in surface tension gradients in the interface.

As liquid drains from a foam, the drag of the liquid on the interface stretches the interface. The expansion of the interface reduces the surface concentration of the surface-active component on the interface and establishes a surface tension gradient between the interface in the film and the interface in the meniscus. These surface tension gradients oppose the motion of the interface and thus maintain the interface immobile as the liquid drains between the two near-immobile interfaces. The surface tension gradient also tends to pull the interface from the meniscus back into the film, causing turbulent motion of the interface at the boundary of the film and the meniscus.

2.5 FOAM FORMATION

2.5.1 FACTORS INFLUENCING FOAM FORMATION

2.5.1.1 Elasticity

For true foaming to occur, the presence of a solute, which is able to adsorb at the liquid-gas interface, is required. The presence of a surface-active agent produces lamellae between the gas cells of the foam that have adsorbed monomolecular films of surfactant molecules on each side of the liquid-gas interface. These adsorbing films provide foaming systems with a property that distinguishes it from non-foaming systems: the adsorbing films have the ability to resist excessive localised thinning of the lamellae surrounding the bubble, while general thinning of the lamellae proceeds.

The adsorption of surface-active matter at the gas/liquid interface becomes a stabilising force by lowering the surface tension of the foaming liquid. Liquid lamellae constantly undergo thinning and expanding due to thermal and other external influences. The ability of lamellae to recover an equilibrium thickness is the key factor in maintaining overall stability of a foam. As the thinner sections in the lamellae contain less surface-active matter and have a high local tension, surface-active material migrates towards the lamellae to restore the equilibrium and thus in doing so rectify the potentially unstable situation. This ability to resist film thinning is called *film elasticity* (Rosen, 1978).

Film elasticity (E) is related to the change in surface tension by the following equation (Sebba, 1987):

$$E = \frac{2d\gamma}{d \ln A_F} \quad 2.3$$

where A_F = surface area of foam [m^2]

$d\gamma$ = change in surface tension [N/m]

From Equation 2.3 it can be seen that an incremental increase in the area of the foam (A_F) must be counterbalanced by an increase in the surface tension, causing a surface tension gradient (Johansson & Pugh, 1992).

2.5.1.2 The Gibbs adsorption isotherm

Elasticity exists mainly due to the requirements set by the Gibbs isotherm. The Gibbs adsorption isotherm establishes that there exists an equilibrium between the concentration of the solute in the surface and the concentration of the solute in the bulk phase. The Gibbs isotherm (Equation 2.1) describes the relation between surface tension, surface excess (Γ) and the activity (a) of the surfactant in the bulk liquid phase. This relationship implies that if the temperature is kept constant the surface-active agents that tend to lower the surface tension will have a higher concentration at the surface than in the bulk solution (Sebba, 1987).

Any attempt to disturb the equilibrium results in a force that aims to restore the equilibrium by producing elasticity in thin films (Sebba, 1987). There are two main methods from which this restoring force can result, namely the *Gibbs effect* and the *Marangoni effect*.

Both these theories postulate that elasticity is owing to the local increase in surface tension with any extension of the film. As a local spot thins and stretches and the area of the film increases, its surface tension increases and a gradient of tension is set up. This gradient of tension causes liquid to flow toward the thinning spot from the thicker portions around it. The thinning spot thereby draws liquid from its perimeter and prevents further thinning of the film (Rosen, 1978), as illustrated in Figure 2.6.

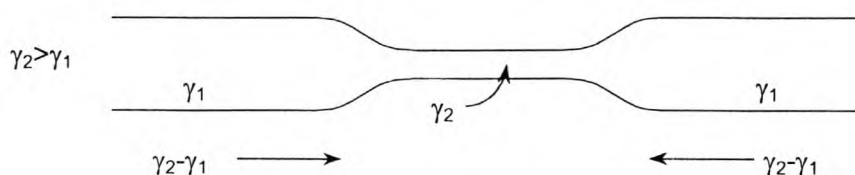


Figure 2.6 Illustration of elasticity mechanism (Rosen, 1978).

2.5.1.3 Gibbs effect

The Gibbs effect only operates in thin films. If a fixed volume of solution contains surfactant, and a section of lamellae is stretched, the surface area increases and the thickness of the film decreases (Rosen, 1978). When the surface is increased, the surfactant molecules have to move to the surface to fulfil the requirements of the Gibbs isotherm. If the film is stretched, more surfactant molecules are adsorbed, lowering the surfactant concentration in the bulk liquid and leading to an increase in surface tension (Walstra, 1989). This increase in surface tension produces the restoring force that resists further thinning (Sebba, 1987). The Gibbs theory of elasticity thus postulates that on thinning and expansion of local areas on the lamellae, the rise of surface tension is due to the depletion of solute from the underlying layer of solution in the interior of the lamellae (Rosen, 1978).

This effect is only significant in a limited concentration range of the solute. If the concentration is very low, the change in surface tension with concentration will be too small and the tension gradient insufficient to prevent any further thinning and eventual rupture of the film. If the concentration is far above the CMC of the solute, the change in surface tension with an increase in area of the film will be too small to prevent rupture, as the surface tension does not vary much with concentration changes. Also, a large reserve of surfactant in the solution will prevent any significant change in surface tension, unless the film becomes very thin (Rosen, 1978).

2.5.1.4 Marangoni effect

The Marangoni effect is different from the Gibbs effect in that it is a dynamic phenomenon that applies to any liquid surface that has a surfactant adsorbed in it and is not confined to thin films only (Sebba, 1987).

As stated, surfactant molecules lower the surface tension of a liquid. If the surface area available for the surfactant molecules is increased it will cause the surfactant molecules to move away from one another. The exposed surface will have the same surface tension than that of the bulk liquid, which is a higher value than the surface where the surfactant is adsorbed. The momentary increase in surface tension must be

restored by a force which will prevent the extension of the surface and this is known as elasticity (Sebba, 1987). The Marangoni effect is related to the change in surface tension with time owing to the diffusion of frother molecules from the interior of the solution to the new surface. This effect is prominent when the surface tension of the frother is considerably lower than the surface tension of the bulk and depends mainly on two factors, namely the lowering of surface tension and the rate of re-establishing the equilibrium over the lamella surface. The extension of the surface reduces the concentration of surface-active agent in the surface layer, providing the diffusion from the bulk of the solution to the surface region is not as rapid as the mechanical movement resulting from the extension (Johansson & Pugh, 1992).

The Marangoni effect is greater in dilute solutions where there are less surfactant molecules present, as the time required for the replacement surfactant molecules to reach the surface to attain the surface concentration will be longer (Sebba, 1987; Rosen, 1978).

2.5.2 FOAM FORMATION METHODS

Foam can be generated by two main methods, namely through dispersion and condensation. In dispersion methods the dispersed phase (gas phase) is originally present as a large separate phase and is then spread through the continuous or liquid phase (Bikerman, 1973). This method can also be described as foam formation by mechanical means, either by injection of gas through narrow openings or beating (Walstra, 1989). An example of foam prepared by this method is surfactant foam.

In condensation methods the dispersed phase is present in the solute originally, i.e. the liquid is supersaturated with gas under pressure (Walstra, 1989) and when molecules combine to form larger bubbles, foam is obtained (Bikerman, 1973). Nucleation is a very important step in this form of foam formation (Walstra, 1989). Gas can be generated either chemically, by microbiological systems (fermentation) or by lowering the pressure in the system (Malysa, 1992). Foam on beer, soft drinks and fire-fighting foams are examples of foams produced by condensation (Bikerman, 1973; Malysa, 1992).

In this section only the formation of foam through dispersion methods will be discussed.

There are several dispersion methods that can be used to form foam. The most common methods are the injection of gas through one or several orifices (Malysa, 1992). However, it is important to employ a method in which the volume of gas injected into the system and the bubble size distribution can be quantified (Bikerman, 1973).

2.5.2.1 Pneumatic methods

All methods through which gas is injected into a liquid through separate capillaries, cloth filters, sinter glass, diffuser stones, spinnerettes, Pasteur-Chamberland filters or any type of sparger falls in this category. The use of single capillaries produces bubbles of relatively uniform size, but the foam formation is relatively slow. When a gas is introduced into a liquid through a capillary, the bubble dimensions can be predetermined and the volume of gas can be controlled (Bikerman, 1973).

Dynamic methods are a subdivision of the pneumatic methods. In these methods the foam height or foam volume produced is measured while the gas continues to produce bubbles. Dynamic equilibrium is attained when the rate of foam formation at the bottom of the column compensates for foam breakage at the top. When this equilibrium is reached the foam volume stays constant. To obtain reliable and reproducible results an experimental method that produces a well defined state is necessary. With dynamic methods the foam at the top, as well as the foam at the bottom are equally well defined, which makes this method ideal for the investigation of foam stability and decay (Iglesias et al., 1995).

2.5.2.2 Shaking tests

Shaking tests are the easiest means to produce foam by agitation. The tests are usually carried out in a closed vessel to ensure the elimination of any evaporation that might occur. This method has two main drawbacks. Firstly, the height and volume of the

foam obtained depend on the details of procedure, volume of air and liquid used, which makes direct comparison between studies difficult. Secondly, the method cannot be used to characterise the foam stability in an absolute manner, as dynamic equilibrium is not obtained in these experiments (Bikerman, 1973).

2.5.2.3 Pour test

This method is very popular and has been adopted by the ASTM (American Society for Testing and Materials). In the Ross-Miles method, 200 ml of a solution of surfactant is contained in a pipette of specific dimensions with a 2.9 mm (id) orifice. The solution is allowed to fall 90 cm onto 50 ml of the same solution contained in a cylindrical vessel at a constant temperature. The height of the foam produced in the cylindrical vessel is read immediately and again after 5 minutes (Rosen, 1978). This method is very sensitive to all the parameters in the test including the volume of the liquid in the cylindrical vessel, the volume of liquid dropped, the height through which the liquid falls and the dimensions of the vessels. A further drawback with this method is that the ambient air has to be incorporated into the liquid when pouring takes place, which makes it difficult to control (Bikerman, 1973).

2.5.2.4 Other methods

Foam can also be produced by other methods, including stirring, whipping and beating. The results are difficult to interpret, as the geometry of instruments used to incorporate the gas into the liquid can be altered in an infinite number of ways. It is impossible to decide which configuration supplies the most fundamental and least arbitrary results. It was found that the precision of a stirring test was better than the pour test when applied to the same system, but no general correlation between the values obtained through the two methods could be found (Bikerman, 1973).

2.6 FOAM LIFETIME (STABILITY)

During the lifetime of a foam four main processes can take place, namely (Bikerman, 1973):

- i Rearrangement of liquid films,
- ii drainage of liquid from lamellae,
- iii rupture of thin films, and
- iv evaporation.

Evaporation occurs due to temperature gradients that create surface tension gradients and induce surface motion in foam films (Bergeron, 1999). In most instances only the first three processes take place, as the evaporation process can be limited with experimental design.

The existence of foam elasticity is necessary to produce foam, but there are other mechanisms that prevent the loss of liquid and gas from the lamellae, as to prevent the liquid films from rupture when the critical thickness is reached (Rosen, 1978). Liquid-based foams are non-equilibrium systems and the stability of these systems depends on the ability of the foam lamellae to resist the mechanisms that play a role in foam decay. These mechanisms are (Beneventi et al., 2001; Malysa, 1992):

- i Gravitational drainage and drainage by capillary suction.
- ii Coalescence and rupture of bubbles.
- iii Gas diffusion through the liquid film or disproportionation.

Drainage of liquid from lamellae cannot be prevented. However, it can be slowed down by preventing direct coalescence of neighbouring bubbles through the correct choice of type and concentration of surfactant. Coarsening (or gas diffusion from small to large bubbles) is driven by surface tension and gradually decreases the interfacial area with time. This phenomenon is present in all foams and cannot be eliminated (The diffusing light web site, 2000).

2.6.1 DRAINAGE OF FILMS AND PLATEAU BORDERS

Liquid lamellae separating the foam cells thin as a result of drainage under gravity and suction into the Plateau borders (Aveyard et al., 1999). Drainage of solution from the interior of the foam lamellae is one of the most important mechanisms that determine foam stability. The drainage discussed in the following section only refers to the drainage of thin films, with a comment on the drainage from the Plateau border. The drainage of concentrated solutions (Nikolov & Wasan, 1989) is not discussed.

2.6.1.1 Films

Drainage occurs under two influences, namely gravity and surface tension. Drainage by gravity occurs when the lamellae are thick and the major factor in determining the rate of drainage due to gravity is the bulk viscosity of the foaming solution. Drainage due to the difference in surface tension is important when the lamellae are thin and it depends on the existence of a pressure difference at various points in the lamellae (Rosen, 1978).

In principal, foam drainage and foam collapse is independent of each other and to estimate the stability of foam from its drainage rate is fundamentally incorrect. As long as the film surrounding gas volume exists the foam exists, and while drainage does render the film thinner, it does not necessary lead to rupture. There is a considerable interplay between collapse and drainage. Drainage is a complex phenomena and its magnitude is determined by two factors, namely proper drainage due to gravitation and bubble rupture. When a bubble ruptures, the liquid present in the bubble flows down in the neighbouring walls and Plateau borders. This drainage of this liquid increases the magnitude of overall drainage (Bikerman, 1973).

2.6.1.2 Capillary Pressure

When a bubble is created in a liquid, work has to be done to create a new surface, which increases in area as the bubble grows. This work is called surface energy and has to be balanced by an increase in pressure in the bubble (Sebba, 1987). This

pressure is called the capillary pressure. In the transition between lamellae and Plateau borders the surface tension of the lamellae is balanced in the force equilibrium by the capillary pressure under the curved surfaces of the Plateau border. It is also because of this pressure that the liquid is sucked out of lamellae (Hédreul & Frens, 2001). The capillary pressure difference between the two phases can be described by the Laplace equation (Bikerman, 1973).

In spherical systems the Laplace equation has the following form (Walstra, 1989):

$$\Delta p = \frac{2\gamma}{r} \quad 2.4$$

where r = radius of the sphere [m]

In non-spherical systems the curvature can be described in terms of the two principal radii, r_1 and r_2 so that the Laplace equation takes on the following form (Aveyard et al., 1999)

$$\Delta p = \gamma \left(\frac{1}{r_1} + \frac{1}{r_2} \right) \quad 2.5$$

The curvature in the lamellae is greatest in the Plateau borders and therefore the pressure across the interface of these regions is larger than in other regions in the foam. The gas pressure in an individual gas cell is the same throughout the cell, but (with reference to Figure 2.2) the liquid pressure inside the lamellae is lower at the highly curved region (B) than at the less curved region (A). This difference in pressure causes liquid to drain from the lamellae into the Plateau border (Rosen, 1978).

2.6.1.3 Mechanisms of drainage through gravity

Gravity is the main driving force behind the drainage of liquid from thin films. Gravity acts on the thin film in two ways, viz. directly on a film that is not horizontal and indirectly through suction of liquid to the Plateau borders by capillary pressure

(Prins, 1988). Drainage is governed by two main mechanisms, which operates independently of each other, namely viscous flow and marginal regeneration.

2.6.1.4 Viscous flow to Plateau borders

Viscous flow through a vertical film takes place in such a way that the liquid moves as if it is between two solid parallel walls as the film surfaces remain motionless due to the Gibbs film elasticity (Prins, 1988). The quantity of liquid leaving the lamellae, per unit time per unit width of the lamellae is given by (Callaghan, 1989):

$$Q = \frac{\rho g \delta^3}{12 \eta_b} \quad 2.6$$

where g = gravity [m/s^2]
 δ = thickness of lamellae [m]
 η_b = viscosity of bulk liquid [Pa.s]
 ρ = density of liquid in foam [kg/m^3]

According to Equation 2.6 the rate of drainage depends on two main factors, namely viscosity and lamella thickness. The higher the viscosity of the liquid, the slower the liquid tends to drain, while a decrease in lamella thickness also decreases the rate of drainage (Callaghan, 1989).

The time needed for drainage to induce a certain critical thickness can be approximated as (Prins, 1988):

$$t(\delta) \approx \frac{6 \eta h_f}{\rho g \delta^2} \quad 2.7$$

where h_f = film height [m]

2.6.1.5 Prevention of drainage

In the process of liquid draining from thin films, the shear stress exerted by the moving liquid on the motionless film surfaces is balanced by a surface tension gradient acting from the top to bottom of the film. This gradient compensates exactly for the weight of the film so that (Prins, 1988):

$$2 \frac{d\gamma}{dz} = \rho g \delta \quad 2.8$$

where $\frac{d\gamma}{dz}$ = surface tension gradient in foam column from top to bottom

It follows from Equation 2.8 that to prevent drainage, a yield stress equal to the stress exerted on the film surfaces must be present. The value of the yield stress is as follows:

$$\sigma_y = \frac{d\gamma}{dz} = \frac{\rho g \delta}{2} \quad 2.9$$

2.6.1.6 Marginal regeneration

Every lamella in a polyhedral foam is completely surrounded by Plateau borders (Callaghan, 1989). Marginal regeneration occurs when the thick part of the lamella is drawn to the Plateau border rather than to the thinner areas in the region, as the pressure difference between the border and the film exert greater force on the thicker part of the film than on the thinner part. The process can only take place in mobile surfaces where the surface shear and dilational parameters are small (Prins, 1988). Marginal regeneration is responsible for the rapid drainage of liquid from the foam lamellae where the magnitude of drainage could not be accounted for by drainage of liquid under gravity alone (Stein, 1991).

In Figure 2.7 the thick and thin parts of the lamellae are located opposite one another for the sake of clarity. In reality the thick and thin parts are in contact with the same Plateau border and lie side by side.

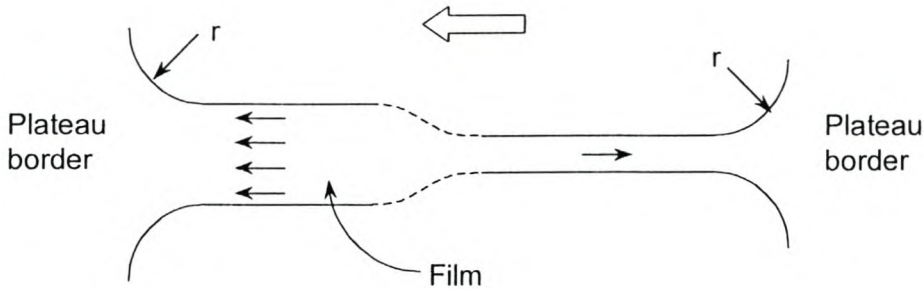


Figure 2.7 Schematic representation of the process of marginal regeneration (Prins, 1988).

Assuming the Plateau borders have the same suction, there is a net force (F) per unit length acting in the direction of the arrow, because the suction Δp is greater at the thick parts of the lamellae than at the thin parts. The net force per unit length is (Prins, 1988):

$$F = \Delta p \Delta \delta \quad 2.10$$

where $\Delta \delta$ = difference in thickness of two parts [m]

The force causes the film to move in the direction of the arrow. The thin part of the film is thus being drawn out by one part of the Plateau border and the thick part of the film is taken up by another part of the Plateau border (Prins, 1988). The areas of thin and thick lamellae move alongside each other but in opposite directions with respect to the Plateau border and the elasticity of the surface layers of the lamellae is the only factor that can inhibit the movement (Callaghan, 1989).

2.6.1.7 Plateau borders

In a new foam the Plateau borders contain excess liquid and this excess liquid must drain away to reach an equilibrium situation. At equilibrium the radius of curvature of the cylindrical Plateau border surface satisfies the following equation:

$$\frac{\gamma}{r} = \rho g H \quad 2.11$$

where H = hydrostatic height [m]

γ = surface tension of Plateau border surface [N/m]

The drainage of liquid from the Plateau border will stop once the suction through capillary pressure equals the hydrostatic pressure of the liquid. As in the case of drainage from liquid films, drainage of the Plateau border can be stopped completely at the presence of a yield stress, provided that the Plateau border surface has an elasticity that is high enough (Prins, 1988).

2.6.2 DIFFUSION OF GAS THROUGH LAMELLAE (DISPROPORTIONATION)

2.6.2.1 Definition

Disproportionation is a coarsening process arising from interbubble gas transport caused by pressure differences between bubbles. According to Laplace's law the pressure is higher in a smaller bubble than in a larger one, if it is assumed that the interfacial tension of the two bubbles is equal. The large bubbles will therefore grow at the expense of the smaller bubbles and the smaller bubbles will eventually disappear. This phenomenon is dependent on the permeability of the adsorbed surface film as can be seen in Equation 2.12 (Gandolfo & Rosano, 1997). The transfer of gas takes place through aqueous pores between the surfactant molecules in the surface films of the lamellae. The gas diffusion through the lamellae will therefore be slower the closer the molecules of the surfactant is packed in the film (Princen et al., 1967).

The rate of diffusion (q) of gas from one bubble to another through the lamella separating them, is given by the following equation (Garrett, 1993):

$$q = -JA_g \Delta p \quad 2.12$$

where A_g = effective perpendicular area through which diffusion occurs [m^2]

J = permeability of diffusion path [s/m]

γ = surface tension of solution [N/m]

and where Δp is the difference in gas pressure between the bubble and a bubble with radius r_{21} so that (Garrett, 1993):

$$\Delta p = 2\gamma \left(\frac{1}{r_{21}} - \frac{1}{r} \right) \quad 2.13$$

Lemlich (1978) developed a theory to predict of the effect of gas diffusion upon bubbles size distribution in a foam where drainage and film collapse is ignored. The derived rate of change in bubble radius with time is:

$$\frac{dR_d}{dt} = K \left(\frac{1}{r_{21}} - \frac{1}{r} \right) \quad 2.14$$

where $K = \frac{2J\gamma RT}{P} \quad [m^2/s]$

It follows from this model that bubbles with a radius so that $r > r_{21}$ grow in size and bubbles with a radius so that $r < r_{21}$ shrink in size and eventually disappear. In the case of extremely small bubbles ($r \ll r_{21}$) the theory predicts that the square of the bubble radius varies linearly with time (Cheng & Lemlich, 1985). In developing the theory, the possible contribution from changes in surface tension due to the effect of surface area changes upon the dilational properties of the solution was ignored. This assumption is reasonable only when the solutions investigated are concentrated

micellar surfactant solutions, where the dilational surface tension changes are minimal (Garrett, 1993).

Monsalve & Schechter (1984) emphasised the importance of the initial bubble distribution of a foam when determining the rate of reduction of surface area due to disproportionation. Foams with the same initial surface area and surface tension, but which differ in initial bubble distribution show different rates of surface area decay. The growth of larger bubbles at the expense of the smaller ones induces a rearrangement of bubbles which may lead to further rupture of the lamellae due to mechanical shock and ultimate collapse of the foam (Gandolfo & Rosano, 1997; Rosen, 1978).

2.6.2.2 Effect of solubility of gas on disproportionation

The more soluble a gas is in the foaming medium, the less stable the foam is (Sharovarnikov et al., 1981). Gases soluble in water, such as CO₂ give less stable foams than less soluble ones such as N₂. As the CO₂ transport across water films is faster (Langevin, 1999), the solubilisation of the gaseous phase enhances the mechanism of disproportionation (Callaghan, 1989). When the composition of the gas is altered to be less soluble, the gas diffusion process is retarded.

2.6.2.3 Retardation of disproportionation

During disproportionation the surface area of a small bubble decreases as the bubble shrinks. As surface-active components are present in the formation of a foam the resulting compression of the surface leads to a lower surface tension. The lowering of surface tension causes a decrease in the rate of disproportionation for both low- and high-molecular weight surfactants, as it leads to a decrease in the driving force described by Equation 2.5.

2.6.3 FACTORS DETERMINING FILM PERSISTENCE

2.6.3.1 Repulsion Force

When liquid films have thinned to such an extent that the films are only a few tens of nanometres thick, the surfaces begin to interact through surface forces. As the liquid film thins, and the thickness reaches the order of the wavelength of incident light, the film will show interference colours. If the lateral pressure is larger than the electrostatic barrier, it is possible to reach a very thin film which will show no colour (Langevin, 1999). When the film reaches this thickness, black spots can be observed and the film is called a black film. These films can be as thin as 10 nm. Both rupture of a thin film and the formation of black spots, occur at the same critical thickness, which is 30 nm for water (Exerowa et al., 1976).

Various authors (Exerowa et al., 1976; Exerowa et al., 1992; Hédreul & Frens, 2001; Mysels et al., 1959) have reviewed the formation of black spots as well as its effect on foam stability and this subject will not be discussed in this study.

The interactions between surfaces result in a change in interface tension and in concomitant changes in the pressure normal to these interfaces. The forces that prevent further thinning of liquid films by preventing further drainage due to gravity are called disjoining forces and are defined as follows (Aveyard et al., 1999):

$$\Pi(\delta) = \left[\frac{\partial G(\delta)}{\partial \delta} \right]_T \quad 2.15$$

where $G(\delta)$ = free energy of interaction per unit area of film [-]

δ = film thickness[m]

These repulsion forces depend on the type of surfactant used and can include coulombic forces and steric repulsion (Aveyard et al., 1999). As films thin, the concentration of the surfactant in the surface will increase and the hydrophilic heads of the surfactant will get closer to each other. These hydrophilic heads have the same

charge and will tend to repel each other, causing a repulsive force known as a coulombic force. This coulombic force, which is inversely proportional to the square of the distance separating the charges, will tend to resist further thinning. When double layer repulsion balances the forces that cause film thinning, equilibrium is reached (Sebba, 1987).

Foams can also be stabilised by non-ionic surfactant, although they do not produce ions. These surfactants are polar but the charge on the dipole heads are the same so there is still a repulsive force active (Sebba, 1987).

2.6.3.2 Dilational viscosity

The rheology of the gas-liquid interface plays a major role in the determining of foam stability (Callaghan, 1989). The stability or instability of foams is largely determined by the surface rheological properties of the adsorption layer at the liquid interface. Surface rheology investigates two-dimensional functional relationships between stress and deformation as well as between stress and the rate of deformation. A complete rheological characterisation of the layers at a liquid interface include the knowledge of surface shear viscosity, surface shear elasticity, surface dilational viscosity and surface dilational elasticity. For foam stability the dilational parameters are especially important, while the shear parameters of adsorption layers of low molecular surfactant molecules are small and can be neglected. In the case of surface active polymer molecules like proteins, the shear parameters play a large role in the stability (Fruhner et al., 1999).

The behaviour of bubbles and thin films can only be understood when the dynamic surface properties are taken into account. The surface dilational viscosity is a measure of the ability of the liquid surface to resist an external disturbance, such as an increase in surface area or the shearing stress exerted by flowing liquid. The surface dilational viscosity is defined as (Prins, 1988):

$$\eta_s = \Delta\gamma \left(\frac{dt}{d \ln A} \right) \quad 2.16$$

In solutions stabilised by low-molecular surfactants, the surface viscosity accounts for the fact that if the surface area enlarges, the transport of surfactant molecules to the depleted area takes a finite time. The existence of a finite surface dilational viscosity implies the presence of a surface tension gradient when liquid flows along the surface (Prins, 1988). By using a new bubble oscillating method, Fruhner et al. (1999) proved that a longer lifetime of liquid lamellae and thus a higher stability can be observed with an increase in surface dilational viscosity. With the advent of the new method, it was shown that the foam lamellae indicate the importance of the surface dilational parameters on the lamella stability. The systems that exhibited viscoelastic properties all formed stable foams.

2.6.4 SPECIAL APPLICATION: FOAM COLUMN COLLAPSE

When foam is generated in a column by a dynamic method, gas is introduced underneath the solution through a sinter disk. The foam is formed either until no solution is left or until equilibrium is reached. The foam column starts shrinking as soon as the introduction of gas stops. This method of measuring the foam lifetime can be argued to be unreliable, as it could be reasoned that as long as bubbles in the lower and central part of the column coalesce but the top layer remains stationary, the impression is created that the foam have not collapsed although many lamellae have been broken. However, this objection is not valid for real foams, as in practice foams start to decay from the top and gradually progress downwards. As the top layer of the foam is exposed to the atmosphere, it is subjected to the process of evaporation, while the layers in the bulk are protected from this process. Drainage does take place in all lamellae and Plateau borders in the top layer as well as in the bulk of the foam. In the bulk the drainage of liquid is almost compensated for by the arrival of liquid from the top layer, while there is no downfall of liquid on the top layer (Bikerman, 1973).

If it is assumed that every bubble, independent of its position has an equal probability to rupture, the number of bubbles still intact after time t can be expressed as follows:

$$n = n_0 e^{-mt} \quad 2.17$$

where $m = \text{constant [s}^{-1}\text{]}$

$n = \text{number of bubbles [-]}$

$n_0 = \text{original number of bubbles (at } t = 0) \text{ [-]}$

If the bubble is most likely to burst when it is a certain time fraction old (Σ) and the probability of bursting decreases at greater and smaller values of time (t) according to a normal distribution curve then,

$$n = \frac{n_0}{s\sqrt{2\pi}} \int_0^t \exp\left[-\frac{(t-\Sigma)^2}{2s^2}\right] dt \quad 2.18$$

In this case the number of bubbles (n) as a function of time (t) will form a sigmoidal-shaped curve: a slow decrease as long as the few short-lived bubbles burst, then a rapid linear decrease including an inflexion point and finally another slow decrease when the few remaining older bubbles bursts.

2.7 CONCLUDING REMARKS

Foam is an agglomeration of gas bubbles separated by liquid films. Wet foams have spherical bubbles separated by thick lamellae, while dry foams consist of a network of thin films and Plateau borders. Foam is generated by two methods, namely dispersion and condensation. The most common dispersion methods are pneumatic methods, shaking tests, pour tests and other methods including beating, whipping and stirring.

No foam is thermodynamically stable and some mechanism must exist to prevent rupture of liquid lamellae, such as high surface viscosity, the elasticity of the film as well as electric double layer repulsion. It is impossible to create a stable foam without a surface active agent. The surfactant adsorbs at the air-liquid interface and lowers the surface tension. It is not through the lowering of the surface tension, but through the variation of surface tension with time and location that the foam is stabilised. The surface tension gradients oppose the motion of the air-liquid interface and maintain it

immobile as the liquid drains. The ability of a liquid film to resist thinning is called elasticity. Two elasticity mechanisms exist, namely the Gibbs effect, active in dilute systems, and the Marangoni effect.

Foam lifetime depends mainly on the drainage of liquid from the films, coalescence and rupture of bubbles as well as disproportionation. Drainage from liquid films occurs under the influence of gravity. Drainage is governed by two mechanisms, namely viscous flow and marginal regeneration. Disproportionation is influenced by the solubility of the gas and the surface viscosity of the system. Forces that prevent thinning of liquid films include disjoining forces such as coulombic forces and steric repulsion. Systems with a high surface dilational viscosity have a longer lifetime and thus a higher stability.

Foam generated in a column has a sigmoidal shaped decay curve.

It is evident from the background discussed in this chapter that foam is a complex phenomenon. There are many characteristics and mechanisms that need to be taken into account when considering the lifetime or stability of a foam. The most important existing stability measurement techniques are discussed in *Chapter 3*.

2.8 SYMBOLS USED IN CHAPTER 2

2.8.1 SYMBOLS

<i>Symbol</i>	<i>Description</i>	<i>Unit</i>
a	Thermodynamic activity of solute	mole fraction
A	Surface area	m ²
C	Concentration	mol/m ³
Δd	Difference in thickness of lamellae	m
E	Film Elasticity	N/m
F	Force	N
g	Specific gravity	m/s ²
G(h)	Gibbs free energy of interaction per unit of film	-
h	Height of film	m
H	Hydrostatic height	m
J	Effective permeability	s/m
K	Parameter	m ² /s
n	Number of bubbles	-
m	Constant	1/s
Δp	Capillary pressure	Pa
P	Gas pressure	Pa
q	Rate of diffusion	kg/s
Q	Liquid flowrate	m ² /s
r	Radius	m
r_1, r_2	Principal radii of curvature	m
r_{21}	Radius of bubble taken by first and second moment	m
R	Gas constant	J/mol.K
R_d	Dimensionless equivalent for bubble radius	-
s	Standard deviation	-
s ²	Variance	-
t	Time	s

T	Temperature	K
z	Distance perpendicular to surface	m

2.8.2 GREEK SYMBOLS

<i>Symbol</i>	<i>Description</i>	<i>Unit</i>
Γ	Surface excess	mol/m ²
Π	Disjoining force	N
Σ	Stability factor/Unit of foaminess	s
γ	Surface tension	N/m
δ	Thickness of film	m
η	Viscosity	Pa.s
ρ	Mass density of liquid	kg/m ³
σ	Stress	Pa

2.8.3 SUBSCRIPTS

<i>Symbol</i>	<i>Description</i>	<i>Unit</i>
b	Bulk liquid	-
f	Film	-
F	Foam	-
g	Bubble	-
L	Solution	-
o	Initial (at time = 0)	-
s	Surface	-
y	Yield	-

CHAPTER 3

LITERATURE SURVEY

3.1 OBJECTIVES

This chapter is a review of the literature concerning the existing methods of foam stability measurements. The specific objectives of this chapter are:

- i Foam stability is defined and the importance of this quantity as well as problems experienced with its measurement is discussed.
- ii Existing methods to measure the stability of dynamic and static foams are discussed and special attention is given to the set conditions and the drawbacks of these methods.
- iii The background of the development of a digital image analysis method to extract froth and foam characteristics from images is discussed.
- iv The Fluxar[®]-SP, an on-line machine vision platform was used to extract the foam characteristics used in this study. The system is discussed briefly with specific focus on the algorithms used to extract parameters.

3.2 STABILITY OF FOAM

There is a large void in the literature describing the experimentally determined characteristics of foam, as in many cases arbitrary methods are used to obtain arbitrary results, which cannot be compared with data obtained elsewhere (Bikerman, 1973). It is impossible to compile foam tables containing information of foam characteristics such as maximum foam height, concentration at which maximum foam

height is obtained, as well as lifetime measurements, as results obtained in various studies seem to be only valid for the instruments used and the experimental procedures followed. In numerous cases only a brief indication of the procedure is given, making repetition impossible (Bikerman, 1973). Direct comparisons between methods are unreasonable if experimental conditions such as modes of foam formation, size of equipment, pressure in the liquid phase and the foam drainage rate are different, as all these parameters have an influence on the lifetime of foam lamellae (Fruhner et al., 1999).

The decay of foam is directly linked to the rate of decrease of total interfacial area and thus any technique giving access to this parameter could be useful in the estimation of foam stability (Lachaise et al., 1990). However, the technique employed to characterise foam stability must involve the measurement of the evolution of the bubble size distribution. Procedures, which require only observation of the change in foam volume, can only lead to a distinction between extremely poor and good foaming agents. Monsalve & Schechter (1984) proved that different measurements of foam stability are possible for the same system, depending on the initial bubble size distribution.

Before the main measurement techniques of foam stability are discussed, two main definitions have to be considered, namely *foamability* and *foam stability*.

3.2.1 FOAMABILITY

Foamability can be defined as the foam-generating power of a liquid (Wilson, 1996) or the capacity of the continuous phase to include the gaseous phase (Prins, 1988). Foaming ability is determined by the increase of foam volume after the introduction of gas into the solution and mostly computed by the initial value of overrun (Raymundo et al., 1998).

$$\text{overrun} = \frac{V_F - V_L}{V_L} \times 100 \quad 3.1$$

where v_F = volume of foam [m^3]
 v_L = volume of liquid [m^3]

The foamability of a substance is directly linked to parameters that influence and maintain foam stability such as surface tension and viscosity (Ross, 1969).

3.2.2 FOAM STABILITY

Foam stability can be defined as the ability of a foam to retain gas for a period of time (Prins, 1988). Foams can be categorised according to their time scale of stability. There are two main types, namely foams with low stability and those with high persistence against mechanisms inducing film thinning. In the case of the former, bubbles rapidly coalesce causing lamellae to rupture, while in the case of the latter, some additional energy barrier resists the collapse. This energy barrier arises from surface-force interactions (Hédruel & Frens, 2001; Bergeron, 1999).

3.3 MEASUREMENT TECHNIQUES OF FOAM STABILITY

There are two main types of foams that are investigated regarding foam stability namely, dynamic foam and static foam. A dynamic foam exists if dynamic equilibrium between the rate of decay at the top of the foam column and the rate of formation at the bottom of the column has been reached. In a static foam no state of equilibrium is reached and the foam is allowed to collapse after formation. Dynamic foam measurements are applicable to transient foam, while static foam measurements are applicable to foam of high stability (Nishioka et al., 1996).

There are many techniques that can be used to estimate the stability of foam. Some of the most widely used methods are reviewed here. The review includes the theory behind the method, the conditions under which the experiments must be performed, as well as further processing of data required to obtain a valid and comparable stability parameter.

3.4 STABILITY MEASUREMENTS OF DYNAMIC FOAM

The simplest method for the estimation of foam stability is to monitor the change in foam volume with time. The actual state of the foam depends strongly on the method of foam generation. If a foam is generated and poured into a vessel the foam will react differently according to physical phenomena from a foam that is generated in a column. To obtain reliable and reproducible results, foam should be generated in such a manner that the foam generated first is as well defined as the foam generated last. In Bikerman's classic dynamic method, dynamic equilibrium is attained in which the formation of foam at the bottom compensates exactly for the breaking of foam at the top. The equilibrium obtained in Bikerman's experiment can thus be taken as the original state or zero time in the investigation of foam decay.

3.4.1 BIKERMAN'S DYNAMIC METHOD

3.4.1.1 Theory

In Bikerman's original method foam is generated in a glass column, 70 cm high and 3 cm in diameter. The dispersed phase is distributed through the column with a glass frit. In some variations, the gas used as dispersion medium is thermally equilibrated, saturated with vapour from the sample liquid and then bubbled through a volume of liquid (50 ml). The apparatus is illustrated in Figure 3.1.

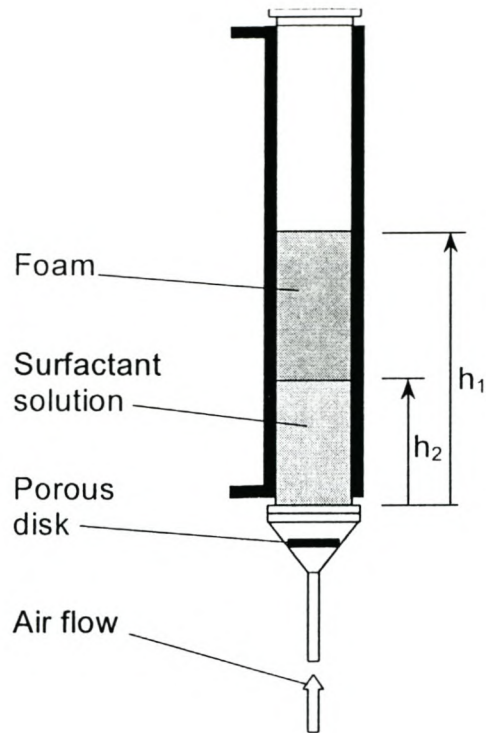


Figure 3.1 Schematic diagram of apparatus for measurement of dynamic foam stability (Beneventi et al., 2001).

When gas injection in a foaming solution starts and continues at a constant rate, the foam height increases with a constant linear velocity. The velocity with which the foam volume increases, gradually decreases and after a certain time period the foam reaches a constant height.

In a measuring cylinder of constant cross-section, a constant foam height implies a constant foam volume (Bikerman, 1973):

$$v_F = A_c h_F \quad 3.2$$

where A_c = cross section area of column [m^2]

h_F = foam height [m]

v_F = foam volume [m^3]

Equally so, if a gas is injected with a linear velocity the volume rate of gas is defined as:

$$\frac{V}{t} = uA_c \quad 3.3$$

where t = time [s]

u = linear gas velocity [m/s]

V = volume of gas injected [m³]

By combining Equations 3.2 and 3.3 it can be seen that the ratio of constant foam height and linear gas velocity is:

$$\frac{h_F}{u} = \frac{v_F}{V/t} \quad 3.4$$

Both the left-hand side and the right-hand side of Equation 3.4 can be an estimate of foam lifetime, based on foam volume measurements. It is important to investigate which one of these ratios remains nearly constant when the cross-section area of the cylinder used is not uniform. Bikerman (1973) found that when investigating two cylinders of different diameters (2.5 cm and 4 cm), the foam height varies in the ratio 3.14:1 while the quantity vt/V decreased only in the ratio 1.23:1. By using the parameter that is least sensitive to a change in the cross-sectional area of the cylinder, the unit of foaminess is defined as:

$$\Sigma = \frac{v}{V/t} = \frac{v_F t}{V} \quad 3.5$$

The values of V and t can be replaced with the gas flowrate to modify Equation 3.5 as follows (Beneventi et al., 2001)

$$\Sigma = \frac{v_F}{U_g} \quad 3.6$$

where U_g = gas flowrate [m^3/s]

The unit of foaminess is a measure of the average time that gas remains entrained in the foam (Nishioka et al., 1996). Bikerman's dynamic method established foaminess (or foam persistence) as a definite physical property of a liquid, independent of the apparatus used and as having a definite physical dimension (Bikerman, 1938).

3.4.1.2 Variations on Bikerman's method

Johansson & Pugh (1992) characterised froths by both dynamic and static tests using a variation on Bikerman's classical method in a mineral flotation application. The dynamic test determined the state of equilibrium of the froth and the static test determined the rate of collapse of the froth.

By using a dynamic test similar to Bikerman's (1938), it was again showed that the dynamic froth stability factor (Σ) is independent of the dimensions of the apparatus. In this study, the dynamic froth stability factor was determined from the linear slope of the equilibrium height (h_e) versus gas flowrate (U_g) curve, multiplied by the area of the column as follows (Johansson & Pugh, 1992)

$$\Sigma = \frac{\Delta h_e}{\Delta U_g} \times A \quad 3.7$$

where A = area [m^2]

h_e = equilibrium height [m]

U_g = gas flowrate [m^3/s]

Static froth stability measurements are characterised by the froth breakdown rate or speed of collapse (S). The time (t) for the foam to collapse from the maximum equilibrium height measured, to the original height at zero flowrate is determined. The speed of collapse is defined as follows (Johansson & Pugh, 1992)

$$S = \frac{h_{e,\max} - H_0}{t} \quad 3.8$$

- where $h_{e,\max}$ = maximum equilibrium foam height obtained [m]
 H_0 = original liquid height at zero flowrate [m]
 t = time of collapse [s]

3.1.4.3 Comments on Bikerman's dynamic method and variations

Bikerman's dynamic method results in foam that is well characterised and while the foam generation method is one of the best possible methods to use considering foam classification, there are a few constraints to the measurement of the foam stability. Several problems are encountered when the method was applied to experimental procedure. In the following section the assumptions made in the derivation of the applicable equations as well as the drawbacks of the measurements are discussed.

1. The following assumptions are made regarding Equation 3.6 (Malysa, 1992).

- i When the liquid height (H) of the solution studied is large enough so that its magnitude does not influence the ratio vt/V and the gas velocity is not too low or too high, the foaminess (Σ) is independent of:
 - a Gas flowrate,
 - b shape and dimensions of measuring cylinder, and
 - c average pore size of the sinter glass used for gas dispersion.
- ii The unit of foaminess (Σ) is equal to an average bubble lifetime in the foam if bubble coalescence in the foam, as well as the liquid in the foam can be neglected. This assumption is not reasonable when working with wet foams, as the liquid content in the foam can be as high as 40 percent (%).

2. In the dynamic method, the foam height or foam volume produced is measured while the gas continues to produce bubbles. The reading of the various values of foam

and liquid height may lead to errors and some systems can prove to be problematic. The following comments can be made concerning the recording of values in the dynamic method (Bikerman, 1973).

- i In most cases the measurement of the foam height does not give any difficulty, as the top of the foam column does not vary along the circumference of the tube by more than one or two millimetres. This does not produce a serious error if the total height obtained is considerably high.
- ii If the bottom of the foam column is not sufficiently definite, as there is no sharp boundary between the gas emulsion below and the true foam formation, the lower boundary of the foam must be taken as the original gas-liquid interface before foaming.
- iii Care should be taken to operate at low flowrates to ensure that there is a significant volume of liquid left in the column when dynamic equilibrium is reached (Nishioka et al., 1996).

3. The following comments are made on the variation of Bikerman's method as used for the characterisation of froth stability by Johansson & Pugh (1992).

- i The equilibrium height used in Equation 3.7 is the summation of the froth height and the liquid height, as measurements of the froth height alone was difficult.
- ii For some frothers the relationship between the equilibrium height and the flowrate was not constant at high flowrates and deviated from linearity. In those cases the dynamic stability factor (Σ) was determined only from the linear section of the equilibrium height-gas flowrate graph.
- iii At high flowrates the experiments were found to be less reproducible.

5. Another application of Bikerman's dynamic method was an investigation by Beneventi et al. (2001) into the effect of surfactant structure on foam stability. The following remarks on Bikerman's method in this application are made.

- i The foam stability was obtained by using Bikerman's original experimental method, but a greater volume of liquid was used to prevent total consumption of liquid during the experiments.
- ii The foam behaviour did not reach a steady state and in many cases the first growth phase in foam volume was followed by a decrease.
- iii Equilibrium could not be reached and the foam stability factor (Σ) was calculated using the maximum value of foam volume obtained.

It is evident from the comments above that although Bikerman's method proves to generate a well-defined foam, the measurements needed to calculate the foam stability has some shortcomings. Firstly, the method can not be applied to all types of foams, due to the application Equation 3.6 was derived for, secondly the measurement of the foam and liquid height can be problematic and thirdly, dynamic equilibrium is not reached in all cases.

3.4.2 OTHER APPLICATIONS

Apart from the above-mentioned measurement problems that are experienced in some systems, there is another problem concerning Bikerman's method, which is the interpretation of the data obtained. The foam column height and thus the decay rate observed are related to the stability of the foam, as well as the foamability of the foam. By using this method it is possible to see whether one foam is more stable than the next, but the extent to which the foams differ according to their stability cannot be quantified. In the following two applications Bikerman's method is used, but no foam stability factor is calculated. Instead a method where the data from the experiment are further processed to obtain a descriptive equation is suggested.

3.4.2.1 Application of a two-phase foam

Iglesias et al. (1995) investigated the foam stability of short life foams. The decay of short life foams is governed by drainage and film breaking but not by gas diffusion. These foams typically have a lifetime of less than an hour. A method was developed that makes it possible to quantify the effect of different additives on foam stability of specific surfactant solutions.

The dynamic method of Bikerman was followed for the formation of the foam. Gas was introduced into the column until dynamic equilibrium was reached, where after the gas input was closed and the change of the foam height with time was observed. The experimental data was plotted and it was found that for the same surfactant solution containing different additives, the heights versus time curves obtained were well ranked in some cases, so that it was obvious which foam is more stable than the others. However, this was not always the case. Some decay curves showed overlapping which imply that the stability of the foam solutions is ranked differently at different time steps. As this representation is not appropriate for deciding whether a given foam is two or three times more stable than another, the data needed to be further processed in order to make it more interpretable.

To ensure this, the data was plotted as a semi-log graph and it was found that the decay is represented as a straight line on such a plot. The height versus time curve can be plotted as such a straight line as follows:

$$h = -a \log t + b \quad 3.9$$

where $a, b = \text{constants [-]}$

From Equation 3.9 the rate of change in foam height is calculated as:

$$\frac{dh}{dt} = -\frac{m}{t} \quad 3.10$$

From Equation 3.10 it is clear that the rate of change in the column height or the thickness of the foam layer that collapses over time is inversely proportional to its age. As the initial conditions of the foam in the column (at $t = 0$) is not well defined because of the initial short drainage time, the last bubble to burst may be out of line with the other data. To rectify this, and to ensure the reproducibility of the results, the best option is to use a *half decay time* ($t_{1/2}$) as a reference. The half decay time is defined as the time passed when half the original height obtained by Bikerman's dynamic method is reached, as this is the most secure part of the linear variation.

If the data obtained are plotted in dimensionless form as h/h_0 versus $\log(t/t_{1/2})$, all straight lines describing different foams pass through the same point (0, 0.5) in the plane. The general equation for this line is wrongfully given by Iglesias et al. (1995) as:

$$\frac{h}{h_0} = -\lambda \log\left(\frac{t}{t_{1/2}}\right) \quad 3.11$$

where h = foam height [m]
 h_0 = initial foam height after formation [m]
 t = time [s]
 $t_{1/2}$ = half decay time [s]
 λ = decay constant [-]

Equation 3.11 is wrong as the constant in the equation is missing due to a numerical error. Turner et al. (1999) defines the equation for the line rightly as:

$$\frac{h}{h_0} = -\lambda \log\left(\frac{t}{t_{1/2}}\right) + \frac{1}{2} \quad 3.12$$

Iglesias et al. (1995) found that all sets of data for a specific surfactant system will pass through the point (0,0.5) in the plane and trace an identical line. Every surfactant system has a specific decay constant (λ) for a specific combination of surfactant, as well as a specific collapse mechanism. A change in mechanism is reflected by a

change in the slope of the straight line. The decay constant is linked to the surfactant used, as well as the mechanism of collapse, while the half lifetime quantifies the rate of collapse for a given mechanism (Turner et al., 1999).

3.4.2.2 Application of a three-phase foam: Foamed emulsion

Turner et al. (1999) applied the method proposed by Iglesias et al. (1995) to foamed emulsions. Foamed emulsions consist of three phases viz. an oil phase, an emulsifying surfactant phase and a dispersed phase. Viscous foamed emulsions (VFEs) have a high viscosity (in the order of 1 Pa/s) owing to the emulsion phase, which retards bubble movement. The small gas fraction in VFEs ensures a thicker interstitial layer than in common foam, so that it displays a greater resistance to Ostwald ripening (diffusion of gas through lamellae). In foamed emulsions the main mechanisms governing foam instability are not gas diffusion, liquid drainage or evaporation. Foam stability of foamed emulsions solely depends on the elasticity and stability of the inter-bubble emulsion layers. In the study of Turner et al. (1999) the lifetime of VFEs were forced to be short-lived by imposing a mechanical force by using an IKA Vibrax rotary vibrator.

The evolution of gas from foam, characterised by negligible drainage, is inversely proportional to time and can be described by (Turner et al., 1999):

$$\frac{dV}{dt} = -\frac{\lambda V_0}{t} \quad 3.13$$

where t = time [s]

V_0 = volume of gas initially present in foam sample [m³]

λ = proportionality constant [-]

Equation 3.13 applies to aqueous three-phase foams and dry aqueous foams. As in the case of two-phase foams, the half decay time is the best reference to use for further data analysis. Equation 3.13 when integrated with the reference condition of $V=V_{1/2}$ at $t=t_{1/2}$, takes the following form:

$$\frac{V}{V_0} = -\lambda \ln \left(\frac{t}{t_{1/2}} \right) + \frac{1}{2} \quad 3.14$$

where $t_{1/2}$ = half life of foam [s]

$V_{1/2}$ = half of original gas volume left in foam [m³]

If an experiment is carried out in a closed vessel with constant cross-sectional area, then:

$$v = v_F - v_{L,0} = A_c (h_F - h_{L,0}) \quad 3.15$$

and

$$v_0 = v_{F,0} - v_{L,0} = A_c (h_{F,0} - h_{L,0}) \quad 3.16$$

where v_F = volume of foam [m³]

v_L = volume of foam solution [m³]

$v_{F,0}$ = initial volume of foam after aerating [m³]

$v_{L,0}$ = initial emulsion volume before aerating [m³]

Combining Equations 3.14, 3.15 and 3.16 leads to:

$$\frac{h_F - h_{L,0}}{h_{F,0} - h_{L,0}} = -\lambda \ln \left(\frac{t}{t_{1/2}} \right) + \frac{1}{2} \quad 3.17$$

where h_F = foam height [m]

$h_{L,0}$ = initial emulsion height before aeration [m]

$h_{F,0}$ = initial foam height after aeration [m]

Equation 3.17 is simplified for dry aqueous foams as

i $h_{F,0} \gg h_{L,0}$ and $h_F \gg h_{L,0}$, and

ii t is far away from t_∞

so that:

$$\frac{h_F}{h_{F,0}} = -\lambda \ln \left(\frac{t}{t_{1/2}} \right) + \frac{1}{2} \quad 3.18$$

This equation has the same form as the equation as derived by Iglesias et al. (1995) for two-phase foams (Equation 3.12). It has to be noted that in the equation of Iglesias the values for the x-axis are calculated as the *log* value, while in the case of Turner et al. (1999) the x-axis values are calculated as a *ln* value.

Just as Iglesias et al. (1995) found that the decay of two-phase foams shows a high linearity, Turner et al. (1999) showed that the same is applicable to foamed emulsions. In both cases a decay constant could be obtained for every unique system. For foamed emulsions, this decay constant confirms changes in mechanisms of foam decay and quantifies the intrinsic foamed-emulsion stability. For foamed emulsions the decay constant has a certain value (0.2) above and under which different systems can be classified. Smooth decay of foamed emulsions take place when $\lambda < 0.2$ and catastrophic decay when $\lambda > 0.2$ (Turner et al., 1999).

3.4.2.3 Comments on the stability parameter calculation followed by Iglesias et al. (1995) and Turner et al. (1999)

1. The approach as quantified by Iglesias et al. (1995) and Turner et al. (1999) can be applied to systems with a smooth decay but not if:

- i The system follows catastrophic decay.
- ii The mechanism of interbubble diffusion plays a substantial role in foam instability.

2. The following remarks can be made for the foamed emulsion systems (Turner, 1999):

- i Significant errors are incurred in the early stages of decay due to:
 - a uneven foam surface, and
 - b initial high rate of collapse.

3. The equations used in the data analysis are only valid for certain systems and the constraints are as follows:

- i In the case of short life foams the decay for 20 to 80 percent (%) of the decay time can be plotted as a straight line.
- ii Equation 3.18 cannot be made to fit the data once approximately 80 percent (%) of gas is lost from the foam, as when $t \rightarrow t_{\infty}$ the approximation $h_f \gg h_{L,0}$ breaks down.

4. No such work has been done on long life foams where the decay is longer than an hour and the decay of the foam is influenced by disproportionation. Iglesias et al. (1995) did apply their method to a long life foam of Sodium dodecyl sulfate (SDS) but the approximation that the data points can be described by a straight line is noticeably inaccurate.

3.4.3 OTHER METHODS

Watkins (1973) postulated a model of foam decay that explains why a cylindrical container may be a poor design to describe the decay of foam. He proved by statistical analysis that the cylindrical vessel is prone to a lack of reproducibility. Ross & Suzin (1985) developed the means to analyse dynamic foams by using a conical shaped container as illustrated in Figure 3.2.

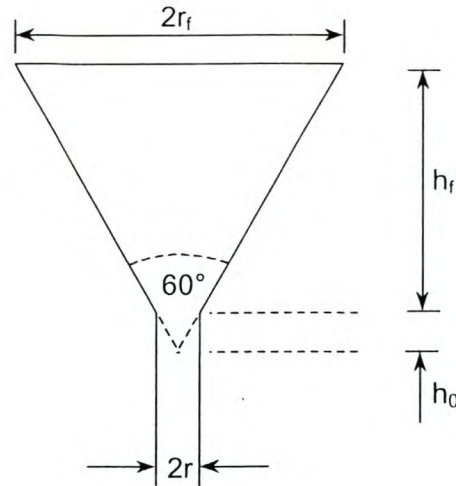


Figure 3.2 Conical foam meter (Nishioka et al., 1996).

With this method the stability of dynamic foams that is dependent upon the geometry of the experimental vessel can be calculated, but it can also be used for foams that is independent of vessel geometry. The study states that the vessel shape plays a role in the quantity of foam produced as well as the variation of the foam quantity with temperature (Ross & Suzin, 1985). Experimental data showed that with this method two regions of flow decay are identified. The first is a linear region, where the bubble lifetime is independent of flow conditions and from which the unit of foaminess (Σ) can be calculated. The second region shows exponential behaviour. In this region the bubble lifetime is dependent on flow conditions (Nishioka et al., 1996).

3.5 STABILITY MEASUREMENTS OF STATIC FOAMS

3.5.1 EXCESS PRESSURE

The excess pressure method can be used for the measurement of stability of static foams and is based on the following reasoning. A foam contains cells, either spherical or polyhedral, filled with gas. From the Laplace equation (Equation 2.4) it is clear that the smaller the radius of a bubble the greater the pressure inside the bubble. As foam

collapses, the pressure above the foam increases, and if the pressure is measured in a closed vessel, the increase in pressure is directly proportional to the rate of collapse of the foam (Wilson, 1996).

3.5.1.1 Theory

The total area of the foam is related to temperature, pressure, volume and quantity of gas by the following foam equation of state (Ross, 1969):

$$P_x V_g + \frac{2}{3} \gamma A = n_g RT \quad 3.19$$

where A = area of liquid surface in the foam [m^2]
 n_g = number of moles of gas in foam [mole]
 P_x = pressure external to foam [Pa]
 R = gas constant [J/mol.K]
 T = absolute temperature [K]
 V_g = volume of gas in foam [m^3]
 γ = interfacial tension [N/m]

If a closed system is considered, the total amount of gas in the system before decay and after decay stays constant so that (Nishioka, 1986):

$$n_x + n_g = n'_x + n'_g \quad 3.20$$

where the prime indicates values in decay after a time t

since

$$n_x + n_g = \frac{P_x V_x}{RT} + \frac{P_x V_g + \frac{2\gamma A}{3}}{RT} \quad 3.21$$

and

$$n'_x + n'_g = \frac{P'_x V'_x}{RT} + \frac{P'_x V'_g + 2\gamma A'}{3RT} \quad 3.22$$

Equation 3.21 and Equation 3.22 can be substituted into Equation 3.20 and rearranged, to obtain the following equation:

$$3V\Delta P + 2\gamma\Delta A = 0 \quad 3.23$$

$$\text{where } \Delta A = A' - A$$

$$\Delta P_x = P'_x - P_x$$

and the volume (V) is defined as (Nishioka & Ross, 1981):

$$V = v_t - v_L \quad 3.24$$

where v_t = total volume of the vessel [m³]

v_L = volume of solution [m³]

The interfacial area of the foam after complete collapse is thus given by (Nishioka & Ross, 1981)

$$A' = \frac{3V}{2\gamma} (\Delta P'_x - \Delta P_x) \quad 3.25$$

or

$$A(t) = \frac{3V}{2\gamma} \{\Delta P_\infty - \Delta P(t)\} \quad 3.26$$

where P_∞ is obtained by letting the foam decay for a sufficiently long time or by injecting an amount of anti-foam into the system.

The interfacial area of the foam can thus be measured by monitoring the change in pressure external to a foam in a container of constant volume and temperature (Nishioka, 1986).

3.5.1.2 Further analysis of data

Nishioka & Ross (1981) proposed the average lifetime of a unit area of liquid surface in a foam as a stability parameter. A surface area-time profile can be drawn up and the foam lifetime can be calculated by integrating the curves of height versus time as set out in Equation 3.27.

$$L_F = \frac{1}{H_0} \left(\int_0^{\infty} H(t) dt \right) \quad 3.27$$

According to Equation 3.27, the average lifetime of a foam can be defined as the area under the drainage profile divided by the initial foam height. The foam height/time profile can be calculated by optical transmission methods, visual recordings of height and time or the pressure excess method (Callaghan, 1989).

3.5.1.3 Comments on the Excess Pressure method

1. There are many drawbacks in using the excess pressure method and many set conditions apply:

- i Equation 3.26 is not valid for spherical cells since the hydrostatic effects create an additional pressure increase. Equation 3.26 thus only holds for (Nishioka et al., 1996):
 - a Dry foams that have a polyhedral structure.
 - b Foam which have a density that is much lower than that of the liquid.
- ii No set zero decay time is defined to ensure the same quality of foam for each experiment. The zero decay time is to be assumed to coincide with

the end of the so-called bubble emulsion state and the beginning of a bonded structure. This corresponds to a maximum of 15 volume percent (%) liquid in the foam.

- iii The largest source of error in this technique is the insertion of the foam into the sample chamber. The back pressure the generator encounters is not controlled and may affect the foam's structure. In addition, the foam ages for a certain time period between the time it is generated and inserted in the sample chamber. Part of the decay curve is thus not measured (Nishioka, 1986).
- iv The quantity of foam inserted in the sample chamber can be different for every sample tested.
- v The following relationship between the variables (defined in Equation 3.28) can cause several severe inaccuracies in the pressure value measured:

$$\frac{\Delta P}{P} = \frac{\Delta T}{T} \tag{3.28}$$

The method thus demands very accurate control of temperature.

2. The excess pressure method is an uncertain method to predict foam stability as:

- i The method fails as a comparative measurement for different substances (Lachaise et al., 1990).
- ii The results obtained from these experiments are not reproducible, as the decay is sensitive to the initial bubble distribution of the foam (Monsalve & Schechter, 1984) and it is not possible to ensure a similar bubble distribution in every sample.

Because the excess pressure method relies heavily on the assumption that the experimental conditions is isothermal, an apparatus was designed where better temperature control is possible. Dickinson (1992) designed such an apparatus for monitoring time-dependent pressure changes above the bulk of unstable foams. The apparatus works on the same principles as discussed in the previous section (3.5.1.1), but is designed to eliminate errors in data acquisition. The apparatus is illustrated in Figure 3.3.

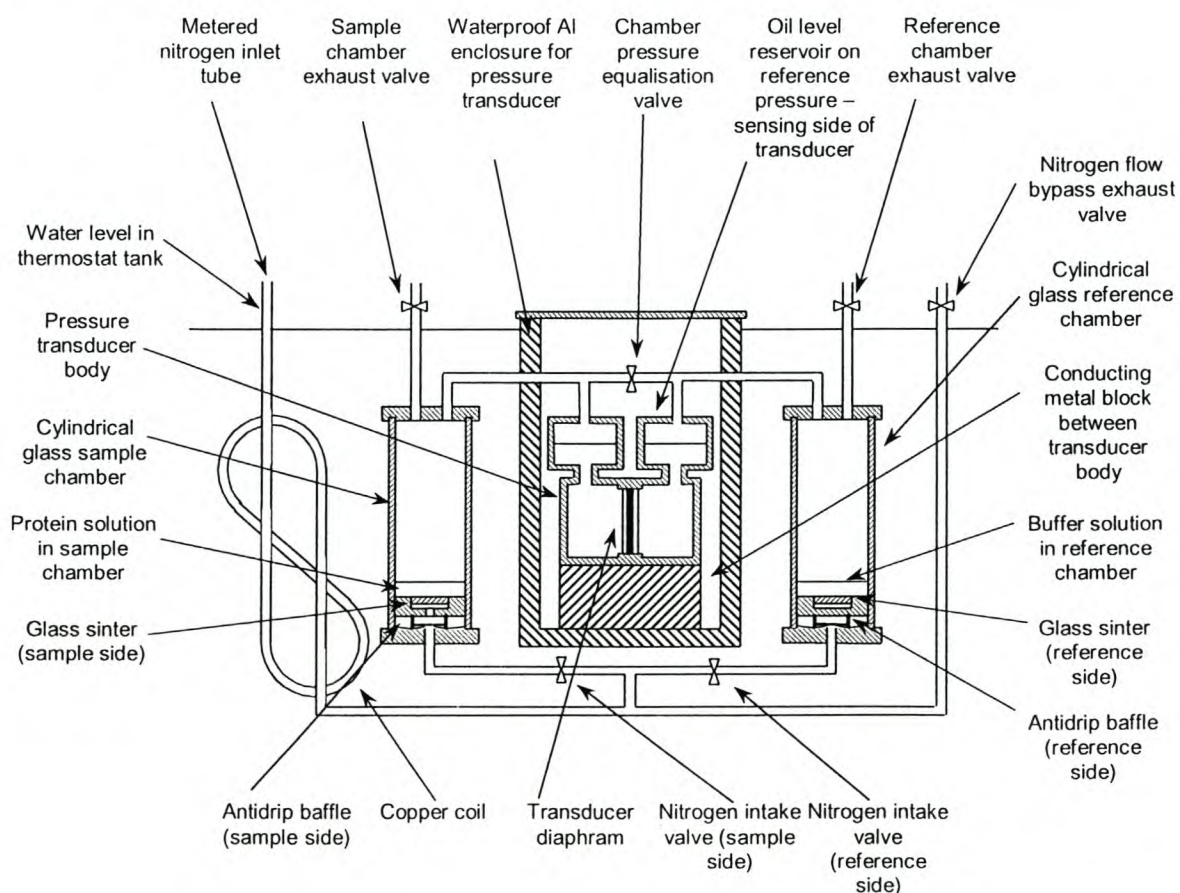


Figure 3.3 Dickinson's pressure chamber (Wilson, 1996).

The apparatus consists of two chambers connected by a differential pressure transducer. The foam from a surfactant solution is formed in the chamber by the diffusion of gas through a sinter glass, thus eliminating problems encountered when the foam is generated elsewhere. In order to overcome problems arising from ambient

temperature fluctuations, the apparatus is immersed in a thermostatically controlled water bath. The temperature is held constant within 0.005 K (Wilson, 1996).

3.5.2 LIGHT TRANSMISSION METHODS AND REFLECTOMETRY

As mentioned, the decay of foam can be directly linked to the decrease in total interfacial area. The following two methods are based on this assumption, namely light transmission methods and reflectometry methods.

Light transmission methods show the variation of interfacial area in a foam (Clark & Blackman, 1948) and can thus be used to characterise the internal dynamics of foam (Wilson, 1996).

3.5.2.1 Theory on light transmission

In the light transmission method the foam is generated in a glass cell and one side of the cell is illuminated with a plane wave of light ($\lambda = 488 \mu\text{m}$) generated from a laser (Wilson, 1996). If the incoming beam has a cross sectional area A_c and an intensity I_0 the intensity of the light leaving the foam is (Nishioka et al., 1996):

$$I = \frac{A_c I_0}{A_x} \quad 3.29$$

where A_x = external surface area of foam [m^2]

In using Equation 3.29 it is assumed that the external area (A_x) is representative of all surfaces in the foam so that measuring changes in I/I_0 yields the change in the relative total area of the foam (Nishioka et al., 1996).

3.5.2.2 Comments on the light transmission method

Light transmission methods can only be applied to foam with certain characteristics and thus the application of the method is limited. The following comments are made on the accuracy and applicability of the method.

- i The accuracy of the light transmission method could be impaired due to some defraction light intensity measured.
- ii It is only possible to use light transmission methods in foams that are relatively transparent or in samples of the foam that produces a thin layer. However, little can be concluded about the characteristics of the bulk foam when looking at a single layer or sample (Turner et al., 1999).

As in the case of light transmission methods, reflectometry can be used to estimate the stability of foam by estimating the decrease in interfacial area.

3.5.2.3 Theory on reflectometry

The light flux reflected by a spherical surface in a direction 2α from the incidence comes from the portion of surface intersected by the two cones of a half-angle α and $\alpha + d\alpha$. Lachaise et al. (1990) assume in their method that the reflected flux in the direction α is proportional to the square of the radius, or the surface area of the bubble so that the total reflected flux comes from all the illuminated bubbles. The illuminated bubbles are those that are at the free surface and those, which are reached by the light after a few refractions. Therefore only the first few layers of bubbles are reached. The deeper the bubble, the smaller the contribution it makes to the reflected light (Lachaise et al., 1990).

For non-spherical bubbles the same result can be achieved by the averaging of the directions of the films. Each contribution is proportional to the surface and therefore the total flux is expected to be proportional to the foam surface area in the first few

layers. If the foam is homogenous, this area is proportional to the interfacial area of the whole foam so that:

$$K \frac{I}{I_0} = \frac{A}{A_0} \quad 3.30$$

where I = instantaneous flux reflected in direction of detection [W/m^2]
 I_0 = initial flux reflected in direction of detection [W/m^2]
 K = proportionality constant [-]

Nishioka et al. (1996) stated that the inference of the proportionality between the reflected flux and surface area as defined in Equation 3.30 is incorrect and that the equation can not be experimentally verified. Lachaise et al. (1990) assumed an analogy between the reflectance of a single bubble and the reflectance from a foam. A single bubble reflects more light as it grows when the bubble radius is smaller than that of the incident beam. The reflectance increases because the bubble's cross section to the incident beam increases. This is however not the case when the beam is incident on a large coarsening foam. In this case the cross-section of the foam illuminated by the beam is constant and determined by the beam diameter, and thus Lachaise et al. (1990) assume the analogy incorrectly.

3.5.2.4 Comments on the reflectometry method

The following comments can be made regarding this method (Lachaise et al., 1990):

- i It is possible to compare foams according to their stability, based on the change in flux.
- ii Classification can be made at an early stage when the foam is too opaque for other methods to produce reliable results.

- iii This method is experimentally convenient and insensitive to temperature fluctuations and hydrostatic effects, and the method merits further examination.
- iv A rigorous analysis is required to relate the reflectance changes in the area of the foam (Nishioka et al., 1996).

3.5.3 OTHER METHODS

There are a variety of other techniques used to obtain fundamental information regarding foam stability. These include:

- i Conductivity measurements (Kato et al., 1983; Chang & Lemlich, 1980).
- ii Photographic techniques used to investigate bubble distributions in foam after the foam sample is flash frozen (Chang et al., 1956).
- iii Forced destruction techniques where α particles are used to induce foam collapse (McEnke & Mysels, 1969).
- iv An optical fiber-based method (Bisperink et al., 1992) used to measure size distributions in foam.

3.6 IMAGE ANALYSIS

Machine vision was initially investigated especially for the control of froth flotation systems. Machine vision systems utilised in automatic flotation control have several advantages. It is a cost effective solution, has low maintenance, the measurements made are immediately available and it yields consistent parameters (Botha, 1999a). The relation between the characteristics of the flotation froth and the flotation performance is used to adjudicate the performance of the system. The output of a computer vision system can however also give insights into the characteristics of foam and froth which makes it a powerful research tool.

3.6.1 OVERVIEW OF DEVELOPMENT

Recent research on the feasibility of a machine vision system for flotation control was initiated by Woodburn et al. (1989). Further contributions were made by Symonds & De Jager (1992), who proposed the segmentation of froth structures into bubbles using morphological methods. The morphological segmentation algorithm they proposed, was a residual edge detector utilising a spherical structuring element (SE). By opening and closing the image with a spherical SE (so-called rolling ball algorithm) and then subtracting the opened and closed images from the original image, a peak image and a valley image could be obtained (Botha, 1999a). The identification of individual bubbles was complex, the study was case specific and performed off-line (Moolman et al., 1995b).

Sun & Wee (1983) developed a method based on neighbouring grey level dependence matrices (NGLDM), with which the textural features of an image can be computed. This method, using second order statistics, was used by Siew et al. (1988) and Moolman et al. (1995b) to characterise the textural properties of flotation froths. Moolman et al. (1995c) refined the method and classified froth structure features by using spatial grey level dependence matrix (SGLDM) methods as well as neighbouring grey level dependence matrix (NGLDM) methods. The combination of the methods improved accurate structure identification up to 90 percent (%).

Eksteen (1995) used the algorithms and image processing software developed by Moolman et al. (1994). His work focussed on providing a knowledge base for research and development of vision-based automatic froth control systems from a chemical engineering viewpoint. He concluded that a vision-based system for automatic flotation control was a commercially viable venture, and has set out the necessary factors pertinent to the development of a complete vision-based automatic control system (Botha, 1999a).

There are thus two basic approaches in the visual analysis of froth surfaces. The first attempts to analyse the froth structure in a hierarchical and direct manner by attempting accurate segmentation of the froth surface into bubbles to then calculate

higher level parameters using this segmentation (Symonds & de Jager, 1992). The second approach relates froth types to textural properties and derives other surface visual parameters from the texture.

Several contributions were made to render the system viable for on-line control of the flotation process. Sadr-Kazemi & Cilliers (1997) successfully segmented froth images into bubbles by the morphological watershed algorithm. Moolman et al. (1995c) and Eksteen (1995) investigated foam mobility by using the NGLDM second moment. They found that the NGLDM second moment, calculated on a blurred image (caused by a slightly longer than normal exposure on video capturing equipment) gave an accurate measure of froth speed. Francis & de Jager (1998) used a standard block-matching algorithm (BMA) based method to calculate froth mobility. BMA methods calculate motion by attempting to match small regions of a source image with corresponding regions on a target image where the source and target image are images of the same scene taken apart over a segment of time. On-line and off-line image processing techniques has been used to link froth structure with kinetics. Woodburn et al. (1994) proposed a kinetic model based on the specific surface of the bubbles estimated by off-line image processing.

Moolman et al. (1995c) proved that the machine vision system shows several benefits if employed as an on-line control system. With an on-line system, more efficient data acquisition in industrial flotation plants would be possible and it would aid development in the flotation process. JKFrothCam is a commercially available system for the on-line monitoring of flotation froth developed at the Julius Kruttschnitt Mineral Research Centre (JKMRC) in Australia. It captures, digitises and analysis images from video obtained from monitoring the froth surface. The system computes three surface characteristics namely average bubble size, froth texture and froth velocity (Holtham, 1999).

Botha (1999a) documented the development of an on-line machine vision froth analysis platform. A complete set of flotation froth surface computational vision analysis algorithms for flotation froths were investigated and implemented. With these algorithms a static and dynamic analysis of digital images of froth surfaces can be performed. The static analysis includes complete bubble segmentation, where the

perimeter of each bubble is determined using watershed morphology. A practical application, the Fluxar[®]-SP has been created as a measurement component to aid in advanced plant control systems as well as in academic research. This application was used in the current study and the parameters extracted as well as the algorithms used are discussed in detail in the following section.

3.6.2 IMAGE PROCESSING

All of the following discussion comes from Botha (1999a).

Two main classes of low-level image algorithms were developed to perform a static analysis and a dynamic analysis on digital images of froth or foam. Algorithms for static analysis extract all information from a single static image. This includes information on the texture and structure of the froth. Dynamic analysis refers to algorithms that utilise two or more images to extract information on froth motion.

3.6.2.1 Static Analysis

Static analysis implements a bubble segmentation algorithm, fine froth detection and the calculation of global second order statistical textural properties. It includes all parameters that can be determined from a single image and excludes any motion and other dynamic analysis.

Bubble segmentation

In his work, Botha (1999a) used full bubble segmentation in addition to the textural analysis for static analysis. Extracting structural bubble characteristics, such as size and shape, are more accurately calculated by physically segmenting bubbles and calculating the true quantities rather than using a measure that is related indirectly to these quantities. In addition, having structural information available for each bubble makes it possible to calculate complete parameter histograms. Element marker-

extraction followed by watershed segmentation as documented by Vincent & Soille (1991) and Vincent (1993) were used for the general case and the application to froth images followed Sadr-Kazemi & Cilliers (1997).

Before the watershed algorithm is applied, the image needs to be pre-processed in order to prevent over-segmentation. This pre-processing includes a binary marker for each expected element, i.e. for each bubble that is expected to segment out, precisely one contiguous collection of co-ordinates within the area of that bubble is required. In practical set-ups it is found that each bubble displays a localised reflection due to the spotlight used in the camera set-up. These localised reflections are always present where there is only one dominant light source. The h-dome extraction (Vincent, 1993) was used to extract the localised reflections. This transform is able to extract regions of pixels, which are brighter than their immediate surroundings.

Homotopic modification utilises the extracted markers and modifies the image in such a way that:

- i The image's only minima are located on the extracted markers,
- ii all the other minima in the image is suppressed, and
- iii significant intensity divisions between marker positions are preserved.

These changes prevent the watershed algorithm from over segmenting the image that is to be analysed. The homotopically modified image appears with less noise than unmodified images.

In the watershed algorithm every bubble in the image is segmented out in an image of the flotation froth. Each bubble is a highly irregular dome and the lowest elevation or altitude is where the bubbles meet and the highest point coincides with the localised light reflection if the light source is close to the normal axis of the froth surface. If the elevation map is inverted, the result of the watershed lines (connecting catchment areas that are at the minima) coincides with the bubble boundaries as illustrated in Figure 3.4.

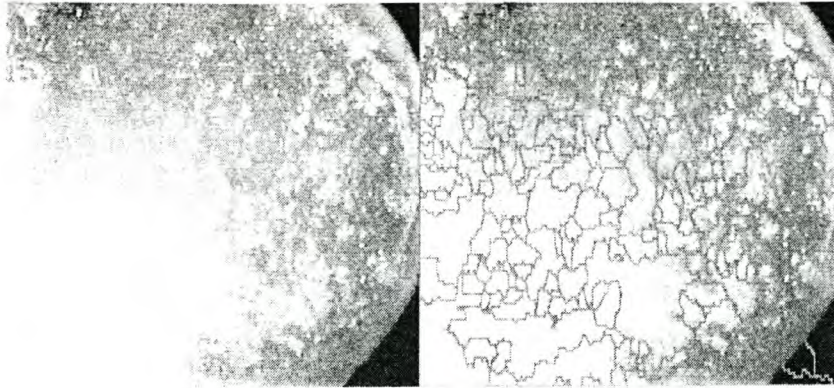


Figure 3.4 Watershed Segmentation of froth

It has to be noted that there are occasions where an irregularity in the bubble dome causes major discontinuities, which in turn causes darker lines in the localised light reflections that are used as markers. These discontinuities result in more than one marker being found for a bubble, which leads to over-segmentation. Darker regions represent higher intensity regions of the image and because the darker discontinuity is indicated in the localised reflection, two markers are extracted.

A post-segmentation over-segmentation correction algorithm is used to remedy over-segmentation of bubbles. Each boundary is examined for pixels that have values over a certain high threshold. If such pixels are found, it is assumed that they sit on false boundaries (i.e. boundaries that intersect a localised light reflection). The first neighbouring pixel belonging to a different catchment basin is found and the two catchment basins are then merged.

Other textural properties

The textural information of the image region is described by the Neighbouring Grey Level Dependence Matrix (NGLDM). The NGLDM, as calculated on an image, contains information about the relationship between each of the pixels and its neighbouring pixels at a certain distance d . The grey dependence level of each pixel is calculated and compared to its neighbour's grey level. It is assumed that all textural information is contained in the neighbouring grey level dependence matrix, Q , where

$Q(k, s)$ can be considered as frequency counts of greyness variation of a processed image. The dimensions of the array is $k \times s$, where k represents the number of grey levels and s the number of possible neighbours to a pixel in an image. The Q matrix is computed by counting the number of times that the difference between each element in the image function $f(i,j)$ and its neighbours is equal or less than the direction specified by a (a grey level parameter) at a certain distance d .

The following image features can be extracted (Moolman, 1995a):

$$i \quad \text{Small Number Emphasis:} \quad SNE = \frac{\sum_k \sum_s \left[\frac{Q(k, s)}{s^2} \right]}{N}$$

$$ii \quad \text{Large Number Emphasis:} \quad LNE = \frac{\sum_k \sum_s [s^2 Q(k, s)]}{N}$$

$$iii \quad \text{Number Nonuniformity:} \quad NNU = \frac{\sum_s \left[\sum_k Q(k, s)^2 \right]}{N}$$

$$iv \quad \text{Second Moment:} \quad SM = \frac{\sum_k \sum_s [Q(k, s)]^2}{N}$$

$$v \quad \text{Entropy:} \quad \mathcal{E}_N = - \frac{\sum_k \sum_s \{Q(k, s) \log[Q(k, s)]\}}{N}$$

where N is a normalising factor defined as (Sun & Wee, 1983):

$$N = \sum_k \sum_s Q(k, s)$$

Though it is more difficult to attach physical meaning to the parameters in this method, the parameter SNE can be seen as an indication of the fineness of the image, whereas LNE is a measure of the coarseness of the texture. SM is a measure of the homogeneity of the image, and the NNU and ϵN parameters are related to the coarseness of the image. In the present study only the SNE is used.

Fine froth segmentation

In froth images certain areas contain bubbles that are too fine to be taken into account in the analysis of the image. These regions however need to be compensated for. The watershed segmentation segments out this fine froth areas as large bubbles.

3.6.2.2 Dynamic Analysis

For the dynamic analysis two images of the same froth scene are taken a short time interval apart. The first is known as the *source image* and the second as the *target image*. These two images are combined to form a new sum-image. Marker extraction is performed on the source, target and sum images. The markers extracted from the sum-image can be used to determine the markers in the target image, which match the markers in the source image. Matching source and destination markers determine the motion that the source marker underwent to reach the target marker position. The motion of the bubble is approximated as the motion of the marker.

3.6.3 PARAMETER EXTRACTION

3.6.3.1 Extractable parameters

Several parameters describing the physical properties of the froth surface can be calculated from low-level image processing data. Most of these parameters are large vectors describing either all the bubbles in an image or describing motion vectors in

the region of interest. The data are further processed at a later stage by a combination of circular statistics calculation and histogramming.

Area

The area of the bubble is approximated with the number of area units or pixels that the segmented two-dimensional projection of the bubble occupies. Bubble area is calculated by counting the exact number of pixels contained in its tessellated two-dimensional projection. This is done for every bubble in the image. The counting is done by performing a sum on the run length pixel information for that bubble.

Bubble count

This refers to the total number of bubbles in a froth image, excluding fine froth. The number of bubbles can also be used as an indication of stability of the froth. If the bubble count shows dramatic variations in sequences of consecutive images, it indicates that bubbles are bursting or being formed at a high rate, which indicates instability. If the bubble count deviates only as much as expected for normal motion it can be considered as a stable froth.

Bubble base motion

Each marker or bubble that moves has a horizontal and a vertical differential motion pair. The horizontal and vertical differential motion pair is a two element vector describing how many pixels the marker has been translated in the time interval between the algorithm's two input images. Motion direction and motion magnitude are calculated by using these vectors.

Colour information

Intensity information, which includes the average red, green and blue components, are calculated. The intensity information is related to the type and concentration of the mineral being floated. In some minerals, such as copper, this can be very important, while in others, such as coal or platinum, colour information is less important.

Perimeter

The perimeter is the pixel perimeter of the segmented bubble projection. A bubble tracing algorithm yields a list of pixel chain codes describing the Euclidean perimeter of the bubble.

3.6.3.2 Statistics

All parameters, which have distinct values for each bubble, pixel or partitioned motion block (multi-valued parameters), are summarised with statistical values. This includes the calculation of a minimum, maximum, standard deviation, mean and median value. Before the values are calculated on the extracted data, parts of the data, which might affect the accuracy of the statistics, are discarded. Firstly all regions of fine froth is discarded, secondly the highest 0.5 percent (%) and lowest 5 percent (%) of area and perimeter values are discarded and similar percentage ratios for all other parameters. In the present study only *average* values were used.

3.6.3.3 Histogramming

Even though a good summary can be obtained from the statistical values, a more detailed summary in the form of a non-accumulative distribution is needed. The histogram is a plot of the number of occurrences versus a bin number. Each bin number represents a certain range of values for the data being examined.

Histograms are calculated for each image that is captured and analysed. Histograms can be accumulated to represent the froth characteristics over time. When accumulative histograms are used, a forget factor is incorporated to divide the influence of the histograms. This is done to eliminate the effect of process disturbances.

3.6.4 CHARACTERISATION OF FROTH/FOAM STABILITY

Stability of froth can be characterised by the degree to which consecutive froth images tend to remain unchanged (Eksteen, 1995). If the rate of bubble collapse in a froth is slow, fewer local changes in light intensity between successive frames should occur than in an unstable froth. In an unstable froth a quick change in the highlights on the top of bubbles and bubble boundaries are observed due to the high rate of bubble collapse and formation of new bubbles (Moolman, 1995a).

The sum of statistical distribution of the grey level values of the difference in pixel values, can be used to describe froth stability (Moolman, 1995a):

$$SB = \sum \sum f(x) \quad 3.31$$

where $f(x)$ is the matrix:

$$f(x) = \begin{cases} 1 & \text{if } |x_1 - x_2| \geq q \\ 0 & \text{if } |x_1 - x_2| < q \end{cases} \quad 3.32$$

where x_1, x_2 = the pixel grey levels of the two successive frames [-]

q = value of the selected grey level threshold [-]

The value of the stability parameter (SB) calculated with Equation 3.31 can be seen as the number of localised variations between the successive frames and hence a rough indication of the instability of the froth/foam. Although there is no explicit stability measure against which the parameter (SB) can be compared, a good qualitative indication of the results can be obtained by a comparison of the results with what is visually observed and with process parameters that are known to affect the froth stability (Moolman, 1995a).

3.6 CONCLUDING REMARKS

Foam stability is defined as the ability of a foam to retain gas for a period of time. Much difficulty is experienced in the measurement of foam stability. Foam characteristics are very sensitive to experimental conditions and the initial state of the foam and it can thus be said that there are as many results as there are methods. For the measurement of dynamic foam, the method of Bikerman (1973) is extensively used. The method generates the most defined foam, but many problems regarding the measurement of experimental values are experienced. The unit of foaminess (Σ) as proposed by Bikerman (1973) can not be applied as a parameter of stability in all foam systems and dynamic equilibrium is not reached in all cases. The work of Iglesias et al. (1995) and Turner et al. (1999) regarding the decay of short-life foams are promising, but the experimental results obtained need to be verified for long-life foams. Measurements of static foam stability include the excess pressure method as well as light transmission and reflectometry methods. These methods are also limited in applicability. The excess pressure method is sensitive to temperature fluctuations and foam type, while little can be concluded about the characteristics of a bulk foam by looking at a single layer of foam, as in the case of light transmission and reflectometry methods.

Monsalve & Schechter (1984) stated that neither the method of Bikerman, nor the pour test of Ross and Miles, optical transmission methods or the excess pressure method gives a measure of foam stability that is reproducible. Without reproducible

results, these methods can not be used to assess the influence of a change in a single variable, such as surfactant concentration, has on foam stability.

Image analysis has found extensive application in the flotation industry, specifically with regards to control. Botha (1999a) documented the development of Fluxar[®] – SP, the machine vision froth analysis platform used in this study. The image analysis includes both static and dynamic analysis. The static analysis implements a bubble segmentation algorithm, while the dynamic analysis use a source image and a target image to detect changes and movement in the system. This machine vision system is applied to two case studies. The first is a mineral flotation application discussed in *Chapter 4* and the second the investigation into the nature of foam decay investigated in *Chapter 5*.

3.7 SYMBOLS USED IN CHAPTER 3

3.7.1 SYMBOLS

<i>Symbol</i>	<i>Description</i>	<i>Unit</i>
a	Constant	-
<i>a</i>	Grey level parameter in NGLDM method	-
A	Area	m ²
b	Constant	-
h	Height	m
H	Liquid height	m
I	Light intensity	W/m ²
k	Number of grey levels	-
L	Lifetime	s
m	Constant	-
n	Number of moles	mole
N	Normalising factor	-
P	Pressure	Pa
Q	Neighbouring grey level dependence matrix	-
q	Grey level threshold	-
R	Gas constant	J/mol.K
s	Number of possible neighbours	-
S	Speed of collapse	m/s
SB	Stability	-
t	Time	s
T	Absolute temperature	K
u	Linear gas velocity	m/s
U	Flowrate	m ³ /s
v	Volume	m ³
V	Gas volume	m ³
x	Pixel grey level	-

3.7.2 GREEK SYMBOLS

<i>Symbol</i>	<i>Description</i>	<i>Unit</i>
Σ	Stability factor/Unit of foaminess	s
α	Angle	-
λ	Decay constant	-
γ	Surface tension	Pa.s

3.7.3 SUBSCRIPTS

<i>Symbol</i>	<i>Description</i>	<i>Unit</i>
c	Cross Sectional	-
e	Equilibrium	-
f	Final	-
F	Foam	-
g	Gas	-
L	Solution	-
o	Initial (at time = 0)	-
t	Total	-
x	External	-

CHAPTER 4

FLOTATION FROTH FEATURES

4.1 OBJECTIVES

The main objective of this chapter is twofold. Firstly, the application of the image analysis system for laboratory use is investigated by its ability to define foam characteristics and differentiate between systems with different characteristics. Secondly, the aim is to assess the image analysis system's measurement of foam and froth stability as to investigate the influence of experimental conditions and additives on stability. The case study of quartz flotation with cetyltrimethylammonium bromide and octadecylamine is studied to quantify the effect of solid particles on the stability of foam. It has to be emphasised that the main objective of this chapter is the adjudication of the image analysis system as a measurement of stability and different froth characteristics and that the type of solid particles used in this study and the effectiveness of the flotation are of lesser importance.

The specific objectives of the chapter are:

- i Flotation as industrial process is described, including the main mechanisms in the process. The types of flotation and the factors influencing the flotation rate are discussed.
- ii Particle characteristics such as size and hydrophobicity play a role in the stability of froth. The mechanism of foam breaking by particles is described and previous studies regarding this effect is discussed.
- iii The ability of the image analysis system to differentiate between two-phase systems of different surfactant concentration as well as systems that differ in phase i.e. two-phase and three-phase systems are investigated. Emphasis is put

on the classification of the groups as well as the unique characteristics defining every system. The correlations between the image variables extracted are also discussed.

- iv The stability of the two-phase system (foam) and three-phase system (froth) as computed by the image analysis system is discussed. A special emphasis is put on the effect of a change in surfactant concentration as well as the effect of different particle sizes on foam/froth stability. The recovery of quartz particles is discussed with specific focus on the effect of surfactant concentration and particle size on the percentage recovery.

4.2 THE FLOTATION PROCESS

4.2.1 DEFINITION

Flotation is a unit operation used to separate liquid phases or a solid phase from a liquid phase (Vrablik, 1959). Unlike most separation processes, which rely on the bulk properties of the solid phase, flotation relies on the surface properties of the solid phase, such as adsorption, wetting and adhesion. If a surface is hydrophobic it will rather attach to the gas phase (air bubble) than attach to the water phase. Most minerals surfaces are however hydrophilic and are not naturally inclined to be floated. The main challenge in flotation is to alter the surface properties of the solid phase in order to optimise the separation of the desired material from the gangue or unwanted material (Prud'homme & Warr, 1996).

The separation of particles from a liquid phase by air flotation is a method that applies the principle of buoyancy (Gopalratnam et al., 1992). Flotation is accepted as a method of solid-liquid separation only when classic separation techniques, such as sedimentation and filtration is ruled out (Zlokarnik, 1998). The success of the flotation process depends on the ability of bubbles to collect particles from the suspension and carry them to the surface where a layer of froth forms (Jameson, 1999).

Air flotation has been used for many years in the beneficiation of ores as well as in wastewater treatment, including the flotation of suspended solids, fibres and other low-density solids. Flotation is also used for thickening of activated sludge and flocculated chemical sludge. As the process is reliable and effective, air flotation is also used for the removal of oils and greases from wastewater (Bennett, 1988).

4.2.2 PROCESS DESCRIPTION

Separation of particles by flotation adheres to the same laws as sedimentation but in a “reverse field of force”. Flotation utilises the difference in density between the gas phase, to which particles become attached, and the liquid phase. The apparent density of the solid phase which is to be removed is reduced by the adsorption of gas bubbles (Vrablik, 1959). Since the agglomerates have a lower density than the medium they are immersed in, they rise to the surface where they can be removed (Bennett, 1988).

In flotation cells in general, the overall flotation rate is a combined result of a number of phenomena. The removal of a solid or liquid phase through flotation follows the following steps (Bennett, 1988):

- i Introduction of gas bubbles into the liquid phase.
- ii Collision between gas bubbles and the suspended matter.
- iii Attachment of fine bubbles to the surface of the suspended matter.
- iv Upward rise of floc structures.

These basic steps have an important influence on the success of the flotation process and each of them will now be discussed briefly.

4.2.2.1 Bubble generation

Bubble size is the most important dependent variable in air flotation systems (Bennett, 1988). The method of bubble generation determines the bubble size and the gas concentration in the flotation cell (Strickland, 1980). Both these variables influence

the contact efficiency between bubble and the suspended matter and therefore have an effect on the removal rate.

There are three main methods to produce bubbles, namely (Strickland, 1980):

- i Dissolution of gas from a supersaturated solution or dissolved gas flotation.
- ii Mechanical mixing of gas and liquid or dispersed gas flotation.
- iii Direct gas injection by means of a sparger as used in froth flotation.

In dissolved air flotation the gas bubbles produced has an average particle size of 10 to 100 μm (Churchill & Tacchi, 1978). In dispersed air flotation the bubble size is an order of magnitude larger, having diameters in the range of 400 to 2000 μm (Van Ham et al., 1983).

4.2.2.2 Bubble/Suspended matter contact

In all methods of flotation the bubble-particle interaction is of primary significance. Various mechanisms have been proposed to describe this phenomenon, including (Churchill & Tacchi, 1978):

- i Adhesion of a bubble to a particle, which includes
 - a precipitation of a bubble on a particle surface, or
 - b collision between a particle and a bubble.
- ii Trapping of a bubble in a coagule or a floc structure.
- iii Absorption of a bubble into a coagule or floc as it forms.

The various mechanisms of bubble/suspended matter contact are illustrated in Figure 4.1.

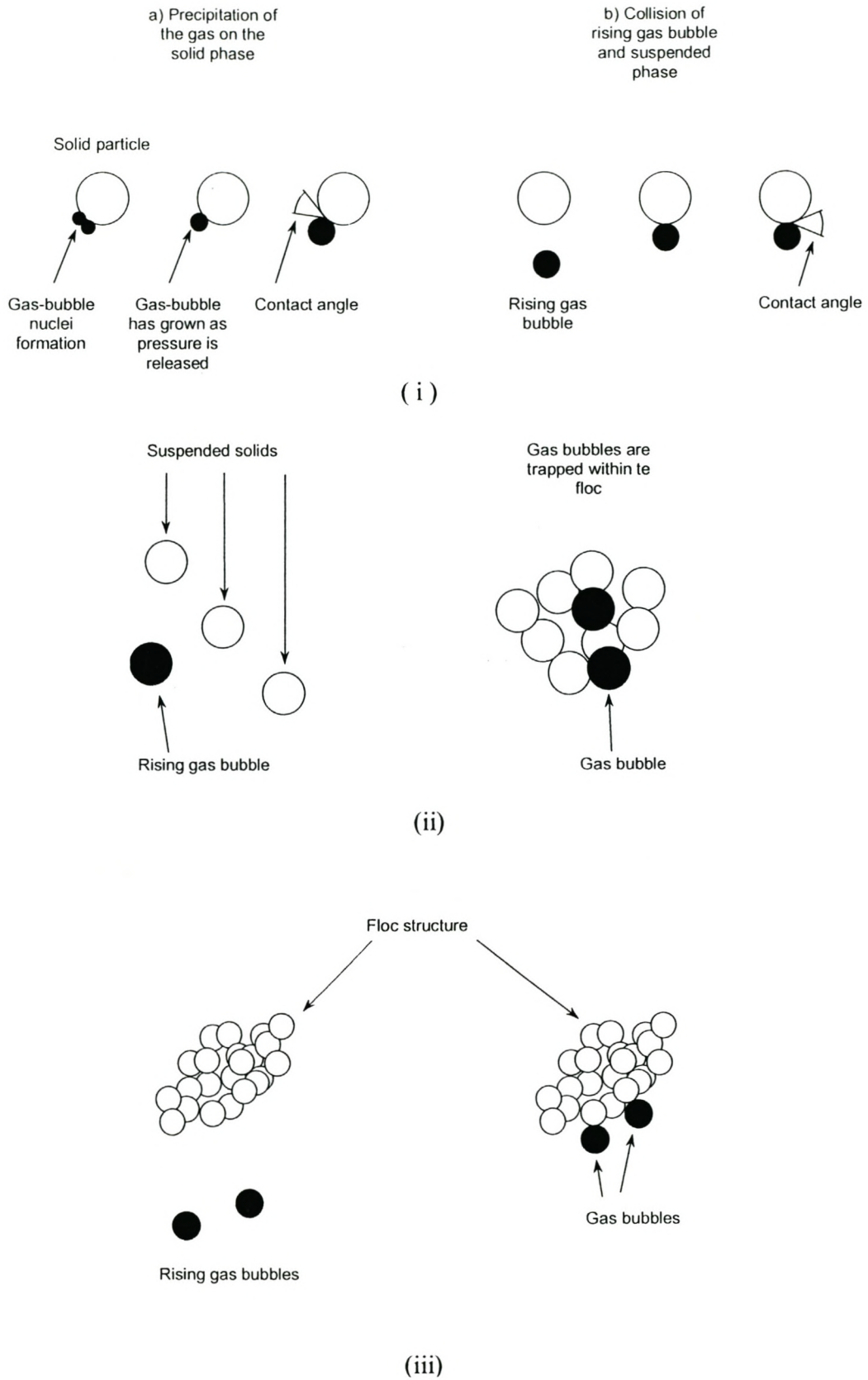


Figure 4.1 Mechanisms of bubble/solid contact (Bennett, 1988).

In mineral processing the particles to be floated are first made hydrophobic or non-wetting and through the collision mechanism the hydrophobic particle attaches to the bubble by the formation of a finite contact angle at the gas-liquid-solid contact line. There are some cases where the particles to be removed has to be flocculated as they are hydrophilic of nature. In these cases the bubbles must be physically trapped within the flocs (Jameson, 1999).

The suspended phase is usually static of movement while the gaseous phase is dynamic and has flow lines established around the bubbles. The suspended phase and the gas bubbles have viscous motion and the suspended phase will tend to follow the flow lines, which will result in no contact between bubble and solid. The rising bubbles need to contact the suspended phase directly, otherwise the suspended phase will not be removed (Vrablik, 1959).

4.2.2.3 Bubble/Suspended matter attachment

For flotation to be successful, the suspended matter have to attach to the bubble that it collides with, and stay attached until the bubble/drop combination reaches the surface. In bubbles-solid adhesion there is always a thin layer of water between the particle and the gas bubble. This layer must rupture in the time that the bubble and solid are in contact for attachment to occur (Strickland, 1980). The thickness of this film depends on the interactions between the air-solid and liquid-solid phases. These interactions are termed the disjoining pressure. The disjoining pressure (as defined in Section 2.6.3) opposes the thinning of the film. With solid particles, the behaviour can range from attractive (non-wetting) to repulsive (wetting). The net interaction between a mineral surface and the gas phase (air) must be attractive to lead to the thinning of the aqueous film and hence solid-bubble adhesion (Prud'homme & Warr, 1996).

Bubbles must be able to attach themselves to particulate matter for flotation to take place. When an approaching gas bubble adheres to a solid particle, it forms a positive contact angle at the line where the gas, liquid and solid phases meet as illustrated in Figure 4.2.

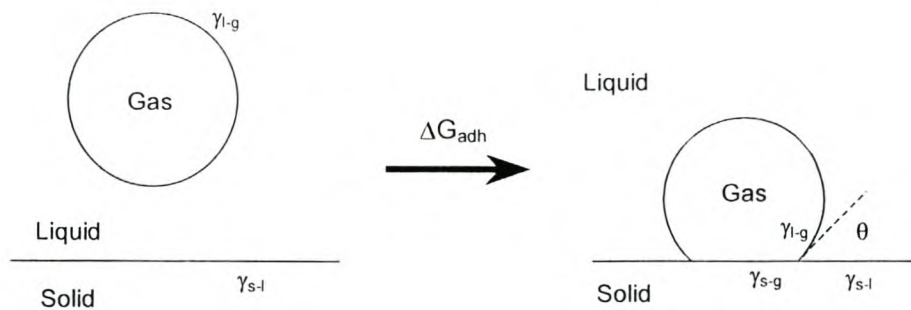


Figure 4.2 Schematic diagram of gas phase (bubble) adhering to solid phase (Prud'homme & Warr, 1996).

If the contact angle is positive, the bubble can carry the particle with it and rise to the surface. If the contact angle is zero then the liquid is said to wet the surface and the bubble will not stick. Thus, to ensure bubble-particle attachment the particle must not be wetted. The larger the contact angle, the stronger the bubble-particle attachment.

Once the bubbles have attached themselves to the ore particles, the bubble-ore agglomerates rise in the pulp. First, a lattice is formed which appears like a loose sponge and later the bubbles tighten into a froth. This tightening process squeeze out a great part of the occluded water, which detaches the gangue (Crozier, 1992). The fraction of suspended matter that attaches to the bubbles is called the attachment efficiency. Various factors, such as surface electric charge, interfacial tension, interfacial tension gradient and viscosity influence the film-thinning process and therefore the attachment efficiency (Strickland, 1980).

For the flotation process to be effective, the bubble and particle must remain together until the froth layer is collected. Flow around the bubble exerts tangential shear forces that tend to cause detachment of the particles. The surface forces at the interface oppose this detachment force (Strickland, 1980).

4.2.3 TYPES

There are essentially five types of flotation systems, namely (Bennett, 1988):

- i Dissolved air flotation (DAF) – Fine gas bubbles are generated from a supersaturated solution as a result of pressure reduction.
- ii Induced air flotation (IAF) – Gas and liquid are mechanically mixed to induce bubble formation.
- iii Froth flotation – Bubbles are directly injected by a sparger.
- iv Electrolytic flotation – Bubble generation occurs as a result from electrolysis of water.
- v Vacuum – Air is extracted from a saturated solution by negative pressure.

The classification of the different types of flotation is made on the difference in bubble formation. The first two systems are currently widely used in the industry. The drawback of induced air flotation is that most of the studies done focussed on the use of induced air flotation in agitated vessels (Feng & Aldrich, 2000). Mechanical agitation in induced air flotation leads to high turbulent flow that breaks up suspended matter which complicates removal (Volesky & Agathos, 1974; Sylvester & Byeseda, 1980). With the development of induced air flotation columns where the air is introduced into the system with a distributor, this disadvantage can be overcome. Froth flotation is used to separate minerals suspended in liquids by attaching them to gas bubbles to provide selective levitation of the solid particles. It is the most extensively used process for the separation of chemically similar materials (Crozier, 1992). Electro-flotation is a variation of the gas flotation process in which the gas is generated by an electric field. Several advantages have been claimed for this method including the formation of small bubbles, minimum turbulence and uniform contact between the gas and the dispersed phase (Churchill & Tacchi, 1978).

4.2.4 FACTORS INFLUENCING FLOTATION RATE

Optimum flotation is a function of the attachment-detachment forces acting on a bubble-particle aggregate (Ahmed & Jameson, 1985). The flotation rate is a balance of various factors such as bubble size, particle density and agitation. In the following section a short description of each factor is given.

4.2.4.1 Bubble size

The most important dependent variable in air flotation systems is bubble size (Bennett, 1988). Bubble-particle collision is necessary for successful flotation. For the same overall flowrate, the number of bubbles in the suspension and hence the surface area available for contact with the particle increases with a decrease in bubble size. Large solid particles can pose a problem as the bubbles that are too small cannot provide the buoyancy to lift large particles, but this is not a limitation with fine particles. In the impeller region the speed of rotation of an eddy with a bubble at the centre will increase as the bubble size decrease and will therefore increase the detachment force (Ahmed & Jameson, 1985).

Bennett et al. (1958) reported that small bubbles result in a more efficient removal of coal. De Vivo & Karger (1970) used two bubble sizes in flotation columns to float kaolin and found that smaller bubbles do increase flotation efficiency.

4.2.4.2 Agitation

Whatever the size of the bubble or the particle, an increase in agitation cause a greater detachment force between a bubble and a particle caught in a turbulent field around the impeller. In the region close to the impeller, the forces that tend to rupture bubble-particle aggregates show an increase. Elsewhere in the stirred cell, where the turbulence levels are less than in the impeller region, it is likely that an increase in

impeller speed will lead to an increase in the rate of particle capture by the bubbles. The turbulence in the cell increases as the impeller speed increases. The rate of collision between particles and bubbles are enhanced in regions far away from the impeller by larger stir speeds (Ahmed & Jameson, 1985).

In the case of quartz, where the minimum agitation is 100 rpm to float the particles, it was found that the benefit of using smaller bubbles decreases with agitation. This is owing to the fact that although frequency of particle-bubble collision increases with agitation, the detachment forces become dominant at a very low agitation due to higher particle density. Low density fines like coal flotation or water effluent treatment shows very slow recovery. In such systems the use of small bubbles at a high agitation rate proves beneficial (Ahmed & Jameson, 1985).

The typical bubble size for a conventional flotation cell is quoted by Harris (1976) to be in the range of 100 and 1000 μm . If the average bubble size is thus taken as 600 μm it can be said that, for the use in flotation cells, high flotation rates of particles with high density could only be obtained with the use of moderate to high agitation.

4.2.4.3 Particle density

High density particles increase the rate of capture as the particles have more inertia and are less influenced by the fluid around the bubble area. However, the detachment force on a bubble-particle in the impeller region increases as the density increase. When floating high-density particles the optimum results are obtained with small bubbles and low impeller speeds. For particles of low density, the flotation rate increases with agitation (Ahmed & Jameson, 1985).

4.2.5 EFFECT OF PARTICLES ON FROTH STABILITY

It is generally accepted that a froth of proper stability is essential to achieve a good recovery of minerals of a good grade. However, the froth stability depends more on the properties and amount of solids it contains than on the properties of the froth itself

(Dippenaar, 1982a). If the froth is not sufficiently stable, the mineralised bubbles will rupture before being scraped over the weir, which will result in the mineral particles detaching and falling back into the pulp (Feng & Aldrich, 2000). If the froth is too stable the froth could entrain gangue and this will lead to the recovery of a lower grade product. A froth of correct stability provides additional selectivity as slow coalescence of bubbles creates overcrowding of particles at the liquid-air interface, which cause the ejection of particles of lower hydrophobicity from the froth back to the pulp (Dippenaar, 1982a). The foam should thus be stable enough to enable concentration processes to occur but it must simultaneously rupture quickly outside the flotation vessel (Malysa, 1992).

There are many characteristics that influence the effect of solid particles on froth stability. The main characteristics are hydrophobicity, particle size and solid concentration and these characteristics affect froth stability interactively (Tao et al., 2000). The reports concerning the influence of the above-mentioned factors are inconsistent and the inconclusive results are due to the different conditions and methods employed in previous studies.

4.2.5.1 Particle Hydrophobicity

When a hydrophobic particle touches both surfaces of a film, the contact angle forces the film surfaces that are in contact with the particle to take on a convex shape. If a film has thinned to such an extent that a particle can bridge the film, and the degree of hydrophobicity of the particle is correct, the Laplace pressure in the film next to the particle becomes positive (Walstra, 1989). This region of increased pressure leads to liquid flowing away from the particle to a region of lower pressure. This film thinning process continues until the film ruptures and breaks contact with the particle. To ensure rupture the particle has to touch both film surfaces, which means that the particle diameter has to be at least equal to the film thickness (Prins, 1988). Film rupture by hydrophobic particles is illustrated in Figure 4.3.

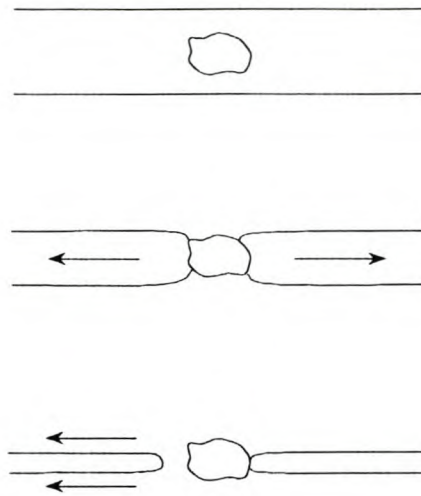


Figure 4.3 Film breaking by hydrophobic particles (Walstra, 1989).

The particles in froth must have a sufficient degree of hydrophobicity to have a favourable interaction with the gas-liquid interface and thus increase froth stability (Johansson & Pugh, 1992). The presence of smaller particles with moderate hydrophobicity ($55^\circ < \theta < 65^\circ$) at the interface of the Plateau border increases the rigidity and surface viscosity of the froth, while particles with a high hydrophobicity ($\theta > 90^\circ$) penetrated the gas-liquid interface (Moudgil & Gupta, 1989). Particles with low hydrophobicity ($\theta < 40^\circ$) remain in the bulk liquid and do not affect froth stability (Tao et al., 2000).

Klassen & Mokrousov (1963) reported that the more hydrophobic particles are, the greater the stabilising effect. Kulkarni et al. (1977) attributed the froth-breaking property of hydrophobic particles to their ability to adsorb the layer of surfactant at the air-water interface, leaving the surface unstable. Johansson & Pugh (1992) stated that small particles (26-44 μm) with low hydrophobicity have little effect on the stability of the froth, while particles with an extremely high hydrophobic interaction ($\theta > 90^\circ$) can penetrate the air-solution interface to a much larger extent and cause film rupture. An intermediate hydrophobicity was also found where the dynamic froth stability can be maximised and the rate of collapse minimised. In agreement with this, Dippenaar (1982a) stated that all particles with a very high contact angle ($\theta = 102^\circ$) destroyed froth immediately and suggested a bridging-dewetting mechanism.

4.2.5.2 Particle Size

Studies on the influence of particle size on the stability on froth generally show that there are some particles that tend to stabilise froth, while others tend to destabilise it. Although some behavioural trends could be identified for some minerals, no general conclusion could be reached (Harris, 1982), owing to the fact that different particle types, concentrations, shape and roughness were used in the experiments (Johansson & Pugh, 1992). There are many contradictive studies concerning the effect of particle size and hydrophobicity of particles on the stability of froth. Livshits & Dudenkov (1965) believed that only coarse particles could act as buffers between bubbles to prevent them from rupture. More conclusive results have been obtained by Dippenaar (1982a) who based his static studies of foam stability on the model of thin films. Systematic use of photographic techniques made it possible to obtain reliable results concerning the kinetics of bubble-wall rupture and the mechanisms of rupture. Dippenaar (1982b) found through empirical experiments with hydrophobic quartz and galena particles that the mass of particles necessary to obtain a decrease in foam volume in a shake test is directly related to the particle size. It was also stated that if a large number of fine particles are present, a foam film could be stabilised by the particles. The fines form a closed packed monolayer, which prevents particles to be forced out of the film and the interfaces to touch.

Johansson & Pugh (1992) showed that quartz particles in a sparsely mineralised froth (2 weight percent), in the size range of 74-106 μm generally increase froth stability. They also concluded that small particles (26-44 μm) at an intermediate hydrophobicity stabilise froth. Szatkowski & Freyburger (1985) found that fine quartz particles (20+ μm) render bubbles to be more resistant to coalescence and thus promoted froth stability. Moudgil & Gupta (1989) investigated phosphate fines and observed, similar to Johansson & Pugh (1992) that the size and hydrophobicity of phosphate fines have a major influence on froth stability. They found that small particles with low hydrophobicity have no effect on froth stability but if the particles are made more hydrophobic, that the particles stabilise the froth. Tao et al. (2000) investigated the stability of froth containing pulverised coal particles and established that particles between 30 and 150 μm stabilise froths. Their results that any particles

smaller than 30 μm destabilises froth as smaller particles show longer froth-destabilising ability, are in accordance with Dippenaar (1982b). They also showed that for small particles there are a maximum solid concentration above which the froth structure is totally destroyed. At low concentrations, coarse particles destabilise froth, but if the solid concentration is increase to 25 percent (%) the froth is stabilised. Increased froth stability at higher solid concentrations is attributed to the increase in viscosity of the froth, which hinders drainage.

4.3 CASE STUDY: THE FLOTATION OF QUARTZ

4.3.1 EXPERIMENTAL SET-UP

All flotation experiments were carried out in an open top Leeds laboratory cell. The flotation cell has a volume of 3 litre (L). A vertical impeller was used as an agitator. Aeration air was supplied from an air cylinder and the airflow was measured by a rotameter. The air was finely dispersed by the agitator and flowed from the bottom of the cell through the liquid. The froth structures were monitored with an ELMO colour charged coupled device (CCD). The CCD was mounted on a bracket, which prevented vibration in the cell from affecting the images. The distance from the lens to the cell was 485 mm to ensure images with a clear focus. The CCD was connected to a personal computer equipped with frame grabber, which captured and digitised the images. Light was provided by a 100 W light bulb next to the CCD. The experimental set-up is illustrated in Figure 4.4.

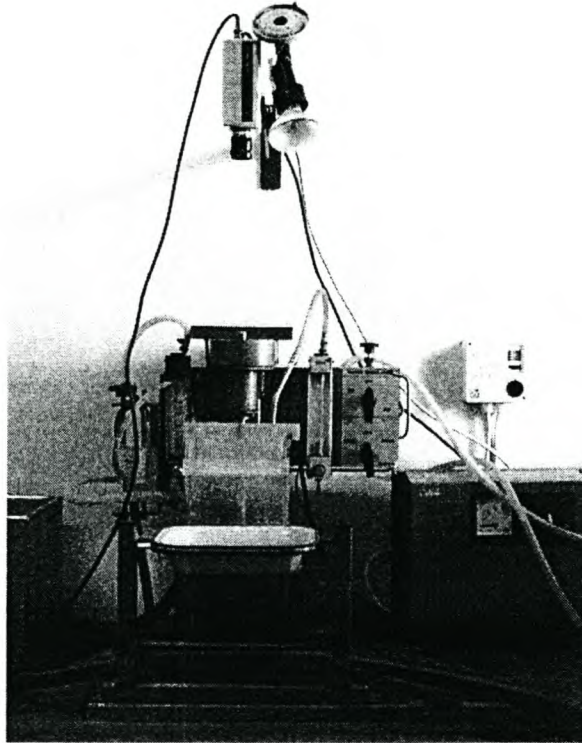


Figure 4.4 Experimental set-up for flotation cell study

4.3.2 QUARTZ AND REAGENTS

In this study a two and three-phase system were investigated. For the investigation of the two-phase study, the surfactants cetyltrimethylammonium bromide (CTAB), with 99 percent (%) purity and octadecylamine (ODA) with 97 percent (%) purity, both obtained from Sigma-Aldrich, were used. The chemical structures of these surfactants are illustrated in Figure 4.5 and Figure 4.6. The two surfactants were used in different ratios, namely 100 percent (%), 90 percent (%) and 80 percent (%) with CTAB as the dominant surfactant.

To investigate the three-phase system, 400 grams (g) of quartz in the form of silica sand (4%-75 μ m) was used as the solid phase. The solid concentration in the system was 14 weight percent (%). This inert solid was used as the main aim of the study was to investigate the behaviour of the system and therefore it was necessary that other interference such as different mineral reactions needed to be excluded. Quartz has a negative zeta-potential for all pH ranges and should be floated by cationic surfactants

(Chen et al., 1991). The same surfactants used in the two-phase system were applied at the same conditions for use in the three-phase system. Approximately five kilograms (kg) of quartz was milled at a time in a ceramic ball-mill. Four solid fractions of quartz were investigated namely $-75\ \mu\text{m}$, $75\text{-}106\ \mu\text{m}$, $106\text{-}150\ \mu\text{m}$ and $150\text{+}\ \mu\text{m}$.

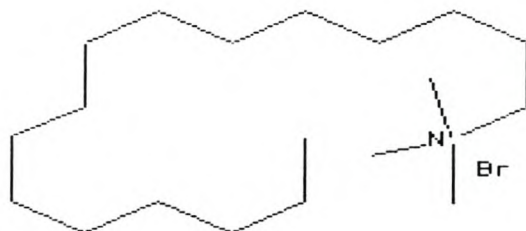


Figure 4.5 Chemical structure of cetyltrimethylammonium bromide



Figure 4.6 Chemical structure of octadecylamine

4.3.3 TEST PROCEDURE

Stock solutions for the two surfactants, CTAB and ODA were made up. The stock solutions' concentrations were 25 millimolar (mM). To ensure that all the crystals in the surfactant stock solution were dissolved, both the solutions were heated in a water bath. The CTAB was heated to $35\ ^\circ\text{C}$ and the ODA to $55\ ^\circ\text{C}$. The stock solutions of the CTAB was permitted to cool down to $25\ ^\circ\text{C}$, but the stock solution of ODA was kept in the water bath at $30\ ^\circ\text{C}$ to ensure that the thick gel formed still flowed. The viscosity of the stock solutions was determined by means of an Ostwald viscometer. The viscosity of the CTAB was $0.998\ \text{mNs/m}^2$ and that of the ODA, $2.390\ \text{mNs/m}^2$.

Three (3) litres (L) of distilled water was used in the flotation cell for the investigation of the two-phase (gas/liquid) system. The required surfactant volume for every experiment was injected into the cell with the use of an Eppendorf Micropipette. Chen et al. (1991) showed that the isoelectric point (iep) for CTAB is at a concentration of 1 millimolar (mM). At this point the zeta potential is zero and at higher concentrations (10 mM) the solution disperses which leads to a decrease in flotation recovery. The best flotation recovery for quartz with CTAB is below the iep and thus the surfactant concentration was held constant at 0.1 millimolar (mM). The surfactant mixture was stirred after injection for 2 minutes at an impeller speed of 1000 rpm before gas introduction. After gas introduction, flotation was permitted for 5 minutes. The aeration rate in the flotation cell was kept constant at 3 litres per minute (l/min). The experiments were carried out at an ambient temperature of 25 °C.

In the case of the three phase (solid/liquid/gas) system, the total volume of the cell, namely three (3) litres (L) was kept constant throughout all experiments. For the three-phase system the surfactants and quartz were once again added to the distilled water. A high agitation speed was used as quartz is a high density particle and in flotation cells high recoveries of high density particles can only be obtained with high agitation speeds (Ahmed & Jameson, 1985). The impeller was started and the mixture was conditioned for 5 minutes before aeration, to ensure that the contents were well mixed. After gas introduction, flotation was permitted for 5 minutes. The recovery of the quartz was investigated by collecting the floated solids and drying it in an oven. The solids were weighed and the percentage recovery calculated. Five different surfactant ratio's were used to test the solid recovery, namely 100 percent (%) CTAB, 90 percent (%) CTAB, 80 percent (%) CTAB, 50 percent (%) CTAB, 80 percent (%) ODA and 100 percent (%) ODA. The recovery of three solid fractions, 75-106 μm , 106-150 μm and 150+ μm were investigated.

4.3.4 IMAGE ANALYSIS

For the aim of this study seven (7) parameters, each describing some physical property of the froth surface were extracted from the froth images. These parameters are vectors that describe either the bubbles in the image or their motion. The

parameters extracted were the average area, average perimeter, average grey level, average speed, number of bubbles, SNE (Small number emphasis, a measure of fineness) and stability. These parameters were extracted every 30 seconds for a total time of 300 seconds per run. All the variables extracted were used in describing the difference between the two and three-phase systems.

4.4 RESULTS AND DISCUSSION

4.4.1 FOAM AND FROTH STRUCTURES

The seven image variables extracted from the image analysis system were used to investigate the structure of a two-phase system (foam) and a three-phase system (froth). These variables were statistically analysed to establish whether the image analysis system could distinguish between systems with different characteristics, as well as to investigate the correlations between the image variables.

4.4.1.1 Two phase system

Principal component analysis

As means to attempt to identify any underlying variables or factors that explain the patterns of correlations within the set of seven observed variables, a principal component analysis (PCA) or factor analysis was performed. Principal component analysis is used as a data reduction technique to identify a small number of factors that explain most of the variance observed in a large number of manifest variables. In this case the seven image variables extracted were reduced to three principal components.

The results from two different two-phase runs, hereafter called Run A and Run B is discussed in the following section. As the same trend could be identified for all two-

phase runs, the results of the remaining three two-phase runs are given in Appendix A. The results from all the two-phase runs are explained in the text.

The variance in the data set explained by the three principal components for the five different runs are summarised in Table 4.1. The variance explained by the three principal components are very high for Run A and Run B, which indicates that the three factors describe the system better than in the case of Run C, Run D and Run E. In all cases the principal components describe more than 84 percent (%) of the variance in the data set.

Table 4.1 Variance explained by principal components in two-phase system

<i>Run</i>	<i>Variance</i>
<i>A</i>	93.6%
<i>B</i>	94.3%
<i>C</i>	85.5%
<i>D</i>	84.4%
<i>E</i>	87.1%

In the first case (Run A), the three principal components explained 93.6 percent (%) of the variance in the data set, while in the second (Run B) the three factors described 94.3 percent (%) of the variance in the data set. The factor matrix shows to what extent the seven parameters are correlated with the factors. The loadings of the variables on the factors show that every factor describe a definite group of foam characteristics. To simplify the interpretation of the factors, the Varimax factor rotation method was used where the projection of the variables is located at the extremities of the factors. The loadings of the factors for Run A and Run B are illustrated in Table 4.2 and Table 4.3. The factor loadings for the remaining three runs (Run C, Run D and Run E) are given in Appendix A. All variables significantly loaded on a factor are marked in bold.

Table 4.2 Factor loadings for three surfactant ratios for Run A

	<i>Factor 1</i>	<i>Factor 2</i>	<i>Factor 3</i>
<i>Average area</i>	0.941	-0.162	0.200
<i>Average grey</i>	0.696	-0.614	0.182
<i>Average perimeter</i>	0.967	0.066	0.069
<i>Average speed</i>	0.167	-0.208	0.951
<i>Number of bubbles</i>	0.705	0.603	-0.204
<i>SNE</i>	-0.044	0.918	-0.302
<i>Stability</i>	-0.660	0.644	0.301

From Table 4.2 it is evident that the first principal component describes the characteristics of the bubbles, including size (*average area*, *average perimeter*), number of bubbles, colour (*average grey*) and stability. The second principal component describes the colour (*average grey*), the fineness (*SNE*) and the stability of the froth and the third component, the movement (*average speed*) of the froth.

Table 4.3 Factor loadings for three surfactant ratios for Run B

	<i>Factor 1</i>	<i>Factor 2</i>	<i>Factor 3</i>
<i>Average area</i>	0.926	-0.349	-0.005
<i>Average grey</i>	0.649	-0.719	-0.009
<i>Average perimeter</i>	0.951	-0.245	-0.006
<i>Average speed</i>	0.128	-0.124	0.951
<i>Number of bubbles</i>	-0.832	0.476	-0.133
<i>SNE</i>	-0.390	0.883	0.0016
<i>Stability</i>	-0.295	0.513	0.740

The foam characteristics explained by the principal components for Run B are summarised in Table 4.3. The first principal component describes, as in the case of Run A (Table 4.2), the bubble characteristics, including area, perimeter, colour (*average grey*) and number of bubbles. The second principal component describes the

colour (*average grey*) and fineness (*SNE*) of the froth and the third principal component, the movement (*average speed*) and stability of the froth.

From the factor loadings of all five runs it is evident that the three principal components describe the following foam characteristics. The one factor describes bubble characteristics, mostly *average area*, *average perimeter* and the *number of bubbles*. The loading of these parameters on the same factor is expected as perimeter and area are both indications of the bubble size. The second describes the colour of the foam (*average grey level*) and the third the movement of the foam (*average speed*). Two variables, namely *stability* and *SNE* are not confined to a specific factor. This is owing to the high correlations between the stability and the other bubble characteristics and the *SNE* with the *number of bubbles*.

As an illustration of how well the image analysis can classify a certain image to a specific group with unique characteristics, the scores of the principal components of the variables extracted from the froth for two different runs are shown in Figure 4.7 and Figure 4.8. The variance of the data explained by the three principal components is shown on every axis. The three different surfactant ratios are identified by different markers: 80% CTAB is identified by the circular marker, the 90% CTAB by the triangle and the 100% CTAB by the square.

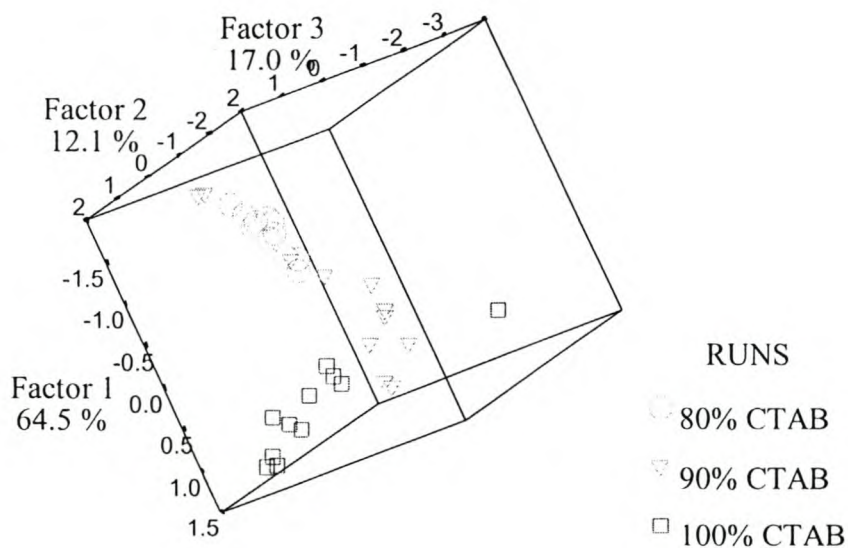


Figure 4.7 Principal Component Analysis for the two-phase system (Run A)

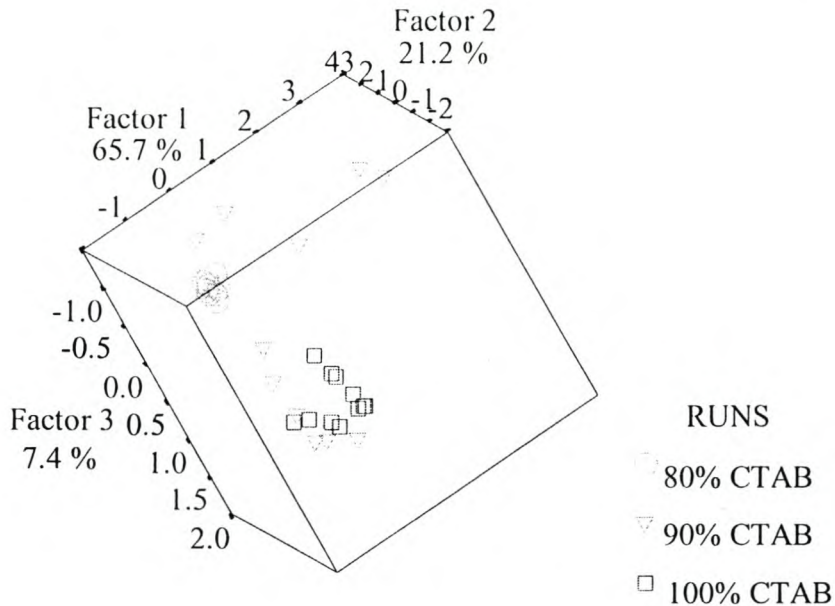


Figure 4.8 Principal Component Analysis for the two-phase system (Run B)

In Figure 4.7 it is clear that three distinct areas are ascribed to the three different surfactant ratios. There is a slight overlapping of values between the 80 percent (%) CTAB and the 90 percent (%) CTAB areas as the 90 percent (%) CTAB group was not as closely grouped together as the other two ratios. The same observation can be made in Figure 4.8 where the 90 percent (%) group again shows overlapping of the other two groups, while the 100 percent (%) and 80 percent (%) groups show definite grouping areas.

It is clear from the results above that the image analysis system can successfully distinguish between different surfactant concentrations in a mixed surfactant system. Every surfactant mixture has unique characteristics and the extent to which these characteristics change with a change in concentration of either surfactant can be quantified by observing the factors, which characteristics they describe, and to what extent they are influenced.

Correlations between variables

As the principal component analysis attempts to identify patterns of correlations between sets of variables, the extent to which the seven image variables are related was established by performing a bivariate correlation on the data. In the bivariate method, Pearson's correlation coefficient is calculated and the results show whether the variables are related within the 0.05 or the 0.01 level. The 0.01 level is indicated with a double asterisk (**) while the 0.05 level is marked by a single asterisk (*). The results of the correlations for the two data sets (Run A and Run B) are given in Table 4.4 and Table 4.5.

Table 4.4 Correlations between seven image variables describing Run A

	<i>Area (Ave)</i>	<i>Grey (Ave)</i>	<i>Perimeter (Ave)</i>	<i>Speed (Ave)</i>	<i>Number Bubble</i>	<i>SNE</i>	<i>Stability</i>
<i>Area (Ave)</i>	1	-	-	-	-	-	-
<i>Grey (Ave)</i>	-0.630**	1	-	-	-	-	-
<i>Perimeter (Ave)</i>	-0.777**	0.495**	1	-	-	-	-
<i>Speed (Ave)</i>	-0.858**	0.607	-0.805**	1	-	-	-
<i>Number Bubble</i>	0.780**	-0.280	-0.653**	-0.779**	1	-	-
<i>SNE</i>	-0.713**	-0.168	-0.640**	-0.711**	0.926**	1	-
<i>Stability</i>	0.409*	-0.459**	0.006	-0.448**	0.367*	0.228	1

**Correlation is significant at the 0.01 level

*Correlation is significant at the 0.05 level

It is evident from Table 4.4 that a strong correlation between the *stability* and the other variables investigated, excluding *average perimeter* and *SNE* exists. The

stability is related within the 0.01 level with the colour (*average grey level*) and the movement of the bubbles (*average speed*) and within the 0.05 level with the size (*average area*) and *number of bubbles*. As expected the *SNE* and *number of bubbles* are highly correlated as it is known that the *SNE* is a useful secondary indication of bubble size (Botha, 1999a). As the *SNE* is a measurement of fineness, a high value of *SNE* is obtained when an image consists of many grey level variations per area. A smooth area will have a lower *SNE* value.

The correlations between the seven image variables for Run B are given in Table 4.5.

Table 4.5 Correlations between seven image variables describing Run B

	<i>Area</i> (<i>Ave</i>)	<i>Grey</i> (<i>Ave</i>)	<i>Perimeter</i> (<i>Ave</i>)	<i>Speed</i> (<i>Ave</i>)	<i>Number</i> <i>Bubble</i>	<i>SNE</i>	<i>Stability</i>
<i>Area</i> (<i>Ave</i>)	1	-	-	-	-	-	-
<i>Grey</i> (<i>Ave</i>)	0.844**	1	-	-	-	-	-
<i>Perimeter</i> (<i>Ave</i>)	0.969**	0.782**	1	-	-	-	-
<i>Speed</i> (<i>Ave</i>)	0.108	0.080	0.098	1	-	-	-
<i>Number</i> <i>Bubble</i>	-0.914**	-0.879**	-0.866**	-0.275	1	-	-
<i>SNE</i>	-0.685**	-0.852**	-0.611**	-0.101	0.724**	1	-
<i>Stability</i>	-0.484**	-0.625**	-0.451**	0.523**	0.383*	0.520**	1

**Correlation is significant at the 0.01 level

*Correlation is significant at the 0.05 level

For Run B, the *stability* of the froth is correlated, either on the 0.01 or the 0.05 level with all other six variables. The stability of the froth is thus dependent on all the other characteristics of the froth analysed here. The correlation tables show that the bubble

characteristics such as *average area*, *average perimeter* and *number of bubbles* are highly correlated as expected. As in the case of Run A, the *SNE* and *number of bubbles* are highly correlated. It should also be noted that the average speed is highly correlated with the stability, implying that the movement of the foam in the cell will have a substantial effect on the foam stability.

4.4.1.2 Three phase system

It is clear that the image analysis system can differentiate between foam of different concentrations and that each system has unique characteristics. To determine whether the image analysis system can differentiate between systems that contains no solids and those that do contain solids, a three-phase system was investigated.

Principal component analysis

In this section two systems, a three-phase system and a two-phase system, discussed in Section 4.4.1.1) are compared. In each case the two-phase system at a certain surfactant ratio is compared to one of the quartz particle sizes tested at the same surfactant ratio, i.e. a two-phase system at 100 percent (%) CTAB is compared with a three-phase system at 100 percent (%) CTAB.

As in the case of the two-phase system a principal component analysis was performed to identify underlying variables or factors that explain the patterns of correlations within the set of observed variables. The seven image variables extracted for the three-phase system were reduced to three principal components.

The variance explained by the three principal components in each of the four solid particle sizes are summarised in Table 4.6 while the factor loadings for the remaining three-phase systems are given in Appendix A.

Table 4.6 Variance explained by principal components in two-phase and three-phase systems

Particle size [μm]	100 % CTAB [%]	90 % CTAB [%]	80 % CTAB [%]
-75	94.1%	89.9%	91.9%
75-106	92.0%	88.4%	89.0%
106-150	94.8%	90.1%	95.7%
150+	91.9%	92.1%	93.1%

The three principal components characterise the system very well as it explain more than 88 percent (%) of the variance in all four cases.

Just as in the case of the two-phase system, the loadings of every variable on the factors can be observed. The factor loadings for the three-phase system containing different surfactant concentrations and a solid particle size of 106-150 μm are summarised in Table 4.7 to Table 4.9. The factor loadings for the remaining three quartz particle sizes are given in Appendix A.

Table 4.7 Factor loadings for three-phase system with 100% CTAB and solid particle size 106-150 μm

	Factor 1	Factor 2	Factor 3
Average area	0.916	0.326	-0.138
Average grey	0.547	0.700	-0.303
Average perimeter	0.934	0.257	-0.132
Average speed	-0.139	0.078	0.985
Number of bubbles	-0.677	0.683	0.053
SNE	-0.198	0.957	-0.015
Stability	-0.609	0.711	0.287

Table 4.8 Factor loadings for three-phase system with 90% CTAB and solid particle size 106-150 μm

	<i>Factor 1</i>	<i>Factor 2</i>	<i>Factor 3</i>
<i>Average area</i>	-0.734	0.561	0.180
<i>Average grey</i>	-0.057	0.942	0.156
<i>Average perimeter</i>	-0.730	0.583	-0.035
<i>Average speed</i>	0.087	0.184	0.968
<i>Number of bubbles</i>	0.500	-0.652	-0.369
<i>SNE</i>	0.937	-0.240	-0.062
<i>Stability</i>	0.872	0.095	0.364

Table 4.9 Factor loadings for three-phase system with 80% CTAB and solid particle size 106-150 μm

	<i>Factor 1</i>	<i>Factor 2</i>	<i>Factor 3</i>
<i>Average area</i>	0.953	0.234	0.123
<i>Average grey</i>	0.590	0.009	0.777
<i>Average perimeter</i>	0.957	0.147	0.092
<i>Average speed</i>	0.553	0.814	0.029
<i>Number of bubbles</i>	-0.904	-0.270	-0.197
<i>SNE</i>	-0.005	0.318	0.928
<i>Stability</i>	0.115	0.920	0.329

In Table 4.7 to Table 4.9 the factor loadings for the solid particle size 106-150 μm in the three different surfactant concentrations are shown. The factor loadings for the 100 percent (%) CTAB case show that the first factor describe the bubble size characteristics, namely *average area*, *average perimeter*, *number of bubbles* as well as the *stability* of the bubbles. The second factor describes the colour (*average grey*), fineness (*SNE*) and *stability* of the bubbles, while the third factor describes the bubble movement (*average speed*). The factor loadings of the second case, 90 percent (%) CTAB is very similar to that of the 100 percent (%) scenario. The first factor

describes the bubble size characteristics including the *stability*, the second the colour (*average grey*) and the fineness (*SNE*) and the third the movement (*average speed*) of the bubbles. In the case of the 80 percent (%) CTAB concentration, the factor loadings differ from that of the 100 percent (%) and 90 percent (%) cases. The first factor describes only the bubble characteristics that have to do with the shape and size of the bubbles (*average area, average perimeter and number of bubbles*), the second describes the *average speed* and *stability* of the bubbles and the third describes the colour (*average grey*) and fineness (*SNE*) of the bubbles.

Considering the results from all the particle sizes, the general trend for the factor loadings is the same as for the two-phase system. The bubble size characteristics (*average area, average perimeter and number of bubbles*) are explained in the first factor, the colour of the foam (*average grey*) in the second and the movement of the foam in the third (*average speed*). Once again the variables *stability* and *SNE* cannot be restricted to a specific factor.

The scores of the three principal components of the variables extracted from the froth associated with the two-phase system and with the three-phase system for the particle size 106-150 μm , are illustrated in Figure 4.9 to Figure 4.11. The scores of the three principle components for the remaining three particle sizes are given in Appendix A.

It has to be noted that the two-phase system in all four cases are four different runs executed on the same day as the three-phase system to ensure the same experimental conditions as far as possible. Figure 4.9 shows the results for the flotation of 106-150 μm quartz with a 100 percent (%) CTAB concentration, Figure 4.10 the results at 90 percent (%) CTAB and Figure 4.11 the results at 80 percent (%) CTAB. The three different surfactant ratios are identified by different markers: 80% CTAB is identified by the circular marker, the 90% CTAB by the triangle and the 100% CTAB by the square. The diamond marker identifies the three-phase group.

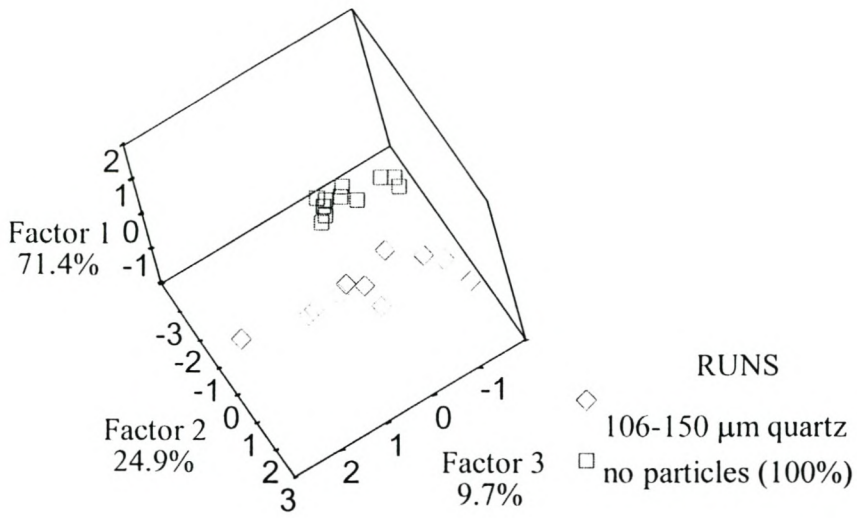


Figure 4.9 Principal Component Analysis for two-phase and three-phase system containing 106-150 μm particles at 100% CTAB

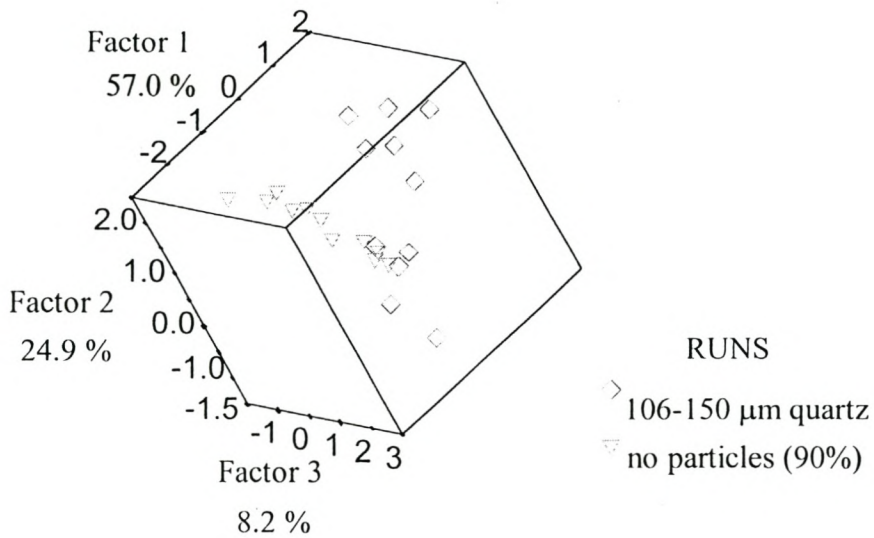


Figure 4.10 Principal Component Analysis for two-phase and three-phase system containing 106-150 μm particles at 90% CTAB

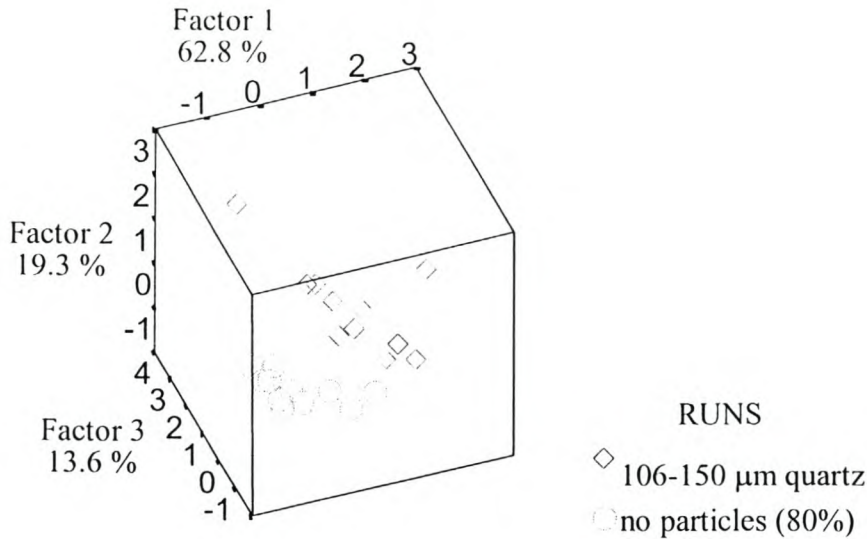


Figure 4.11 Principal Component Analysis for two-phase and three-phase system containing 106-150 μm particles at 80% CTAB

A successful distinction between all solid particle sizes and the case where 100 percent (%) CTAB was used can be observed. Less distinct areas are observed in the case of the 90 percent (%) CTAB as the three-phase system is spread out and has more outliers. The system can thus also successfully distinguish between two different phase groups and it is possible to predict the change in foam characteristics when particles are present by interpreting the foam characteristics entailed by each factor and observing the change between the two groups.

Classification of groups

To investigate how well the image analysis system predicts an image as belonging to a specific system from its characteristics correctly, a linear discriminant analysis was done. A predictive model of group membership based on the observed characteristics of each case was build. A discriminant function is generated, based on linear combinations of the predictor variables that provide the best discrimination between

groups. The discriminant function is generated from a sample of cases for which the group membership is known.

Two different scenario's were investigated, namely the two-and three-phase system as a whole (thus including all three concentrations without solids as one group and the same runs with solids as the other) and all six runs separately. All results from the classification of the four three-phase systems are summarised and discussed in detail. The three-phase system containing 106-150 μm solids is given as illustration while the detailed tables for the classification of groups for the other three solid particle sizes are given in Appendix A.

The classification between the two main groups for the system containing 106-150 μm particles is summarised in Table 4.10. The first group is the two-phase group of 11 cases each of 100 percent (%) CTAB, 90 percent (%) CTAB and 80 percent (%) CTAB. The second group is the same surfactant ratios as mentioned above, containing solids of the particle size 106-150 μm . It was found that the image analysis system can identify between the two-and three-phase runs and classifies them 98.5 percent (%) accurately into their correct groups.

Table 4.10. Classification results between two main groups for the solid particle size 106-150 μm

<i>Actual group</i>	<i>Cases</i>	<i>Predicted group membership</i>	
		1	2
1	33	33	0
%		100	0
2	33	1	32
%		3	97.0

Percentage of "grouped" cases correctly classified: 98.5%

In the second case all six runs had to be classified into their own group and not just into their type. A distinction is thus made between all concentrations with and without solid particles. As can be observed in Table 4.11, the model showed an accurate classification of 75.8 percent (%).

Table 4.11 Classification results for six groups for the solid particle size 106-150 μm

Actual group	Cases	Predicted group membership					
		1	2	3	4	5	6
1	11	9	2	0	0	0	0
%		81.8	18.2	0	0	0	0
2	11	1	6	2	2	0	0
%		9.1	54.5	18.2	18.2	0	0
3	11	0	0	11	0	0	0
%		0	0	100	0	0	0
4	11	0	0	1	10	0	0
%		0	0	9.1	90.9	0	0
5	11	0	0	1	1	6	3
%		0	0	9.1	9.1	54.5	27.3
6	11	0	0	0	0	3	8
%		0	0	0	0	27.3	72.7

Percent of “grouped” cases correctly classified: 75.8%

where the groups describe the following concentrations:

- 1 100% CTAB
- 2 90% CTAB
- 3 80% CTAB
- 4 100% CTAB containing quartz
- 5 90% CTAB containing quartz
- 6 80% CTAB containing quartz

From Table 4.11 it is evident that the foam from the 100 percent (%) CTAB concentration with and without solids are classified very well with correct classification of 81.8 percent (%) and 90.9 percent (%) respectively. The classification of the foam generated from 80 percent (%) CTAB with and without solids also show high correct classification, with values of 100 percent (%) and 72.7 percent (%)

respectively. However, the groups of 90 percent (%) CTAB were classified poorly into correct groups. This is in accordance with the factor analysis graphs where the data points belonging to 90 percent (%) CTAB group did not form a close group, but instead some data points seem to group with either the 100 percent (%) CTAB or 80 percent (%) CTAB groups.

The poor classification of the group containing 90 percent (%) CTAB as well as the findings that the data points belonging to the 90 percent (%) group is scattered in the factor analysis graph may be as a results of the nature of the ODA liquid. The stock solution of ODA has a high viscosity, which makes injection of the surfactant into the cell with the Eppendorf Micropipette difficult. It is thus possible that the high viscosity of the ODA lead to inaccurate surfactant dosage, which explains the tendency of the 90 percent (%) to scatter. It is thus recommended that a less viscous surfactant be used for future flotation studies if a high repeatability of results is required.

The classification for the remaining three particle sizes is summarised, with the results for the 106-150 μm particle size in Table 4.12 and Table 4.13. The complete tables showing the classification of the remaining three particle sizes are given in Appendix A.

Table 4.12 Classification results between two main groups for all solid particle sizes

<i>Particle size [μm]</i>	<i>Groups classified correctly [%]</i>
-75	97.0
75-106	93.8
106-150	98.5
150+	98.5

Table 4.13. Classification results for six groups for the all solid particle sizes

Particle size [μm]	Groups classified correctly [%]
-75	65.2%
75-106	66.2%
106-150	75.8%
150+	74.2%

The system therefore classifies the data into the correct group above 95 percent (%) accurate when two groups, namely the two-phase and three-phase groups are considered, and above 65 percent (%) when there is differentiated between the runs in the two groups. The data obtained by the image analysis system can thus be classified very successfully for both phase systems but with a substantially higher accuracy when the two main groups as a whole are compared.

4.4.2 COMPARISON OF THE STABILITY OF FOAM AND FROTH

The stability of the two-phase foam and the three-phase froth was extracted as an image variable by the image analysis system. For investigation of the two-phase system, the stability of the three different surfactant ratios, 100 percent (%) CTAB, 90 percent (%) CTAB and 80 percent (%) CTAB are compared to one another. The stability of the four quartz sizes at every surfactant concentration is compared to investigate the effect of particle size on the stability of froth.

The data points obtained for each run is the average value of the total number of runs done for that specific concentration or solid particle size. The data is illustrated from 30 seconds (s) to 300 (s) as the values of the stability obtained by the image analysis system at time zero could be inaccurate due to slow initial foam formation for some of the surfactant ratios. It should be noted that the *y-axis* in all the figures in this section describes the *instability* of the foam/froth where a value of zero (0) is the most stable value and a value of one (1) the least stable.

4.4.2.1 Influence of surfactant concentration on stability

Stability of foam

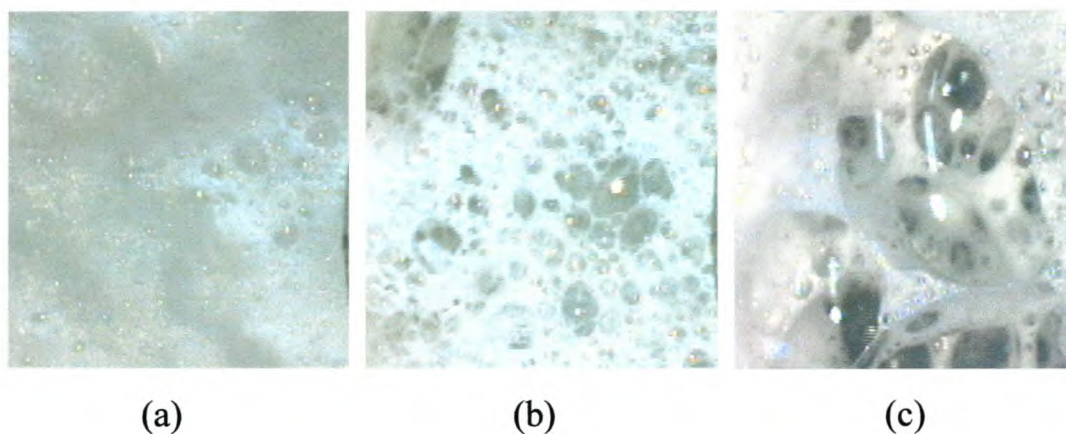


Figure 4.12 Foam images showing 100% CTAB, 90% CTAB and 80% CTAB

The state of the foam for the different CTAB and ODA concentrations are illustrated in Figure 4.12. It is evident from the foam images that the CTAB form a foam that consists of small bubbles which are very closely packed. As the quantity of ODA in the foam mixture increases, the foam appearance change from being small bubbles to a foam that produces less dense foam with big bubbles. The ODA produces oily foam with big unstable bubbles that burst rapidly.

The difference in stability for three surfactant ratios is shown in Figure 4.13. The foam of 100 percent (%) CTAB is the most stable for the first 200 seconds (s) and again after 240 seconds (s). The starting value of the 90 percent (%) CTAB curve is higher than that of the 80 percent (%) curve, but no conclusion can be made on the rank of stability between the 90 percent (%) CTAB and the 80 percent (%) CTAB curves. The two curves seem to have the same form in regards to peaks, but the graphs are constantly crossing each other so that no conclusion regarding the rank of

stability can be drawn. The foam generated from the 100 percent (%) CTAB is thus more stable than any combination of CTAB and ODA.

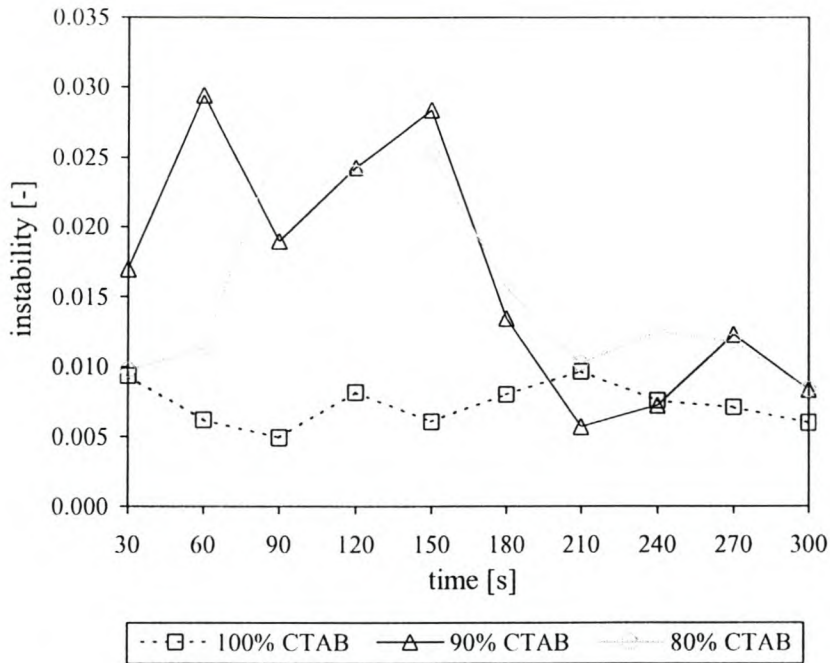


Figure 4.13 Influence of surfactant concentration on foam stability

To verify whether the peaks observed in the stability data extracted from the flotation cell runs are due to movement in the cell, a stability test was done where the foam from a 100 percent (%) CTAB run was generated and removed from the running cell. To quantify the stability measurements of the image analysis system where there is no movement of the foam other than bubble coalescence or collapse, a foam layer of approximately 200 millimetres (mm) thick was put in a container. Three main regions in the instability curve were observed. The regions are illustrated by three foam images, Figure 4.15a to 4.15c.

From Figure 4.14, it is evident that the foam reaches a constant stability value immediately. The foam is a fine dense white foam and the bubble collapse and the drainage of the liquid film are slow. This value is retained for 66 minutes. (Figure 4.15a). After this period, the figure shows a sudden jump in instability. The instability increases as the foam becomes more transparent and more bubble boundaries appear.

This increase in instability reaches a maximum and decrease thereafter for a period of 40 minutes (Figure 4.15b). The instability decreases as more bubble coalesces and less bubble boundaries are visible. This decrease continues until only a water layer (which is interpreted as being stable) is left with a small bubble layer with stable individual bubbles (Figure 4.15c).

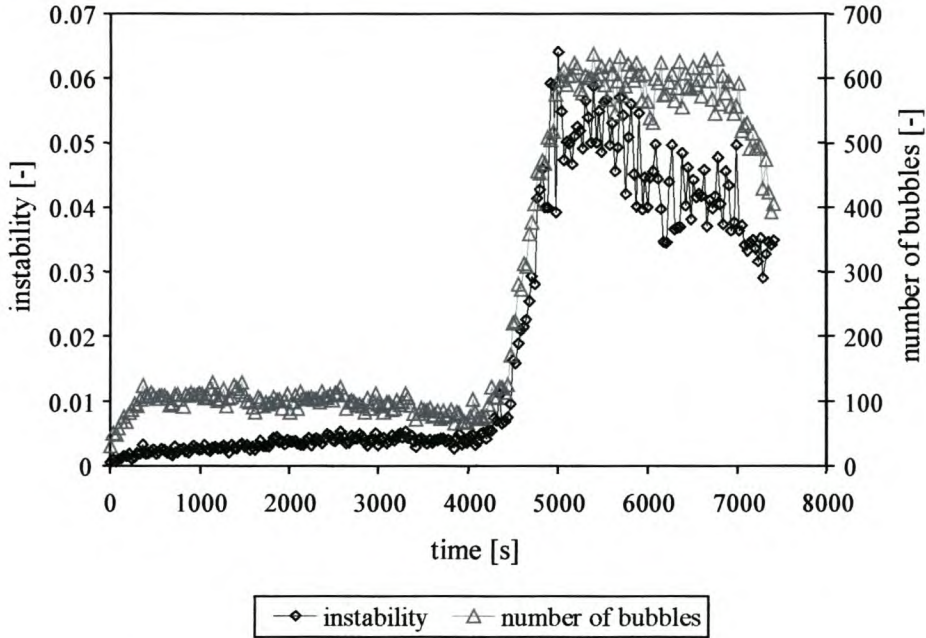


Figure 4.14 Stability test

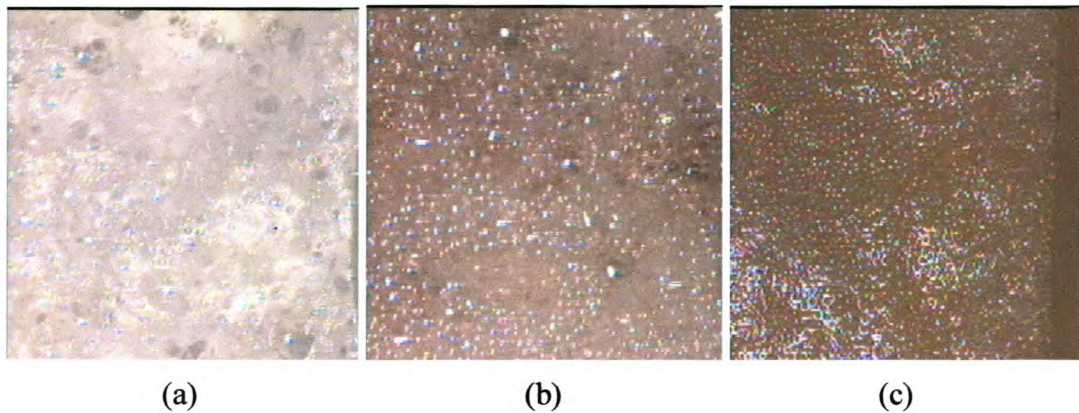


Figure 4.15 Froth images at different time steps in stability test

The bubble size distribution (Figure 4.14) follows a similar trend as the stability of the froth and the number of bubbles is strongly correlated. The number of bubbles is high

in the beginning as the CTAB forms a dense foam that contains a high number of small bubbles. It can however be seen that between 0 and 4000 seconds (s) the system recorded the number of bubbles lower or around 100 per frame. Compared with the visual observation this is not correct. This incorrect calculation of the number of bubbles is caused by the measurement problem in the system caused by fine bubbles (Botha, 1999a). As the liquid film drains and larger bubbles are formed, the system is able to recognise bubbles size and give the correct number of bubbles in each frame. This explains the rapid jumps to higher bubble numbers after 4000 seconds (s).

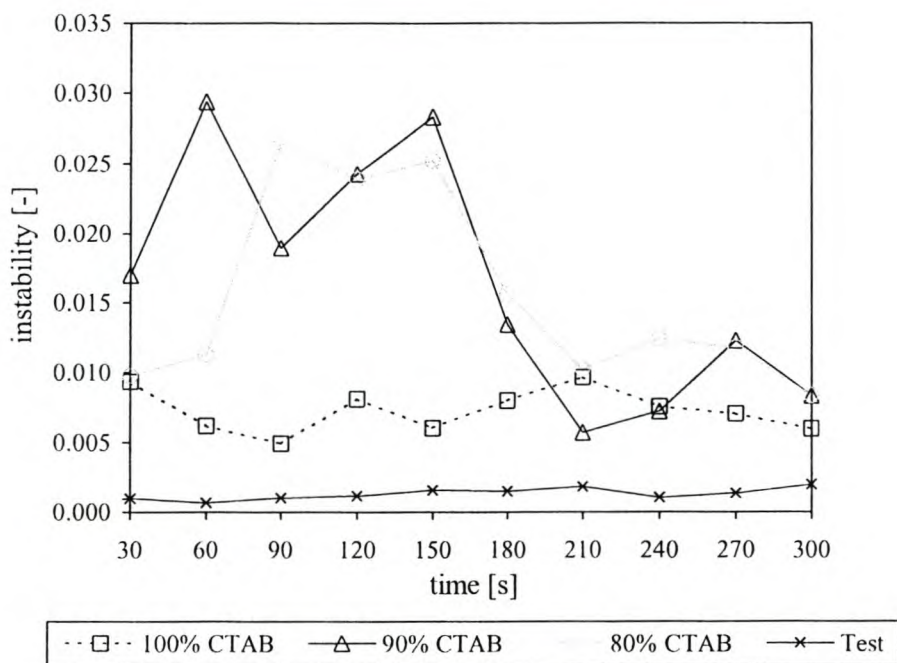


Figure 4.16 Comparison of stability of foam in flotation cell and stability test curve

Figure 4.16 shows the difference between the instability curve obtained from the stability test and the curves obtained from the flotation cell. It is evident that peaks in all three instability curves from the flotation cell is absent in the stability test curve. These peaks are thus as a result of movement in the flotation cell and can be ascribed to the time in the cell operation where the foam layer overflowed and a high speed of froth flow in the horizontal direction was achieved. The peaks do not always occur at the same time as the characteristics of the three foams were different and the foams were not scraped at the same time of operation. After every maximum peak a valley

can be observed as the layer of foam underneath the top layer is observed by the system. This layer is more stable than the top layer that has been scraped off.

To support this statement that high stability values are caused by the movement of foam in the cell, the average speed values obtained by the image analysis system are compared to the stability curves. The average speed is a measure of any movement of the foam. The average speed and stability curves for the three surfactant concentrations are illustrated in Figure 4.17 to Figure 4.19.

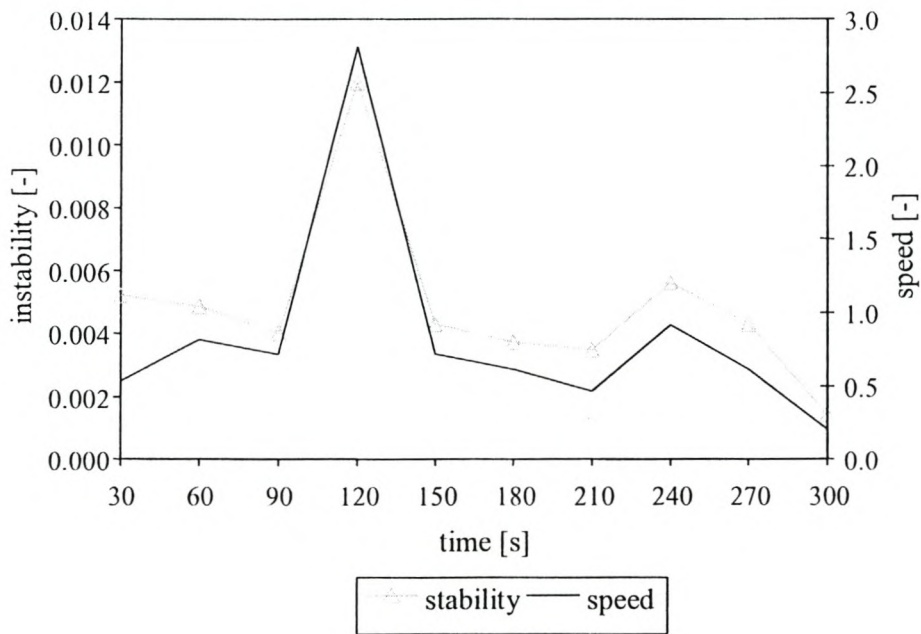


Figure 4.17 Average speed and stability of foam for 100% CTAB

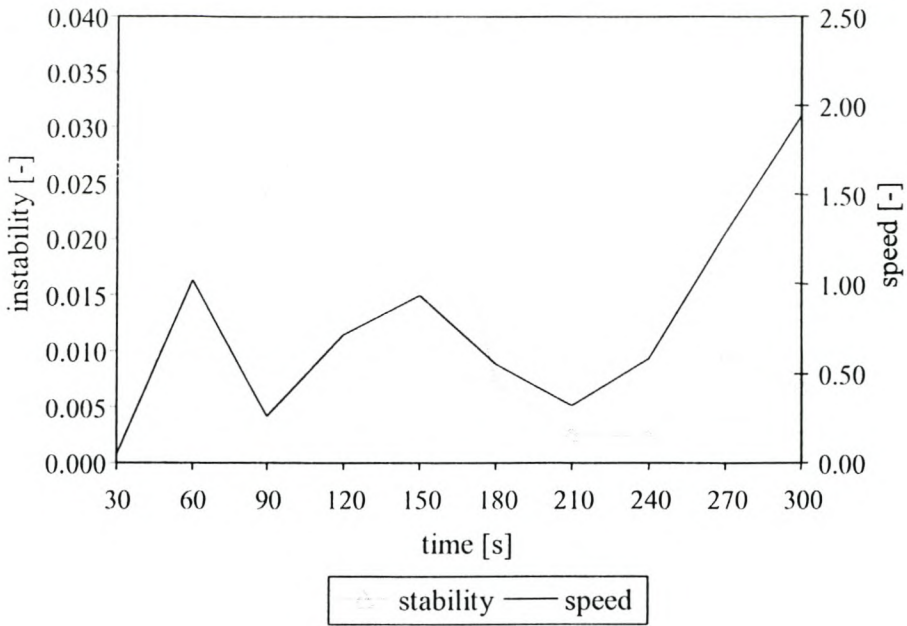


Figure 4.18 Average speed and stability of foam for 90% CTAB

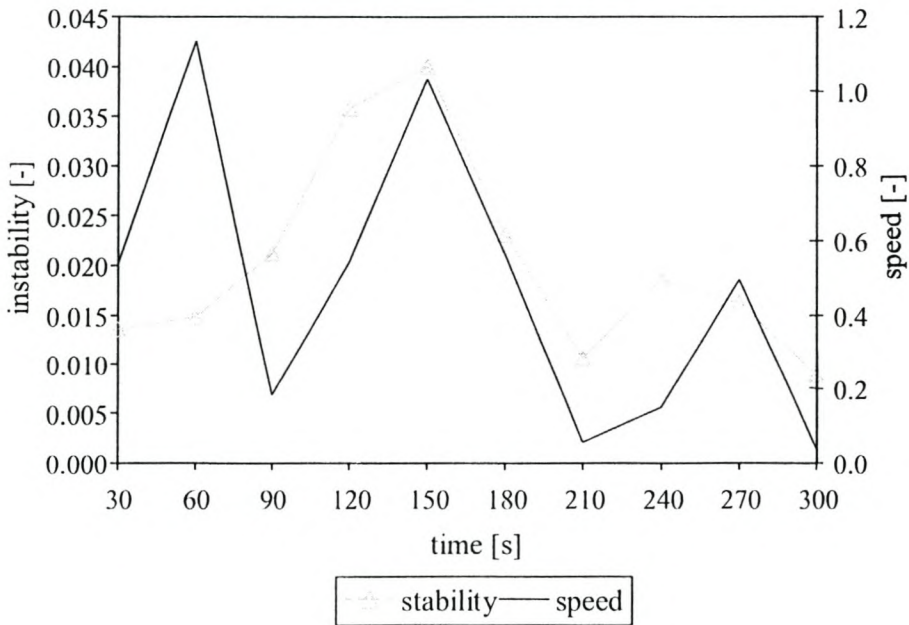


Figure 4.19 Average speed and stability of foam for 80% CTAB

It is evident from Figure 4.17 to Figure 4.19 that the highest stability values corresponds with high values obtained for the average speed at the beginning of the flotation run, with the exception of the average speed peak at 60 seconds (s) in the run illustrating the 80 percent (%) CTAB concentration. High values of average speed is

also obtained later in the flotation run at 300 seconds (s) for the 90 percent (%) CTAB concentration and at 270 seconds (s) for the 80 percent (%) concentration. These large speed values are not accompanied by very high instability values as most of the foam has been scraped off the cell. The instability values obtained at these times point to bubble formation or bubble coalescence and although the movement is still evident in the system, the stability value is smaller as in the beginning of the cell.

Stability of froth

The stability curves for specific quartz sizes at three CTAB concentrations are illustrated in Figure 4.20 to Figure 4.23. In none of the graphs can an accurate conclusion be made on the instability difference between the three concentrations. The curves show similar peaks at some points and inverse peaks at others. The curves cross one another repeatedly so that no curve is ranked more unstable than the others over the total time of 270 seconds (s) but only over certain time instances.

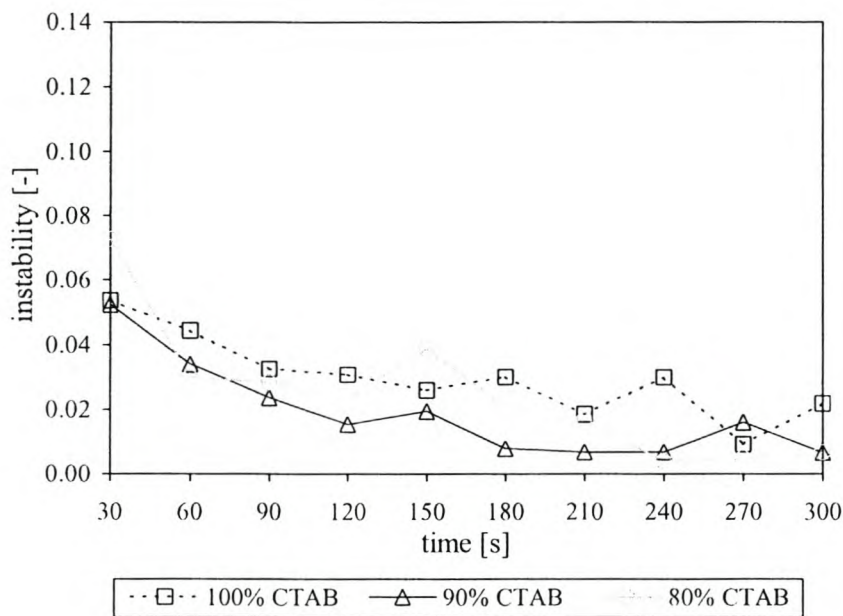


Figure 4.20 Influence of surfactant concentration on froth stability containing $-75 \mu\text{m}$ quartz particles

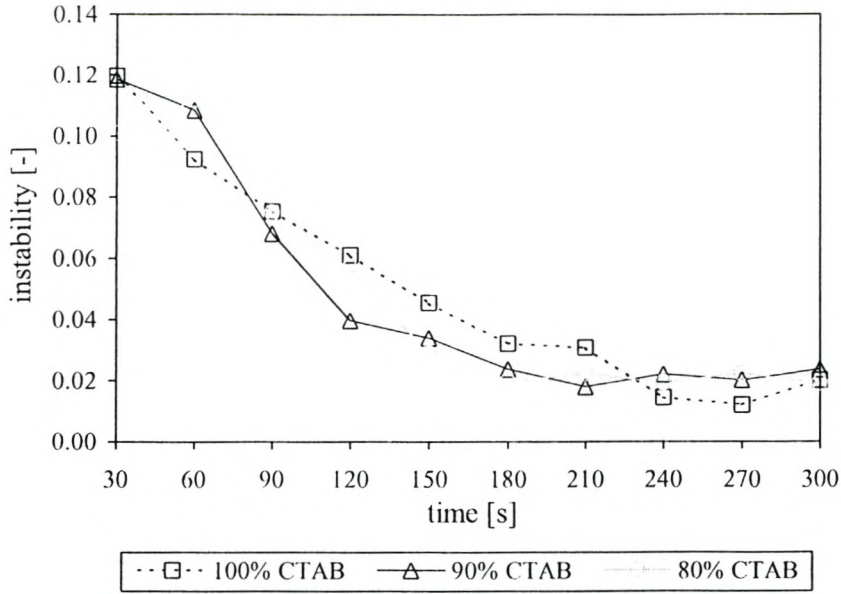


Figure 4.21 Influence of surfactant concentration on froth stability containing 75-106 μm quartz particles

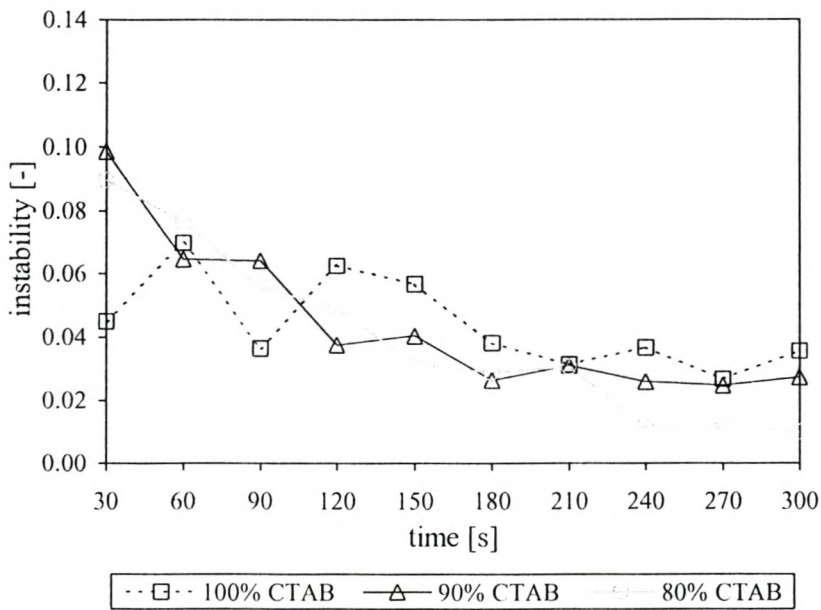


Figure 4.22 Influence of surfactant concentration on froth stability containing 106-150 μm quartz particles

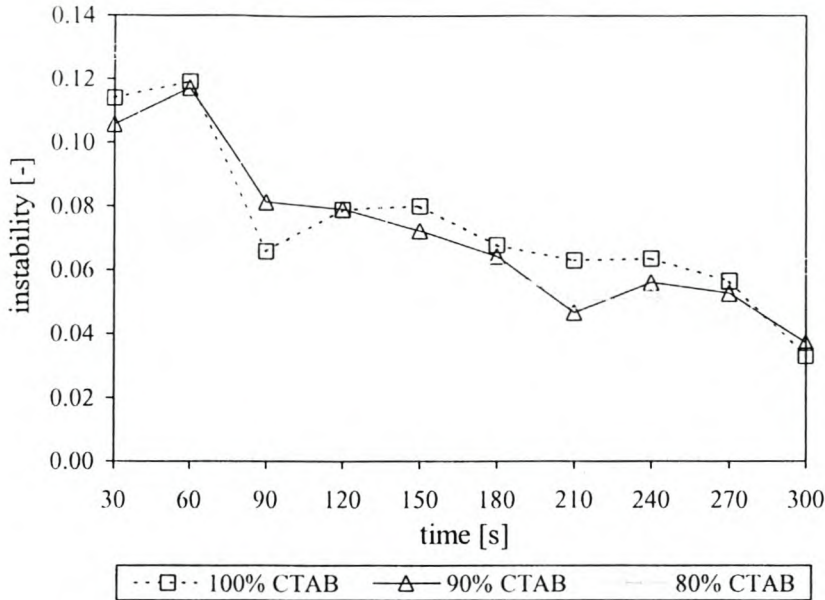


Figure 4.23 Influence of surfactant concentration on froth stability containing 150+ μm quartz particles

4.4.2.2 Influence of particles on stability

From Figure 4.20 to Figure 4.23 it seems as if, although no conclusion can be made on the effect a difference in surfactant concentration has on froth stability, that the instability is different for every particle size. To investigate the effect of particle size on the instability of froth, the four particle sizes are compared for all three surfactant concentrations in Figure 4.24 to Figure 4.26. In all three figures, the froth containing the $-75 \mu\text{m}$ solids are the most stable, and the froth containing the $150+ \mu\text{m}$ solids the most unstable. This behaviour is the same throughout except for the minimum peak of the $150+ \mu\text{m}$ curve at 60 seconds (s) and the maximum peak of the $-75 \mu\text{m}$ curve at 150 seconds (s) in the figure describing the 80 percent % CTAB concentration. Similar peaks can be observed in the 100 percent (%) CTAB concentration curves where the $150+ \mu\text{m}$ curve have a maximum value at 90 seconds (s) and the $-75 \mu\text{m}$ curve a minimum value at 240 seconds (s).

The curves describing the intermediate fractions, 75-106 μm and 106-150 μm show the same behaviour in all three figures. For the first ± 120 seconds the froth containing 106-150 μm sized particles is more stable than that containing 75-106 μm particles. After ± 120 seconds (s) the curves cross and the froth containing particles of size 75-106 μm shows a lower value of instability than that containing 106-150 μm . In the figure showing the stability at 80 percent (%) CTAB the two curves make another cross-over to change the instability with respect to one another.

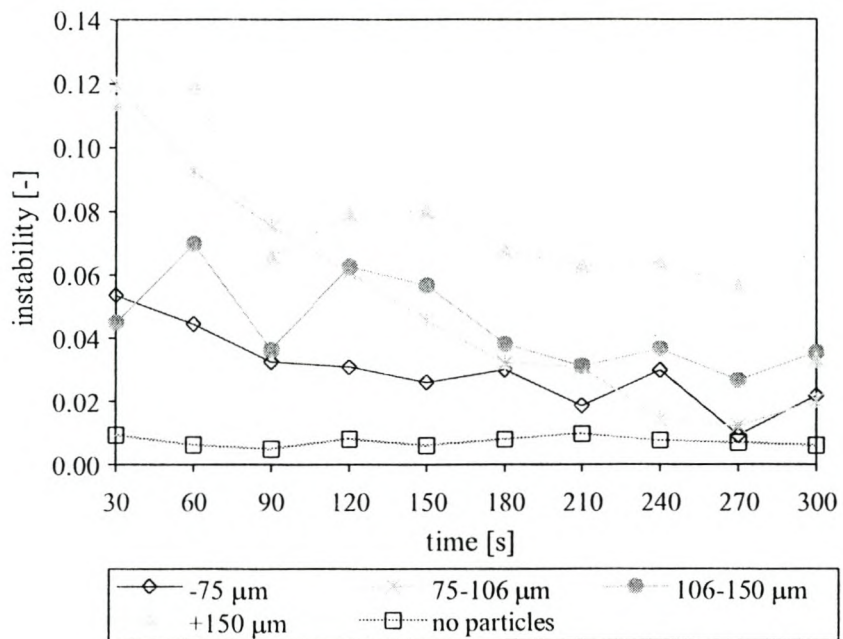


Figure 4.24 Influence of particle size on froth stability for 100% CTAB

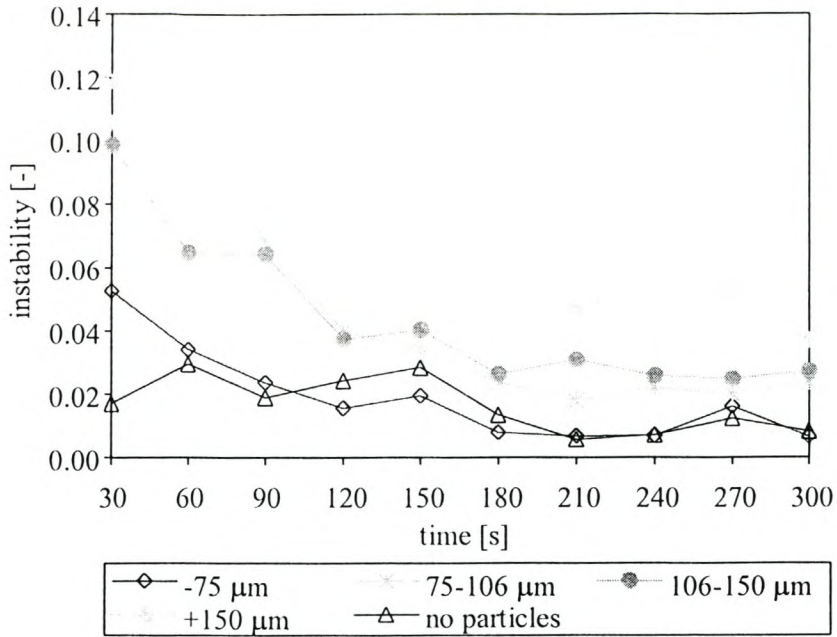


Figure 4.25 Influence of particle size on froth stability for 90% CTAB

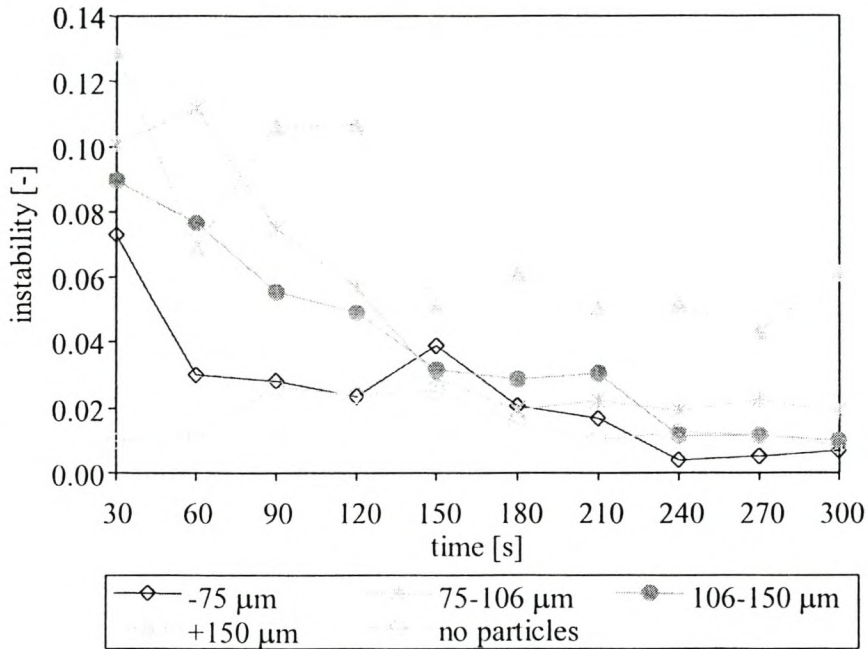


Figure 4.26 Influence of particle size on froth stability for 80% CTAB

To conclude whether the particles destabilise or stabilise a froth, the instability of the clean runs (no particles) are compared to all particle sizes at the same surfactant

concentration in Figure 4.24 to Figure 4.26. In Figure 4.24 it is evident that the 100 percent (%) CTAB concentration the clean run is more stable than any of the particle runs. In the 90 percent (%) (Figure 4.25) and 80 percent (%) (Figure 4.26) CTAB concentrations, the instability of the run containing $-75 \mu\text{m}$ solid particles is very close to the instability values obtained for the runs containing no solids. In some instances the runs containing $-75 \mu\text{m}$ particles are more stable than the runs containing no particles. The stability behaviour of the smallest fraction is in accordance with Dippenaar (1982a), who stated that the higher stability froth containing small particles might be due to the large number of fines present. The fines form a packed monolayer and this prevents the particles to be forced out of the froth structure. Szatkowski & Freyburger (1985) also found that fine quartz particles render bubbles to be more resistant to coalescence. Jameson (1999) found that the contact angle of CTAB on silica quartz is 60° . As this is a moderate hydrophobicity, the results are also in accordance with Johansson & Pugh (1992) and Moudgil & Gupta (1989). In both these studies it was proven that small particles ($<44 \mu\text{m}$) with hydrophobicity between 50° and 65° stabilise froth.

The other three particle sizes are less stable than the clean runs in all CTAB concentrations. The same peaks and valleys, due to horizontal movement of the froth, as described for the foam without solids can be observed in the froth stability curves. To investigate the effect of froth movement on froth stability in the three-phase system, the average speed curves is compared to the instability curves as recorded by the image analysis system. The system containing the particle size $106\text{-}150 \mu\text{m}$ is illustrated for all three surfactant concentrations in Figure 4.27 to Figure 4.29. From the figures it is evident that a higher value of instability is obtained when the froth displays high movement.

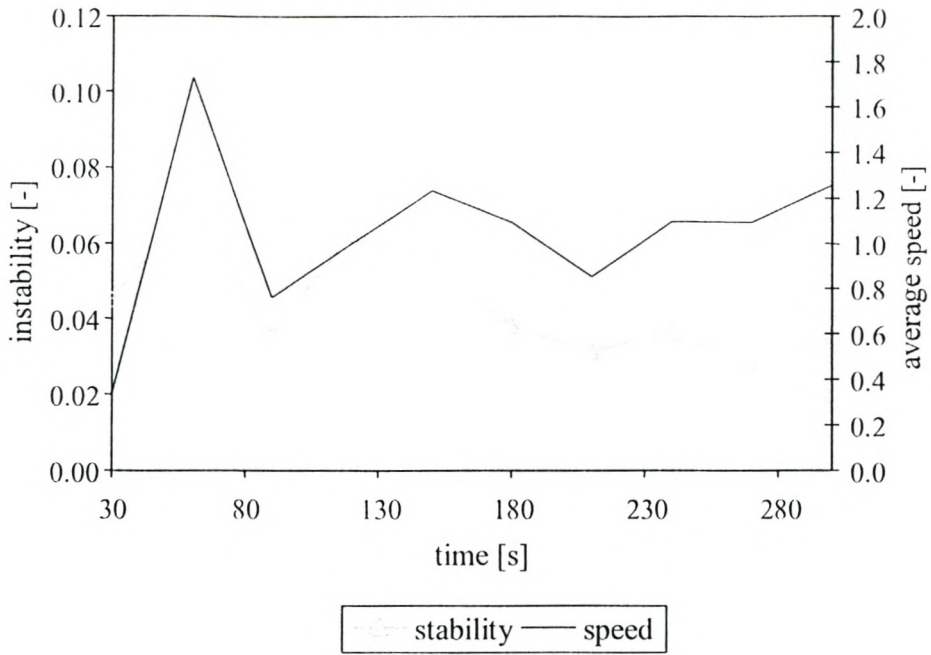


Figure 4.27 Average speed of foam for 100% CTAB containing 106-150 μm quartz particles

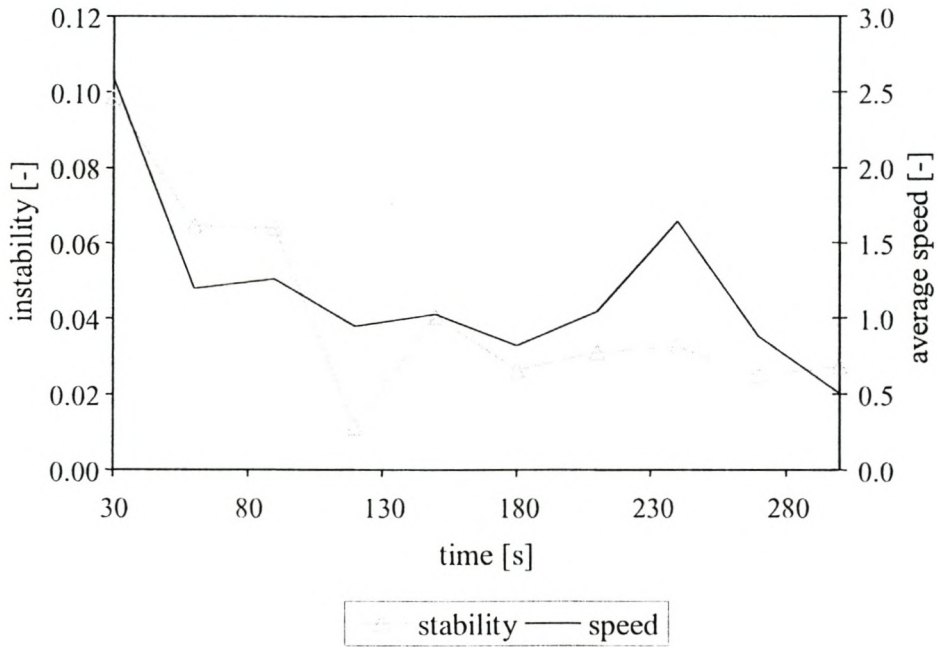


Figure 4.28 Average speed of foam for 90% CTAB containing 106-150 μm quartz particles

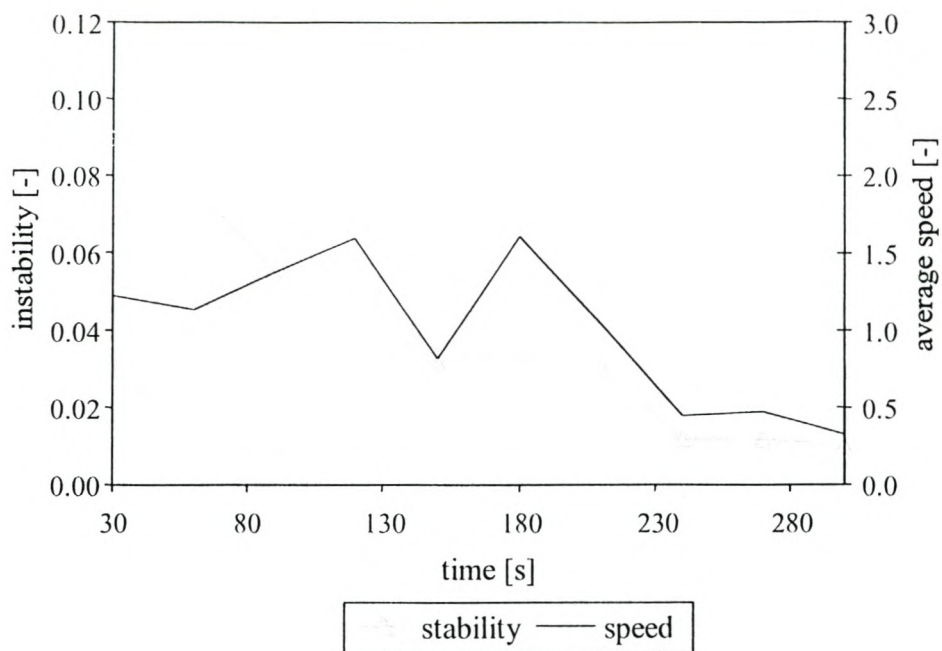


Figure 4.29 Average speed of foam for 80% CTAB containing 106-150 μm quartz particles

4.4.3 RECOVERY

4.4.3.1 Influence of surfactant concentration on recovery

Six different concentration ratios for CTAB and ODA were investigated to obtain the percentage recovery of quartz particles at different surfactant concentrations. Three solid particle sizes were investigated, namely 75-106 μm , 106-150 μm and 150+ μm . Figure 4.30 summarises the results of the three solid fractions with varying surfactant concentration.

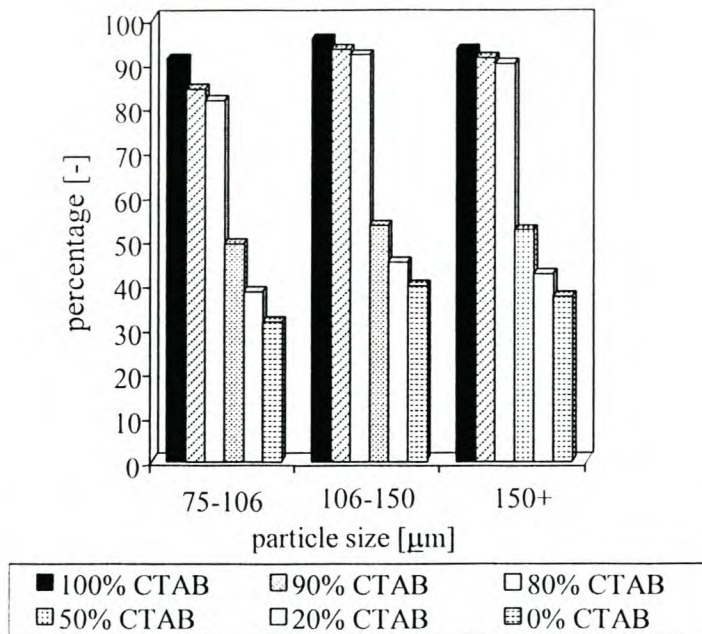


Figure 4.30 Influence of surfactant concentration on solid recovery

From Figure 4.30 it is clear that the recovery of solid particles, irrespective of particle size, decrease with a decrease in CTAB concentration. The maximum recovery of quartz is at 100 percent (%) CTAB with recovery varying between 91 percent (%) and 96 percent (%). This is in accordance with Chen et al. (1991) who showed that quartz flotation exhibits its highest recovery (>95%) at a concentration below the isoelectric point (at 1×10^{-3} moles per litre CTAB) as in the case of this study. The recovery of quartz particles is above 80 percent (%) for 80 percent (%) CTAB. At 50 percent (%) CTAB and concentrations where the main surfactant present is ODA, recoveries are between 31 percent (%) and 53 percent (%). The cationic collector cetyltrimethylammonium bromide is thus a far better collector than octadecylamine.

4.4.3.2 Influence of particles size on recovery

Bustamante & Warren (1984) stated that for the recovery of coal particles two opinions concerning the recovery of particles exists. The first group proved that the recovery increases with a decrease in particle size below $500 \mu\text{m}$ while the second group proved that recovery is the highest at some intermediate particle size when

investigating particles between 53 μm and 500 μm (Bennett et al., 1958; Lynch et al., 1981; Sun & Zimmerman, 1950). Figure 4.31 shows the recovery of quartz particles of size, 75-106 μm , 106-150 μm and 150+ μm as a function of different surfactant concentrations. It is clear that the intermediate size 106-150 μm shows the best recovery for all surfactant ratios. The percentage recovery for the 106-150 μm particle size ranges between 39.63 percent (%) at 100 percent (%) ODA to 95.50 percent (%) at 100 percent (%) CTAB. The particle size 150+ μm has the second best recovery for all surfactant concentrations and 75-106 μm the worst recovery of the three sizes. The recovery for the particle size 75-106 μm varies between 37.2 percent (%) and 93.2 percent (%).

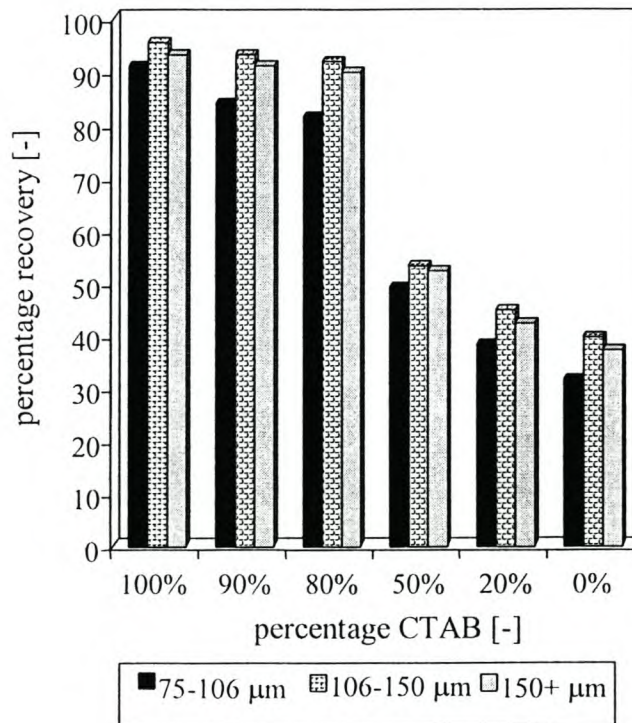


Figure 4.31 Influence of particle size on solid recovery

4.5 CONCLUDING REMARKS

From the experimental results in this chapter it is clear that the image analysis system differentiates well between systems with unique characteristics. Through principal

component analysis it was shown that experimental runs of different concentration and mineral content occupy a unique region in the 3D factor plot. Every factor describes certain froth characteristics and the characteristics of a group can be identified by investigating the position of the group in the plot. In the flotation of quartz particles it was shown that quartz particles of $-75\ \mu\text{m}$ tend to stabilise froth while coarser particles destabilise froth. It was shown in this chapter that the characteristics of foam and froth such as bubble size, colour and movement play a substantial role in the stability measurement of the foam. To investigate the stability measurements of the image analysis system closer, the system was applied to the decay of CTAB foam. This characterisation of foam decay is discussed in *Chapter 5*.

CHAPTER 5

DYNAMIC MODELLING OF FROTH STABILITY

As was discussed previously, the growth and decay of froths and foams are dynamic processes and should be treated as such. Observation of the stability of foam or froth yields one or more time series, regardless of the way in which the stability is measured. A time series is a potentially rich source of information with reference to the system being observed, but exploitation of the information is not trivial. This is particularly so if the time series is non-linear as it can not be fully characterised by its mean and frequency spectrum. Owing to the diversity and complexity of non-linear behaviour, new established methods are available to deal with non-linear systems. Of these, the method of surrogate data is widely used.

The main purpose of time series analysis is to take the order of the observations and try to learn something about the data set such as periodicity, trends or repeating. These characteristics can then be used to infer something about the process being observed. Time series analysis strives to meet two goals (Singular-Spectrum Analysis Toolkit, 2001):

- i Identifying the nature of the phenomenon represented by the sequence of observations, and
- ii predicting future values of the time series variable.

Both of these goals require that the pattern of observed time series data is identified and more or less formally described.

5.1 OBJECTIVES

The objectives of this chapter are as follows:

- i To determine the nature of foam decay of CTAB foam through the application of time series analysis on the stability data obtained through image analysis. A generalised approach to time series analysis, as recently proposed by Barnard et al. (2001) is used to characterise the dynamics of foam stability. This entails Monte Carlo methods (surrogate data analysis) to assess the determinism or stochasticity of the system, followed by system identification with appropriate models and interpretation of the models. Embedding of the time series is fundamental in all these techniques.
- ii To determine whether the nature of decay of long life foams can be classified in the same manner as short life foams (Iglesias et al., 1995) and viscous emulsions (Turner et al., 1999) by using a manual method.

5.2 OUTLINE OF THIS CHAPTER

As this chapter contains a vast amount of information about the generation as well as the analysis of the time series obtained, a short summary of the methodology as well as an explanation of the steps followed are given. The theory describing the background of the time series analysis approach is discussed in detail in Appendix B.

- i The case study is the decay of cetyltrimethylammonium bromide foam in a glass column. The behaviour of the foam was investigated at two surfactant concentrations. Two possible methods were used to investigate the change in foam stability with foam decay.
 - a In the first method an image analysis system was used to obtain the instability data. The instability curves obtained from this method are illustrated and discussed. The instability curves obtained showed that the original instability

time series was not stationary. The original time series was transformed to obtain two new time series. The first series (Series A) is called a time series of first differences and consists of the differences between successive time intervals. The second series (Series B) consists of residual values from subtracting a predicted instability value (obtained through linear regression) from the original instability value at a specific time interval.

- b The second method used to obtain stability measurements was the manual method described by Iglesias et al. (1995) and Turner et al. (1999). Using Bikerman's dynamic method (Bikerman, 1938) to generate the foam, the decay of the foam was characterised by the decrease in foam volume with time. The foam decay was investigated to see whether the decay of a long-life foam follows the same trends as was proven by Iglesias et al. (1995) for short-life foams and Turner et al. (1999) for foamed emulsions. These results are given as supplementary results at the end of the chapter in Section 5.9.
- ii The sample distributions of the original time series as generated by the image analysis system as well as the two series obtained through transformation of the data were plotted to show the distribution of each series and to demonstrate specific structures in the time series.
- iii The first step in non-linear time series analysis is state space reconstruction. The single variable time series was used to recreate a full n-dimensional state space. Singular spectrum analysis was used for the embedding of the time series.
- iv After the embedding of the data, the attractor for every time series was plotted. The reconstructed attractors in state space were inspected to conclude whether the attractors showed a pattern and defined a limited region in the state space. To interpret the attractors obtained, a random stochastic series was generated and its attractor plotted. The attractors generated from Series A and Series B are compared to the stochastic attractor to highlight differences and point to possible determinism of the time series.

- v The presence of non-linearity in the time series was investigated by using the method of surrogate data. By statistically assessing the difference between the original time series and the surrogates generated from it, the time series were classified as stochastic or deterministic.
- vi Multi-layer perceptron neural networks are a popular approach to non-linear modelling and were used to model the deterministic time series. The models are trained with the Levenberg-Marquart training function and cross validation are done on the last 200 data point. The models are validated by using the significance of R^2 as an indicator of how well the models perform.

5.3 CASE STUDY: CETYLTRIMETHYLAMMONIUM BROMIDE

5.3.1 EXPERIMENTAL SET-UP

To investigate the stability of foam, experiments were carried out in a glass column. The glass column had a diameter of 55 millimetres (mm), a length of 302 millimetres (mm), and a thickness of 2 millimetres (mm). At the bottom of the column a number 3 (40-60 μm) sinter disk was used to distribute the air. Pure grade nitrogen was used as the gas phase and was supplied from a gas cylinder. The gas flowrate was measured by a rotameter and kept at 0.005 L/min for all experiments. The froth structures were monitored with an ELMO colour charged coupled device (CCD). The CCD was mounted on a bracket, which prevented vibration in the cell from affecting the images. The distance from the lens to the cell was 455 mm to ensure images with a clear focus. The CCD was connected to a personal computer equipped with frame grabber, which captured and digitised the images. Light was provided by a 100 W light bulb next to the CCD. The experimental set-up is illustrated in Figure 5.1.

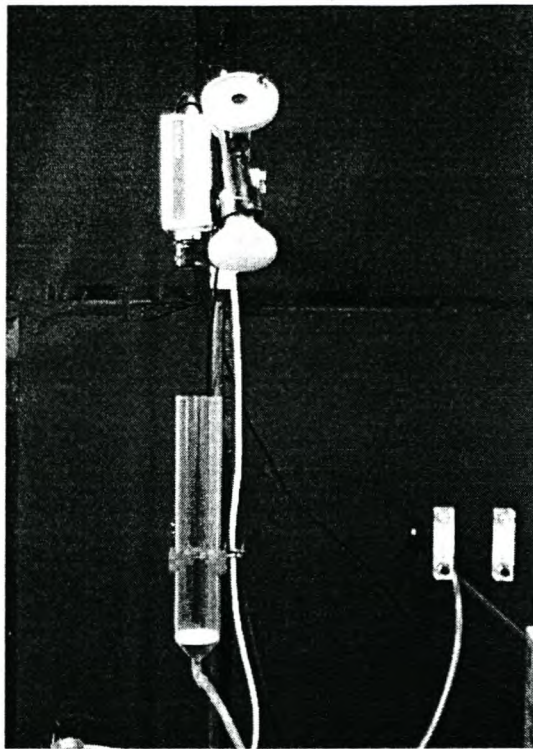


Figure 5.1 Experimental set-up for flotation column study

5.3.2 REAGENTS

Cetyltrimethylammonium bromide (CTAB), with 99 percent (%) purity was obtained from Sigma-Aldrich. The critical micelle concentration (CMC) of CTAB is 0.92 millimolar (mM). Stock solutions of two concentrations of CTAB were used to investigate the stability namely, 0.8 millimolar (mM) a concentration just below the CMC and 9 millimolar (mM), approximately ten (10) times the CMC.

5.3.3 TEST PROCEDURE

Stock solutions for the CTAB were made up. The stock solutions' concentrations were respectively 9 millimolar (mM) and 0.8 millimolar (mM). To ensure that all the crystals in the surfactant stock solution were dissolved, the CTAB solutions were heated in a water bath to 35°C. Seventy (70) millilitres (ml) of the foaming solution was used in the investigation of the concentration above CMC and 40 millilitres (ml) of the solution for the concentration under the CMC. The foaming solution was

slowly injected into the column by using a 50 ml and 20 ml pipette. Care was taken not to wet the sides of the glass column as to ensure the even formation of the foam surface. The foaming solution was introduced in the glass column very slowly to ensure that no foam was formed on the liquid surface before foam generation by aeration took place.

The gas supply was opened after the solution was introduced into the column. The flowrate of the nitrogen into the column was kept constant at 0.005 l/min. In the case of the high concentration (9 mM) the nitrogen flow was permitted until no foaming solution was left, after which the gas supply in the cylinder was closed. Dynamic equilibrium was reached where the lower concentration (0.8 mM) was used after which the nitrogen flow was closed and foam decay commenced. The foam column was positioned as far as possible at a constant height from the camera (455 mm) to ensure the same focus depth for all images recorded. The time of foam generation was measured with a stopwatch and the maximum foam height obtained measured with a measuring tape. The decay of the foam was followed by measuring the time for a millimetre (mm) of the foam height to drop. The increase in solution height at the bottom of the column was also measured against time.

5.4 EXPERIMENTAL DATA

5.4.1 INSTABILITY CURVES

As described in Chapter 3, the following function is used in the image analysis system to calculate the foam stability (Moolman, 1995a):

$$SB = \sum \sum f(x) \quad 3.31$$

where $f(x)$ is the matrix:

$$f(x) = \begin{cases} 1 & \text{if } |x_1 - x_2| \geq q \\ 0 & \text{if } |x_1 - x_2| < q \end{cases} \quad 3.32$$

where x_1, x_2 = the pixel grey levels of the two successive frames [-]

q = value of the selected grey level threshold [-]

The stability values calculated with Equation 3.31 for every time increment lie between zero (0) and unity (1), zero (0) being the most stable value and unity (1) the most unstable value.

The instability curves in Figure 5.2 to Figure 5.12 describe the decay of the foam. An instability value as calculated by the image analysis system was recorded, either every 10 seconds (s) or every 20 seconds (s), depending on the set time interval. The stability of the CTAB foam was investigated for two main scenarios: above CMC, where the change in surface tension is negligible and close to the CMC where the surface tension effect is at its highest. Two runs describe the foam decay at the surfactant concentration of 9 millimolar (mM) or ten times the CMC namely Run A and Run B, where Run B is merely a repetition of Run A. The foam decay at a surfactant concentration of 0.8 millimolar (mM) or below CMC are described by Run C and Run D, where Run D is once again merely a repeat run. Below every instability curve the foam images as recorded by the image analysis system are illustrated. The first image (a) was recorded at the start of the decay (after 10 or 20 seconds depending on the set time interval), the second image (b) illustrates the state of the foam at highest instability value (maximum peak) and the third image (c) illustrates the last image recorded for that specific system. A full collection of foam images for the four specific foam systems, illustrating the foam state every 30 minutes, can be viewed in Appendix C.

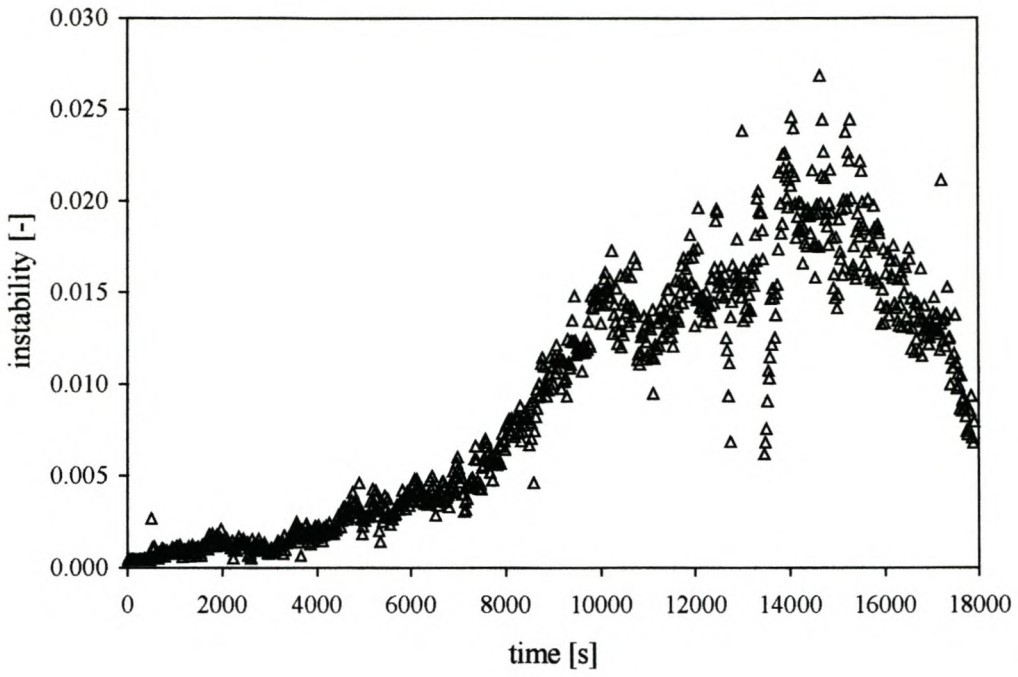


Figure 5.2 Instability curve for Run A

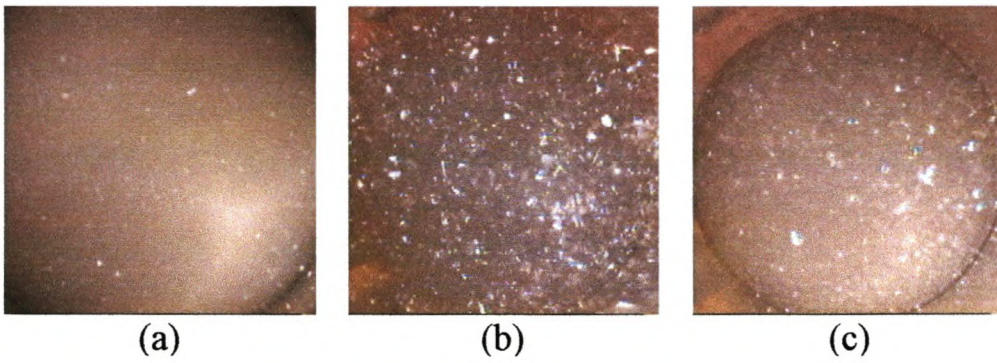


Figure 5.3 Foam images for Run A

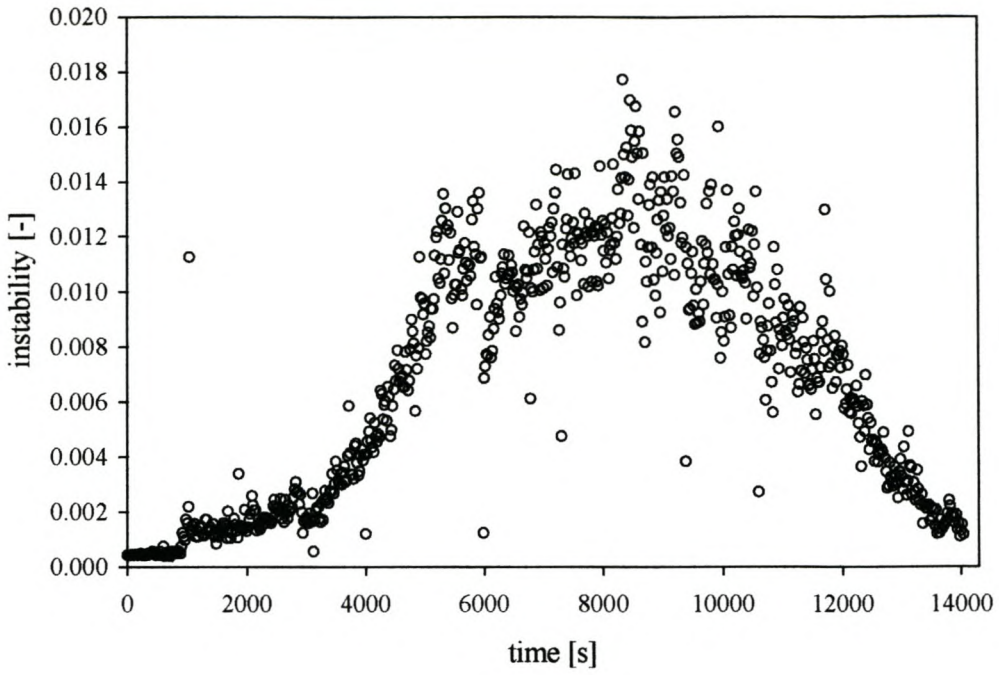


Figure 5.4 Instability curve for Run B

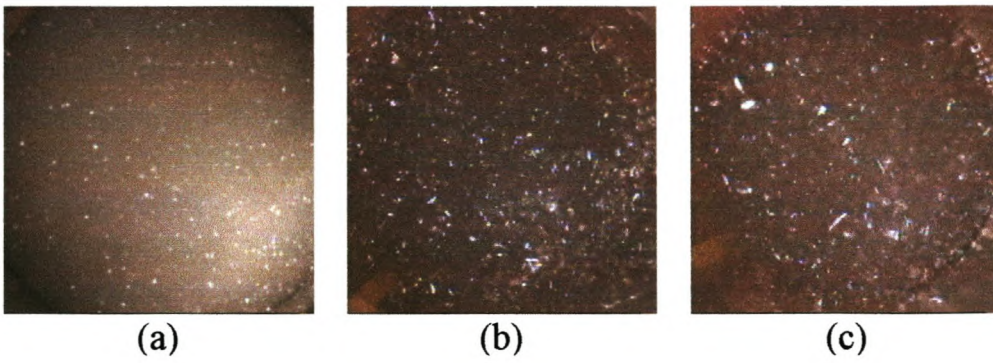


Figure 5.5 Foam images for Run B

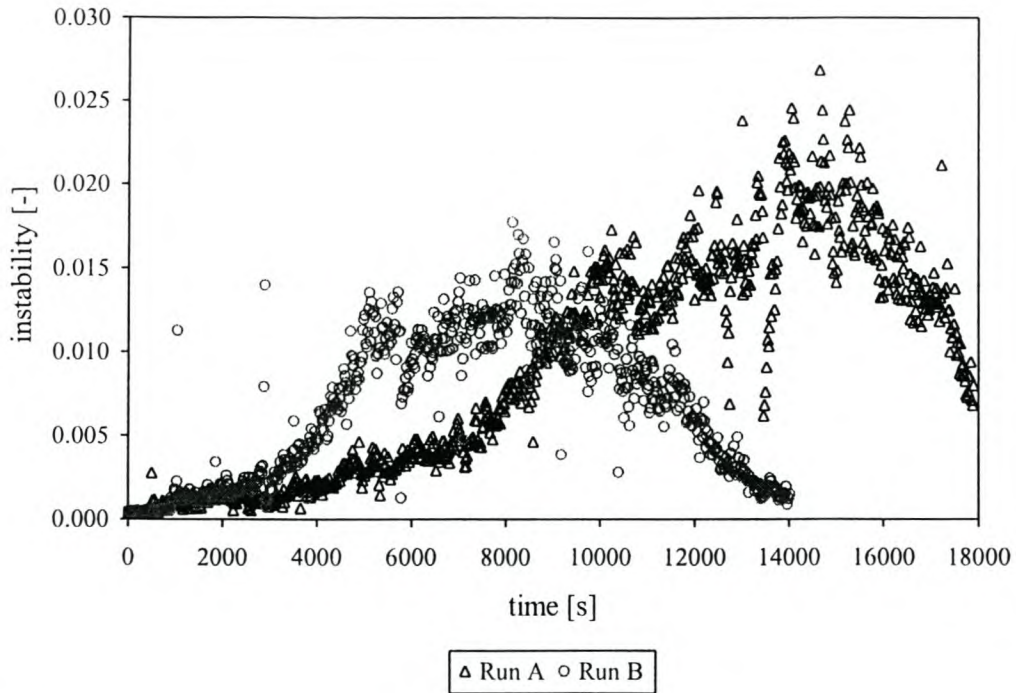


Figure 5.6 Instability curve comparison for Run A and Run B

The instability curves for Run A (Figure 5.2) and Run B (Figure 5.4) demonstrate that the stability measurements, as extracted from the image analysis system show that the foam is stable in the beginning, then increases in instability up to a maximum point and then show a decrease to a stable value. As evident from Figure 5.6, the instability curves for both runs have the same shape, but Run A is more unstable. The maximum peak in the curve describing Run A is at a higher instability value (0.0268) as opposed to the maximum value obtained in Run B (0.0177). The instability curve obtained in Run A also shows a longer increase in instability before the maximum peak range and the decrease in instability. The instability in Run A peaks after 15 000 seconds (s) while the maximum peak in Run B is obtained in 8000 seconds (s). As the shape of the instability curve is the same for the two runs, it is possible that evaporation played a greater role in the decay of the foam in Run B than in Run A, hence the shorter time period in which total decay of the foam takes place. Both the curves show single maximum and minimum points of the instability over the whole time range.

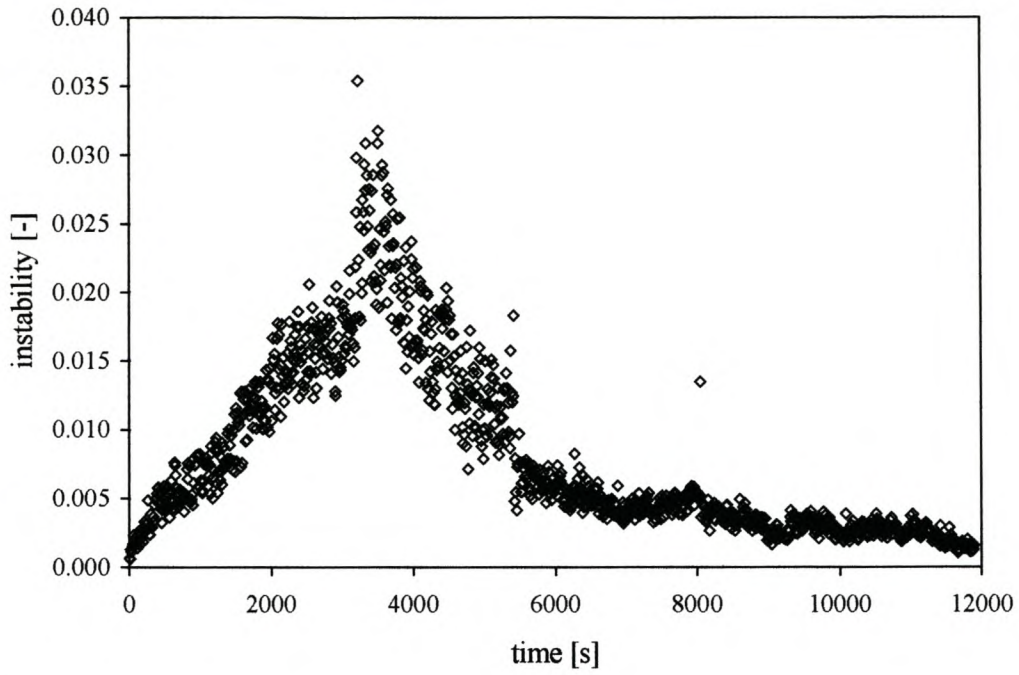


Figure 5.7 Instability curve for Run C

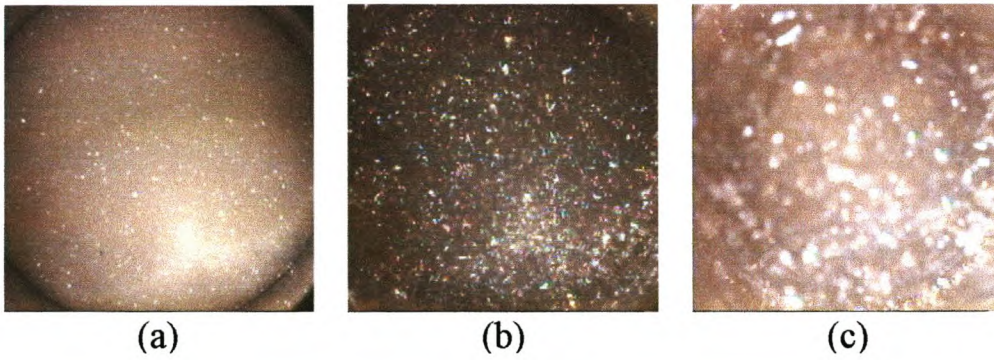


Figure 5.8 Foam images for Run C

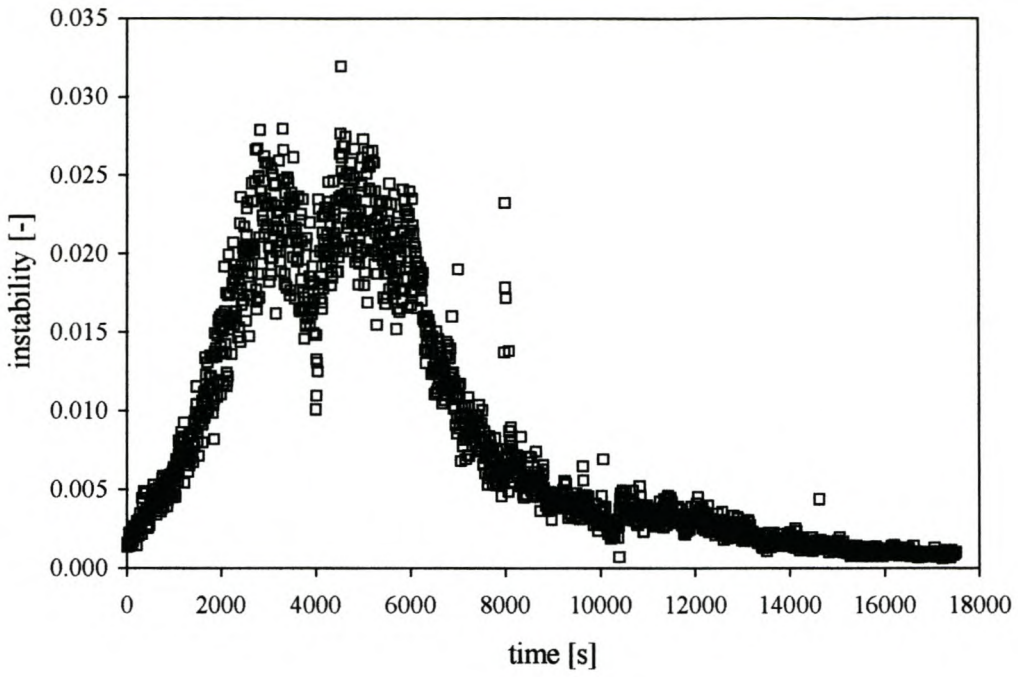


Figure 5.9 Instability curve for Run D

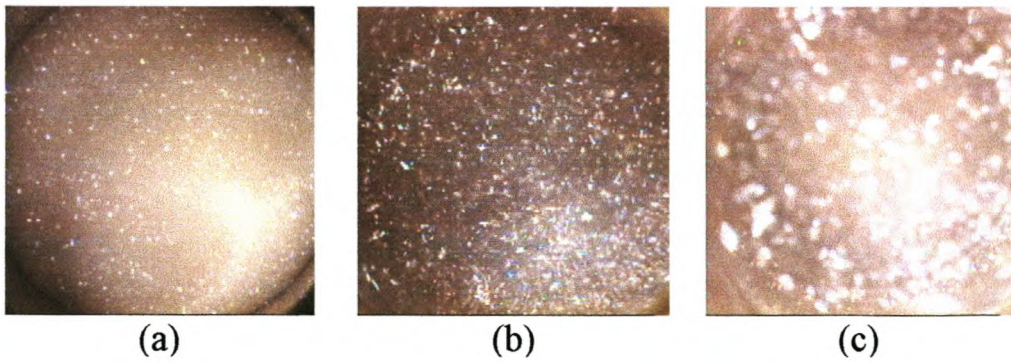


Figure 5.10 Foam images for Run D

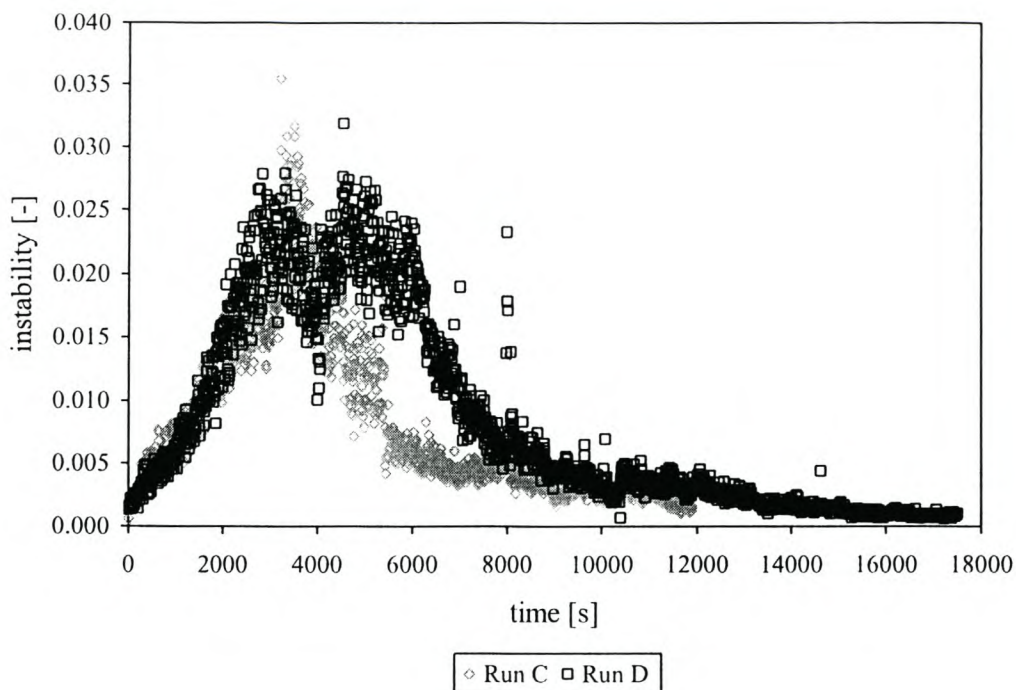


Figure 5.11 Instability curve comparison for Run C and Run D

The instability curves obtained at 0.8 mM CTAB (as illustrated in Run C and Run D in Figure 5.7 and Figure 5.9 respectively) show a similar trend to that of the 9 mM concentration (as illustrated in Run A, Figure 5.2 and Run B, Figure 5.4). For the instability curves generated in Run C and Run D both curves show an instability increase, a maximum value and then a decrease. The instability curve in Run C show a strong sharp peak at the maximum instability while the curve in Run D show two maximum peaks separated by a lower region of instability. The instability in Run C decreases more rapidly than Run D.

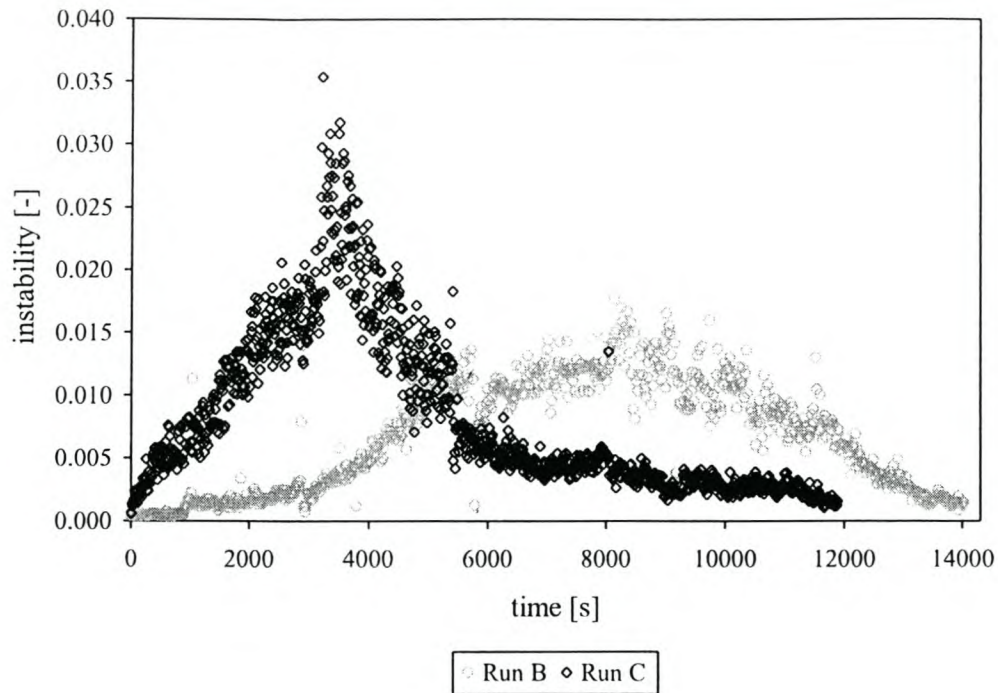


Figure 5.12 Instability curve comparison for Run B and Run C

To compare the instability of the two surfactant concentrations, the instability curves of Run B and Run C are shown in Figure 5.12. The foam generated with the surfactant concentration under the CMC (Run C) shows a higher instability value (0.0354) than the equivalent curve generated at ten times the CMC (0.0177). The instability curve for Run C peaks much faster than that of Run B, shows a higher peak value and a quicker descend. The instability curve generated in Run B show an outstretched peak and there is a region of maximum instability but not a pronounced peak as in the case of Run C. The region where an increase in instability can be observed is longer in the case of Run B, while the decrease in instability is observed over a longer time period in the case of Run C. The foam at the higher CTAB concentration show a slow instability increase as the foam bubbles are closely packed and bubble coalescence are slower. The machine vision system cannot identify foam bubbles of such small diameter and only recognises the coalescence of bubbles when the bubbles are of satisfactory size.

The behaviour of the two systems can be explained by micellar formation. The maximum foam stability for a surfactant solution should be obtained under the critical micelle concentration (CMC). At concentrations just above the CMC the surfactant monolayer is depleted slightly but restored to quickly for the film to show elasticity. The film thus resists the Gibbs-Marangoni effect and results in an unstable foam (Sebba, 1987). Above the CMC the concentration of dispersed surfactant molecules are constant and little variation in the surface tension is observed. Micelles are shaped spherical around the CMC but are shaped non-spherical at concentrations around ten times the CMC. At such high concentrations the micelles form extended parallel sheets, with individual molecules orientated perpendicular to the plane of the sheet. In other cases, micelles take on the form of long cylinders pack together. These extended micelle structures are called *lyotropic mesomorphs* or a *liquid crystalline phase*. The formation of this viscous liquid crystalline phase in the bulk solution increase the stability of the foam by retarding the drainage (Rosen, 1978). The formation of micelles thus explains the higher stability of the more concentrated solution.

5.4.2 TRANSFORMATION OF DATA

The time series that describes the original instability series (as illustrated in Figure 5.2, Figure 5.4, Figure 5.7 and Figure 5.9) is not stationary. Two new time series were obtained by transformation of the original time series to investigate whether a more stationary series can be obtained from the data. The manner in which the transformation was done as well as the results obtained with further investigation into the determinism of the time series is discussed in the following sections. The first time series is referred to as Series A and the second transformation, Series B.

5.4.2.1 Series A: Instability differences

The first transformation is a series of first differences. To obtain Series A the difference in successive instability values were used. If the original time series is defined as follows:

$$z(n) = \{z_1, z_2, z_3, \dots, z_n\} \quad 5.1$$

The series of differences can be defined as follows:

$$z(n-1) = \{z_{1-2}, z_{2-3}, \dots, z_{(n-2)-(n-1)}\} \quad 5.2$$

As the series of differences consists of the difference in instability of successive observations, the series has one less observation than the original time series. The descriptive curves obtained for the four runs are illustrated in Figure 5.13 to Figure 5.16.

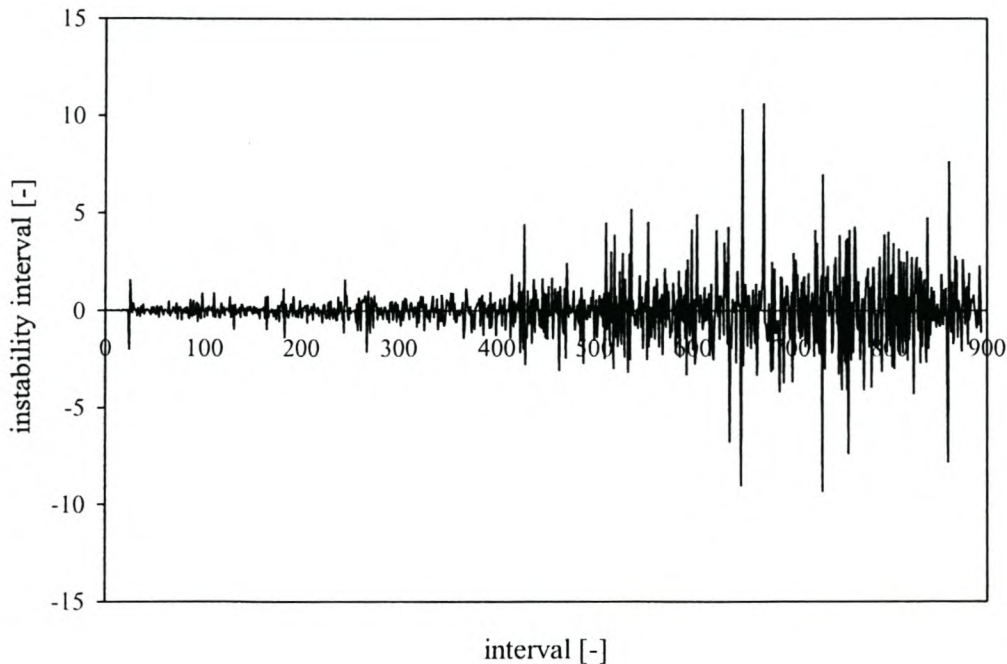


Figure 5.13 Instability curve for Series A, Run A

Figure 5.13 illustrates the series of successive differences in instability for Run A. It is clear that there is a small difference in instability over the first 400 intervals. This is the period where a slow increase in instability can be observed in Figure 5.2. A bigger difference between instability values is observed in the region of the maximum instability peak. As the period of recording of the decrease in instability was relatively

short and not followed until total decay was reached, the successive differences remain high over the last intervals.

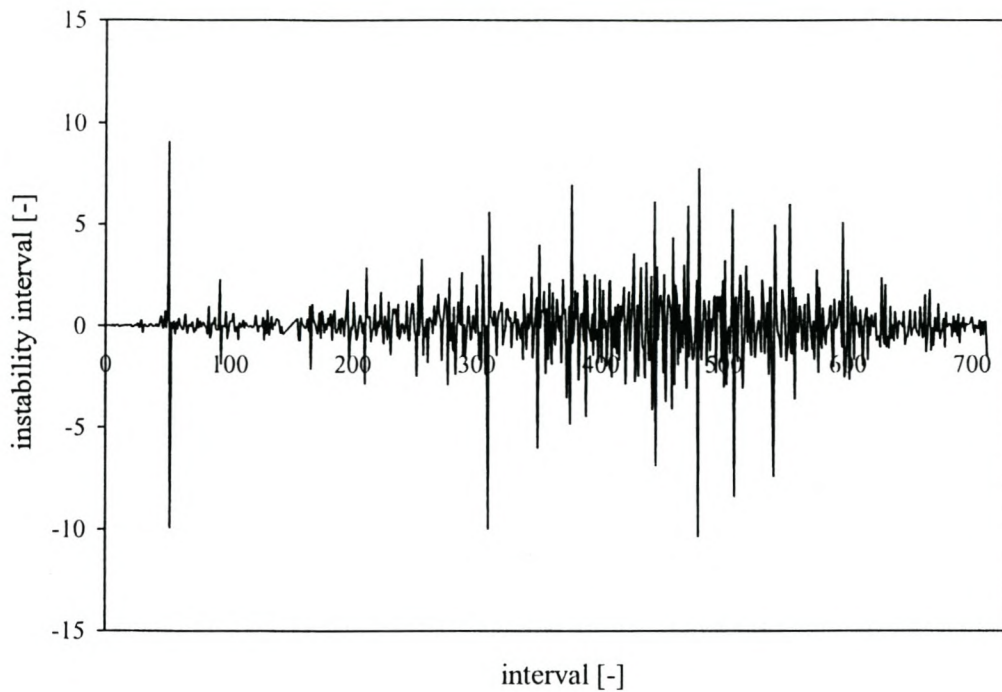


Figure 5.14 Instability curve for Series A, Run B

The curve describing the successive difference in instability for Run B, Figure 5.14, show a small difference in instability in the beginning of the foam instability (150 observations), an increase over the long outstretched peak area and a small difference over the last 150 observations that represents the decrease in instability.

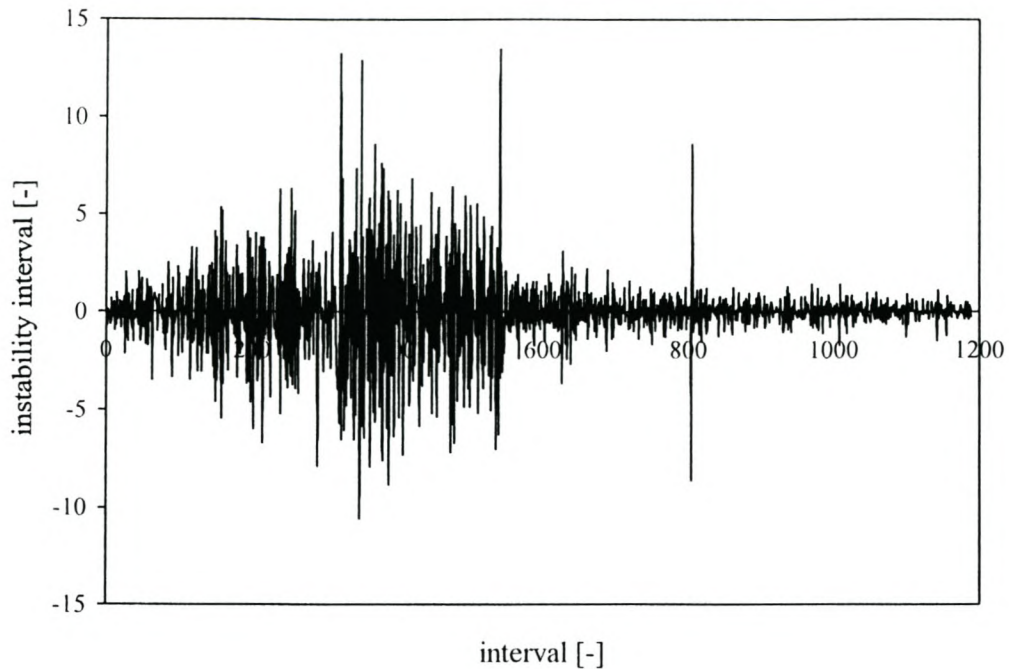


Figure 5.15 Instability curve for Series A, Run C

In contrast to the curve obtained in Run B (Figure 5.14), Run C (Figure 5.15) shows an immediate difference in instability between successive observations. The difference is substantial for the first 400 intervals and after which the difference decreases over the next 800 intervals. The large difference in instability in the beginning is due to the steep increase in instability up to the maximum instability peak. The decrease in instability takes place over a much longer range and thus explains the 800 intervals where the difference in instability are small in comparison with the first 400 intervals.

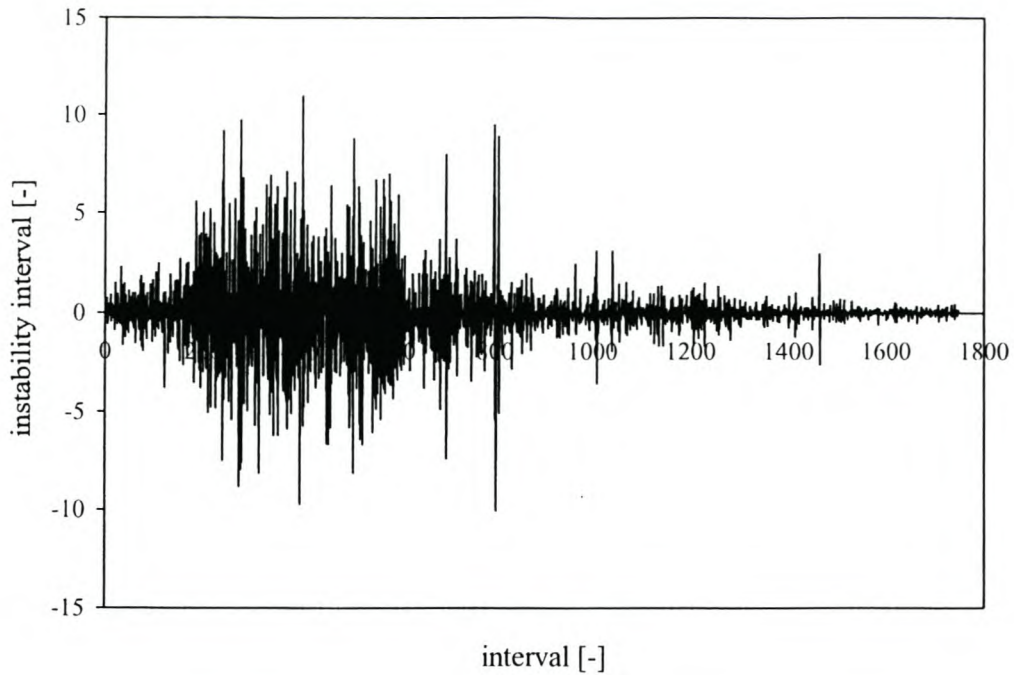


Figure 5.16 Instability curve for Series A, Run D

The time difference curve for Run D, as illustrated in Figure 5.16 shows the same trend as Run C (Figure 5.15). The region where the highest instability can be observed is reached rapidly (200 intervals), but the decrease in instability show a period of slow decrease in instability over 600 observations.

5.4.2.2 Series B: Residual value from linear regression

The second series was derived from the original instability time series by subtracting a predicted value of the instability (obtained through linear regression) from the original instability value for a specific observation time. An explanatory regression model was derived with the use of *Microsoft Excel* of the instability time series data. The linear regression tool in *Microsoft Excel* performs linear regression by using the least-squares method to fit a line through a number of observations. The residual values formed the new series and the descriptive curvature of the series for the four runs are illustrated in Figure 5.17 to Figure 5.20.

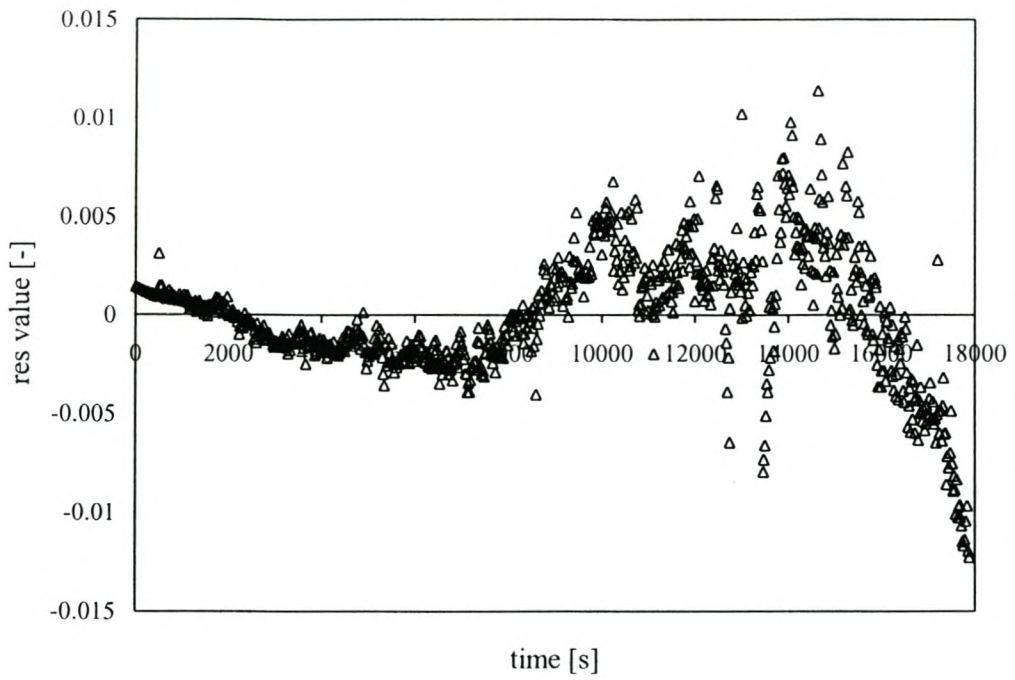


Figure 5.17 Instability curve for Series B, Run A

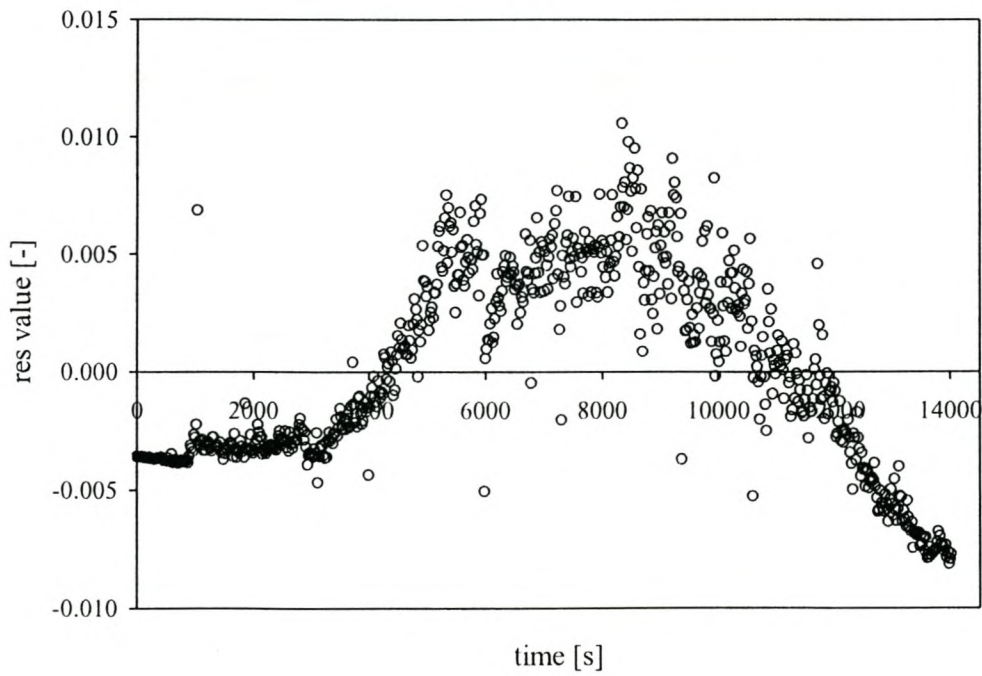


Figure 5.18 Instability curve for Series B, Run B

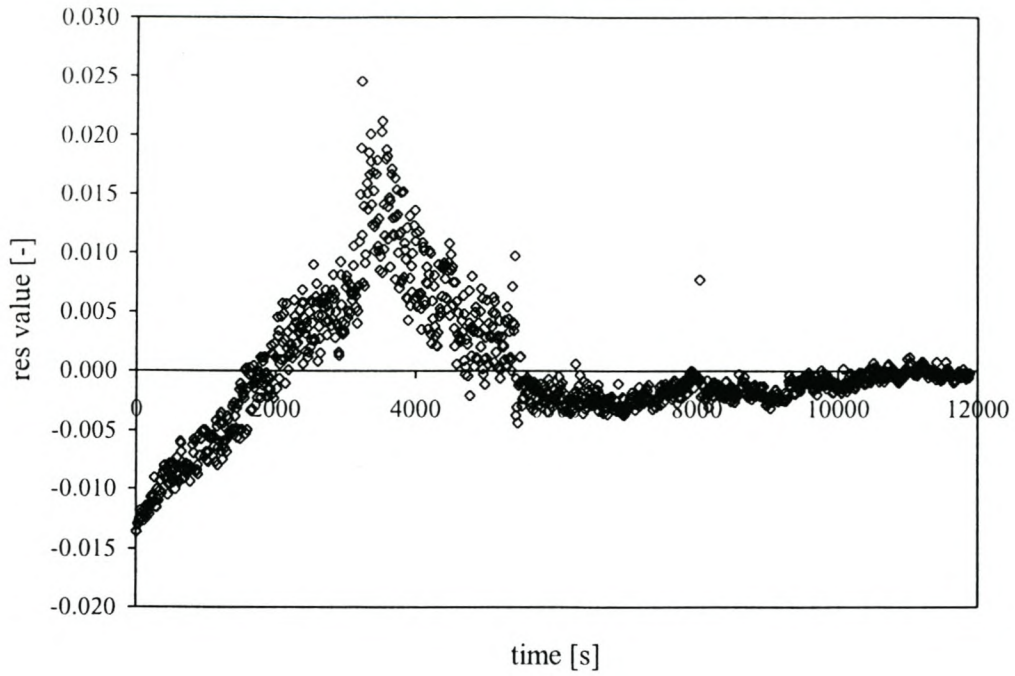


Figure 5.19 Instability curve for Series B, Run C

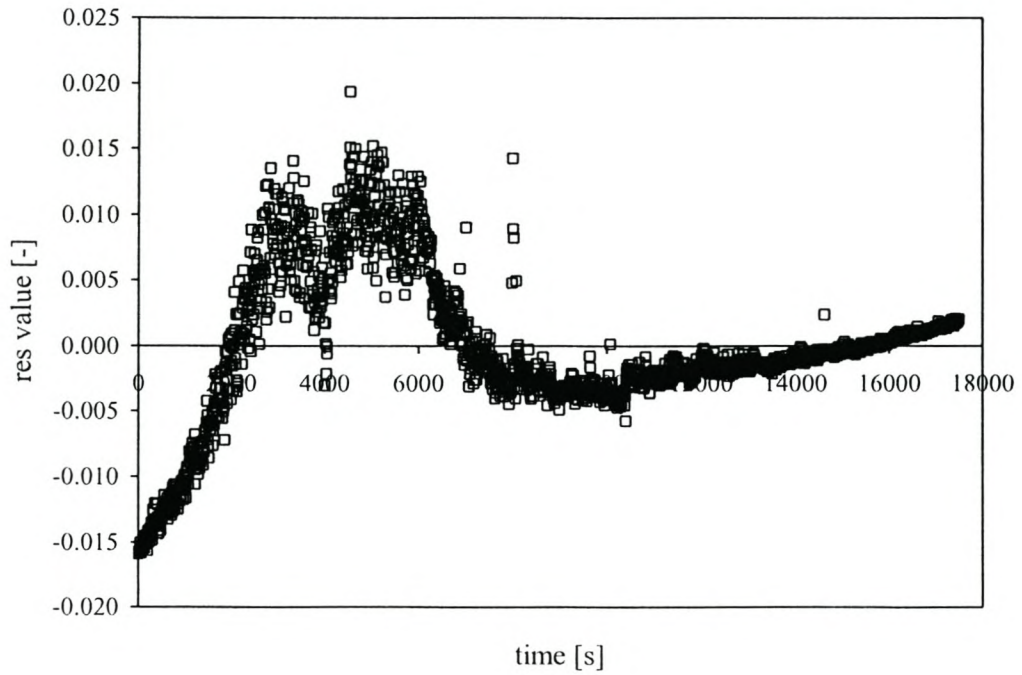


Figure 5.20 Instability curve for Series B, Run D

In all four cases the shape of the curves describing the reconstructed data as illustrated in Figure 5.17, Figure 5.18, Figure 5.19 and Figure 5.20 is the same as that of the original instability data (See Figure 5.2, Figure 5.4, Figure 5.7 and Figure 5.9). The curves are however shifted in a downward direction with reference to the y-axis.

5.5 SAMPLING DISTRIBUTIONS

The histograms of all three data sets, namely the original data series, Series A and Series B were plotted for all four runs. The sample distributions of Run B are given in the following section (Figure 5.22 to Figure 5.24), while the histograms of the remaining three runs (Run A, Run C and Run D) are given in Appendix C.

The sample distribution of the instability data generated was investigated to identify any existing structure in the data. A histogram of the instability data with a normal distribution curve as reference was plotted. The histogram illustrating a random set of data generated to have a normal distribution is given in Figure 5.21, while the descriptive statistics of the distribution is given in Table 5.1

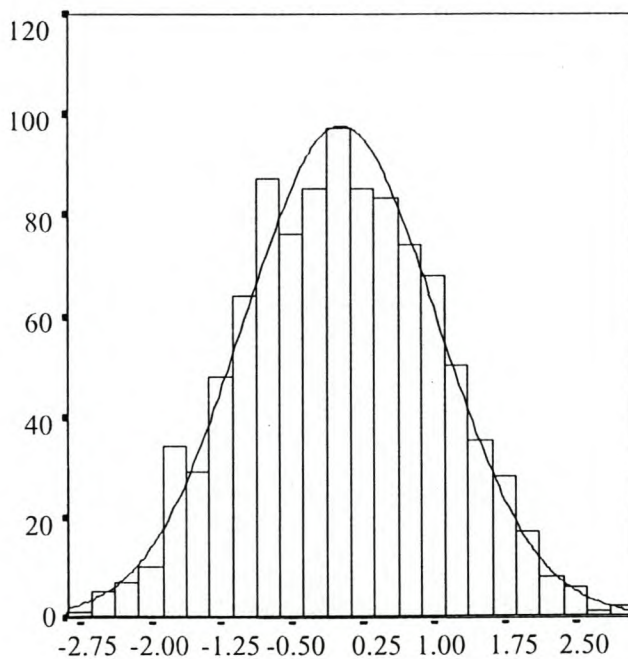


Figure 5.21 Histogram illustrating normal distribution

Table 5.1 Descriptive statistics of normal distribution

<i>Number of observations</i>	1000
<i>Mean</i>	0.003
<i>Standard deviation</i>	1.020
<i>Sample variance</i>	1.040

The sample distribution of the original stability time series for Run B is illustrated in Figure 5.22 it is clear that the distribution show two peaks. This is known as a bimodal distribution. Bimodality is a strong indication that the variable in the population is not normal. The distribution of the remaining three original stability time series runs (Run A, Run C and Run D) show two peaks as illustrated here for Run B (See Figure C.5, Figure C.8 and Figure C.11). The descriptive statistics for the bimodal distribution is given in Table 5.2.

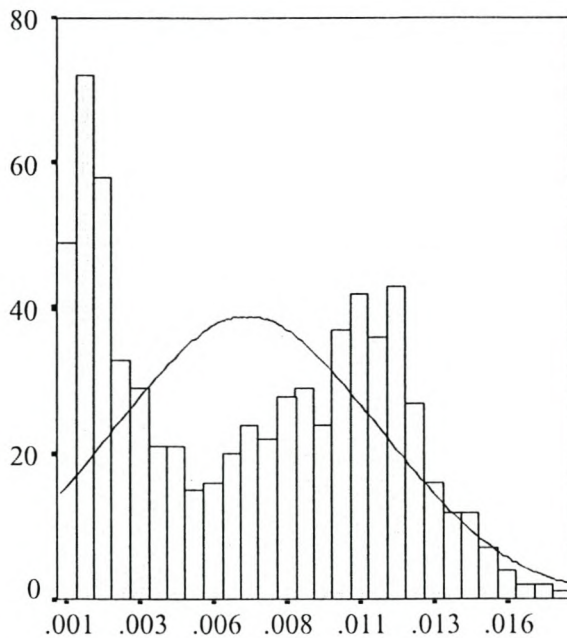
*Figure 5.22 Histogram showing distribution of original time series, Run B*

Table 5.2 Descriptive statistics of original time series, Run B

<i>Number of observations</i>	702
<i>Mean</i>	6.78E-3
<i>Standard deviation</i>	4.49E-3
<i>Sample variance</i>	2.02E-5

The sample distribution of the first series obtained through the transformation of data, namely Series A show a distribution with a very high peak at zero (0), as the one illustrated in Figure 5.23 showing the distribution of Run B (Series A). This is due to the fact that Series A is a series of first differences and the probability that two consecutive instability values will have the same value is very high. As can be seen in Table 5.3, the distribution has a very small mean and a very high standard deviation. This is the case for all four runs as can be seen in Table C.3, Table C.6 and Table C.9.

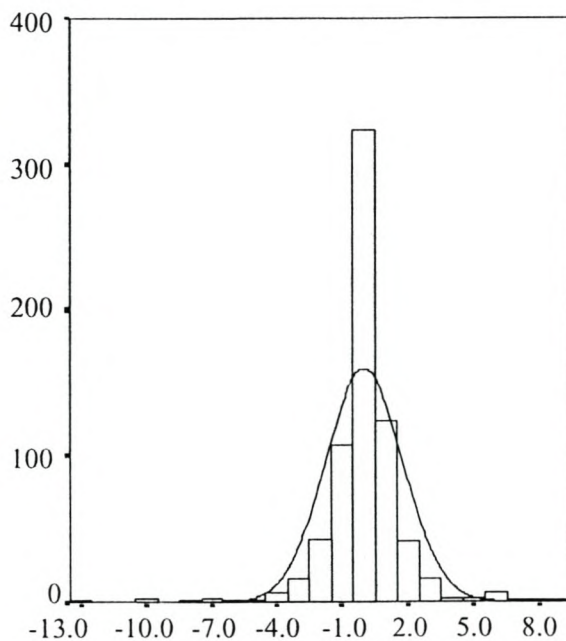
*Figure 5.23 Histogram showing distribution of Series A, Run B*

Table 5.3 Descriptive statistics of Series A, Run B

<i>Number of observations</i>	701
<i>Mean</i>	0.001
<i>Standard deviation</i>	1.751
<i>Sample variance</i>	3.065

The distribution describing Series B show bimodality in the case of Run B (see Figure 5.24 illustrated below) and Run D (Figure C.13) but not in the case of Run A (Figure C.7) and Run C (Figure C.10). In all cases the mean of the distribution, as seen for Run B in Table 5.4, is very low ($-0.0004 < \text{mean} < -8.6 \times 10^{-18}$) and the standard deviation lies between 0.003 and 0.006.

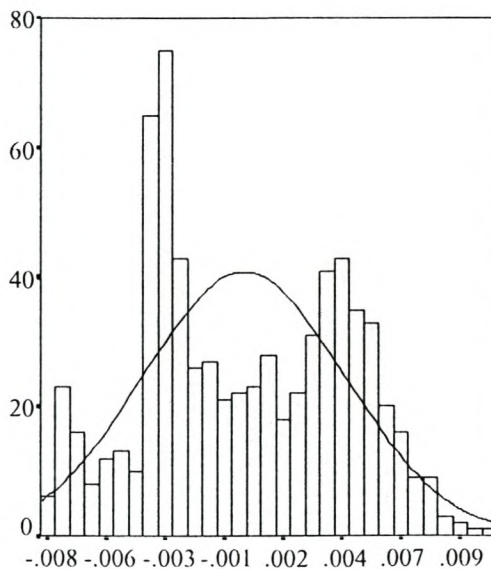


Figure 5.24 Histogram showing distribution of Series B, Run B

Table 5.4 Descriptive statistics of Series B, Run B

<i>Number of observations</i>	702
<i>Mean</i>	2.06E-4
<i>Standard deviation</i>	4.27E-3
<i>Sample variance</i>	1.83E-5

5.6 EMBEDDING USING SINGULAR SPECTRUM ANALYSIS

A brief discussion on the basic principles of embedding and background on the method of Singular Spectrum Analysis is given respectively in Section B1 and Section B2 of Appendix B.

As mentioned previously, the embedding of the time series were done through singular spectrum analysis. The data was embedded with a lag of unity and the embedding dimension was taken as the number of singular vectors that explain 98 percent (%) of the variance in the data set. The attractors were plotted for every time series and are shown here as means of interpretation of the complexity of the system.

In the aid of interpretation of the attractors generated from Series A and Series B, a random stochastic time series was generated. The attractor of the stochastic time series was plotted, as to provide a standard stochastic attractor with whom the attractors generated in this work can be compared and is given in Figure 5.25.

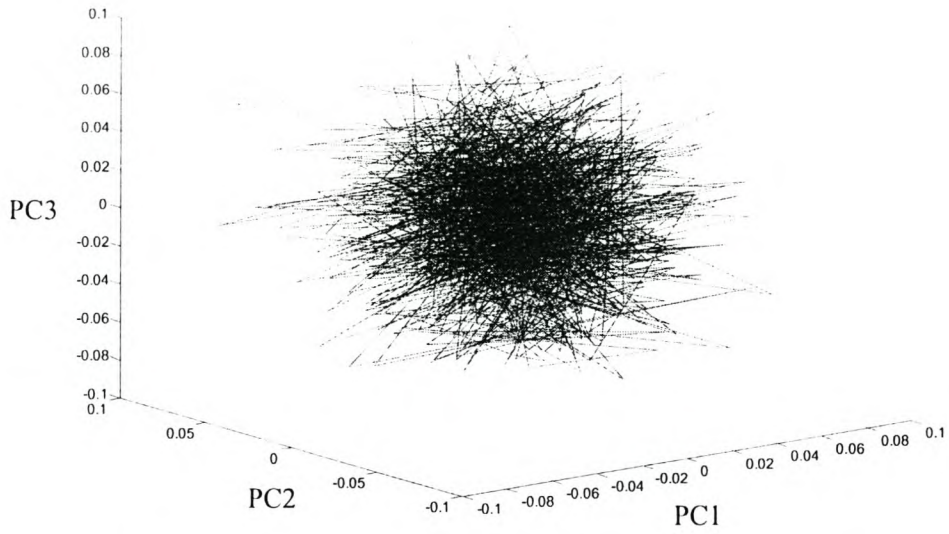


Figure 5.25 Attractor describing stochastic process

5.6.1 SERIES A

The reconstructed attractors for Series A are illustrated in Figure 5.26 to Figure 5.29.

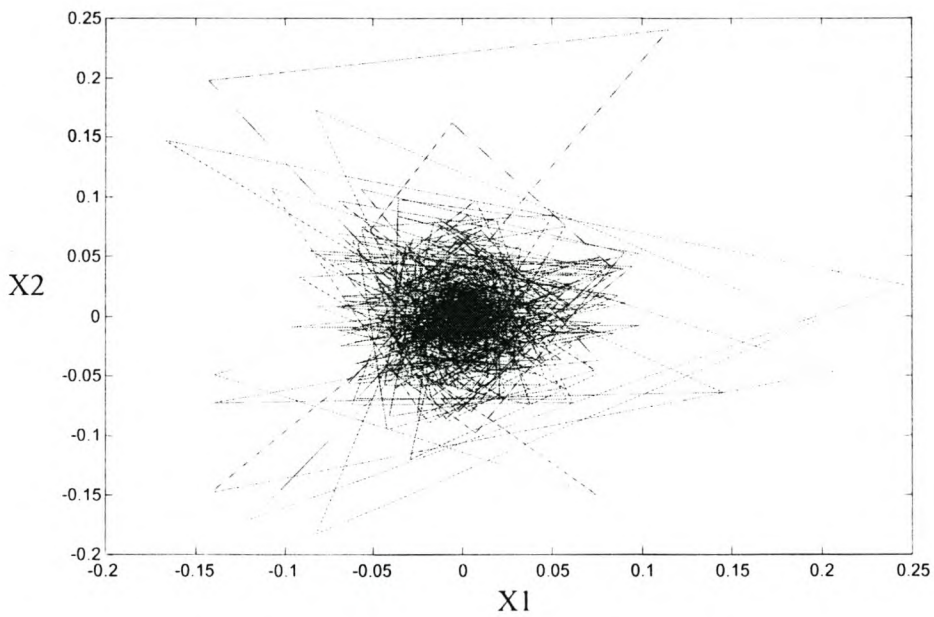


Figure 5.26 Attractor for Series A, Run A

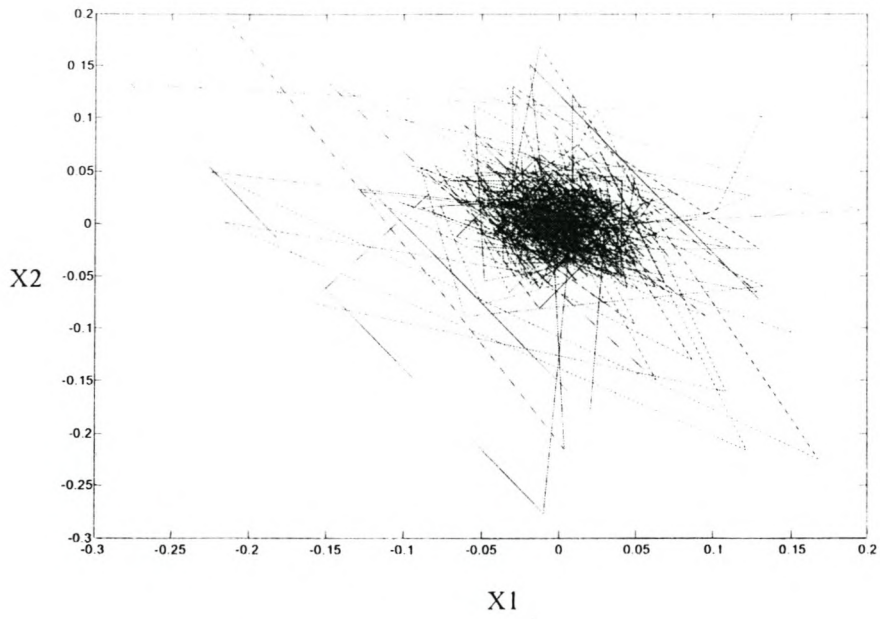


Figure 5.27 Attractor for Series A, Run B

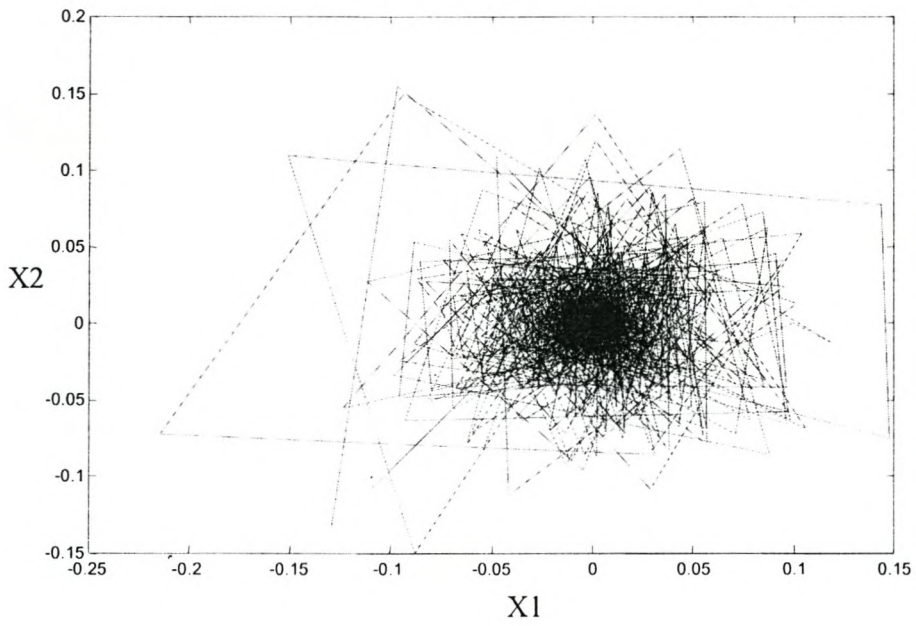


Figure 5.28 Attractor for Series A, Run C

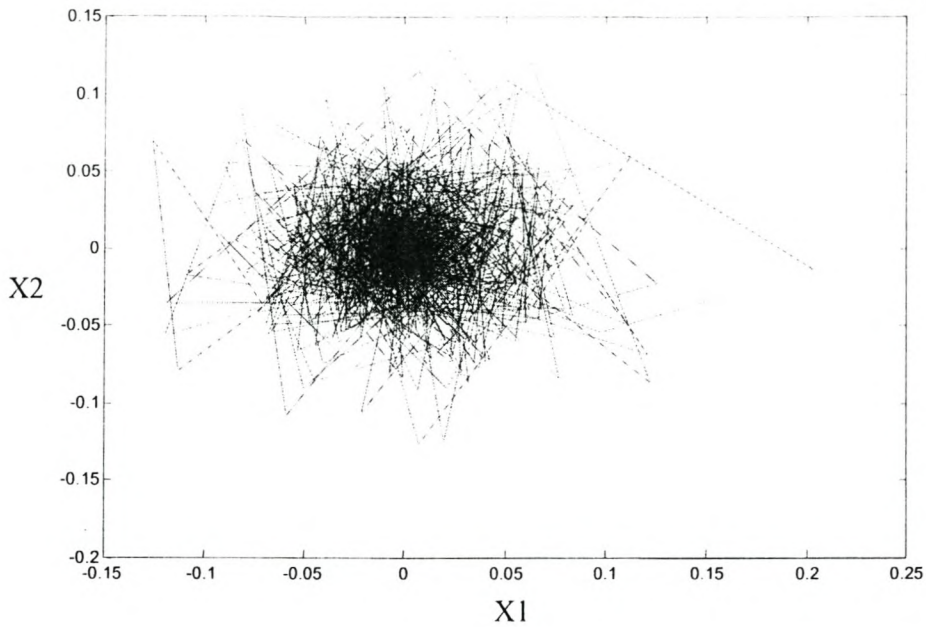


Figure 5.29 Attractor for Series A, Run D

In all four cases, the attractors plotted for Series A (Figure 5.26 to Figure 5.29) are complex, owing to the presence of dynamic and measurement noise. When compared with the attractor describing the stochastic series (See Figure 5.25) it is clear that Series A is not stochastic. The attractors do show some pattern and the attractor is limited to a region in the state space, which implies that the order of the data points is not random.

5.6.2 SERIES B

The reconstructed attractors for Series B are illustrated in Figure 5.30 to Figure 5.33.

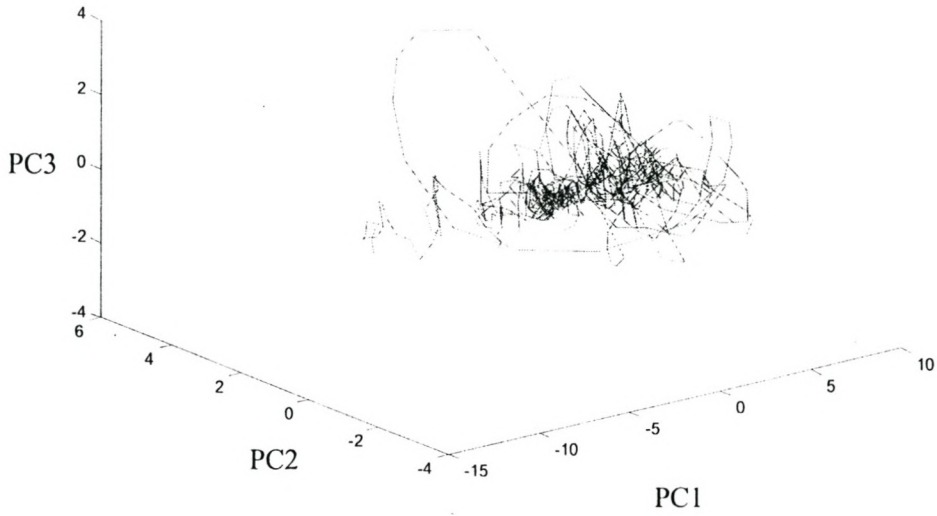


Figure 5.30 Attractor for Series B, Run A

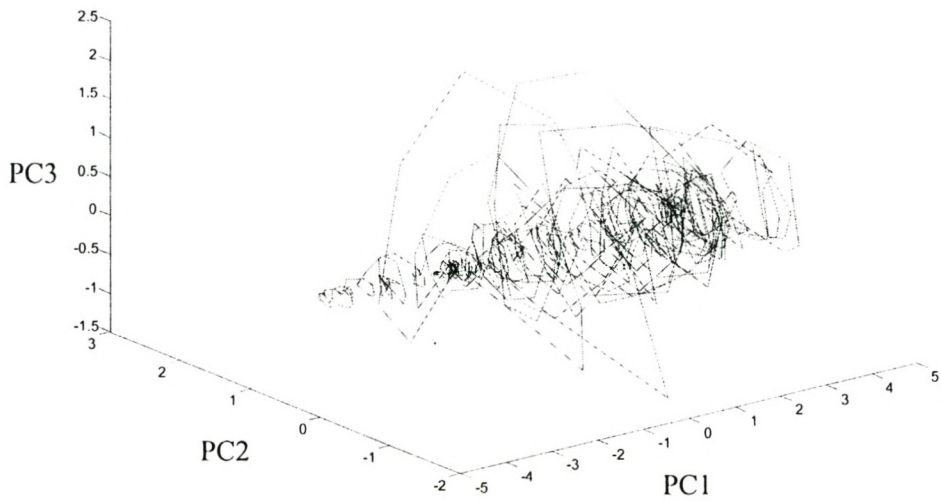


Figure 5.31 Attractor for Series B, Run B

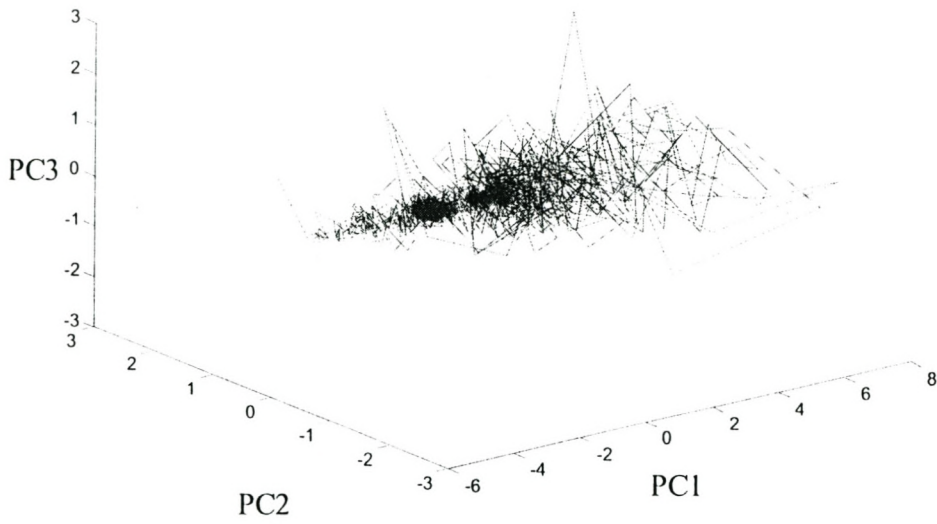


Figure 5.32 Attractor for Series B, Run C

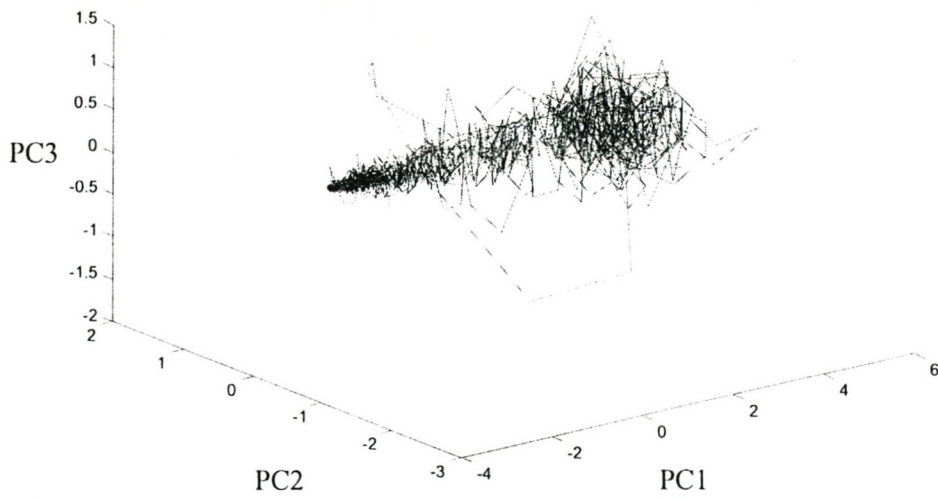


Figure 5.33 Attractor for Series B, Run D

The attractors generated from the runs with Series B show a much more definite pattern when compared to the attractors generated from Series A. The attractors for Series B occupy a limited region in the state space and points to determinism in the data series.

5.7 SURROGATE DATA

The background of the surrogate data technique including a definition of the correlation dimension is given in Section B3 in Appendix B.

The surrogate data technique was used to investigate whether the time series is stochastic or deterministic. A deterministic system is one where the later states evolve from the earlier ones according to fixed law. The correlation dimension curves for Series A and Series B are illustrated in the following section.

5.7.1 SERIES A

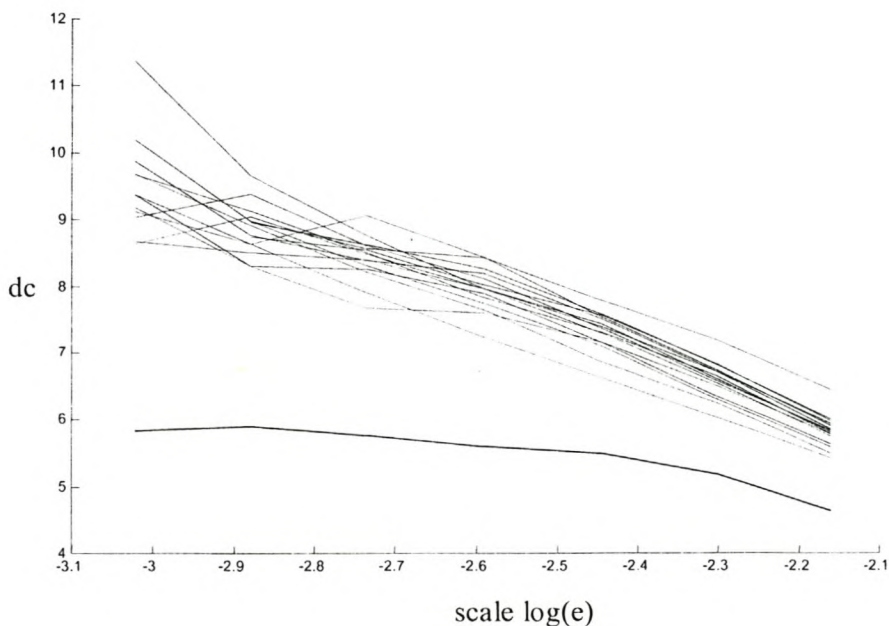


Figure 5.34 Surrogate data curves for Series A, Run A

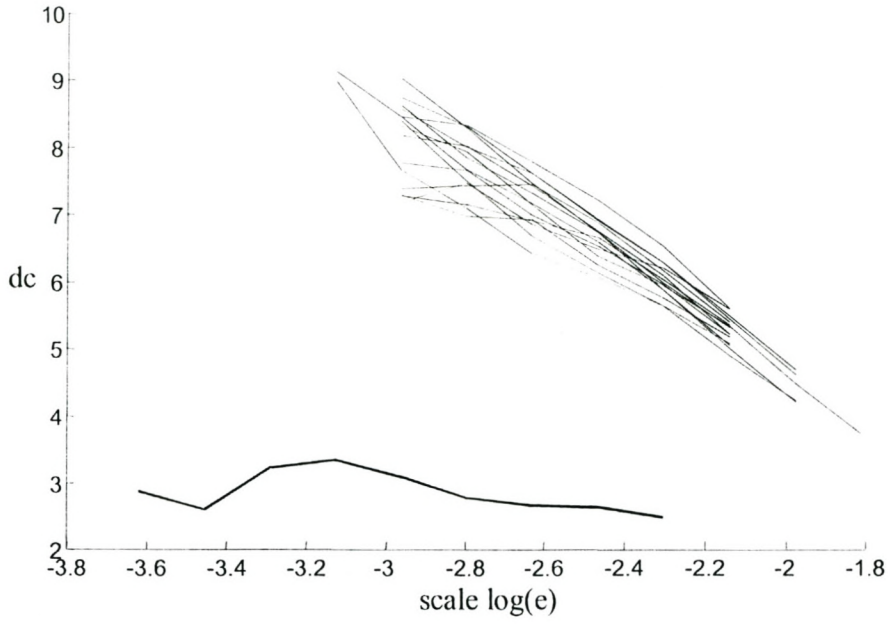


Figure 5.35 Surrogate data curves for Series A, Run B

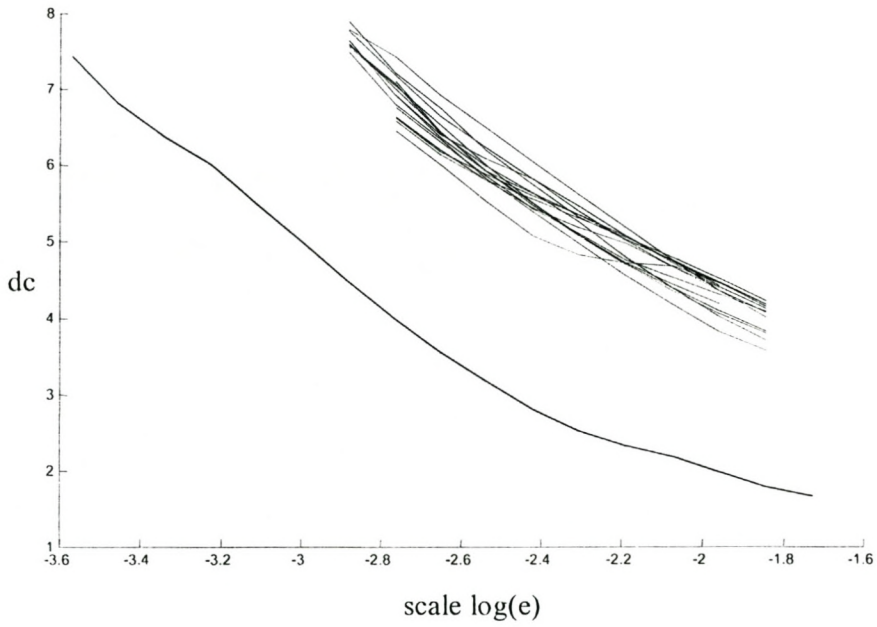


Figure 5.36 Surrogate data curves for Series A, Run C

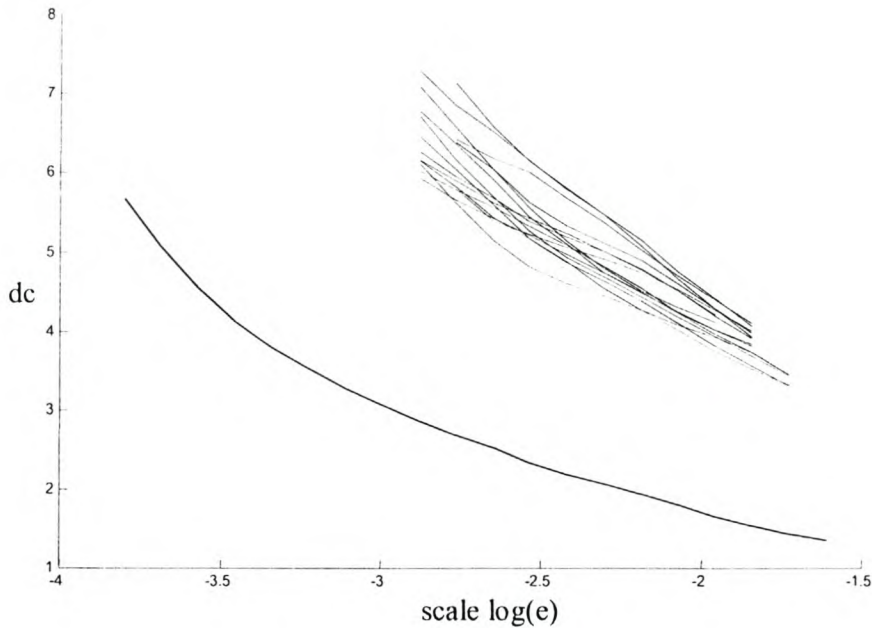


Figure 5.37 Surrogate data curves for Series A, Run D

Although the correlation dimension curves for Series A (Figure 5.34 to Figure 5.37) show no overlapping between the curve depicting the time series and the surrogate data curves which implies that the data is deterministic, the attractor has a complex structure. For data with measurement noise the correlation dimension curve has higher values than that of data without noise. A higher correlation dimension at small scales indicates more complex detail dynamics in the system caused by dynamic noise. A higher correlation dimension at all scales indicates an overall more complex structure in the attractor (Barnard, 1999). A higher correlation dimension is observed for Run A and Run C at small scale, while Run B and Run D exhibit low correlation dimension values.

5.7.2 SERIES B

In the correlation dimension curves for Series B, the deterministic character of the data is evident for Run A (Figure 5.38), Run B (Figure 5.39) and Run D (Figure 5.41). In the case of Run C (Figure 5.40) no distinction can be made between the original data set and the surrogates, which implies that the data is stochastic. The correlation

dimension has relatively low values at small scales for Run B and Run D, while Run A shows higher values.

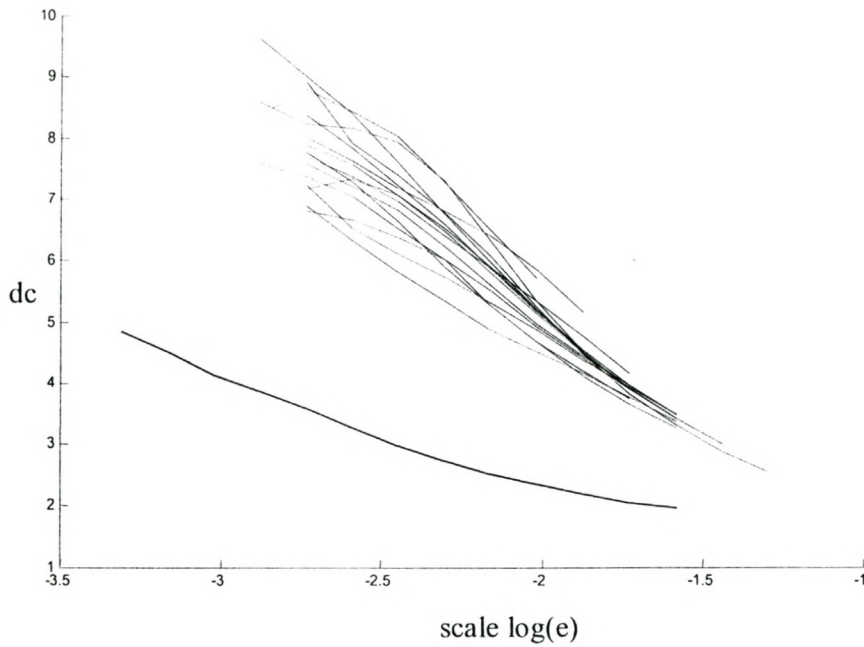


Figure 5.38 Surrogate data curves for Series B, Run A

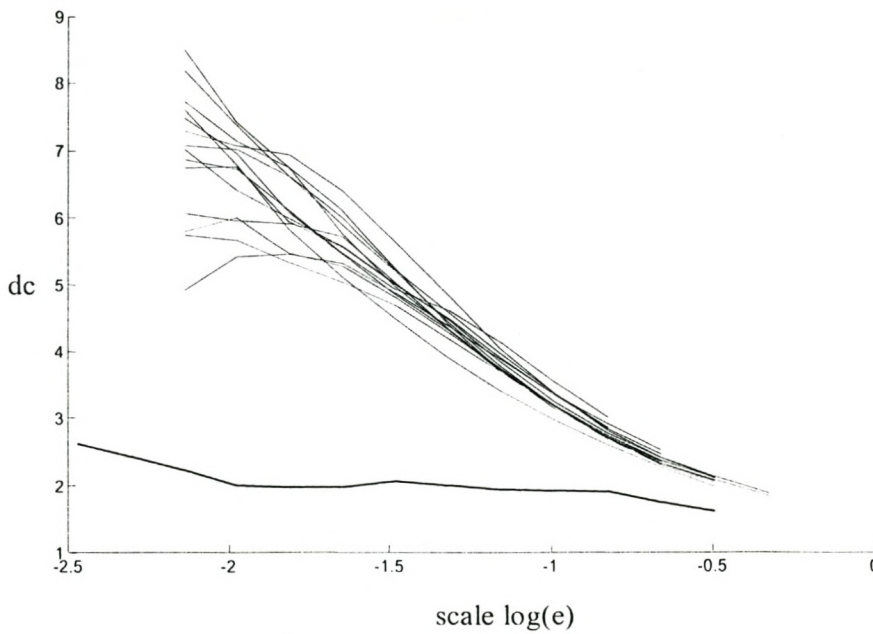


Figure 5.39 Surrogate data curves for Series B, Run B

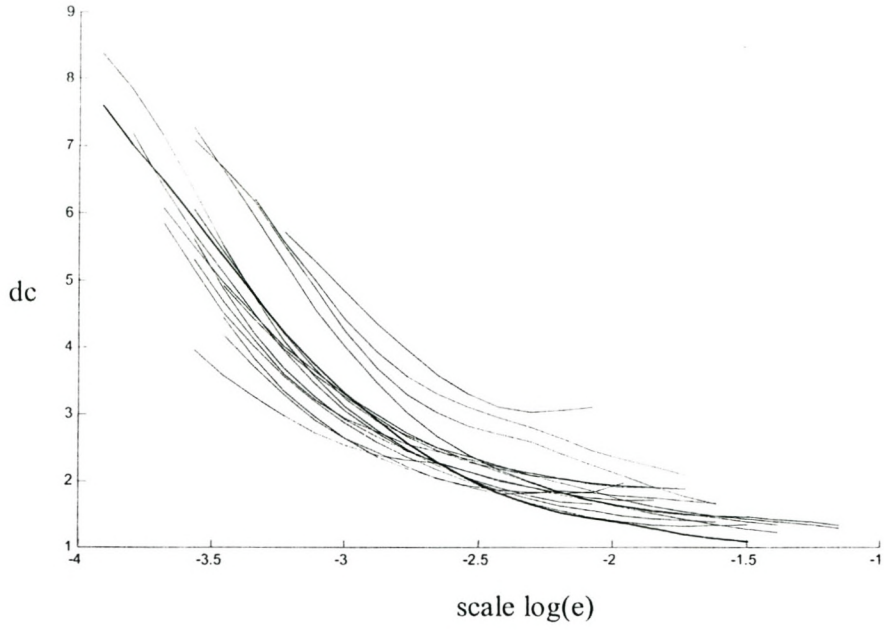


Figure 5.40 Surrogate data curves for Series B, Run C

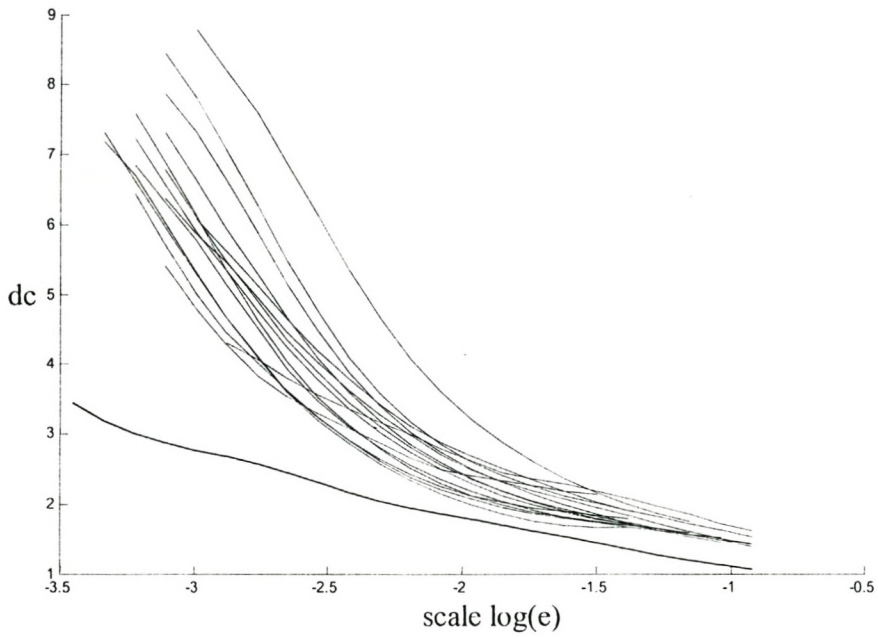


Figure 5.41 Surrogate data curves for Series B, Run D

5.8 MODELLING

A brief discussion on multi-layer perceptron neural networks as well as model validation is given in Section B4 of Appendix B.

The functional approximations for the data sets in Series A and Series B were done with a multi-layer perceptron neural network. The training function used was the Levenberg-Marquardt algorithm as it converges faster than most other training algorithms. Proper model validation ensures the reliable application of the model on new observations from the same process and was based on the significance of R^2 .

5.8.1 SERIES A

Modelling of Series A with the multi-layer perceptron network showed that no run in the series could be modelled with this method. As is evident from Table 5.5 the training and hence the cross-validation of the models in all runs were poor. Although some trend could be observed in the attractors and the surrogate data pointed towards determinism, the series are not predictable. The surrogate data obtained for Series A (Figure 5.34 to Figure 5.37) does show that the system is not stochastic but it does imply complexity.

Table 5.5 Table of R^2 values for training and cross validation for Series A

<i>Run</i>	<i>Training R^2</i>	<i>Cross-validation R^2</i>
<i>Series A, Run A</i>	0.2297	0.2611
<i>Series A, Run B</i>	0.3157	0.1365
<i>Series A, Run C</i>	0.2742	0.1524
<i>Series A, Run D</i>	0.2661	0.0806

From Figure 5.13 to Figure 5.16 it is clear to see why the validation R^2 for the models of Series A are so poor. As the cross-validation is done on the last 200 points of the

data set the poor validation can be explained by the instability difference curves. It is evident from the instability difference curves that the last 200 points is not a representative sample of the data, as the data show small instability differences in the beginning and at the end and large differences over a middle range of observations.

Two explanations can possibly be given for the fact that Series A could not be modelled. Firstly, the accuracy of the surrogate data curves obtained for Series A can be questioned. Although the null hypothesis was rejected implying that the system is non-linear and deterministic, signals that are non-stationary is not covered by most null hypothesis. An element of non-stationary in the series can be the reason why the hypothesis was rejected falsely. Secondly, the model fitted may not have been the correct choice and another model should be tested to investigate whether the data is predictable.

5.8.2 SERIES B

The modelling of Series B with the multi-layer perceptron network proved to be very successful, as illustrated in Table 5.6.

Table 5.6 Table of R^2 values for training and cross validation for Series B

<i>Run</i>	<i>Training R^2</i>	<i>Cross-validation R^2</i>
Series B, Run A	0.8055	0.0645
Series B, Run B	0.8638	0.8293
Series B, Run C	0.8956	0.3276
Series B, Run D	0.9201	0.8960

All four the runs of Series B showed excellent R^2 for training. However, the cross-validation was only successful for Run B and Run D. Figure 5.17 illustrates the curve for Series B, Run A. From the curve it is evident that the last 200 point used for cross-validation is not representative of the data sample. The decrease in instability was not recorded fully as recording of values was stopped at a relatively high instability value

when compared with the other trends (Run B, Run C, Run D). This is possibly the reason for the poor cross-validation R^2 obtained from the model. In the case of Run C, a long time interval, between 6000 seconds to 12000 seconds (s) is observed where the instability value remains relatively constant as illustrated in Figure 5.19. The data points used for cross-validation is taken from that constant period and would therefore explain the poor cross-validation R^2 . It would thus be recommended that the points for cross-validation should rather be 200 random data points, which should prove to be more representative of the instability data sample.

5.8.3 MODELS

From Table 5.2, as suggested by the low correlation dimension values obtained at micro-scale in the surrogate data curves, it is clear that Run B and Run D of Series B could be successfully modelled. In each case two figures illustrate the successful modelling. Figure 5.42 and Figure 5.44 show the data points as generated from the model versus the experimental values of the corresponding point. The R^2 summarised in Table 5.2 is a criterion of how well the model fits the data. In Figure 5.43 and Figure 4.45 the observed data is directly compared with the predicted data. The experimental values are shown as a line (observed data), while the corresponding data point generated from the model is marked as a black point (predicted data).

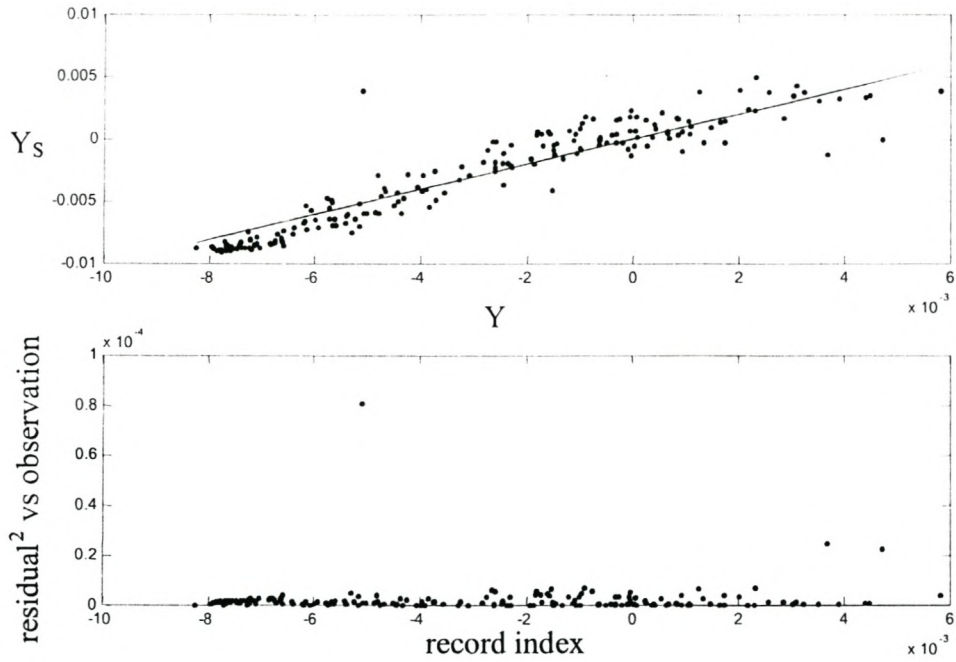


Figure 5.42 Multi-layer perceptron model for Series B, Run B

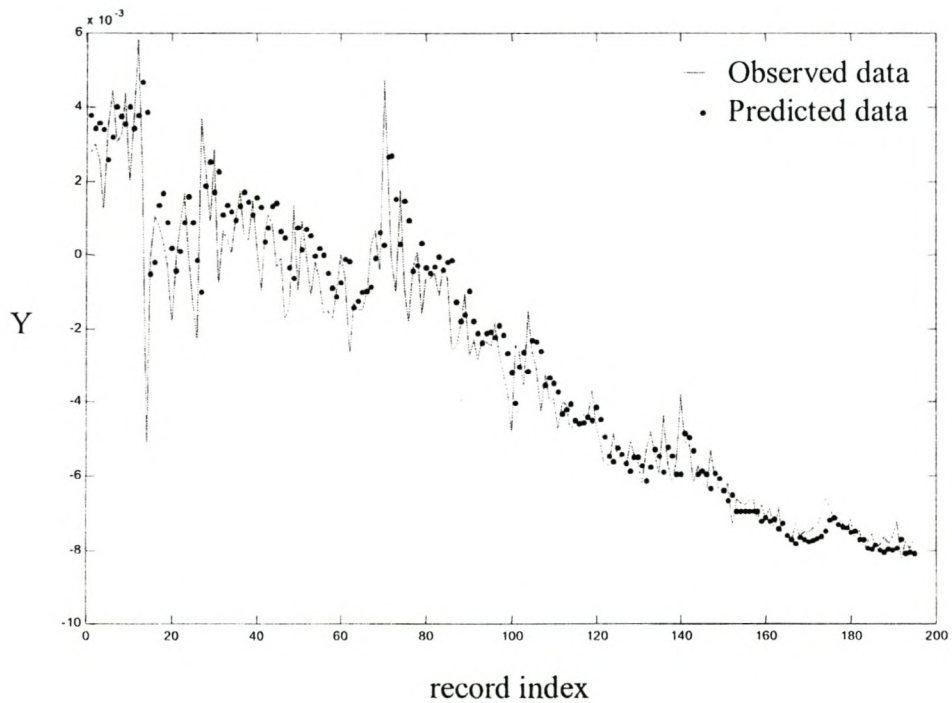


Figure 5.43 Predicted data vs Observed data for Series B, Run B

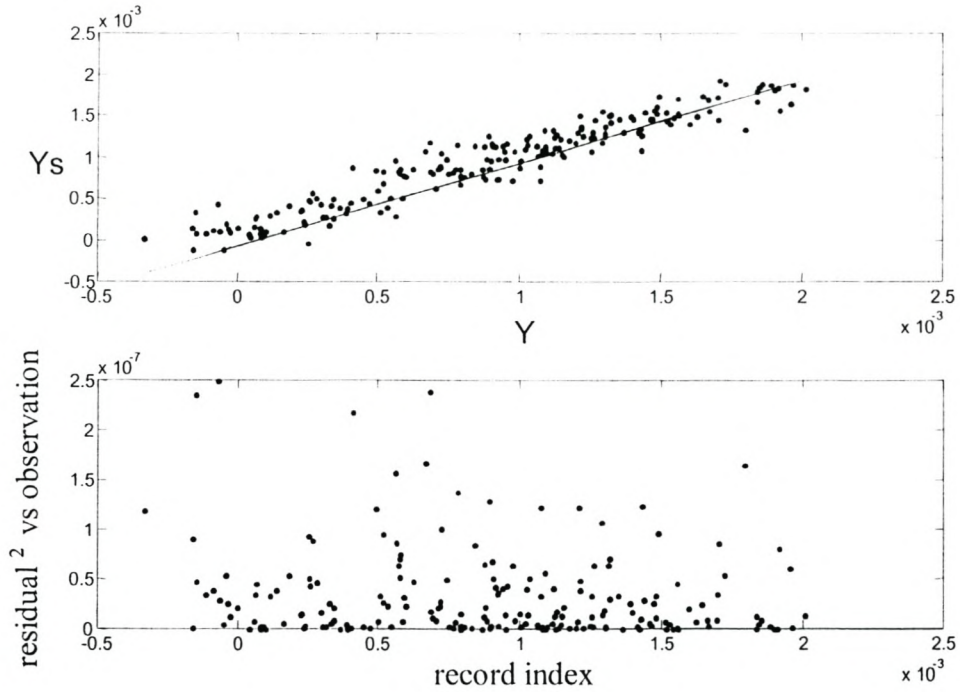


Figure 5.44 Multi-layer perceptron model for Series B, Run D

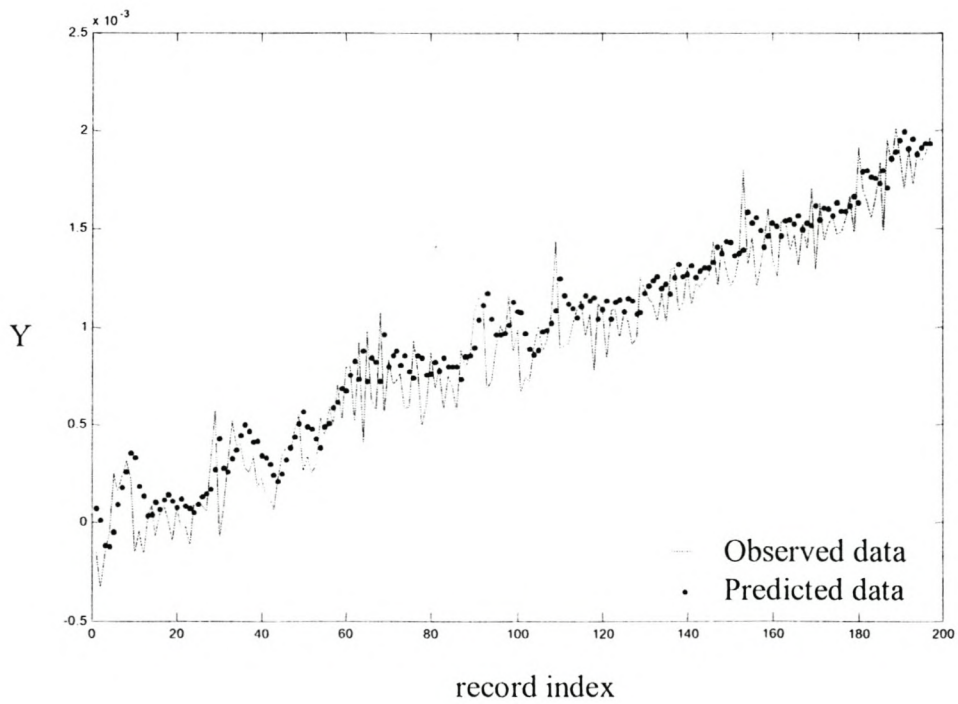


Figure 5.45 Predicted data vs Observed data for Series B, Run D

5.9 CONCLUDING REMARKS FOR TIME SERIES ANALYSIS

In the time series analysis used to characterise the stability of foam the first step was the state space reconstruction through singular spectrum analysis. The reconstructed attractors obtained for Series A and Series B defined a limited region in the state space and some pattern could be recognised implying that the order of the data points are not random. The surrogate data curves pointed towards determinism although high values for the correlation dimension at micro-scale was identified in Run A and Run C. The modelling of the two series showed that Series A could not be modelled but that successful models for Run B and Run D for Series B could be obtained.

5.10 CALCULATION OF STABILITY PARAMETER THROUGH MANUAL METHOD (SUPPLEMENTARY RESULTS)

As stated in Chapter 3, the decrease in foam volume can be used as a measure of foam stability. Iglesias et al. (1995) and Turner et al. (1999) found that the decay of short life foams as well as the decay of viscous foamed emulsions (made short-lived by vibration) follows an exponential trend. In both the studies the data was further processed to obtain a dimensionless plot of foam height (h) versus time (t) with reference to the initial height (h_0) and the half decay time ($t_{1/2}$). It was found that data points describing foams of the same concentration lie on the same line and it was proposed that the slope of the line is unique to a surfactant system of specific concentration. The half decay time ($t_{1/2}$) as well as the initial foam height (h_0) obtained was used as stability parameters, which can be used in the comparison of different foams. The method used by Iglesias et al. (1995) and Turner et al. (1999) is described in Chapter 3, Section 3.4.2.

The case study of the decay of cetyltrimethylammonium bromide as used for the investigation of the foam decay with the image analysis system was also used to obtain manual experimental data. The same runs, Run A (9 mM CTAB), Run B (repetition of Run A) and Run C (0.8 mM CTAB) recorded by the image analysis system and described in Section 5.3 were simultaneously monitored to investigate

whether the findings of Iglesias et al. (1995) and Turner et al. (1999) are applicable to long life foams. In the figure describing the decay of CTAB foam, Figure 5.46, the first run, Run A can be identified by the triangular marker, the second, Run B by the diamond marker and the third, Run C by the square marker.

From Figure 5.46 it is evident that the decay of foam generated from cetyltrimethylammonium bromide have a sigmoidal shaped curve as described by Bikerman (1973) for foam decay in a column (Section 2.6.4). There is a period where a very slow decrease in foam volume is observed (± 3000 seconds) after which a linear decrease in foam volume is observed. An explanatory regression model of the instability time series data was derived with the use of *Microsoft Excel*. The linear regression tool in *Microsoft Excel* performs linear regression by using the least-squares method to fit a line through a number of observations. The characteristics of the fitted linear curves are summarised in Table 5.7. It is evident from the high adjusted R^2 obtained that the linear model fits the data extremely well.

Table 5.7 Characteristics of linear regression curves describing Run A, Run B and Run C

<i>Run</i>	<i>Gradient</i>	<i>Intercept</i>	<i>Adjusted R^2</i>
A	0.001	23.07	0.995
B	0.001	20.32	0.972
C	0.0008	27.56	0.994

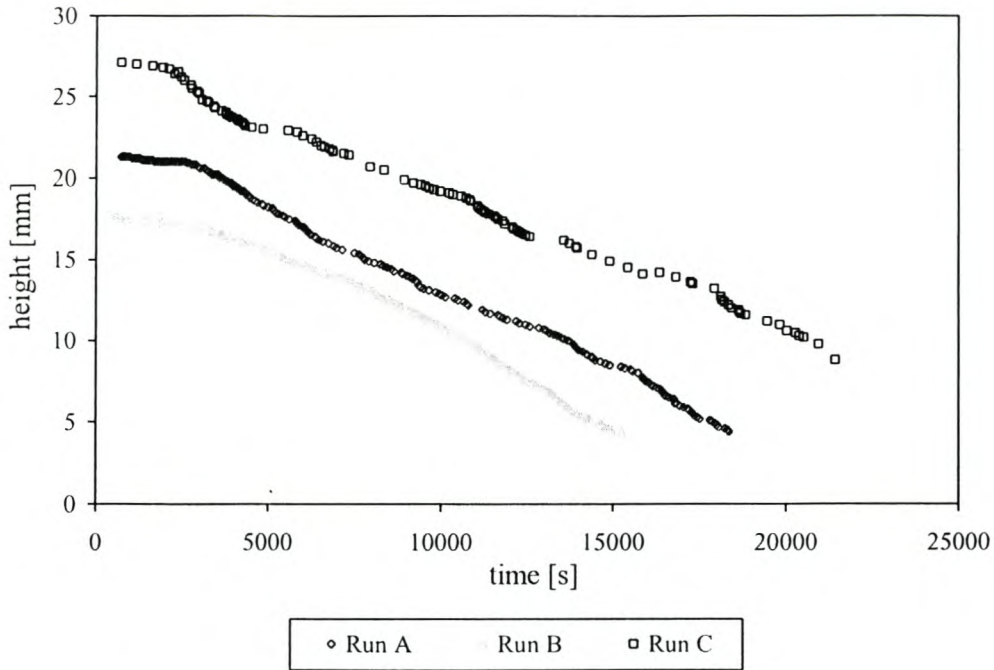


Figure 5.46 Foam height versus time for Run A, Run B and Run C

From Table 5.7 it is evident that Run A and Run B have the same gradient. The two runs is a repetition of the same experiment and as expected the runs show the same rate of decay. A higher foam volume was obtained for Run C (0.8 mM CTAB) than for Run A and Run B (9 mM CTAB), which explains the higher intercept of the curve.

The decay of long-life foam as illustrated in Figure 5.46 is not exponential, as is the case for short-life foams, but linear. The only further data processing done to test whether the curves do fall on the same curve as found by Iglesias et al. (1995) is to plot the data in dimensionless form.

The foam decay curves are described by the following equation:

$$h = -at + b \quad 5.3$$

The half decay time ($t_{1/2}$) is used as reference in order to plot the graph in dimensionless form. If it is assumed that the curves will pass through the point (1, 0.5) Equation 5.3 ideally takes on the following form:

$$\frac{h}{h_o} = -a \left(\frac{t}{t_{1/2}} \right) + \left(\frac{1}{2} + a \right) \quad 5.4$$

As expected the curves pass through the point (1,0.5) where the curves of Iglesias et al. (1995) passed through the central point (0,0.5). This is owing to the fact that they used a semi-log plot to transform the original exponential curve into a linear curve. In order to investigate the linear section of the curves, only the data obtained between 20 percent (%) and 80 percent (%) of the time measured was used, thereby excluding the period of slow decrease in the beginning.

Figure 5.47 illustrates the curves of Run A and Run B as well as a run (Run D) of the same surfactant concentration as Run A and Run B but containing 1 weight percent (%) NaCl. Run A is identified by the triangular marker, Run B by the diamond marker and Run D by the circular marker.

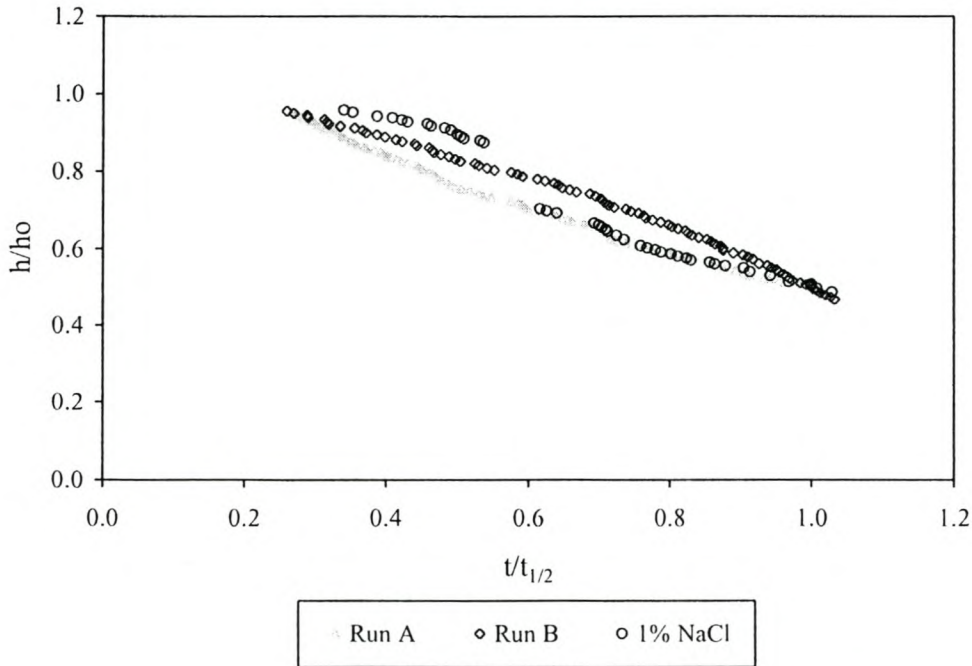


Figure 4.47 Dimensionless foam decay curves over 20 percent to 80 percent of decay time

It is evident from Figure 5.47 that the curves do not coincide on the same straight line but that a large portion of Run D follows the same trend than the curve of Run B. Once again the linear curves describing the curves were obtained through linear regression. The characteristics of the equations describing the three curves are summarised in Table 5.8.

Table 5.8 Characteristics of linear regression curves describing Run A, Run B and Run C in dimensionless plot

<i>Run</i>	<i>Gradient</i>	<i>Intercept</i>
A	0.63	1.09
B	0.62	1.14
D	0.79	1.25

It is evident from Table 5.8 that the gradients of the linear curve describing Run A and Run B are very close in value. It could thus be said that although the data points do not lie on the same straight line, the rate of foam decay is essentially the same. The linear curve describing Run D varies from that describing Run B although the curves coincide over a period of time. This is as a result of the difficulty with which the manual values for Run D were obtained. The foam containing 1 percent (%) NaCl did not decrease in volume uniformly as in the case of Run A and Run B. The foam level used as reference showed high peaks at some parts of the column and lower parts on others. The foam decay was fast and a catastrophic collapse was observed between 2550 seconds and 2890 seconds where the foam height decreased from 16.5 centimetres to 13.3 centimetres. From Figure 5.48 it is evident that this catastrophic collapse is the divider between the data points that lie away from the other curves and the data points that coincides with the curve of Run B. A front view of the column shows the non-uniform decrease in foam volume.

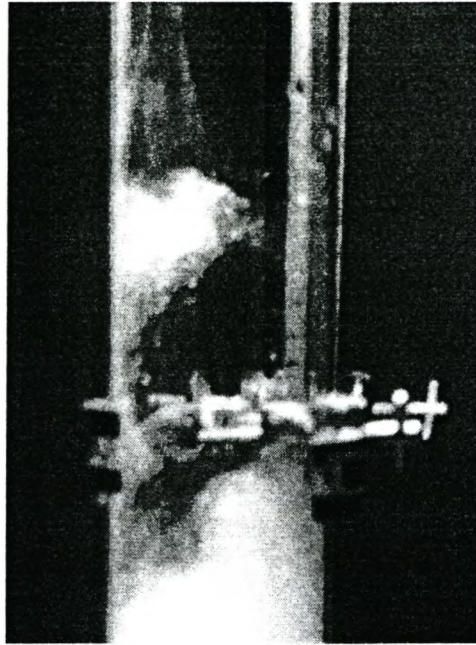


Figure 5.48 Non-uniform foam collapse of CTAB containing 1 percent (%) NaCl

Iglesias et al. (1995) stated that the gradient of the line can be approximated as the decay constant, λ and that it is the same for a specific surfactant system. From Figure 5.47 it is evident that the same conclusion can be drawn for long-life foams.

5.11 SYMBOLS USED IN CHAPTER 5

<i>Symbol</i>	<i>Description</i>	<i>Unit</i>
q	Grey level threshold	-
SB	Stability	-
x	Pixel grey level	-

CHAPTER 6

CONCLUSIONS AND RECOMMENDATIONS

6.1 CONCLUSIONS

The main conclusions drawn from the two case studies in the present study are listed below.

6.1.1 CASE STUDY: FLOTATION OF QUARTZ

6.1.1.1 System differentiating

The image analysis system differentiates well between two-and three-phase systems of different concentration.

- i Through the application of principal component analysis it was shown that experimental runs of different surfactant concentration occupy a limited region in the 3D factor plot. Every limited region represents a combination of the unique characteristics described by the three principal components. The image analysis can differentiate successfully between the three surfactant groups.
- ii The factor matrix shows the loadings of the seven image variables extracted by the image analysis system. In the two-phase and three-phase system the bubble size characteristics such as *average area*, *average perimeter* and *number of bubbles* are loaded on the first factor. The second factor describes the colour of the foam/froth (*average grey level*) and the third factor the movement or *average speed* of the foam/froth.

Two variables, namely *SNE* and *stability* could not be confined to a specific factor.

- iii In both the two-phase and three-phase systems the characteristics of the different groups can be compared by investigating the position of the group in the 3D factor plot. Each group has a unique set of co-ordinates and factor values and thus unique characteristics. The position of the group can be analysed to determine how the characteristics of the groups change with surfactant concentration or addition of particles. For instance, a group that has a higher value for Factor 3 will show an increase in bubble movement.

6.1.1.2 Correlation between extracted variables

The bivariate correlation performed on the seven image variables extracted showed the following correlations in general:

- i The bubble characteristics *average area*, *average perimeter* and *number of bubbles* are highly correlated.
- ii The *SNE* and *number of bubbles* are highly correlated as expected. *SNE* or the measure of fineness is used in the flotation industry as a secondary measurement of the number of bubbles.
- iii The *stability* of the foam shows correlations on the 0.01 and 0.05 level with all other image variables extracted.

6.1.1.3 Identification of groups

The linear discriminant analysis performed on the two -and three- phase systems showed that the image analysis system can successfully group different data points of the same experimental run as belonging to the same group.

The image analysis system has potential as research tool, since it successfully differentiates between systems of different characteristics and the surfactant groups identified have unique characteristics. Through image analysis it is possible to quantify the change in characteristics of a system with the change in surfactant ratio.

6.1.1.4 Stability of foam and froth

The difference in stability of foam for three surfactant ratios was investigated. The same system was applied to the three-phase system where the three surfactant concentrations were investigated with the addition of quartz particles. Four different sized quartz particles were investigated. The following conclusions regarding foam and froth stability are reached:

- i Foam generated from 100 percent (%) CTAB shows higher foam stability than any other CTAB and ODA combination.
- ii No conclusion could be reached regarding the rank in stability between foam of 90 percent (%) CTAB and 80 percent (%) CTAB.
- iii A stability test showed that the high instability peaks present in the stability curves are owing to the movement of the foam in the cell. The comparison of the average speed curve with the stability curve support this finding, as high average speed values corresponds to high instability values.
- iv The image analysis system has difficulty with areas of fine froth, as stated by Botha (1999a). The grouping of areas of fine froth into one bubble leads to inaccurate measurements of the number of bubbles.
- v No conclusion could be reached regarding the rank of the stability of the three surfactant ratios for a specific quartz system. The three curves cross one another repeatedly.

- vi The three phase system containing quartz particles of $-75\ \mu\text{m}$ have the highest stability in the case of the 90 percent (%) and 80 percent (%) CTAB systems. This is in accordance with Dippenaar (1982b), Szatkowski & Freyburger (1985) and Johansson & Pugh (1992). The experimental runs containing $150+\ \mu\text{m}$ particles show the highest instability, while the intermediate particle sizes $75\text{-}106\ \mu\text{m}$ and $106\text{-}150\ \mu\text{m}$ show no definite stability ranking.

- vii As in the case of the two-phase system, stability peaks and valleys are observed in the three-phase system, owing to the movement of the froth in the flotation cell.

6.1.1.5 Recovery

The following trends could be identified in the recovery of quartz particles:

- i CTAB is a better collector than ODA. 100 percent (%) CTAB show recoveries of between 91 percent (%) and 96 percent (%) for all particle sizes, while the recovery range for ODA is between 31 percent (%) and 53 percent (%).

- ii The quartz of intermediate particle size $106\text{-}150\ \mu\text{m}$ shows the highest recovery for all concentrations of CTAB and ODA. This is in accordance with Bennett et al. (1958), Sun & Zimmerman (1950) and Lynch et al. (1981) who found an intermediate size of coal particles to show the highest flotation recovery.

6.1.2 CASE STUDY: DECAY OF CETYLTRIMETHYLAMMONIUM BROMIDE

6.1.2.1 Instability curves

The stability of a cetyltrimethylammonium bromide foam column was investigated by the image analysis system. Two surfactant concentrations were investigated and the following are observed regarding the stability trends:

- i The two runs executed at a concentration of 9 millimolar (mM) have the same shape, but the foam decay in the second is much shorter. This could be owing to evaporation as an open system was used.
- ii The foam of higher concentration (9 mM) is of higher stability (or lower instability) than the foam of 0.8 mM CTAB. This is owing to micelle formation at the higher concentration, which prevents drainage in the system, and thus increases foam lifetime.
- iii The foam at the higher CTAB concentration (9 mM) shows a slow instability increase as the foam bubbles are closely packed and bubble coalescence are slow. The machine vision system cannot identify foam bubbles of such small diameter.

6.1.2.2 Time series analysis

The time series analysis of the instability series as generated from the image analysis system successfully characterised the decay of cetyltrimethylammonium bromide foam. The following characteristics of the system can be summarised:

- i The reconstructed attractors obtained for Series A and Series B imply that neither time series is stochastic. The attractors define a limited region in

the state space and have a definite pattern, which prove that the data points are not random. The attractors in Series A are complex and the complexity indicates that there is a considerable amount of noise in the system.

- ii The surrogate data curves show that the time series are deterministic except for the case of Run C of Series B. The correlation dimension values are low for Run B and Run D for both series (A and B), which implies that there was less measurement noise for these two runs as for Run A and Run C. The high correlation dimension at small scale in the case of Run A and Run C indicates complex dynamics of the system caused by dynamic noise.
- iii The non-linear model used to model the data was a multi-layer perceptron neural network. The data sets in Series A could not be modelled but in the case of Series B all four runs showed very good training R^2 . However, only Run B and Run D performed well under cross-validation. The two models are successful, the predictions are effective and the underlying dynamics of the system have been modelled well.
- iv The failure to model Series A could be owing to a false rejection of the null hypothesis used in the construction of the surrogate data.

The stability of foam or the lifetime of foam is dependent on many factors and many mechanisms such as drainage, disproportionation and evaporation play an intricate role in the decay. The system is complex and it would seem that to model the decay of foam from first principles would be a cumbersome task. *However, from the time series analysis it can be concluded that the decay of foam in a column is non-linear and deterministic.*

6.1.2.3 Stability as measured by manual method

The following conclusions are reached from the application of a manual method to a long-life foam:

- i The decay of the long-life foam cetyltrimethylammonium bromide has a sigmoidal foam decay in accordance with the prediction of Bikerman (1973) and not an exponential decay as in the case of short-life foams (Iglesias et al., 1995) and short-life emulsions (Turner et al., 1999).
- ii The reading of the foam height did prove to be problematic, as foreseen by Bikerman (1973) especially for the system containing NaCl.
- iii The results obtained from the foam decay curves of CTAB shows that if the decay curve is plotted as a straight line, surfactant systems of the same concentration shows the same gradient. This is in agreement with the findings of Iglesias et al. (1995) and Turner et al. (1999) who investigated short-life foams and short-life foamed emulsions. A unique decay constant (λ) can be identified for every surfactant at a specific concentration
- iv Considering the height versus time plot, the statement made by Iglesias et al. (1995) that the same line can describe all the data points of a similar surfactant system appear to be an estimation. The deviations of the data points as found by Iglesias et al. (1995) from the linear approximation are owing to the different initial foam heights obtained. In experimental work many factors influence the foamability of the system. Different values of initial foam height can thus be obtained for the same system firstly owing to experimental conditions and secondly owing to any additives that will alter this value. It is thus a better approximation to state that the curves describing a surfactant of a specific concentration have the same gradient or decay constant.

As the manual method and the image analysis method as measurement techniques were applied to the same system, it can be concluded that the image analysis system is a viable alternative to current stability measurements. Firstly, the system provides a direct stability value at a time interval and no calculation of an indirect stability parameter is necessary. Secondly, the system also computes the bubble size distribution of the sample. Monsalve & Schechter (1984) proved that initial bubble distribution of a foam sample has an effect on the stability of the foam and criticised the existing stability measurement methods as none provided for bubble distributions.

6.2 RECOMMENDATIONS FOR FURTHER RESEARCH

The following comments and recommendations for further research are made:

- i The instability data are very sensitive to its environment and any change in its surroundings. Factors like evaporation, the presence of other particles like dust as well as vibration decreases the persistence of foam lamellae. These are factors little could be done about in the present study but which did affect the instability values obtained and could explain the difference in lifetime of the foams of similar concentration as well as the difference in shape of the instability curves. As the system under investigation is very sensitive, it is proposed that the experimental design of a system used for foam stability testing should be adapted to ensure the minimisation of environmental effects on the foam.
- ii The quality of images obtained from the image analysis system, and thus also the quality of instability values obtained is dependent on the focus length between the camera lens and the foam surface. The focus depth was kept constant as far as possible but after a certain amount of liquid was drained from the foam, the foam layer was too low to ensure a constant focus depth. The reflectance of the light from the side of the glass column causes disturbances of the real image. It is proposed that an alternative camera set-up be explored. Alternatives do exist, but not without disadvantages. The use of a long lens with 25 millimetre field

depth can minimise the problems regarding the focus height, but the drawback of this option is the problem it creates with the sufficient lighting of the foam surface. Another option is the application of a telecentric lens. This lens provides a constant magnification with object position but only has a field depth of 3 millimetres, which would imply that the camera has to be moved for every 3 millimetres that the foam height decreases.

- iii The inability of the image analysis to deal with fine froth needs to be addressed. In the current image analysis system the regions of fine froth are grouped as one bubble. In the laboratory system the typical surfactant system investigated will show a small bubble distribution or a dense foam, as in the case of CTAB. The extent to which the grouping of a fine froth area influence the stability values obtained must be investigated.
- iv The investigation of specific combinations of surfactant types over a spectrum of surfactant concentration and ratio should be conducted to investigate the predictability of the system regarding characteristics of foam. It was proven that the system can successfully identify unique characteristics of different systems, but for the application of surfactant design the system has to be able to predict system characteristics at a set surfactant ratio.
- v The effect of additives such as mineral particles and electrolytes such as sodium chloride on the stability and decay of foam must be investigated in a similar manner in which the foam decay of CTAB was performed. The results will lead to a better understanding of the stability measure as computed by the image analysis system.
- vi The high correlation between movement in a foam or froth and an increase in instability was proved in this study. The extent to which the internal movement of a foam/froth, including bubble coalescence and bubble movement as well as foam/froth movement of an external type

such as overflowing of a cell influence the stability of the foam/froth must be investigated further.

- vii The main reason why inconclusive results are obtained in the investigation of the effect of particles on froth stability is the vast number of different systems used. A study should be conducted which cover different types of particles of different particle sizes and hydrophobicity at different solid concentrations, thus combining the four main factors influencing the effect of particles on a foam system.

The study was an overview of current experimental methods used to determine foam stability. A flowchart is presented in Figure 6.1, which summarises the steps necessary for the measurements of foam stability with Bikerman's dynamic method as well as image analysis.

6.3 FLOW DIAGRAM OF FOAM STABILITY EVALUATION PROCEDURE

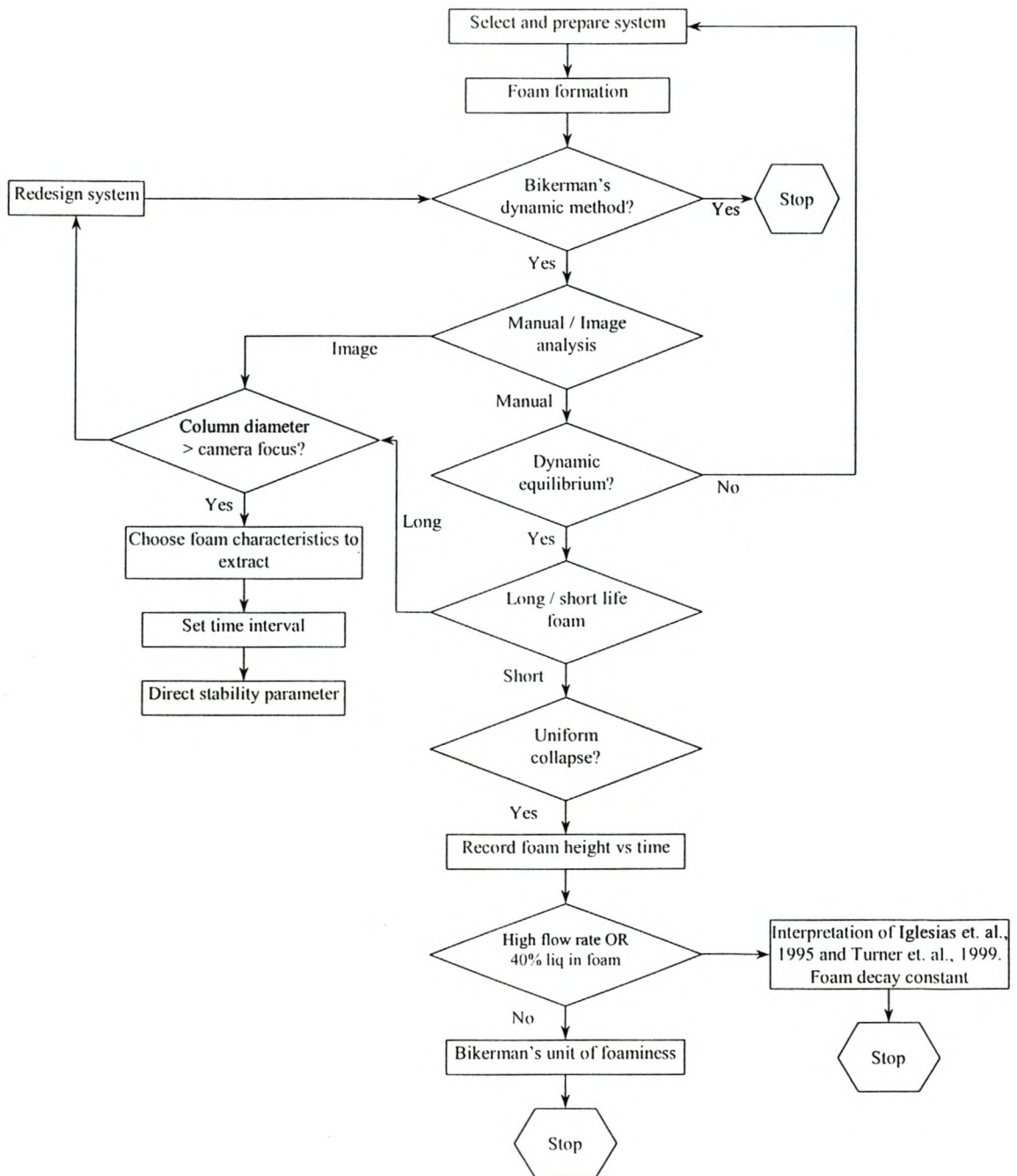


Figure 6.1 Flow diagram of foam stability evaluation process

REFERENCES

- Ahmed, N. & Jameson, G.J., (1985). The effect of bubble size on the rate of flotation of fine particles, *International Journal of Minerals Processing*, Volume 14, pp. 195-215.
- Angarska, J.K., Tachev, K.D., Kralchevsky, P.A., Mehreteab, A. & Broze, G., (1998). Effects of Counterions and Co-ions on the Drainage and Stability of Liquid Films and Foams, *Journal of Colloid and Interface Science*, Volume 200, pp. 31-45.
- Askeland, D.R., (1996). *The Science and Engineering of Materials* (3rd ed.), Chapman & Hall, London.
- Aveyard, R., Binks, B.P., Clint, J.H. & Fletcher, P.D.I., (1999). Foams and Emulsions: Their Stability and Breakdown by Solid Particles and Liquid Droplets. In J.F. Sadoc & N. Rivier (eds.), *Foams and Emulsions* (pp. 21-44). Kluwer Academic Publishers, The Netherlands.
- Barnard, J.P., (1999). *Empirical State Space modelling with Application in On-line Diagnosis of Multivariate Non-Linear Dynamic Systems*, Ph.D. Thesis, University of Stellenbosch, Stellenbosch, South Africa.
- Barnard, J.P., Aldrich, C. & Gerber, M., (2001). Identification of dynamic process models with surrogate data, *AIChE Journal*, Volume 47, Number 9, pp. 2064-2075.
- Beneventi, D., Carre, B. & Gandini, A., (2001). Role of surfactant structure on surface and foaming properties, *Colloids and Surface A: Physicochemical and Engineering Aspects*, Volume 189, pp. 65-73.
- Bennett, A.J.R., Chapman, W.R. & Dell, C.C., (1958). Studies in froth flotation of coal, *Third International Coal Preparation Congress*, Brussels-Liege, June, Paper E2.

Bennett, G.F., (1988). The removal of oil from wastewater by air flotation, *Environmental Control (CRC Critical Reviews)*, Volume 18, pp. 189-253.

Bergeron, V., (1999). An introduction to forces and structures in individual foam and emulsion films. In J.F. Sadoc & N. Rivier (eds.), *Foams and Emulsions* (pp. 45-72). Kluwer Academic Publishers, The Netherlands.

Bikerman, J.J., (1938). The unit of foaminess, *Transactions of the Faraday Society*, Volume 34, pp. 634-638.

Bikerman, J.J., (1973). *Foams*, Springer-Verlag, New York, United States of America.

Bisperink, C.G.J., Ronteltap, A.D. & Prins, A., (1992). Bubble size distributions in foam, *Advances in Colloid and Interface Science*, Volume 38, Number 13, pp. 13-32.

Bлга, A., (1974). Rigid thermosetting Plastic Foams, *Canadian Building Digest* [Online], Volume 168, Available: <http://www.nrc.ca>. [2001, October 25].

Botha, C.P., (1999a). *An On-line Machine Vision Flotation Froth Analysis Platform*, Master's Thesis, University of Stellenbosch, Stellenbosch, South Africa.

Botha, C.P., Weber, D.M., Van Olt, M. & Moolman, D.W., (1999b). Practical system for real-time on-plant flotation froth visual parameter extraction. *IEEE AFRICON Conference*, Volume 1, pp. 103-106.

Beward, C.J.W., Darton, R.C., Howell, P.D. & Ockendon, J.R., (1997). Modelling foam drainage, *Institution of Chemical Engineers Symposium Series*, pp. 1009-1019.

Broomhead, D.S. & King, G.P., (1986). Extracting qualitative dynamics from experimental data, *Physica D*, Volume 20, pp. 217-236.

Bustamante, H. & Warren, L.J., (1984). The joint effect of rank and grain size on the flotation of Australian bituminous coals, *International Journal of Minerals Processing*, Volume 13, pp. 13-28.

Callaghan, I.C., (1989). Non-Aqueous Foams: a Study of Crude oil Foam Stability. In A. J. Wilson (ed.), *Foams: Physics, Chemistry and Structure* (pp.89-104). Springer-Verlag, Great Britain.

Chang, R.C., Schoen, H.M. & Grove, C.S., (1956). Bubble size and bubble size distribution, *Industrial Engineering Chemistry*, Volume 48, pp. 2035-2039.

Chang, K.-S. & Lemlich, R., (1980). A Study of the Electrical Conductivity of Foam, *Journal of Colloid and Interface Science*, Volume 73, Number 1, pp. 224-232.

Chen, Z., Nishimura, S., Sasaki, H. & Usui, S., (1991). Cationic flotation of quartz using dodecyltrimethylammonium bromide (DTAB), *Metallurgical Review of MMIJ*, Volume 8, Number 1, pp. 22-34.

Cheng, H.C. & Lemlich, R., (1985). Theory and Experiment for Interbubble Gas Diffusion in Foam, *Industrial Engineering and Chemistry Fundamentals*, Volume 24, pp. 44-49.

Churchill, R.J. & Tacchi, K.J., (1978). A critical analysis of flotation performance, *AIChE Symposium Series*, Volume 75, Number 190, pp. 290-299.

Clark, N.O. & Blackman, M., (1948). The transmission of light through foam, *Transactions of the Faraday Society*, Volume 44, pp. 7-13.

Croda Fire Fighting Chemicals [Online], (2000). Available: <http://www.croda-firefighting.co.uk>. [2001, October 25].

Crozier, R.D., (1992). *Flotation: Theory, Reagents and Ore Testing*, Pergamon Press, Great Britain.

De Vivo, D.G. & Karger, B.L., (1970). Studies in the flotation of colloidal particulates: Effects of aggregation in the flotation process, *Separation Science*, Volume 5, pp. 145-167.

Dickinson, E., (1992). *An Introduction to Food Colloids*, Oxford University Press, Oxford, Great Britain.

Dippenaar, A., (1982a). The destabilization of froth by solids. I. The mechanism of film rupture, *International Journal of Mineral Processing*, Volume 9, pp. 1-14.

Dippenaar, A., (1982b). The destabilisation of froth by solids. II. The rate determining step, *International Journal of Mineral Processing*, Volume 9, pp. 15-27.

Eksteen, J.J., (1995). *The development and technology transfer of an industrial machine vision system for the control of a platinum flotation plant*, Master's Thesis, University of Stellenbosch, Stellenbosch, South Africa.

Elsner J.B. & Tsonis, A.A., (1996). *Singular Spectrum Analysis: A New Tool in Time Series Analysis*, Plenum Press, New York, United States of America.

Exerowa, D., Khristov, K.H.R. & Penev, I., (1976). Some techniques for the investigation of foam stability. In R.J. Akers (ed.), *Foams* (pp.109-124). Academic Press, Great Britain.

Exerowa, D., Kashchiev, D. & Platikanov, D., (1992). Stability and permeability of amphiphile bilayers, *Advances in Colloid and Interface Science*, Volume 40, pp. 201-256.

Feng, D. & Aldrich, C., (2000). The effect of frothers on bubble size distributions in flotation pulp phases and surface froths, *Minerals Engineering*, Volume 13, Number 10-11, pp. 1049-1057.

Francis, J.J. & De Jager, G., (1998). An investigation into the suitability of various motion estimation algorithms for froth imaging, *Proceedings of the IEEE South Africa Symposium on Communications and Signal Processing*, pp. 139-142.

Fruhner, H., Wantke, K.-D. & Lunkenheimer, K., (1999). Relationship between surface dilational properties and foam stability, *Colloids and Surfaces A: Physicochemical and Engineering Aspects*, Volume 162, pp. 193-202.

Gandolfo, F.G. & Rosano, H.L., (1997). Interbubble Gas Diffusion and the Stability of Foams, *Journal of Colloid and Interface Science*, Volume 194, pp. 31-36.

Garrett, P.R., (1993). Recent developments in the understanding of foam generation and stability, *Engineering Science*, Volume 48, Number 2, pp. 367-392.

Gopalratnam, V.C., Bennett, G.F. & Peters, R.W., (1992). Effect of collector dosage on metal removal by precipitation/flotation, *Journal of Environmental Engineering*, Volume 118, pp. 923-948.

Grassberger, P. & Procaccia, I., (1983). Characterization of strange attractors, *Physical Review Letters*, Volume 50, pp. 346-349.

Harris, C.C., (1976). Flotation machines. In M.C. Fuerstenau (ed.), *Flotation*. (pp.753-815). A.M. Gaudin Memorial Volume, AIME, New York, United States of America.

Harris, P.J., (1982). Frothing phenomena and frothers. In R.P. King (ed.), *Principles of flotation*. (pp.237-250). *South African Institute of Mineral and Metallurgy Monograph Series*, Number 3.

Hédreul, C. & Frens, G., (2001). Foam stability, *Colloids and Surfaces A: Physicochemical and Engineering Aspects*, Volume 182, pp. 73-82.

Holtham, P.N., (1999). JKFrothCam – An on-line vision-based instrument for measuring froth flotation properties [Online], Available from: <http://www.jkrmc.uq.edu.au>. [2001 October 2].

Iglesias, E., Anderez, J., Forgiarini, A. & Salager, J.-L., (1995). A new method to estimate the stability of short-life foams, *Colloids and Surfaces A: Physicochemical and Engineering Aspects*, Volume 98, pp. 167-174.

Jameson, G.J., (1999). Hydrophobicity and floc density in induced-air flotation for water treatment, *Colloids and Surfaces A: Physicochemical and Engineering Aspects*, Volume 151, pp. 269-281.

Johansson, G. & Pugh, R.J., (1992). The influence of particle size and hydrophobicity on the stability of mineralized froths, *International Journal of Minerals Processing*, Volume 34, pp. 1-21.

Judd, K., (1992). In improved estimator of dimension and some comments on providing confidence intervals, *Physica D*, Volume 56, pp. 216-228.

Judd, K., (1994). Estimating dimension from small samples, *Physica D*, Volume 71, pp. 421-429.

Kaplan, D., (2001). Matlab software for non-linear time series [Online], Available from :<http://www.mcalstr.edu/~kaplan/> [2001, September 28].

Kato, A., Takahashi, A., Matsudomi, N. & Kobayashi, K., (1983). Determination of foaming properties of proteins by conductivity measurements, *Journal of Food Science*, Volume 48, pp. 62-65.

Klassen, V.I. & Mokrousov, V.A., (1963). *An Introduction to the Theory of Flotation*, Butterworth, London.

Kulkarni, R.D., Goddard, E.D. & Kanner, B., (1977). Mechanisms of anti-foaming: The role of filler particle, *Industrial Engineering and Chemical Fundamentals*, Volume 16, Number 4, pp. 472-474.

Kugiumtzis, D., (1996). State Space Reconstruction Parameters in the Analysis of the Chaotic Time Series – The Role of the time Window Length, *Physica D: Non-linear phenomena*, Volume 85, Issue 1, pp. 13-28.

Kugiumtzis, D., Lillekjendlie, B. & Christophersen, N., (1994). Chaotic time series Part I: Estimation of some invariant properties in state space, *Modelling, Identification & Control*, Volume 15, Number 4, pp. 205-224.

Lachaise, J., Graciaa, A., Marion, G. & Salager, J.L, (1990). A new reflectometry method to measure a liquid foam stability, *Journal of Dispersion Science and Technology*, Volume 11, Number 4, pp. 409-430.

Lai, Y-C., Lerner, D., (1998). Effective scaling region for computing the correlation dimension from chaotic time series, *Physica D*, Volume 115, pp. 1-18.

Langevin, D., (1999). Surface energy and surface rheology: Relation to foam properties. In J.F. Sadoc & N. Rivier (eds.), *Foams and Emulsions* (pp. 1-19). Kluwer Academic Publishers, The Netherlands.

Lemlich, R., (1978). Prediction of change in Bubble Size Distribution Due to Interbubble Gas Diffusion in Foam, *Industrial Engineering and Chemistry Fundamentals*, Volume 17, Number 2, pp. 89-93.

Livshits, A.K. & Dudenkov, S.V., (1965). Some factors in flotation froth stability. In *Proceedings of the 7th International Mineral Processing Congress* (pp. 367-371), Gordon & Breach, New York.

Lynch, A.J., Johnson, N.W., Manlapig, E.V. & Thorne, C.G., (1981). *Mineral and Coal Flotation Circuits: Their simulation and Control*, Elsevier Publishers, Amsterdam.

Malysa, K., (1992). Wet foams: Formation, Properties and Mechanism of Stability, *Advances in Colloid and Interface Science*, Volume 40, pp. 37-83.

Mathe, Z.T., Harris, M.C., O'Connor, C.T. & Franzidis, J. -P., (1998). Review of froth modelling in steady state flotation systems, *Minerals Engineering*, Volume 11, Number 5, pp. 397-421.

McEnke, W.R. & Mysels, K.J., (1969). Bursting of sub-films. I. An experimental study, *Journal of Physical Chemistry*, Volume 73, pp. 3018-3028.

Monsalve, A. & Schechter, R.S., (1984). The Stability of Foams: Dependence of Observation of the Bubble Size Distribution, *Journal of Colloid and Interface Science*, Volume 97, Number 2, pp. 327-335.

Moolman, D.W., Aldrich, C., Van Deventer, J.S.J. & Stange, W.W., (1994). Digital image processing as a tool for on-line monitoring of froth in flotation plants, *Minerals Engineering*, Volume 7, Number 9, pp. 1149-1164.

Moolman, D.W., (1995a). *The interpretation of flotation froths by using computer vision and connectionist networks*, Ph.D. thesis, University of Stellenbosch, Stellenbosch, South Africa.

Moolman, D.W., Aldrich, C. & Van Deventer, J.S.J., (1995b). The monitoring of froth surfaces on industrial flotation plants using connectionist image processing techniques, *Minerals Engineering*, Volume 8, pp. 23-30.

Moolman, D.W., Aldrich, C., Van Deventer, J.S.J. & Stange, W.W., (1995c). The classification of froth structures in a copper flotation plant by means of a neural net, *International Journal of Minerals Processing*, Volume 43, pp. 193-208.

Moolman, D.W., Aldrich, C., Van Deventer, J.S.J. & Bradshaw, D.J., (1995d). The interpretation of flotation froth surfaces by using digital image analysis and neural networks, *Chemical Engineering Science*, Volume 50, Number 22, pp. 3501-3513.

Moolman, D.W., Eksteen, J.J., Aldrich, C. & Van Deventer, J.S.J., (1996). The significance of flotation froth appearance for machine vision control, *International Journal of Minerals Processing*, Volume 48, pp. 135-158.

Moudgil, B.M. & Gupta, D., (1989). Flotation of coarse phosphate particles. In S. Chander & R.R. Klimpel (eds.), *Advances in Coal and Mineral Processing using Flotation* (pp.164-168). Proceedings of an Engineering Foundation Conference, Palm Coast, Florida, December, Society of Mining, Metallurgy and Exploration Incorporated, Colorado.

Mysels, K.J., Shinoda, K. & Frankel, S., (1959). *Soap films: Studies of Their Thinning and a Bibliography*, Pergamon Press, New York, United States of America.

Nelson Chemistry [Online], (2000). Available: <http://www.nelsonitp.com/chemistry/>. [2001, August 14].

Nichols, J.M. & Nichols, J.D., (2001). Attractor reconstruction for non-linear systems: A methodological note, *Mathematical Biosciences*, Volume 171, pp. 21-32.

Nikolov, A.D. & Wasan, D.T., (1989). Ordered Micelle Structuring in Thin Films Formed from Anionic Surfactant Solutions, *Journal of Colloid and Interface Science*, Volume 133, Number 1, pp. 1-12.

Nishioka, G.M. & Ross, S., (1981). A New Method and Apparatus for Measuring Foam Stability, *Journal of Colloid and Interface Science*, Volume 81, Number 1, pp. 1-7.

Nishioka, G.M., (1986). Stability of Mechanically Generated Foams, *Langmuir*, Volume 2, pp. 649-653.

Nishioka, G.M., Ross, S. & Kornbrekke, R.E., (1996). Fundamental Methods for Measuring Foam Stability. In R.K. Prud'homme & S.A. Khan (eds.), *Foams: Theory*,

Measurements and Applications (pp.275-286). Marcel Dekker, United States of America.

Nutt, C.W. & Burley, R.W., (1989). The Influence of Foam Rheology in Enhanced Oil Recovery Operations. In A.J. Wilson (ed.), *Foams: Physics, Chemistry and Structure* (pp.105-123). Springer-Verlag, Great Britain.

Parlitz, U., (1999). Nonlinear time-series analysis. In J.A.K. Suykens & J. Vande Walle (eds.), *Non-linear modelling*. Kluwer Academic Publishers, Boston, United States of America.

Princen, H.M., Overbeek, J.Th.G. & Mason, S.G., (1967). The permeability of soap films to gases. II. A simple mechanism of monolayer permeability, *Journal of Colloid and Interface Science*, Volume 24, pp. 125-130.

Prins, A., (1988). Principles of Foam Stability. In E. Dickinson & G. Stainsby (eds.), *Advances in Food Emulsions and Foams* (pp.91-122). Elsevier Applied Science Publishers, Great Britain.

Prud'homme, R.K. & Warr, G.G., (1996). Foams in Mineral Flotation and Separation Processes. In R.K. Prud'homme & S.A. Khan (eds.), *Foams: Theory, Measurements and Applications* (pp.511-553). Marcel Dekker, United States of America.

Raymundo, A., Empis, J. & Sousa, I., (1998). Method to Evaluate Foaming Performance, *Journal of Food Engineering*, Volume 36, pp. 445-452.

Rosen, M.J., (1978). *Surfactants and Interfacial Phenomena*, John Wiley & Sons, United States of America.

Ross, S., (1969). Bubbles and foam: New generation law, *Industrial Engineering Chemistry*, Volume 61, Number 10. pp. 48 –57.

Ross, S. & Suzin, Y., (1985). Measurement of Dynamic Foam Stability, *Langmuir*, Volume 1, pp. 145-149.

Rossen, W.R., (1996). Foams in Enhanced Oil Recovery. In R.K. Prud'homme & S.A. Khan (eds.), *Foams: Theory, Measurements and Applications* (pp.413-463). Marcel Dekker, United States of America.

Ruelle, D., (1980). Strange Attractors, *Mathematical Intelligence*, Volume 2, pp. 37-48.

Sadr-Kazemi, N. & Cilliers, J.J., (1997). An image processing algorithm for measurement of flotation froth bubble size and shape distributions, *Minerals Engineering*, Volume 10, Number 10, pp. 1075-1083.

Schreiber, T. & Schmitz, A., (2000). Surrogate time series, *Physica D*, Volume 142, pp. 346-382.

Sebba, F., (1987). *Foams and Biliquid Foams – Aphrons*, John Wiley and Sons, Great Britain.

Sharovarnikov, A.F., Tsap, V.N., Korol'chenko & A Ya, I.A.V., (1981). Study of the Structural Stability of Foams, *Kolloidnyi Zh.*, Volume 43, pp. 808-812.

Siegell, J.H., (1996). Feature Report Part I: A primer on Surfactants, *Chemical Engineering*, Volume 103, Issue 6, pp. 80-81.

Siew, L.H., Hodgson, R.M. & Wood, E.J., (1988). Texture measurement for carpet wear assessment, *IEEE Transactions on Pattern Analysis and Machine Intelligence*, 1988, Volume 10, Number 1, pp. 92-105.

Singular-Spectrum Analysis Toolkit (SSA) [Online], (2001). Available: <http://www.ccpo.odu.edu>. [2001, September 19].

Stein, H.N., (1991). On Marginal Regeneration, *Advances in Colloid and Interface Science*, Volume 34, pp. 175-190.

Strickland, W.T., (1980). Laboratory results of cleaning produced water by gas flotation, *Society of Petroleum Engineering Journal*, Volume 20, Number 3, pp. 175-190.

Sun, C. & Wee, W.G., (1983). Neighbouring grey level dependence matrix for texture classification, *Computer Vision Graphics and Image Processing*, Volume 23, pp. 341-352.

Sun, S.C. & Zimmerman, R.E., (1950). The mechanism of coarse coal and mineral froth flotation, *Minerals Engineering*, Volume 2, pp. 616-622.

Sylvester, N.D. & Byeseda, J.J., (1980). Oil/Water separation by induced-air flotation, *Society of Petroleum Engineering Journal*, Volume 20, Number 6, pp. 579-590.

Symonds, P.J. & de Jager, G., (1992). A technique for automatically segmenting images of the surface froth structures that are prevalent in industrial flotation cells, *Proceedings of the South African Symposium on Communications and Signal Processing*, pp. 111-115.

Szatkowski, M. & Freyburger, W.L., (1985). Kinetics of flotation with fine bubbles, *Transactions of the Institution of mining and metallurgy, Section C*, Volume 94, pp. C61-70.

Takens, F., (1981). Detecting strange attractors in turbulence. In D.A. Rand & L.S. Young (eds.), *Lecture notes in mathematics* (pp. 346-382), Volume 898, Springer-Verlag, Berlin.

Takens, F., (1993). Detecting non-linearities in stationary time series, *International Journal of Bifurcations and Chaos*, Volume 3, pp. 241-256.

Tao, D., Luttrell, G.H. & Yoon, R.-H., (2000). A parametric study of froth stability and its effect on column flotation of fine particles, *International Journal of Mineral Processing*, Volume 59, pp. 25-43.

Taylor, B., (2000). *Phases and Equilibrium*, Class notes (Physical Chemistry 1) [Online], University of Texas at Tyler, Available from: <http://chemistry.uttyler.edu>. [2001, October 2].

The diffusing light web site [Online], (2000). Available from: <http://www.physics.ucla.edu>. [2001, August 14].

Theiler, J. & Pritchard, D., (1996). Constrained realization Monte Carlo method for hypothesis testing, *Physica A*, Volume 94, pp. 21-235.

Theiler, J. & Rapp, P.E., (1996). Re-examination of the evidence for low-dimensional non-linear structure in the human electroencephalogram, *Encephalography and Clinical Neurophysiology*, Volume 98, pp. 213-222.

The Surfactants Virtual Library [Online], 1996. Available: <http://www.surfactants.net>. [2001, April 17]

Tsujii, K. (ed.), (1998). *Surface Activity: Principles, Phenomena and Applications*, Academic Press, United States of America.

Turner, D., Dlugogorski, B. & Palmer, T., (1999). Factors affecting the stability of foamed concentrated emulsions, *Colloids and Surfaces A: Physicochemical and Engineering Aspects*, Volume 150, pp. 171-184.

Van Ham, N.J.M., Behie, L.A. & Svrcek, W.Y., (1983). The effect of air distribution on the induced air flotation of fine oil in water emulsions, *Canadian Journal of Chemical Engineering*, Volume 61, pp. 541-547.

Vincent, L. & Soille, P., (1991). Watersheds in digital spaces: An efficient algorithm based on immersion simulations, *IEEE Transactions on Pattern Analysis and Machine Intelligence*, Volume 13, pp. 583-598.

Vincent, L., (1993). Morphological grayscale reconstruction in image analysis: Applications and efficient algorithms, *IEEE Transactions on Pattern Analysis and Machine Intelligence*, Volume 2, pp. 176-201.

Volesky, B. & Agathos, S., (1974). Oil removal from refinery wastes by air flotation, *Water Pollution Research Canada*, Volume 9, pp. 328-339.

Vrablik, E.R., (1959). Fundamental Principles of dissolved-air flotation of Industrial Wastes, *Proceedings of Purdue Industrial Waste Conference*, Volume 14, pp. 743-779.

Walstra, P., (1989). Principles of Foam Formation and Stability. In A.J. Wilson (ed.), *Foams: Physics, Chemistry and Structure* (pp.1-16). Springer-Verlag, Great Britain.

Watkins, R.C., (1973). An Improved Foam Test for Lubricating Oils, *Journal of the Institute of Petroleum*, Volume 59, pp. 106-113.

Weaire, D., Phelan, R. & Verbist, G., (1999). The structure and geometry of foams. In J.F. Sadoc & N. Rivier (eds.), *Foams and Emulsions* (pp. 287-302). Kluwer Academic Publishers, The Netherlands.

Wilson, A.J., (1996). Experimental techniques for the Characterisation of Foams. In R.K. Prud'homme & S.A. Khan (eds.), *Foams: Theory, Measurements and Applications* (pp.243-274). Marcel Dekker, United States of America.

Woodburn, E.T., Stockton, J.B. & Robbins, D.J., (1989). Vision based characterization of three-phase froths, *International Colloquium Developments in Froth Flotation, South African Institute of Mining and Metallurgy*, Volume 1, pp. 1-30.

Woodburn, E.T., Austin, L.G. & Stockton, J.B., (1994). A froth based flotation kinetic model, *Transactions of the Institute of Chemical Engineering, Section A*, Volume 72, pp. 221-226.

Zhu, H. & Rohwer, R., (1996). No free lunch for cross-validation, *Neural Computation*, Volume 8, pp. 1421-1426.

Zlokarnik, M., (1998). Separation of activated sludge from purified waste water by induced air flotation (IAF), *Water Research*, Volume 32, Number 4, pp. 1095-1102.

APPENDIX A

ADDITIONAL TABLES AND FIGURES FOR CHAPTER 4

A.1 FACTOR LOADINGS

The factor loadings for the two phase system not shown in Chapter 4, namely Run C, Run D and Run E are illustrated below. All variables significantly loaded on a factor are marked in bold.

Table A.1 Factor loadings for two-phase system (Run C)

	<i>Factor 1</i>	<i>Factor 2</i>	<i>Factor 3</i>
<i>Average area</i>	0.968	0.094	-0.040
<i>Average grey</i>	0.076	0.260	-0.812
<i>Average perimeter</i>	0.960	0.076	-0.306
<i>Average speed</i>	-0.095	-0.913	0.288
<i>Number of bubbles</i>	0.850	0.092	-0.010
<i>SNE</i>	0.038	0.953	-0.142
<i>Stability</i>	0.037	-0.126	0.881

Table A.2 Factor loadings for two-phase system (Run D)

	<i>Factor 1</i>	<i>Factor 2</i>	<i>Factor 3</i>
<i>Average area</i>	0.974	-0.123	0.022
<i>Average grey</i>	0.304	-0.803	0.163
<i>Average perimeter</i>	0.952	-0.153	0.008
<i>Average speed</i>	0.097	0.304	-0.798
<i>Number of bubbles</i>	-0.645	0.543	0.412
<i>SNE</i>	0.019	0.114	0.905
<i>Stability</i>	0.059	0.888	0.022

Table A.3 Factor loadings for two-phase system (Run E)

	<i>Factor 1</i>	<i>Factor 2</i>	<i>Factor 3</i>
<i>Average area</i>	-0.177	0.939	0.098
<i>Average grey</i>	-0.845	0.257	0.042
<i>Average perimeter</i>	-0.118	0.966	-0.101
<i>Average speed</i>	0.041	-0.095	0.969
<i>Number of bubbles</i>	0.756	-0.539	-0.0005
<i>SNE</i>	0.727	0.219	-0.361
<i>Stability</i>	0.883	-0.204	0.298

The factor loadings for the three-phase system containing different surfactant concentrations and the three remaining solid particle sizes, -75 μm , 75-106 μm and 150+ μm are summarised in Table A.4 to Table A.12.

A.1.1 PARTICLE SIZE –75 MICRON*Table A.4 Factor loadings for three-phase system with 100% CTAB and solid particle size -75 μm*

	<i>Factor 1</i>	<i>Factor 2</i>	<i>Factor 3</i>
<i>Average area</i>	0.457	-0.752	-0.332
<i>Average grey</i>	0.897	-0.406	-0.120
<i>Average perimeter</i>	0.907	-0.320	-0.178
<i>Average speed</i>	-0.068	0.133	0.978
<i>Number of bubbles</i>	-0.771	0.532	-0.095
<i>SNE</i>	-0.442	0.881	-0.062
<i>Stability</i>	-0.348	0.846	0.295

Table A.5 Factor loadings for three-phase system with 90% CTAB and solid particle size -75 μm

	<i>Factor 1</i>	<i>Factor 2</i>	<i>Factor 3</i>
<i>Average area</i>	-0.954	0.092	0.132
<i>Average grey</i>	0.094	-0.913	-0.290
<i>Average perimeter</i>	-0.909	-0.182	0.079
<i>Average speed</i>	-0.136	0.214	0.944
<i>Number of bubbles</i>	0.888	0.205	-0.172
<i>SNE</i>	0.491	0.793	0.003
<i>Stability</i>	0.794	0.098	0.490

Table A.6 Factor loadings for three-phase system with 80% CTAB and solid particle size $-75 \mu\text{m}$

	<i>Factor 1</i>	<i>Factor 2</i>	<i>Factor 3</i>
<i>Average area</i>	-0.435	0.843	-0.296
<i>Average grey</i>	0.713	-0.306	0.573
<i>Average perimeter</i>	-0.249	0.917	-0.280
<i>Average speed</i>	-0.936	0.167	0.129
<i>Number of bubbles</i>	0.743	-0.446	0.431
<i>SNE</i>	0.768	-0.431	-0.252
<i>Stability</i>	-0.145	-0.268	0.864

A.1.2 PARTICLE SIZE 75-106 MICRON

Table A.7 Factor loadings for three-phase system with 100% CTAB and solid particle size $75-106 \mu\text{m}$

	<i>Factor 1</i>	<i>Factor 2</i>	<i>Factor 3</i>
<i>Average area</i>	-0.430	0.885	0.047
<i>Average grey</i>	-0.258	-0.644	0.591
<i>Average perimeter</i>	-0.458	0.801	0.118
<i>Average speed</i>	0.219	-0.270	-0.872
<i>Number of bubbles</i>	0.861	-0.431	0.019
<i>SNE</i>	0.343	-0.164	0.917
<i>Stability</i>	0.950	-0.144	-0.006

Table A.8 Factor loadings for three-phase system with 90% CTAB and solid particle size 75-106 μm

	<i>Factor 1</i>	<i>Factor 2</i>	<i>Factor 3</i>
<i>Average area</i>	-0.296	0.927	-0.052
<i>Average grey</i>	-0.213	-0.203	0.850
<i>Average perimeter</i>	-0.230	0.918	0.101
<i>Average speed</i>	-0.229	-0.453	-0.748
<i>Number of bubbles</i>	0.798	-0.536	0.123
<i>SNE</i>	0.970	-0.057	0.015
<i>Stability</i>	0.811	-0.298	-0.196

Table A.9 Factor loadings for three-phase system with 80% CTAB and solid particle size 75-106 μm

	<i>Factor 1</i>	<i>Factor 2</i>	<i>Factor 3</i>
<i>Average area</i>	-0.748	-0.169	0.576
<i>Average grey</i>	0.003	0.203	-0.923
<i>Average perimeter</i>	-0.708	-0.213	0.571
<i>Average speed</i>	0.115	-0.924	0.200
<i>Number of bubbles</i>	0.791	0.554	0.048
<i>SNE</i>	0.420	0.809	-0.221
<i>Stability</i>	0.902	-0.101	0.022

A.1.3 PARTICLE SIZE 150+ MICRON*Table A.10 Factor loadings for three-phase system with 100% CTAB and solid particle size 150+ μm*

	<i>Factor 1</i>	<i>Factor 2</i>	<i>Factor 3</i>
<i>Average area</i>	-0.354	0.904	-0.046
<i>Average grey</i>	-0.912	0.250	0.032
<i>Average perimeter</i>	-0.268	0.936	-0.060
<i>Average speed</i>	0.032	-0.047	0.987
<i>Number of bubbles</i>	0.661	-0.571	-0.291
<i>SNE</i>	0.901	-0.285	0.103
<i>Stability</i>	0.699	-0.561	0.332

Table A.11 Factor loadings for three-phase system with 90% CTAB and solid particle size 150+ μm

	<i>Factor 1</i>	<i>Factor 2</i>	<i>Factor 3</i>
<i>Average area</i>	-0.685	0.606	0.226
<i>Average grey</i>	-0.115	0.951	0.203
<i>Average perimeter</i>	-0.676	0.630	-0.006
<i>Average speed</i>	0.067	0.192	0.976
<i>Number of bubbles</i>	0.363	-0.873	-0.124
<i>SNE</i>	0.912	-0.328	-0.035
<i>Stability</i>	0.928	-0.079	0.181

Table A.12 Factor loadings for three-phase system with 80% CTAB and solid particle size 150+ μm

	Factor 1	Factor 2	Factor 3
Average area	0.978	0.138	0.040
Average grey	0.309	0.638	0.575
Average perimeter	0.942	0.215	0.079
Average speed	0.057	0.220	0.955
Number of bubbles	0.230	0.948	0.062
SNE	-0.127	0.903	0.329
Stability	-0.945	0.076	-0.101

A.2 FACTOR ANALYSIS GRAPHS

A.2.1 PARTICLE SIZE -75 MICRON

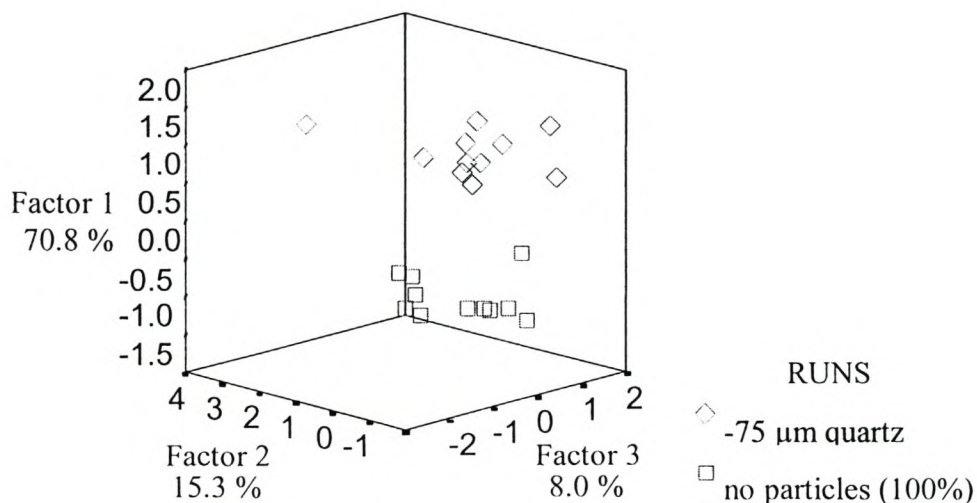


Figure A.1 Principal Component Analysis for two-phase and three-phase system containing -75 μm particles at 100% CTAB

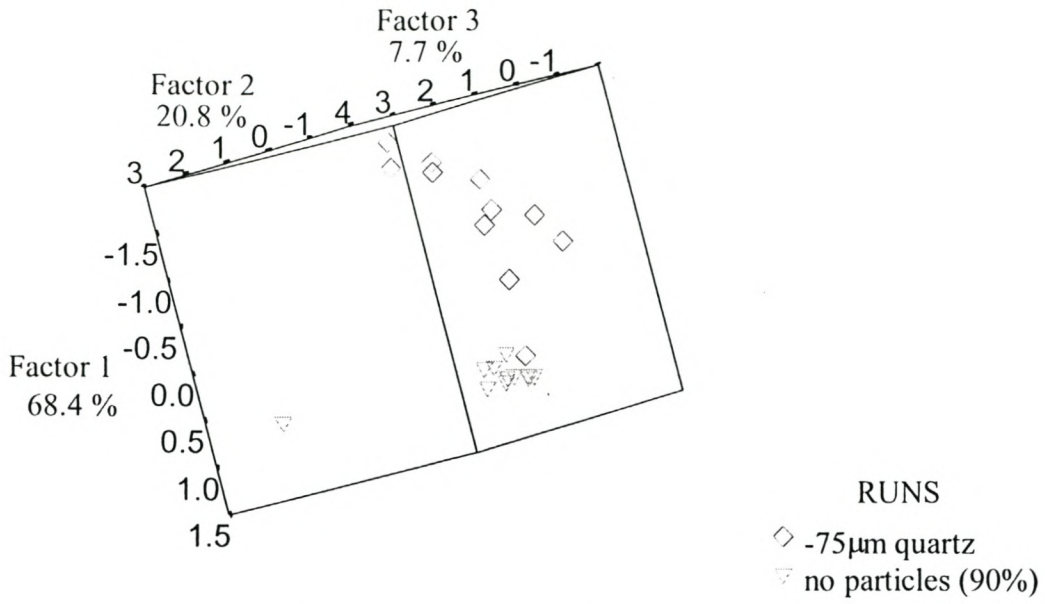


Figure A.2 Principal Component Analysis for two-phase and three-phase system containing -75 µm particles at 90% CTAB

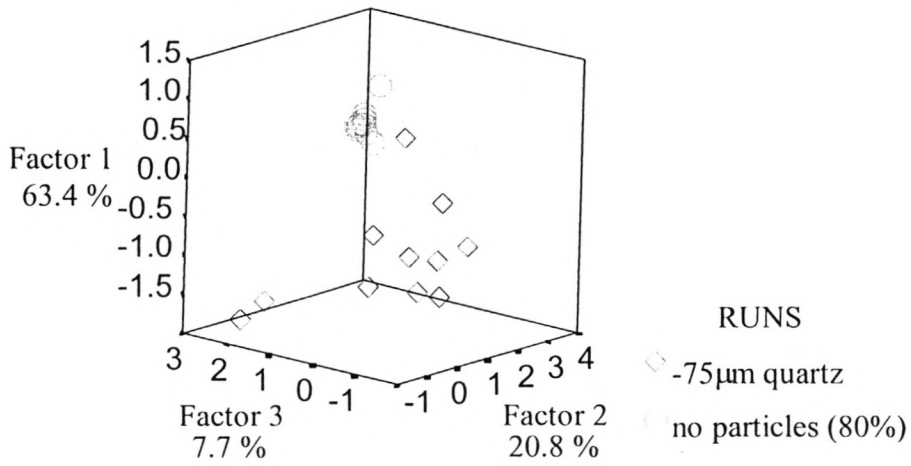


Figure A.3 Principal Component Analysis for two-phase and three-phase system containing -75 µm particles at 80% CTAB

A.2.2 PARTICLE SIZE 75-106 MICRON

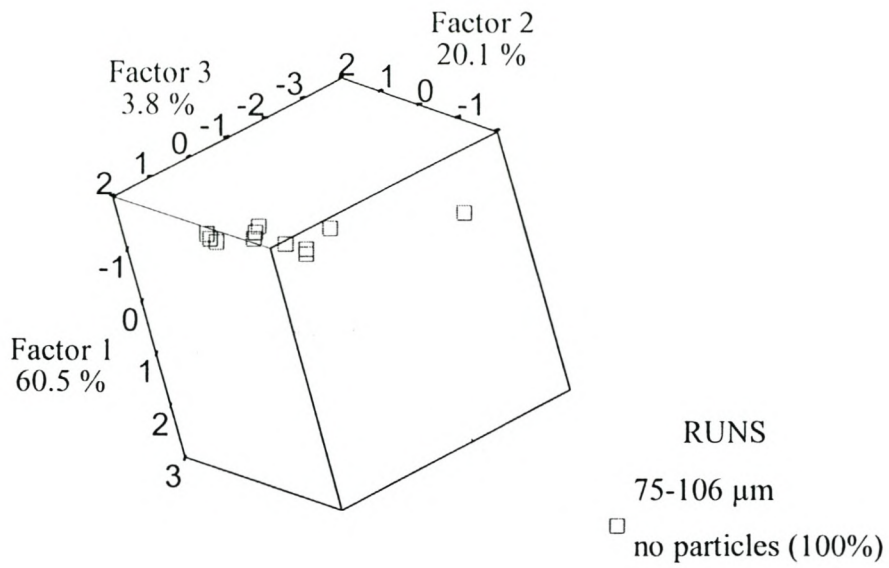


Figure A.4 Principal Component Analysis for two-phase and three-phase system containing 75-106 μm particles at 100% CTAB

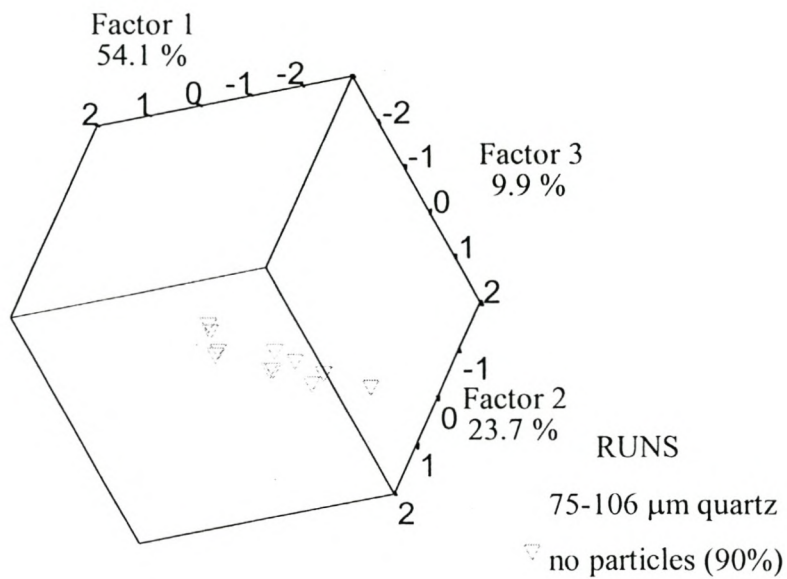


Figure A.5 Principal Component Analysis for two-phase and three-phase system containing 75-106 μm particles at 90% CTAB

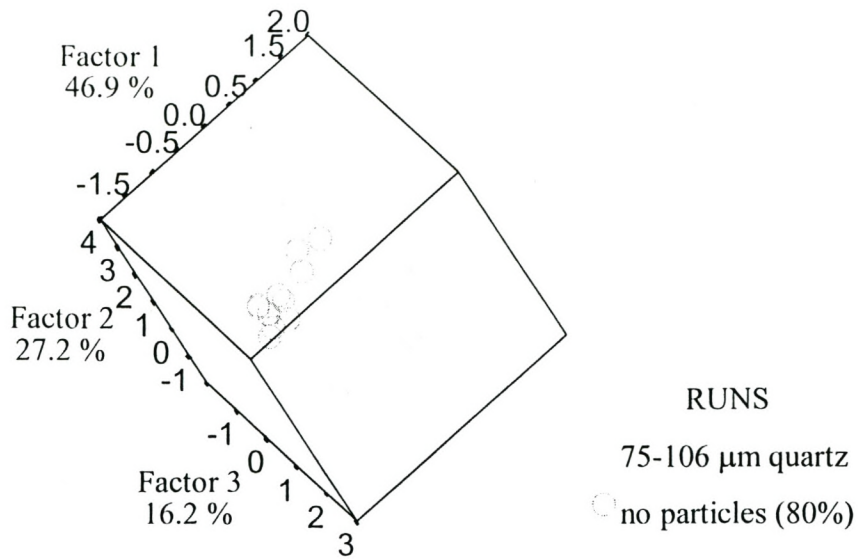


Figure A.6 Principal Component Analysis for two-phase and three-phase system containing 75-106 μm particles at 80 % CTAB

A.2.3 PARTICLE SIZE 150+ MICRON

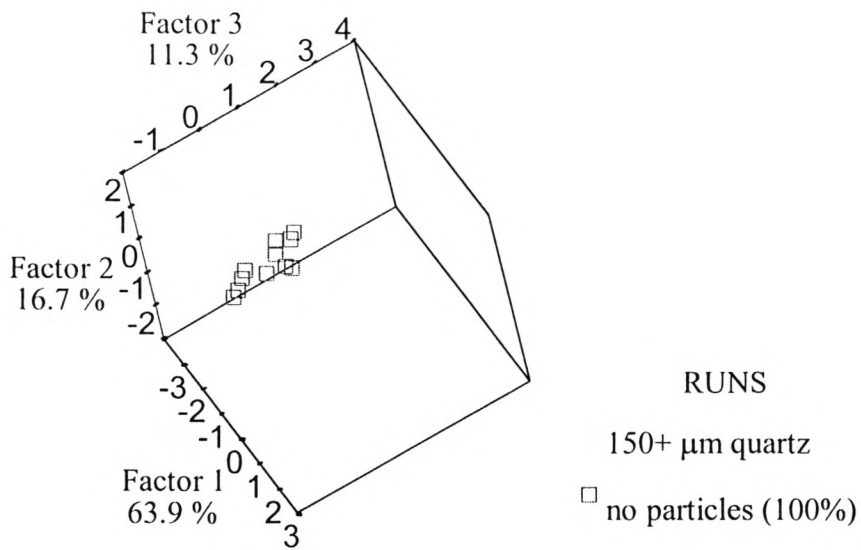


Figure A.7 Principal Component Analysis for two-phase and three-phase system containing 150+ μm particles at 100% CTAB

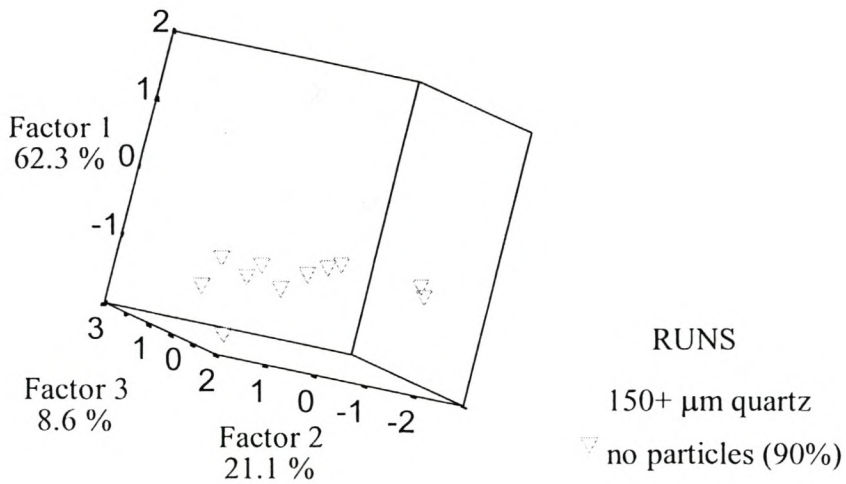


Figure A.8 Principal Component Analysis for two-phase and three-phase system containing 150+ μm particles at 90% CTAB

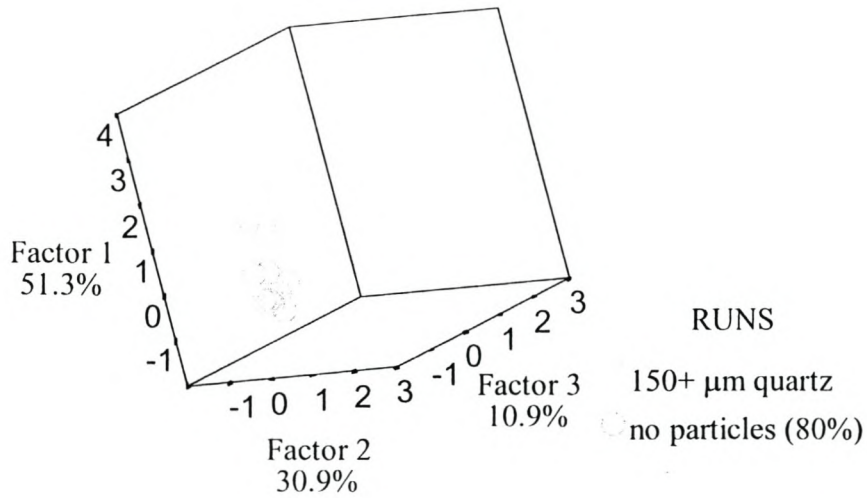


Figure A.9 Principal Component Analysis for two-phase and three-phase system containing 150+ μm particles at 80% CTAB

A.3 CLASSIFICATION OF DATA

The detailed tables for the classification of groups between the two main groups i.e. flotation of two phase and three phase systems for the solid particle sizes, -75 μm , 75-106 μm and 150+ μm are given in Table A.13 to Table A.15. The detailed tables showing the classification results between the six groups (100 % CTAB, 90 % CTAB and 80 % CTAB with and without solids) for the mentioned three particle sizes are given in Table A.16 to Table A.18.

A.3.1 CLASSIFICATION BETWEEN THREE PHASE GROUP AND TWO PHASE GROUP

A 3.1.1 Particle size –75 micron

Table A.13 Classification results between two main groups for the solid particle size - 75 μm

<i>Actual group</i>	<i>Cases</i>	<i>Predicted group membership</i>	
		1	2
1	33	32	1
%		97.0	3.0
2	33	1	32
%		3	97.0

Percentage of “grouped” cases correctly classified: 97.0%

A 3.1.2 Particle size 75-106 micron

Table A.14 Classification results between two main groups for the solid particle size 75-106 μm

<i>Actual group</i>	<i>Cases</i>	<i>Predicted group membership</i>	
		1	2
1	33	28	4
%		87.5	12.50
2	32	0	32
%		0	100.0

Percentage of “grouped” cases correctly classified: 93.8%

A 3.1.3 Particle size 150+ micron*Table A.15 Classification results between two main groups for the solid particle size 150+ μm*

		<i>Predicted group membership</i>	
<i>Actual group</i>	<i>Cases</i>	1	2
1	33	33	0
%		100	0
2	33	1	32
%		3	97.0

Percentage of “grouped” cases correctly classified: 98.5%

A 3.2 CLASSIFICATION BETWEEN ALL GROUPS

A 3.2.1 Particle size –75 micron

Table A.16 Classification results between six groups for the solid particle size -75 μm

<i>Actual group</i>	<i>Cases</i>	<i>Predicted group membership</i>					
		1	2	3	4	5	6
1	11	10	1	0	0	0	0
%		90.9	9.1	0	0	0	0
2	11	6	3	1	1	0	0
%		54.5	27.3	9.1	9.1	0	0
3	11	0	1	10	0	0	0
%		0	9.10	90.1	0	0	0
4	11	0	2	0	8	1	0
%		0	18.20	0	72.7	9.1	0
5	11	0	0	1	1	7	2
%		0	0	9.1	9.1	63.6	18.2
6	11	0	0	0	3	3	5
%		0	0	0	27.3	27.3	45.5

Percent of “grouped” cases correctly classified: 65.2%

where the groups describe the following concentrations:

- 1 100% CTAB
- 2 90% CTAB
- 3 80% CTAB
- 4 100% CTAB containing quartz
- 5 90% CTAB containing quartz
- 6 80% CTAB containing quartz

A 3.2.2 Particle size 75-106 micron*Table A.17 Classification results between six groups for the solid particle size 75-106 μm*

		<i>Predicted group membership</i>					
<i>Actual group</i>	<i>Cases</i>	1	2	3	4	5	6
1	10	9	1	0	0	0	0
%		90.9	9.1	0	0	0	0
2	11	1	10	0	0	0	0
%		9.1	90.9	9.1	9.1	0	0
3	11	2	0	7	1	1	0
%		18.2	9.10	63.6	9.1	9.1	0
4	11	0	0	0	5	4	20
%		0	0	0	45.5	36.4	18.2
5	11	0	0	0	3	6	2
%		0	0	0	27.3	54.6	18.2
6	11	0	0	0	2	3	6
%		0	0	0	18.2	27.3	54.6

Percent of "grouped" cases correctly classified: 66.2%

where the groups describe the following concentrations:

- 1 100% CTAB
- 2 90% CTAB
- 3 80% CTAB
- 4 100% CTAB containing quartz
- 5 90% CTAB containing quartz
- 6 80% CTAB containing quartz

A 3.2.3 Particle size 150+ micron

Table A.18 Classification results between six groups for the solid particle size 150+ μm

Actual group	Cases	Predicted group membership					
		1	2	3	4	5	6
1	11	10	1	0	0	0	0
%		90.9	9.1	0	0	0	0
2	11	0	9	2	0	0	0
%		0	90.9	18.2	0	0	0
3	11	0	0	11	0	0	0
%		0	0	100	0	0	0
4	11	0	2	0	6	4	1
%		0	18.20	0	54.6	36.4	9.10
5	11	0	0	0	2	7	2
%		0	0	0	18.2	63.6	18.2
6	11	0	0	0	2	3	6
%		0	0	0	18.2	27.3	54.6

Percent of “grouped” cases correctly classified: 74.2%

where the groups describe the following concentrations:

- 1 100% CTAB
- 2 90% CTAB
- 3 80% CTAB
- 4 100% CTAB containing quartz
- 5 90% CTAB containing quartz
- 6 80% CTAB containing quartz

APPENDIX B

ADDITIONAL THEORY FOR CHAPTER 5

B.1 EMBEDDING OF TIME SERIES

A discrete time series and its successive shifts by a delay parameter could be sufficient to capture the dynamics of the system (Ruelle, 1980), even if the system is complex and influenced by other variables that are not measured. These lag variables can be regarded as numerical estimations of a set of representative system state variables, provided that they are statistically independent (Barnard et al., 2001).

State space reconstruction is the first step in non-linear time series analysis of data from chaotic systems (Kugiumtzis, 1996). The development of a prediction algorithm involves the reconstruction of the attractor. This can be interpreted as an effort to recreate the full n -dimensional state space using the time series of a single variable. The accuracy of reconstruction is of utmost importance to the development of a useful predictor and hence a good estimation of the prediction error as well as other invariant measures that characterise the system (Nichols & Nichols, 2001).

The main goal of attractor reconstruction is to use a single state variable (system output) to create a new set of coordinates while preserving the invariant properties of the system. Delay coordinates are used to construct a set of state vectors as follows (Nichols & Nichols, 2001).

$$x(n) = \{x(n), x(n + \tau), x(n + 2\tau), \dots, x(n + (d_e - 1)\tau)\} \quad \text{B.1}$$

where d_e = embedding dimension

$x(n)$ = observed state variable at discrete time n

τ = delay

The delay variables are called state variables defining a reconstructed state space (Barnard et al., 2001) and the number of delay variables is the embedding dimension of the system. The optimum choice of the embedding dimension, d_e is the smallest value that provides a proper reconstruction of the attractor. Theoretically the geometric structure of the multivariate dynamics of the system can be unfolded from the observable variable $s(t)$ in the absence of noise in a d_e -dimensional space. An appropriate embedding dimension has to be calculated to ensure that the topology of the map is maintained. According to Takens (1981) the reconstruction of the state space can be done provided that $d_e \geq 2d_A + 1$ where d_A is the fractal dimension of the system. The condition $d_e \geq 2d_A + 1$ is sufficient but not necessary for the reconstruction of the system dynamics.

When the embedding dimension is too large it results in a very thin distribution of the data in the reconstructed space. Likewise, when the dimension is too small the state space will be constructed improperly (Nichols & Nichols, 2001).

B.2 SINGULAR SPECTRUM ANALYSIS

Three main methods can be used for state space reconstruction from a scalar time series, namely derivative co-ordinates, delay co-ordinates and singular spectrum analysis (Parlitz, 1999). Of the three methods, delay co-ordinates and singular spectrum analysis are both extensively used in experimental systems as derivative co-ordinates are not very useful for experimental data, owing to their susceptibility to noise. Singular spectrum analysis (Elsner & Tsonis, 1996) was used in this work as it is significantly more robust to noise than the method of delay coordinates, as discussed in the following section.

Broomhead and King (1986) developed an approach to attractor reconstruction that both eliminates the need for choosing a delay and removes additive noise from the data. This approach relies on singular spectrum analysis to extract qualitative information from experimental data. The main idea of Singular Spectrum Analysis (SSA) is the application of principal component analysis to the trajectory matrix obtained from the original time series with a subsequent reconstruction of the series.

In this method the data are embedded with a delay of unity as the method is based on the theory of singular value decomposition and does not rely on the explicit calculation of the embedding delay. As the calculation of the embedding delay is suspect in the presence of noise, this method's independence from the explicit calculation of the delay is an attractive feature. The embedding dimension is associated with the point of linear decorrelation of the lagged variables i.e. this point is the smaller of either the first minimum or the first zero crossing of the linear autocorrelation sequence (Barnard et al., 2001).

The data are embedded with a delay of unity (1) and an embedding dimension $w \gg d_e$ to form a trajectory matrix which contains a record of the various patterns in the data. The matrix is (Nichols & Nichols, 2001):

$$X = \begin{pmatrix} x(1) & x(2) & x(3) & \dots & x(w) \\ x(2) & x(3) & x(4) & \dots & x(w + 1) \\ \cdot & & & & \\ \cdot & & & & \\ x(n - w) & x(n - w + 1) & x(n - w + 2) & \dots & x(n) \end{pmatrix}$$

The singular values of the covariance matrix are determined and ordered in decreasing rank. The data are decomposed by the use of singular value decomposition (SVD) to yield a set of singular vectors and associated singular values. The singular vectors that correspond to the largest singular values are the direction in the reconstructed state space showing the largest variations in the data (Kugiumtzis et al., 1994). By projecting X onto the d_e most populated directions, a d_e dimensional reconstruction is accomplished. The remaining vectors are discarded, thus removing system noise. The number of vectors chosen to represent the system must capture all the essential dynamics and care must be taken in choosing d_e (Nichols & Nichols, 2001). A criterion used for the discarding of vectors is that the remaining vectors must explain at least 98 percent (%) of the variance in the data set.

Singular spectrum analysis have a robustness against noise in the observed data and shows significant reduction in measurement and dynamic noise (Barnard et al., 2001).

B.3 TESTING FOR NONLINEARITIES

A nonlinear approach to analyse time series can be motivated as follows. Firstly, the time series might contain certain structures that cannot be accounted for by linear methods or secondly, it can be known that the system contains nonlinear components before the time series is tested for linearity. Whatever the reasoning, the application of nonlinear time series methods needs to be justified by establishing nonlinearity in the time series (Schreiber & Schmitz, 2000). This is best done by the use of surrogate data, which is specifically designed to deal with non-linearities in the data. With this method surrogate data series are generated from the original time series. The surrogates are carefully designed to be stochastic but to have the same frequency spectra as the original time series. By statistically assessing the difference between the original time series and the surrogates, the time series can be classified as deterministic or stochastic and be dealt with accordingly.

B.3.1 SURROGATE DATA

The method of surrogate data (Takens, 1993; Theiler & Pritchard, 1996 ; Theiler & Rapp, 1996) involves a null hypothesis against which the data are tested. The data are assumed to belong to a specific class of dynamic process and surrogate data based on the original data set are generated by using the assumed process (Barnard, 1999). An appropriate null hypothesis for many nonlinear dynamic tests is that the data arise from a linear dynamic system (Kaplan, 2001).

It is attempted to reject a null hypothesis by comparing the value of a non-linear parameter taken on by the data with its probability distribution. Since only exceptional cases allow for the exact or asymptotic derivation of this distribution unless other strong assumptions are made, it has to be estimated by a Monte Carlo resampling technique. This procedure is known in the non-linear time series literature as the method of surrogate data (Schreiber & Schmitz, 2000).

Surrogate data attempts to find that the observed dynamics of a time series comes from a distortion by the measurement procedure and that the serial correlations are

due to linear stochastic dynamics. Consider the power spectra of a non-linear time series. To test whether this system is indeed non-linear, the null hypothesis that the data have been generated by a stationary Gaussian linear stochastic process needs to be rejected. If the power spectrum of the time series is tested against the power spectra generated by a stationary Gaussian linear stochastic process, and the spectra agree strongly, the null hypothesis is not rejected. It is then assumed that the time series was indeed generated by a linear process (Schreiber & Schmitz, 2000).

Surrogate data are valuable for the screening of data prior to model building since it helps to determine the degree of determinism or stochasticity (Barnard, 1999).

B.3.2 CORRELATION DIMENSION

A natural approach towards the characterisation of the dynamics of a system is based on the characteristics that are invariant under reconstruction of the attractor of the system. The correlation dimension and correlation entropy in particular are popular measures and can be estimated from correlation integrals.

The calculation of correlation dimension requires embedding of the time series so as to reconstruct the dynamic attractor of the original system in state space. For an observed time series x_t ($t = 1, 2, \dots, n$), sets of $N = n - (w-1)\tau$ reconstruction vectors $\mathbf{v}_t = (x_t, x_{t+\tau}, \dots, x_{t+(w-1)\tau})$ are constructed for consecutive embedding dimensions w . The set of delay vectors constitutes a set of points in \mathfrak{R}^w , which can be regarded as a sample of the underlying probability measure μ_w (provided that the time series is stationary).

The correlation function (C_m) is defined by:

$$C_N(\varepsilon) = \binom{n}{2}^{-1} \sum_{i=1}^{n-1} \sum_{j=i+1}^n \theta(\varepsilon - \|v_i - v_j\|) \quad \text{B.3}$$

where θ = Heavyside function that returns one (1) if the distance between the point i and j is within ε and zero (0) otherwise

n = number of observations in data set

The correlation dimension can be calculated from the correlation function. Strickly speaking the scaling law only holds in the limit as $\varepsilon \rightarrow 0$ and $n \rightarrow \infty$, so that

$$d_c = \lim_{\varepsilon \rightarrow 0} \lim_{n \rightarrow \infty} \frac{\log C_n}{\log \varepsilon} \quad \text{B.4}$$

The Grassberger-Proccaccia algorithm (Grassberger & Procaccia, 1983) requires a linear scaling region to reliably calculate the correlation dimension. In practice, estimates of the correlation integral are not very reliable, owing to noise in the data. As a consequence, one has to find a region (ε -interval) where the scaling law holds approximately, that is where curves $C_m(\varepsilon)$ vs ε on a double logarithmic scale are approximately straight and parallel for consecutive values of m . Lai and Lerner (1998) showed that the scaling region is sensitive to the choice of embedding lag.

Judd (1994) stated that linear correlation in the data set misleads the Grassberger-Proccaccia algorithm to wrongly show convergence to some low dimension, which could then be misinterpreted for inherently low-dimensional dynamics. Earlier, Judd (1992) proposed a different algorithm to calculate correlation dimension. This algorithm replaces the requirement for a linear scaling region by fitting a polynomial of the order of the topological dimension in that region. It finally expresses correlation dimension for inter-point distances below a specific scale ε_0 . Instead of comparing single values of correlation dimension estimates, one rather compares the clustering of correlation dimension estimation curves calculated by the Judd algorithm. This allows

correlation dimension to be used for examining the macro- and micro-scale of the reconstructed dynamic attractor.

Judd proposed that the correlation dimension be estimated as a function of scale ϵ_0 using the equation, which is valid for $\epsilon < \epsilon_0$:

$$C_m(\epsilon) \approx \epsilon^{d_c} q(\epsilon) \quad \text{B.5}$$

where $q(\cdot)$ = a polynomial of order of the topological dimension.

B.4 MODELLING

B.4.1 MODEL CLASS

There are several non-linear empirical model classes that can be used for functional approximation. Examples are linear and non-linear polynomial regression, non-linear piecewise regression, regression trees (CART), projection pursuit regression, multiple-adaptive regression splines (MARS), support vector machines, kernel based models, such as radial basis function (RBF) neural networks and multiple layer perceptron neural networks (Barnard et al., 2001).

One of the most popular approaches to non-linear modelling is based on the use of multi-layer perceptrons. A multi-layer perceptron model structure is specified in terms of the model class, the topology and the nodal transfer function of each layer. Interconnected nodes arranged in layers form the network. Each node is a numerical processor with a linear or non-linear activation function. Weights are assigned to the connections, which carry out the output of nodes forward from one layer to the next. In addition, the layer can also incorporate a bias constant. The weights and biases constitute the model parameters and are estimated by training or fitting them to the data. The structure of a typical multi-layer perceptron neural network is illustrated in Figure B.1.

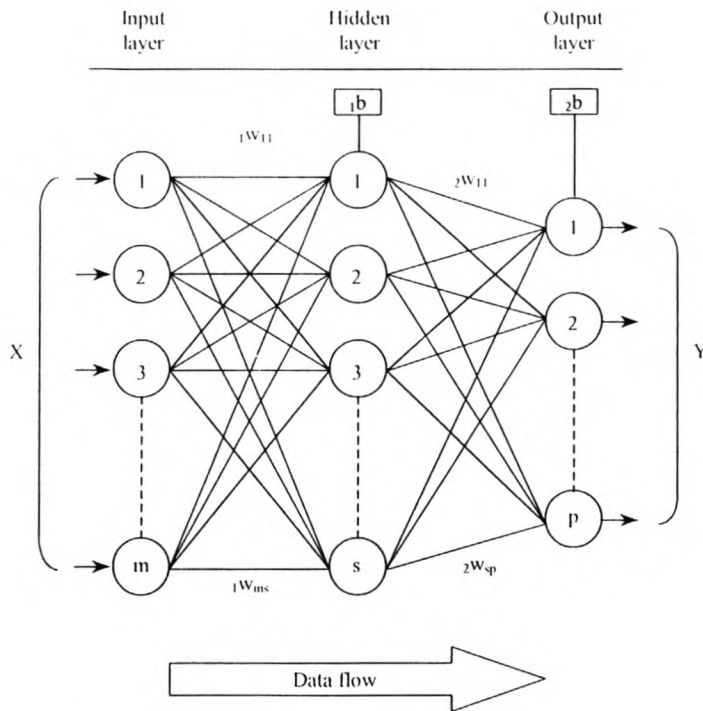


Figure B.1 Schematic representation of a typical multi-layer perceptron network topology

B.4.2 MODEL VALIDATION

Proper model validation ensures the reliable application of the model on new observations from the same process. Model validation is usually based on statistical tests such as the significance of R^2 or RMS criteria derived from actual and predicted values or empirical methods such as cross-validation. These statistics are static measures of the ability of the model to generalise, that is, to capture the underlying trends in the system as opposed to filtering the data or noise.

Model validation based on one-step ahead prediction is not necessarily a good indicator of the ability of the model to generalise the underlying process represented by the data (Zhu & Rohwer, 1996) as it can be influenced strongly by high sampling rates.

B.5. SYMBOLS USED IN APPENDIX B**B.5.1 SYMBOLS**

<i>Symbol</i>	<i>Description</i>	<i>Unit</i>
C_m	Correlation integral	-
d_A	Fractal dimension	-
d_e	Optimum embedding dimension	-
n	Discrete time	-
q	Polynomial	-
t	Time	-
v	Reconstructed vector	-
w	Embedding dimension	-
X	Trajectory matrix	-

B.5.2 GREEK SYMBOLS

<i>Symbol</i>	<i>Description</i>	<i>Unit</i>
ε	Interval/Scale	-
θ	Heavyside function	-
τ	Embedding delay	-

B.5.3 SUBSCRIPTS

<i>Symbol</i>	<i>Description</i>	<i>Unit</i>
t	Time	s
0	At time zero	-

APPENDIX C

ADDITIONAL TABLES AND FIGURES FOR CHAPTER 5

C.1 FOAM IMAGES

Images of the foam as given by the image analysis system for all four runs are given. The first images (after 10 seconds (s) or 20 seconds (s)) is given and thereafter an image that corresponds to every thirty (30) minutes up to the last image recorded in every case. Table C.1 lists the numbering of the images and the times at which the image was recorded.

Table C.1 Description of numbering of foam images

	<i>Time [s]</i>			
<i>Run number</i>	<i>A</i>	<i>B</i>	<i>C</i>	<i>D</i>
<i>Image number</i>				
<i>A</i>	10	20	10	10
<i>B</i>	1800	1800	1800	1800
<i>C</i>	3600	3600	3600	3600
<i>D</i>	5400	5400	5400	5400
<i>E</i>	7200	7200	7200	7200
<i>F</i>	9000	9000	9000	9000
<i>G</i>	10800	10800	10800	10800
<i>H</i>	12600	12600	11890	12600
<i>I</i>	14400	14040	-	14400
<i>J</i>	17920	-	-	17510

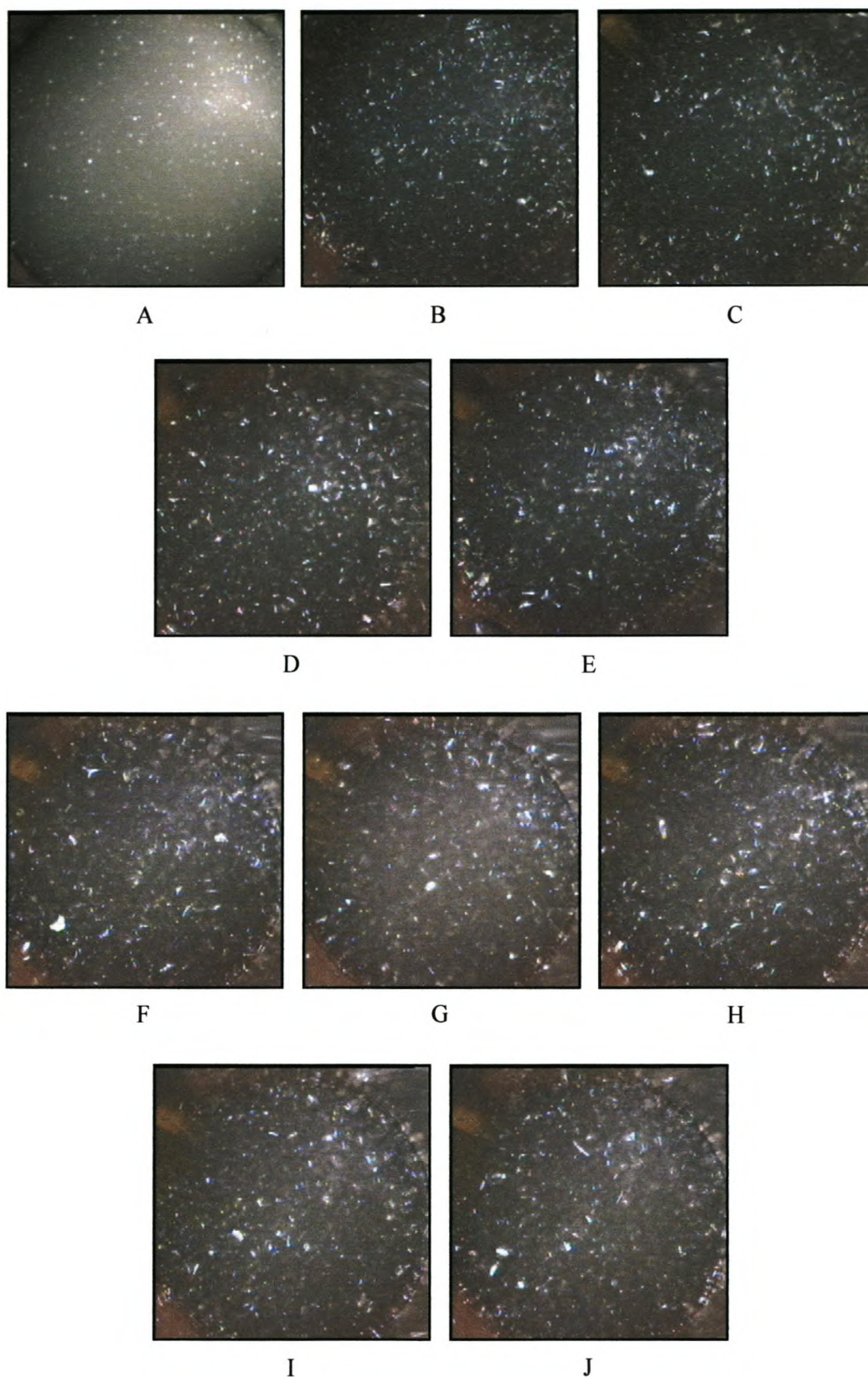


Figure C.1 Foam images for Run A

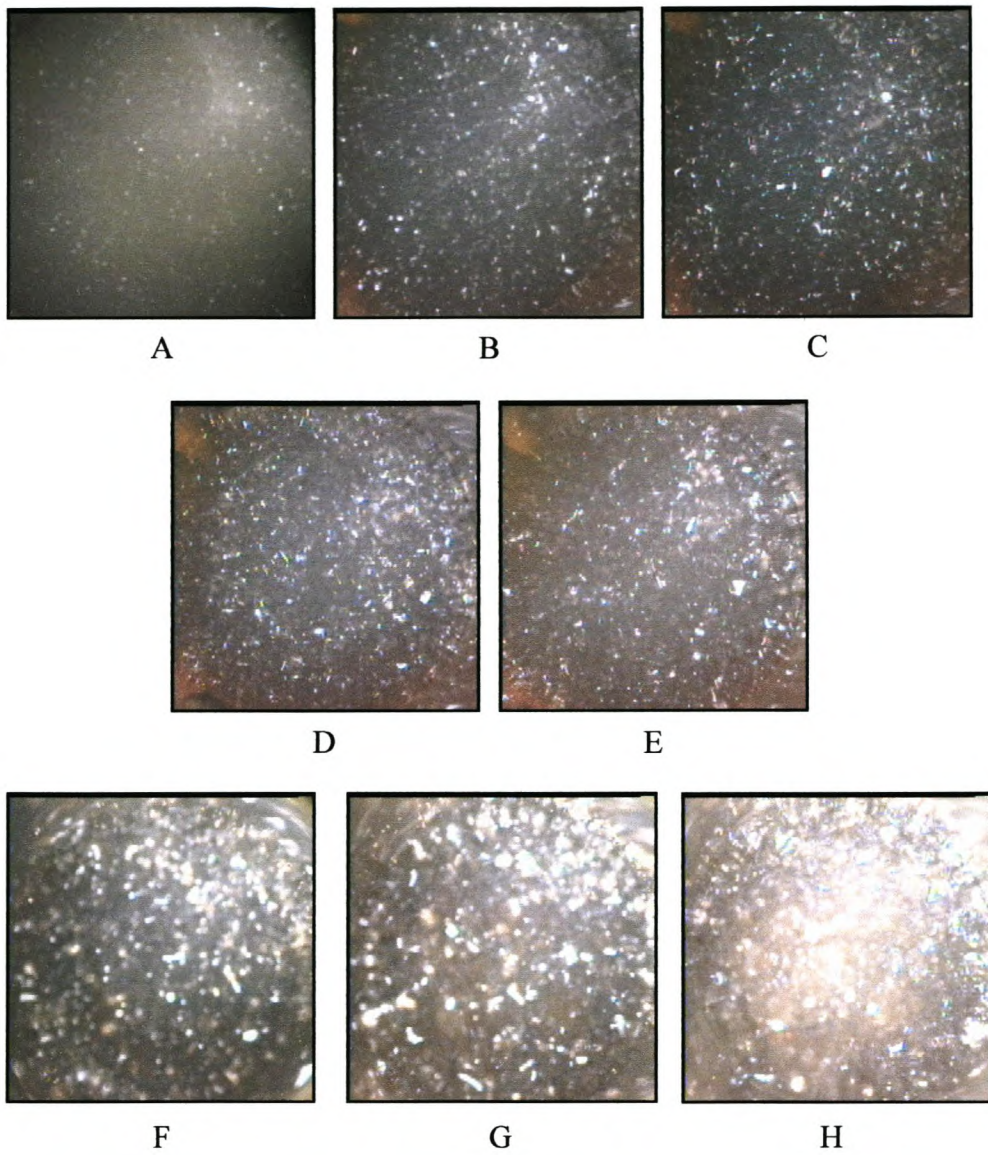


Figure C.2 Foam images for Run B

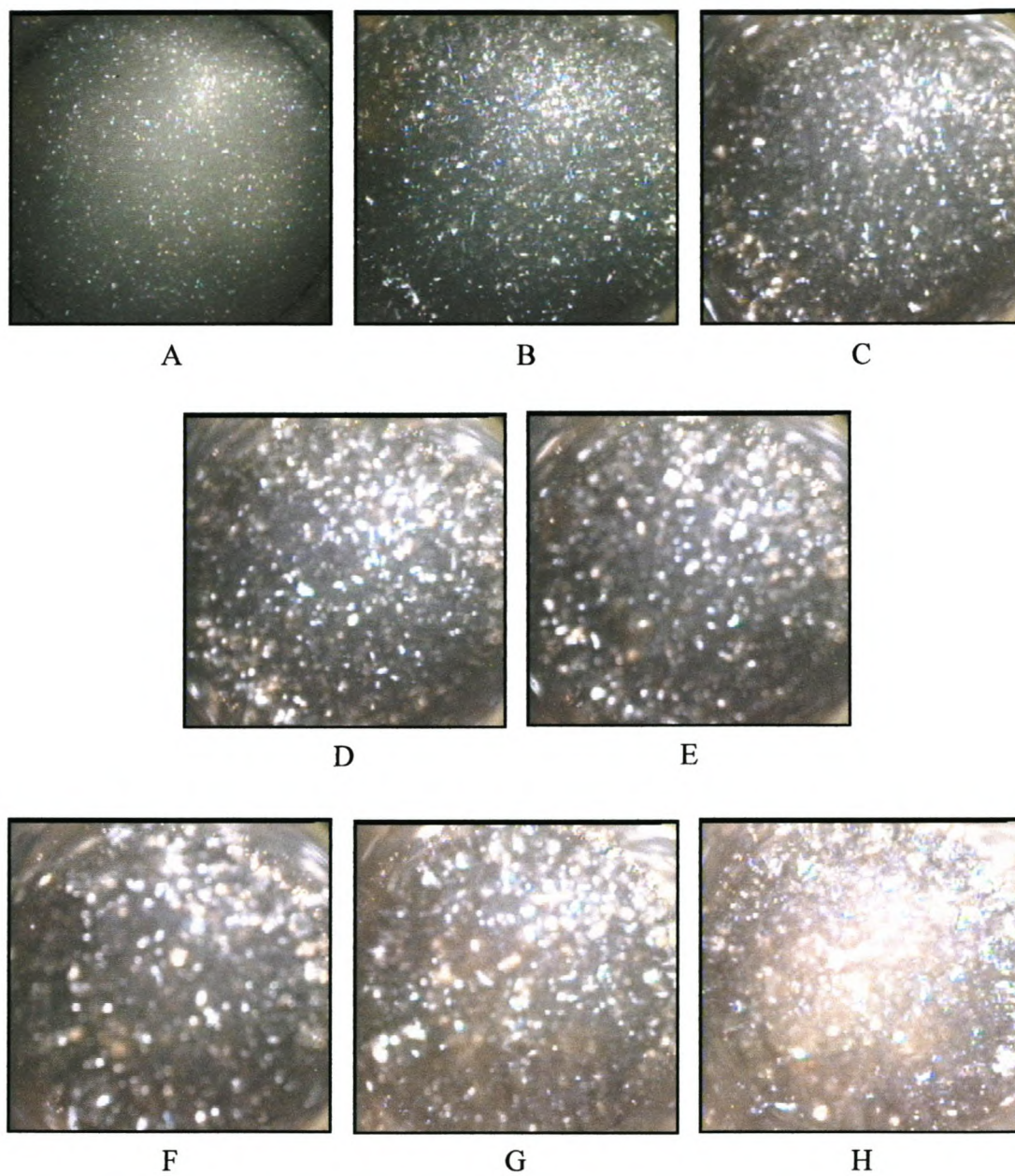


Figure C.3 Foam images for Run C

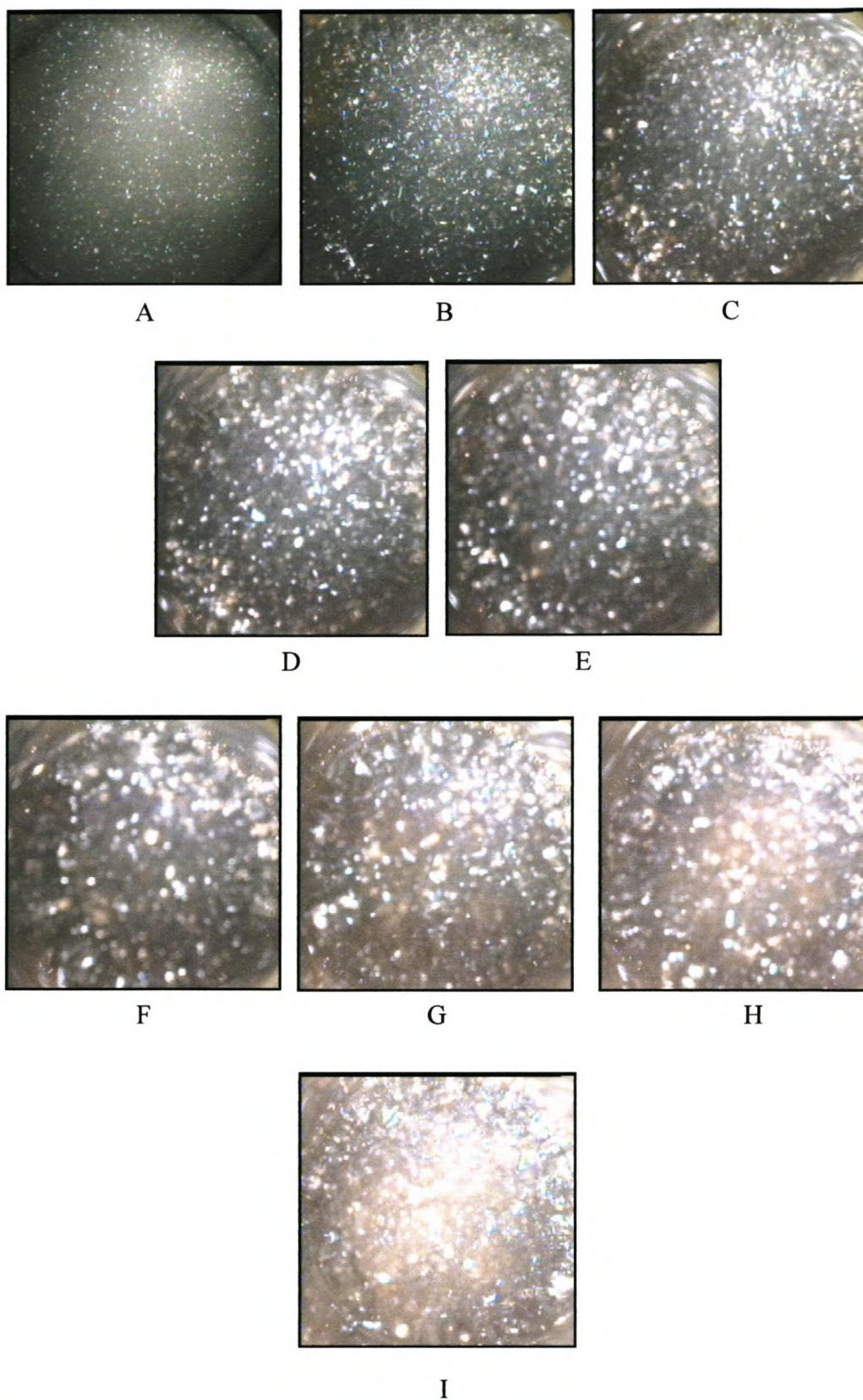


Figure C.4 Foam images for Run D

C.2 SAMPLING DISTRIBUTIONS

The sampling distributions for the three remaining runs, Run A, Run C and Run D are given. The histograms for all three data series, the original series, Series A and Series B are illustrated.

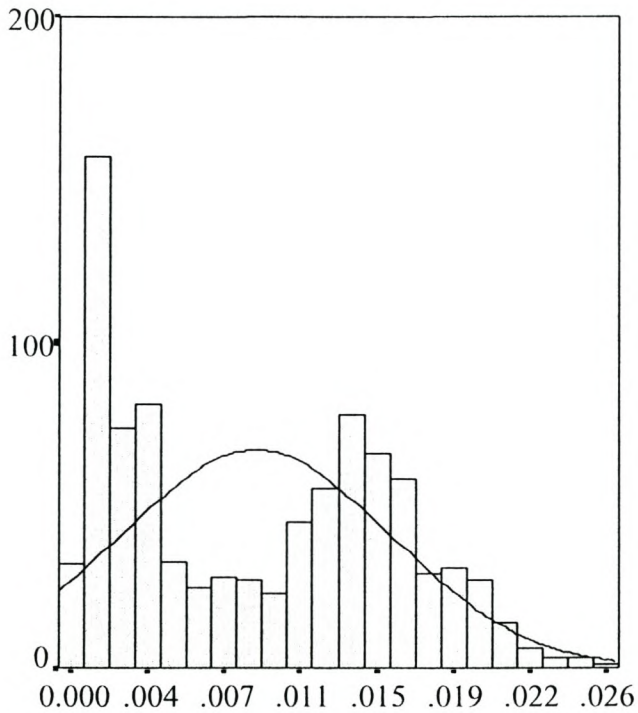


Figure C.5 Histogram showing distribution of original time series, Run A

Table C.2 Descriptive statistics of original time series, Run A

<i>Number of observations</i>	896
<i>Mean</i>	9.05E-3
<i>Standard deviation</i>	6.64E-3
<i>Sample variance</i>	4.41E-5

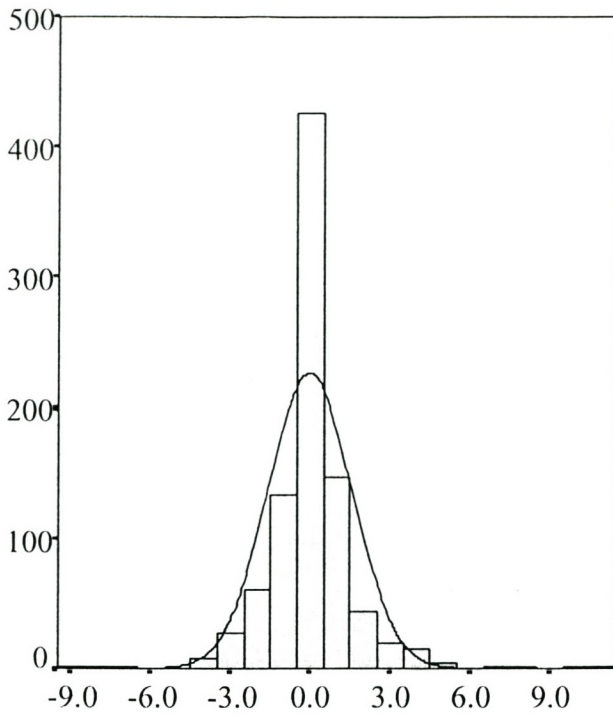


Figure C.6 Histogram showing distribution of Series A, Run A

Table C.3 Descriptive statistics of Series A, Run A

<i>Number of observations</i>	895
<i>Mean</i>	8.43E-3
<i>Standard deviation</i>	1.576
<i>Sample variance</i>	2.484

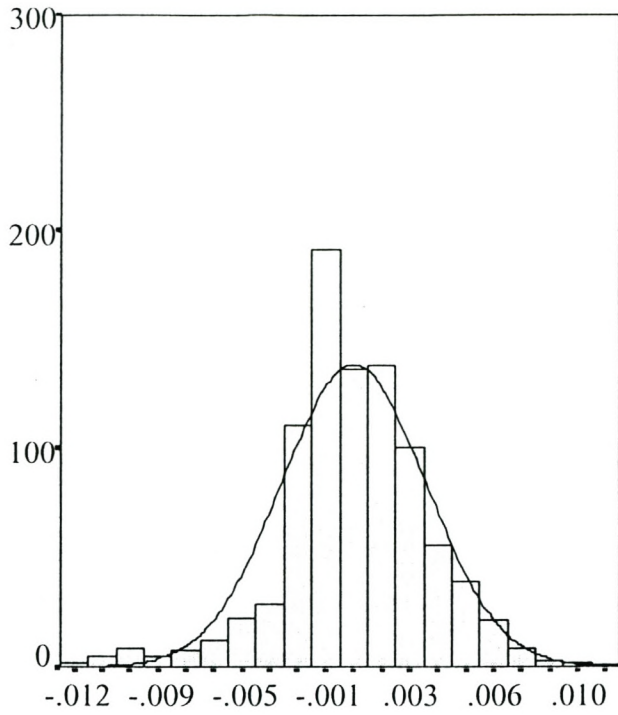


Figure C.7 Histogram showing distribution of Series B, Run A

Table C.4 Descriptive statistics of Series B, Run A

<i>Number of observations</i>	896
<i>Mean</i>	8.44E-18
<i>Standard deviation</i>	3.21E-3
<i>Sample variance</i>	1.04E-5

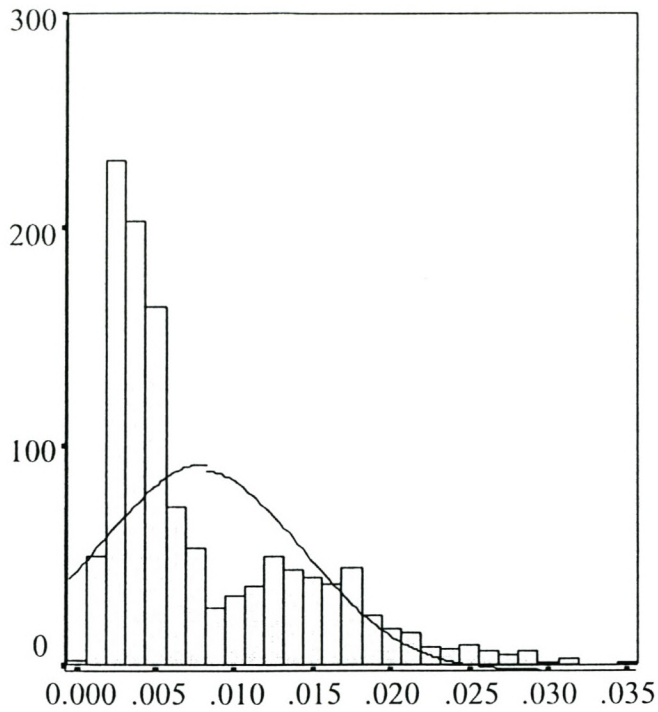


Figure C.8 Histogram showing distribution of original time series, Run C

Table C.5 Descriptive statistics of original time series, Run C

<i>Number of observations</i>	1189
<i>Mean</i>	8.01E-3
<i>Standard deviation</i>	6.44E-3
<i>Sample variance</i>	4.14E-5

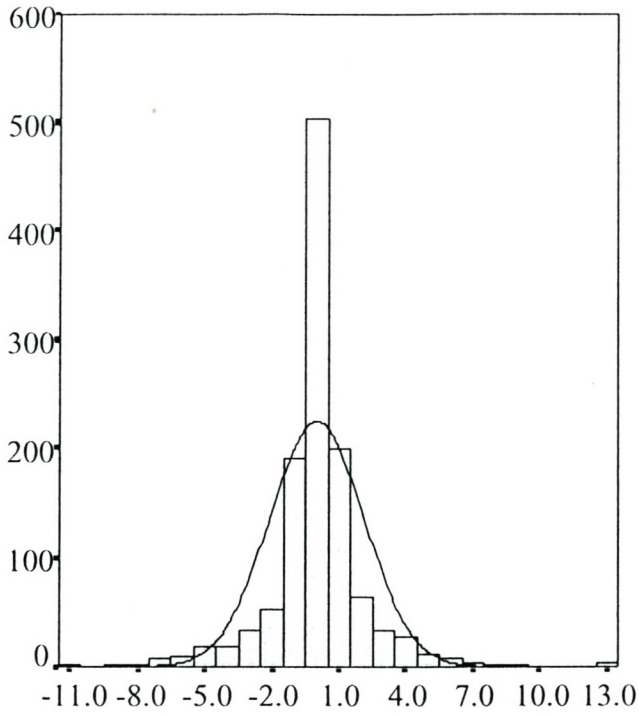


Figure C.9 Histogram showing distribution of Series A, Run C

Table C.6 Descriptive statistics of Series A, Run C

<i>Number of observations</i>	1188
<i>Mean</i>	-5.50E-4
<i>Standard deviation</i>	2.101
<i>Sample variance</i>	4.416

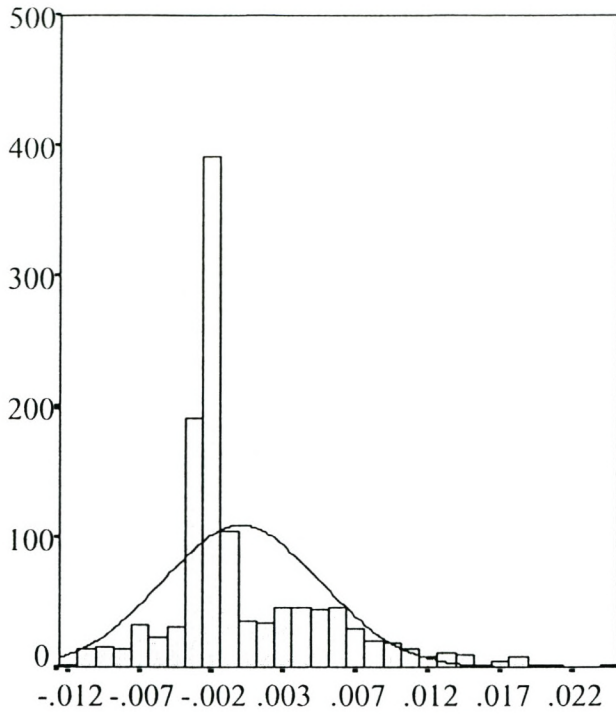


Figure C.10 Histogram showing distribution of Series B, Run C

Table C.7 Descriptive statistics of Series B, Run C

<i>Number of observations</i>	1189
<i>Mean</i>	-4.50E-4
<i>Standard deviation</i>	5.43E-3
<i>Sample variance</i>	2.95E-5

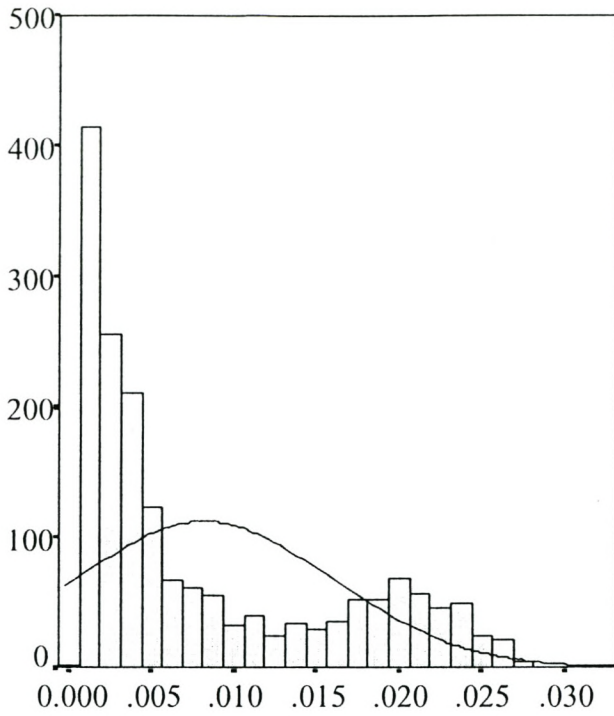


Figure C.11 Histogram showing distribution of original time series, Run D

Table C.8 Descriptive statistics of original time series, Run D

<i>Number of observations</i>	1751
<i>Mean</i>	8.17E-3
<i>Standard deviation</i>	7.78E-3
<i>Sample variance</i>	6.06E-5

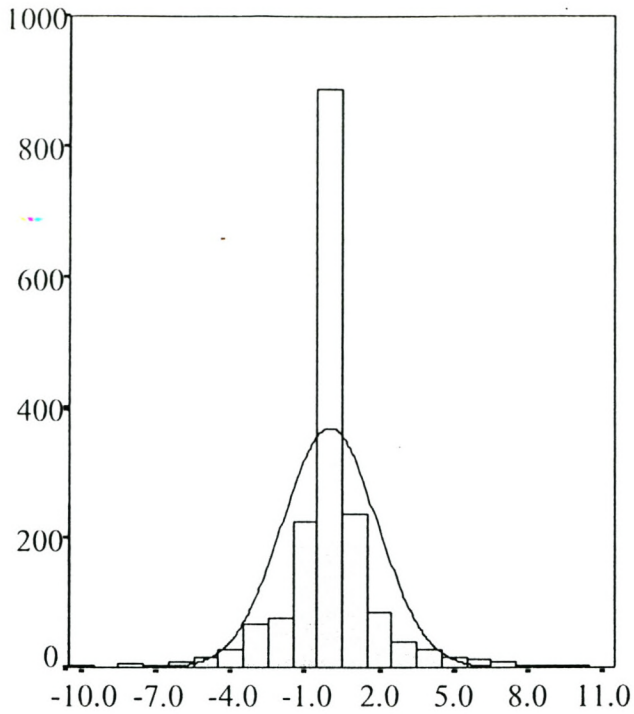


Figure C.12 Histogram showing distribution of Series A, Run D

Table C.9 Descriptive statistics of Series A, Run D

<i>Number of observations</i>	1750
<i>Mean</i>	-1.90E-4
<i>Standard deviation</i>	1.897
<i>Sample variance</i>	3.599

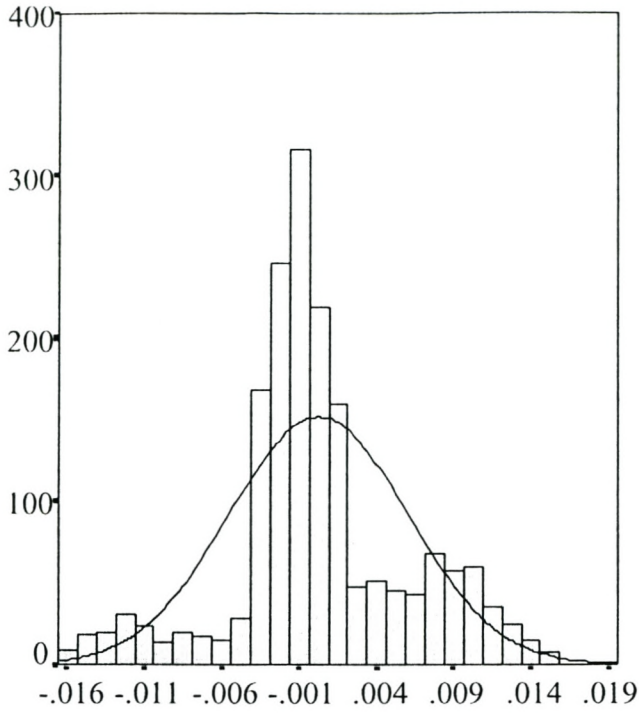


Figure C.13 Histogram showing distribution of Series B, Run D

Table C.10 Descriptive statistics of Series B, Run D

<i>Number of observations</i>	1751
<i>Mean</i>	-8.6E-18
<i>Standard deviation</i>	5.73E-3
<i>Sample variance</i>	3.28E-5